SAND92-0700/2
Unlimited Release
Printed December 1992

Distribution
Category UC-721

# Preliminary Performance Assessment for the Waste Isolation Pilot Plant, December 1992

## Volume 2: Technical Basis

WIPP Performance Assessment Department
Sandia National Laboratories
Albuquerque, New Mexico 87185

## ABSTRACT

Before disposing of transuranic radioactive waste in the Waste Isolation Pilot Plant (WIPP), the United States Department of Energy (DOE) must evaluate compliance with applicable long-term regulations of the United States Environmental Protection Agency (EPA). Sandia National Laboratories is conducting iterative performance assessments (PAs) of the WIPP for the DOE to provide interim guidance while preparing for a final compliance evaluation. This volume contains the technical basis for the 1992 PA. Specifically, it describes the conceptual basis for consequence modeling and the PA methodology, including the selection of scenarios for analysis, the determination of scenario probabilities, and the estimation of scenario consequences using a Monte Carlo technique and a linked system of computational models.

Additional information about the 1992 PA is provided in other volumes. Volume 1 contains an overview of WIPP PA and results of a preliminary comparison with the long-term requirements of the EPA's *Environmental Protection Standards for Management and Disposal of Spent Nuclear Fuel, High-Level and Transuranic Radioactive Wastes* (40 CFR 191, Subpart B). Volume 3 contains the reference data base and values for input parameters used in consequence and probability modeling. Volume 4 contains uncertainty and sensitivity analyses related to the preliminary comparison with 40 CFR 191B. Volume 5 contains uncertainty and sensitivity analyses of gas and brine migration for undisturbed performance. Finally, guidance derived from the entire 1992 PA is presented in Volume 6.

This volume of the report should be referenced as:

WIPP PA (Performance Assessment) Department. 1992. *Preliminary Performance Assessment for the Waste Isolation Pilot Plant, December 1992 — Volume 2: Technical Basis.* SAND92-0700/2. Albuquerque, NM: Sandia National Laboratories.

# ACKNOWLEDGMENTS

The Waste Isolation Pilot Plant (WIPP) Performance Assessment (PA) Department is comprised of both Sandia National Laboratories (SNL) and contractor employees working as a team to produce preliminary comparison with Environmental Protection Agency (EPA) regulations, assessments of overall long-term safety of the repository, and interim technical guidance to the program. The on-site team, affiliations, and contributions to the 1992 performance assessment are listed in alphabetical order:

**Performance Assessment Department**

| Name | Affil.* | Primary Author of Major Code | Area of Responsibility |
|---|---|---|---|
| R. Anderson | SNL | | Department Manager |
| B. Baker | TEC | | SEC02D, Hydrology, Office Manager |
| J. Bean | UNM | | BRAGFLO, 2-Phase Flow |
| J. Berglund | UNM | CUTTINGS | Task Ldr., Cuttings/Cavings/Spallings, Engr. Mech. |
| S. Bertram-Howery | SNL | | PA Liaison with DOE, Criteria Document, Test Phase Plan |
| W. Beyeler | SAI | PANEL, GARFIELD | Geostatistics, Analytical Models, CAMCON Systems Codes |
| K. Brinster | SAI | | Geohydrology, Conceptual Models |
| R. Blaine | ECO | | SEC02D, SECOTP, & CAMCON Systems Codes |
| T. Blaine | GC | | Drilling Technology, Exposure Pathways Data |
| K. Byle | UNM | | Software and Analysis QA |
| J. Chapman | TRI | | Documentation V.3 |
| D. Duncan | MAC | | Data QA |
| K. Economy | ECO | | SEC02D, SECOTP, Hydrology & Transport |
| D. Gallegos | SNL | | Task Ldr., Hydrology, Geostatistics, NEA, PSAG |
| D. Galson | GS | | NEA Working Groups, PSAG, PAAG, Human Intrusion |
| J. Garner | API | PANEL | Source Term, Sens. Anal. |
| A. Gilkey | UNM | | CAMCON Systems Codes |
| L. Gomez | SNL | | Task Ldr., Safety Assessments |
| M. Gruebel | TRI | | EPA Regulations, Documentation V.1, Editor V.1 |
| R. Guzowski | SAI | | Geology, Scenario Construction |
| J. Helton | ASU | CCDFPERM | Task Ldr., Uncert./Sens. Anal., Probability Models, Editor V.4 |
| S. Hora | UHH | | Expert Elicitation, Probability Models |
| R. Iuzzolino | GC | CCDFCALC, CCDFPERM | LHS, CAMCON System Codes, Probability Models |
| R. Klett | SNL | | EPA Regulations |
| P. Knupp | ECO | SECOTP | Comp. Fluid Dyn. |
| M. LaVenue | INT | GRASP-INV | Hydrology/Geostatistics |
| C. Leigh | SNL | GENII-S | Exposure Pathways |
| M. Marietta | SNL | | Dep. Dept. Manager, Tech. Coord. |
| G. de Marsily | UP | | Geostatistics Expert Group Chair |
| R. McCurley | UNM | | CAMCON System Codes |
| B. Napier | PNL | GENII | Safety Assessments |
| A. Peterson | SNL | | Task Ldr., Inventory |

| | | | |
|---|---|---|---|
| B. RamaRao | INT | GRASP-INV | Geostatistics |
| J. Rath | UNM | | CAMCON System Codes |
| R. Rechard | SNL | | Task Ldr., CAMCON, QA |
| P. Roache | ECO | SECO | Task Ldr., Comp. Fluid Dyn. |
| D. Rudeen | UNM | | STAFF2D, SECOTP, Transport |
| J. Ruge | ECO | | Multigrid Methods/BRAGFLO |
| T. Russell | ECO | | Upscaling |
| K. Salari | ECO | SECOTP | Transport, Computational Fluid Dynamics |
| J. Sandha | SAI | | INGRES, PA Data Base |
| J. Schreiber | SAI | | BRAGFLO, 2-Phase Flow |
| D. Scott | TRI | | Documentation V.2 |
| P. Swift | TRI | | Task Ldr., Geology, Climate Var., Documentation V.1 & 2, Editor V.1, 2, 4, & 5 |
| M. Tierney | SNL | | Task Ldr., CDF Constr., Probability Models, Ref. Data, Editor V.2 & 3 |
| K. Trauth | SNL | | Task Ldr., Expert Panels |
| P. Vaughn | API | BRAGFLO | Task Ldr., 2-Phase Flow & Waste Panel Chemistry, Editor V.4 & 5 |
| T. Zimmerman | GRA | | Geostatistics Test Problem |

The foundation of the annual WIPP performance assessment is the underlying data set and understanding of the important processes in the engineered and natural barrier systems. Other SNL Departments are the primary source of these data and understanding. Assistance with the waste inventory comes from Westinghouse Electric Corporation and its contractors. We gratefully acknowledge the support of our departmental and project colleagues. Some individuals have worked closely with the performance assessment team, and we wish to acknowledge their contributions individually:

| | | |
|---|---|---|
| H. Batchelder | WEC | CH & RH Inventories |
| R. Beauheim | SNL | Natural Barrier System, Hydrologic Parameters |
| D. Borns | SNL | Geology, Geophysics |
| B. Butcher | SNL | Engineered Barrier System, Unmodified Waste-Form Parameters, Disposal Room Systems Parameters |
| L. Brush | SNL | Engineered Barrier System, Source Term (Solubility) and Gas Generation Parameters |
| L. Clements | ReS | Computer System Support |
| T. Corbet | SNL | Natural Barrier System, Geologic & Hydrologic Parameters, Conceptual Models |
| P. Davies | SNL | Natural Barrier System, Hydrologic & Transport Parameters, & 2-Phase Flow Mechanistic Modeling |
| P. Drez | DE | CH & RH Inventories |
| R. Finley | SNL | Repository Isolation Systems Parameters |
| F. Gelbard | SNL | Natural Barrier System, Retardation |
| E. Gorham | SNL | Natural Barrier System, Fluid Flow & Transport Parameters |
| R. Holt | CON | Geology |
| S. Howarth | SNL | Natural Barrier System, Hydrologic Parameters |
| R. Kehrman | WEC | Ch & RH Waste Characterization |
| K. Lickliter | BEC | EPA Regulations |
| R. Lincoln | SNL | Room Modeling |
| F. Mendenhall | SNL | Engineered Barrier System, Unmodified Waste Form Parameters, Waste Panel Closure (Expansion) |
| D. Munson | SNL | Reference Stratigraphy, Constitutive Models, Physical & Mechanical Parameters |
| C. Novak | SNL | Natural Barrier Systems, Chemistry |
| E. Nowak | SNL | Room Modeling, Source Term |
| J. Orona | ReS | Computer System Support |
| A. Stevens | SNL | DOE Liaison |
| J. Tillerson | SNL | Repository Isolation Systems Parameters |

| | | |
|---|---|---|
| W. Wawersik | SNL | Fracturing |
| S. Webb | SNL | 2-Phase Flow Sensitivity Analysis & Benchmarking |

* Affiliation

API = Applied Physics Incorporated
ASU = Arizona State University
BEC = Benchmark Environmental Corp.
CON = Consultant
DE = Drez Environmental
ECO = Ecodynamics Research Associates
GC = Geo-Centers Incorporated
GRA = GRAM, Inc.
GS = Galson Sciences
INT = Intera
MAC = MACTEC
PNL = Pacific Northwest Laboratory
ReS = ReSpec
SAI = Scientific Applications International Corporation
SNL = Sandia National Laboratories
TEC = Technadyne Engineering Consultants
TRI = Tech Reps, Inc.
UHH = University of Hawaii at Hilo
UNM = University of New Mexico/New Mexico Engineering Research Institute
UP = University of Paris
WEC = Westinghouse Electric Corporation

## Peer Review

**Internal/Sandia**
L. Gomez
D. Schafer

**Management/Sandia**
W. Weart

**PA Peer Review Panel**

| | |
|---|---|
| R. Heath, Chair | University of Washington |
| R. Budnitz | Future Resources Associates, Inc. |
| T. Cotton | JK Research Associates, Inc. |
| J. Mann | University of Illinois |
| T. Pigford | University of California, Berkeley |
| F. Schwartz | Ohio State University |

**Department of Energy**
R. Becker

## Expert Panels

**Futures**

| | |
|---|---|
| M. Baram | Boston University |
| W. Bell | Yale University |
| G. Benford | University of California, Irvine |
| D. Chapman | The World Bank, Cornell University |
| B. Cohen | University of Pittsburgh |
| V. Ferkiss | Georgetown University |
| T. Glickman | Resources for the Future |
| T. Gordon | Futures Group |
| C. Kirkwood | Arizona State University |
| H. Otway | Joint Research Center (Ispra), Los Alamos National Laboratory |

| | |
|---|---|
| M. Pasqualetti | Arizona State University |
| D. Reicher | Natural Resources Defense Council |
| N. Rosenberg | Resources for the Future |
| M. Singer | The Potomac Organization |
| T. Taylor | Consultant |
| M. Vinovskis | University of Michigan |

**Markers**

| | |
|---|---|
| D. Ast | Cornell University |
| V. Baker | University of Arizona |
| M. Brill | Buffalo Organization for Social and Technological Innóvation |
| F. Drake | University of California at Santa Cruz |
| B. Finney | University of Hawaii at Manoa |
| D. Givens | American Anthropological Association |
| W. Goodenough | University of Pennsylvania |
| M. Kaplan | Eastern Research Group |
| J. Lomberg | Consultant |
| L. Narens | University of California at Irvine |
| F. Newmeyer | University of Washington |
| W. Sullivan | University of Washington |
| W. Williams | Case Western Reserve University |

**Source Term**

| | |
|---|---|
| C. Bruton | Lawrence Livermore National Laboratory |
| I-Ming Chou | U.S. Geological Survey |
| D. Hobart | Los Alamos National Laboratory |
| F. Millero | University of Miami |

**Retardation**

| | |
|---|---|
| R. Dosch | Sandia National Laboratories |
| C. Novak | Sandia National Laboratories |
| M. Siegel | Sandia National Laboratories |

**Geostatistics Expert Group**

| | |
|---|---|
| G. de Marsily, Chair | U. of Paris |
| R. Bras | Massachusetts Inst. of Tech. |
| J. Carrera | U. Politécnica de Cataluña |
| G. Dagan | Tel Aviv U. |
| A. Galli | Ecole des Mines de Paris |
| S. Gorlick | Stanford U. |
| P. Grindrod | Intera Sciences |
| A. Gutjahr | New Mexico Tech |
| D. McLaughlin | Massachusetts Inst. of Tech. |
| S. Neuman | U. of Arizona |
| C. Ravenne | Institut Français du Pétrole |
| Y. Rubin | U. of California, Berkeley |

**Report Preparation (TRI)**

Volume 1: M. Minahan (text); D. Marchand (illustrations)
Volume 2: M. Minahan (text); D. Marchand (illustrations)
Volume 3: J. Chapman (text); D. Marchand (illustrations)

D. Rivard and the Word Processing Department
R. Rohac, R. Andree, and the Illustration and Computer Graphics Departments
S. Tullar and the Production Department

# CONTENTS


1. Introduction ..... 1-1
   1.1 Purpose of Volume 2 ..... 1-1
   1.2 Organization of Volume 2 ..... 1-1
   1.3 Code Linkage and Data Flow ..... 1-3
      1.3.1 Data Bases ..... 1-4
      1.3.2 Program Linkage and Model Applications ..... 1-4

2. Conceptual Basis for Consequence Modeling ..... 2-1
   2.1 Introduction ..... 2-1
      2.1.1 Conceptual Models ..... 2-1
      2.1.2 Chapter Organization ..... 2-2
   2.2 Natural Barrier System ..... 2-2
      2.2.1 Regional Geology ..... 2-2
      2.2.2 Stratigraphy ..... 2-10
         2.2.2.1 Bell Canyon Formation ..... 2-10
         2.2.2.2 Capitan Limestone ..... 2-10
         2.2.2.3 Castile Formation ..... 2-11
         2.2.2.4 Salado Formation ..... 2-11
         2.2.2.5 Rustler-Salado Contact Zone ..... 2-12
         2.2.2.6 Rustler Formation ..... 2-12
            The Unnamed Lower Member ..... 2-14
            Culebra Dolomite Member ..... 2-16
            Tamarisk Member ..... 2-23
            Magenta Dolomite Member ..... 2-23
            Forty-niner Member ..... 2-24
         2.2.2.7 Supra-Rustler Rocks ..... 2-24
      2.2.3 Hydrology ..... 2-26
         2.2.3.1 Present Climate ..... 2-26
         2.2.3.2 Paleoclimates and Climatic Variability ..... 2-26
         2.2.3.3 Surface Water ..... 2-29
         2.2.3.4 The Water Table ..... 2-29
         2.2.3.5 Regional Water Balance ..... 2-29
         2.2.3.6 Groundwater Flow Above the Salado Formation ..... 2-30
            Potentiometric Surfaces ..... 2-30
            Groundwater Geochemistry ..... 2-34
            Recharge and Discharge ..... 2-36
      2.2.4 Radionuclide Transport in the Culebra Dolomite ..... 2-38
         2.2.4.1 Expert Judgment Elicitation for $K_d$s ..... 2-39
         2.2.4.2 Planned and Ongoing Experimental Work Related to Radionuclide Transport in the Culebra ..... 2-40
   2.3 Engineered Barrier System ..... 2-41
      2.3.1 The Salado Formation at the Repository Horizon ..... 2-41
      2.3.2 Repository and Seal Design ..... 2-45
         2.3.2.1 Waste Characterization ..... 2-45
         2.3.2.2 Seals ..... 2-48
         2.3.2.3 Backfill ..... 2-48
         2.3.2.4 Engineered Alternatives ..... 2-50
      2.3.3 Radionuclide Inventory ..... 2-50
      2.3.4 Radionuclide Solubility and the Source Term for Transport Calculations ..... 2-52
         2.3.4.1 Expert Judgment Elicitation ..... 2-52
         2.3.4.2 Experimental Work ..... 2-55
      2.3.5 Creep Closure, Fluid Flow, and Room/Waste Interactions ..... 2-55

3. Performance Assessment Methodology ..... 3-1
3.1 Conceptualization of Risk for the WIPP Performance Assessment ..... 3-1
3.1.1 Calculation of Risk ..... 3-2
3.1.2 Characterization of Uncertainty in Risk ..... 3-4
3.1.3 Risk and the EPA Limits ..... 3-8
3.2 Selection of Scenarios ..... 3-9
3.2.1 Conceptual Basis for Scenario Development ..... 3-9
3.2.2 WIPP Performance-Assessment Approach to Scenario Development ..... 3-13
3.3 Determination of Scenario Probabilities ..... 3-15
3.4 Calculation of Scenario Consequences ..... 3-16
3.5 Monte Carlo Analysis Techniques ..... 3-16
3.5.1 Selection of Variables and Their Ranges and Distributions ..... 3-19
3.5.2 Generation of the Sample ..... 3-21
3.5.3 Propagation of the Sample through the Analysis ..... 3-21
3.5.4 Uncertainty Analysis ..... 3-22
3.5.5 Sensitivity Analysis ..... 3-22

4. Scenario Construction ..... 4-1
4.1 Evaluation of Events and Processes ..... 4-1
4.1.1 Identifying Events and Processes ..... 4-1
4.1.2 Classifying Events and Processes ..... 4-3
4.1.3 Screening Events and Processes ..... 4-3
4.1.4 Summary of Screened Events and Processes ..... 4-4
4.2 Summary Scenarios ..... 4-7
4.2.1 Development of Summary Scenarios ..... 4-7
4.2.2 Screening of Summary Scenarios ..... 4-9
4.2.3 Retained Summary Scenarios ..... 4-10
4.2.3.1 Undisturbed Summary Scenario ($S_B$) ..... 4-10
Guidance from 40 CFR 191 ..... 4-10
Base-Case Description ..... 4-11
4.2.3.2 Human-Intrusion Summary Scenarios ..... 4-13
Guidance from 40 CFR 191 ..... 4-13
Intrusion Borehole through a Room or Drift into Pressurized Brine in the Castile Formation (Summary Scenario E1) ..... 4-13
Intrusion Borehole into a Room or Drift (Summary Scenario E2) ..... 4-15
Intrusion Borehole through a Room or Drift into Pressurized Brine in the Castile Formation and Another Intrusion Borehole into the Same Panel (Summary Scenario E1E2) ..... 4-15
4.2.4 Computational Approximations of Scenarios E1, E2, and E1E2 ..... 4-18

5. Drilling Intrusion Probabilities ..... 5-1
5.1 Introduction ..... 5-1
5.2 Probability Computations ..... 5-2
5.3 Lambda Function Generation ..... 5-5
5.3.1 The Expert Judgment Process ..... 5-5
5.3.2 Algorithm for Generating Lambda Functions ..... 5-7
5.3.3 Use of the Lambda Functions ..... 5-8

6. Data and CDFs ..... 6-1
6.1 Conventions ..... 6-1
6.1.1 Probability Distribution Functions ..... 6-1
6.1.2 Empirical Distribution Functions ..... 6-2
6.1.3 Range ..... 6-2
6.1.4 Mean and Sample Mean ..... 6-2
6.1.5 Median and Sample Median ..... 6-2
6.1.6 Variance and Coefficient of Variation ..... 6-2

6.1.7 Categories of Distributions ..... 6-3
6.1.7.1 Continuous Distributions ..... 6-3
6.1.7.2 Discrete Distributions ..... 6-4
6.1.7.3 Constructed Distributions (Data) ..... 6-4
6.1.7.4 Constructed Distributions (Subjective) ..... 6-4
6.1.7.5 Miscellaneous Categories ..... 6-4
6.2 Selection of Parameter Distributions ..... 6-5
6.2.1 Requests for Data from Sandia Investigators and Analysts ..... 6-5
6.2.2 Construction of Distributions ..... 6-6
6.2.3 Some Limitations on Distributions ..... 6-6

7. Consequence Modeling ..... 7-1
7.1 Radioactive Decay ..... 7-1
7.2 Multiphase Flow Through Porous Media ..... 7-1
7.2.1 Features and Capabilities of BRAGFLO ..... 7-2
7.2.2 Interaction of Important Repository Processes ..... 7-3
7.2.3 General Assumptions Used in 1992 PA Two-Phase Flow Modeling ..... 7-3
7.3 Waste-Filled Room Deformation ..... 7-5
7.4 Waste Mobilization ..... 7-7
7.4.1 Assumptions ..... 7-7
7.4.2 Simplified Mathematical Model ..... 7-9
7.5 Groundwater Transmissivity Fields ..... 7-10
7.5.1 Unconditional Simulation ..... 7-10
7.5.2 Conditional Simulation ..... 7-11
7.5.3 Automated Calibration ..... 7-11
7.6 Groundwater Flow and Transport ..... 7-13
7.6.1 Groundwater Flow in the Culebra ..... 7-15
7.6.1.1 Boundary Conditions ..... 7-16
7.6.1.2 Effects of Climate Change ..... 7-16
7.6.2 Solute Transport in Culebra ..... 7-18
7.6.2.1 Modeling Hydrodynamic Dispersion ..... 7-18
7.6.2.2 Modeling Chemical Sorption in Fracture Flows ..... 7-21
7.7 Direct Removal of Waste ..... 7-23
7.7.1 Cuttings ..... 7-25
7.7.2 Cavings ..... 7-25
7.7.2.1 Laminar Flow ..... 7-25
7.7.2.2 Turbulent Flow ..... 7-26
7.7.3 Spallings ..... 7-27

8. References ..... 8-1

Appendix A: BRAGFLO and PANEL ..... A-1

Appendix B: SANCHO ..... B-1

Appendix C: SECO Flow and Transport Model ..... C-1

Appendix D: Culebra Transmissivity Field Simulations ..... D-1

## Figures

1-1 1992 Organization of Programs in CAMCON ..... 1-5
2-1 Generalized geology of the Delaware Basin, showing the location of the Capitan Reef and the erosional limits of the basinal formations ..... 2-4
2-2 Geologic time scale ..... 2-5
2-3 Stratigraphy of the Delaware Basin ..... 2-6
2-4 Schematic east-west cross section through the northern Delaware Basin ..... 2-7

2-5 Schematic north-south cross section through the northern Delaware Basin ..... 2-8
2-6 Map of the WIPP vicinity showing the land-withdrawal area (labeled "WIPP Boundary"), the study area of Brinster, and the location of observation wells ..... 2-9
2-7 East-west cross section showing stratigraphy of the Rustler Formation and the Dewey Lake Red Beds ..... 2-13
2-8 Rustler Formation halite around the WIPP ..... 2-15
2-9 Log hydraulic conductivities of the Culebra Dolomite Member of the Rustler Formation ... 2-17
2-10 Sources of geologic information about the Culebra Dolomite ..... 2-18
2-11 Isopach overburden for the Culebra Dolomite Member ..... 2-20
2-12 Interpreted extent of Salado dissolution ..... 2-21
2-13 Percentage of natural fractures in the Culebra Dolomite Member filled with gypsum ..... 2-22
2-14 Log hydraulic conductivities of the Magenta Dolomite Member of the Rustler Formation .. 2-25
2-15 Estimated mean annual precipitation at the WIPP during the Late Pleistocene and Holocene ..... 2-28
2-16 Adjusted potentiometric surface of the Rustler-Salado contact zone in the WIPP vicinity .... 2-31
2-17 Adjusted potentiometric surface of the Culebra Dolomite Member of the Rustler Formation in the WIPP vicinity ..... 2-32
2-18 Adjusted potentiometric surface of the Magenta Dolomite Member of the Rustler Formation in the WIPP vicinity ..... 2-33
2-19 Hydrochemical facies in the Culebra Dolomite Member of the Rustler Formation ..... 2-35
2-20a Reference local stratigraphy near repository ..... 2-43
2-20b Stratigraphy at the repository horizon ..... 2-44
2-21 Plan view of waste-disposal horizon showing shaft, drift, and panel seal locations ..... 2-46
2-22 Representative shaft and plug seals ..... 2-49
3-1 Estimated CCDF for consequence result **cS** ..... 3-3
3-2 Example distribution of CCDFs obtained by sampling imprecisely known variables ..... 3-6
3-3 Example summary curves derived from an estimated distribution of CCDFs ..... 3-7
3-4 Decomposition of the sample space *S* into high-level subsets ..... 3-10
3-5 Construction of a CCDF for comparison with the EPA release limits ..... 3-12
3-6 Models used in 1992 WIPP performance assessment ..... 3-17
3-7 Distribution function for an imprecisely known analysis variable ..... 3-20
3-8 Example of box plots ..... 3-23
4-1 Potential scenarios for the WIPP disposal system ..... 4-8
4-2 Conceptual model used in simulating undisturbed performance ..... 4-12
4-3 Conceptual model for scenario E1 ..... 4-14
4-4 Conceptual model for scenario E2 ..... 4-16
4-5 Conceptual model for scenario E1E2 ..... 4-17
5-1 A realization of effective drilling intensity $\lambda(t)$ and its associated integrated effective drilling intensity as functions of time ..... 5-9
7-1 Interaction of some important repository processes ..... 7-4
7-2 Surface giving porosity of waste-filled disposal room as a function of total volume of gas produced and time after sealing ..... 7-6
7-3 Idealized collapsed WIPP panel in a PANEL model ..... 7-8
7-4 Conceptual hydrologic model of the Culebra Dolomite Member ..... 7-14
7-5 Example of regional and local grids used for disturbed fluid flow and transport calculations ..... 7-17
7-6 Rotary drilling ..... 7-24

## Tables

2-1 Properties of the Rustler Formation Units and Rustler-Salado Contact Zone ..... 2-14
3-1 Summary of Computer Models Used in the 1992 WIPP Performance Assessment ..... 3-18
4-1 Potentially Disruptive Events and Processes ..... 4-2
4-2 Summary of Screened Events and Processes ..... 4-5

# 1. INTRODUCTION

The Waste Isolation Pilot Plant (WIPP) is planned as a research and development facility to demonstrate the safe disposal of transuranic (TRU) wastes generated by defense programs of the United States Department of Energy (DOE). Before disposing of waste in the WIPP, the DOE must evaluate compliance with applicable long-term regulations of the United States Environmental Protection Agency (EPA), including 40 CFR 191 Subpart B *(Environmental Radiation Protection Standards for Management and Disposal of Spent Nuclear Fuel, High-Level and Transuranic Radioactive Wastes)* [U.S. EPA, 1985]) and 40 CFR 268.6 (U.S. EPA, 1986), which is the portion of the *Land Disposal Restrictions* of the *Hazardous and Solid Waste Amendments* to the *Resource Conservation and Recovery Act* (RCRA) that states the conditions for disposal of specified hazardous wastes. Performance assessments (PAs) will form the basis for evaluating compliance with all applicable long-term regulations of the EPA. The WIPP Performance Assessment (PA) Department of Sandia National Laboratories (SNL) is performing annual iterative preliminary PAs to provide guidance to the Project while preparing for final compliance evaluation. The 1991 preliminary performance assessment for comparison with 40 CFR 191B was documented in 4 volumes (WIPP PA Division, 1991 a, b, c; Helton et al., 1992).

## 1.1 Purpose of Volume 2

This volume describes the technical basis for the 1992 WIPP preliminary PA: conceptual model development, probability modeling, and consequence modeling of the WIPP disposal system for evaluating compliance with the quantitative requirements of applicable long-term regulations. Volume 1 deals primarily with the regulations in Subpart B of 40 CFR Part 191 and their application to the WIPP, but also summarizes aspects of this volume and explains the 1992 status of the WIPP PA. Volume 3 compiles model parameters, constructs cumulative distribution functions (cdfs) and discusses their derivation from the pertinent data of disposal system characterization. Uncertainty and sensitivity analysis results related to 40 CFR 191B are discussed in Volume 4. Uncertainty and sensitivity analysis results of gas and brine migration for undisturbed performance are discussed in Volume 5. Finally, guidance derived from the entire 1992 PA is presented in Volume 6.

## 1.2 Organization of Volume 2

Volume 2 consists of seven chapters and four appendices. This chapter (Chapter 1) describes the organization of Volume 2. The remaining six chapters are organized following the PA methodology described in Volume 1.

- Chapter 2 (Conceptual Basis for Consequence Modeling) describes the conceptual basis for consequence modeling. This chapter is a detailed expansion of the brief discussion in Chapter 2 of Volume 1, and provides a bibliographic mapping into the published literature of the site characterization and engineered design programs.

- Chapter 3 (Performance Assessment Methodology) describes the conceptual model for risk that forms the framework (scenarios, frequency or probability of scenarios, and consequences of scenarios) for the WIPP

PA, presents an outline of the Monte Carlo technique that is used for uncertainty and sensitivity analyses, and discusses the construction of complementary cumulative distribution functions (CCDFs). This chapter is a detailed expansion of Chapter 4 of Volume 1, and is generally unchanged from the 1991 PA.

- Chapter 4 (Scenario Construction) examines the first element (scenarios) of the conceptual model for risk. This chapter discusses the application of the methodology for scenario construction—identifying, screening, and classifying events and processes; developing scenarios using a logic diagram; and screening of scenarios —for the WIPP. Retained scenarios that are analyzed in the 1992 PA are described. This material is generally unchanged from the 1991 PA and therefore references previous documents extensively. Scenarios included in the Monte Carlo analysis in 1991 are included again in 1992.

- Chapter 5 (Drilling Intrusion Probabilities) examines the second element (probabilities or frequencies of scenarios) of the conceptual model for risk. The probability model that is used for the 1992 analysis was presented in the 1991 documentation, so this chapter is a much briefer description that references previous documentation. The significant difference in the application of this model is that time-varying drilling intensities were used in 1992, whereas in 1991 only constant, but imprecisely known, drilling intensities were used. A brief discussion of how these new drilling intensity functions were derived from expert panel output that references material in Volume 3 is included.

- Chapter 6 (Data and cdfs) begins the description of the different steps of the Monte Carlo technique: selection of imprecisely known parameters, construction of ranges and distributions for these parameters, generation of the sample, propagation of uncertainty through the system model, uncertainty analysis, and sensitivity analysis. This chapter briefly describes the first steps: selection of imprecisely known parameters and construction of their ranges and distributions. The entire data base, especially model parameters, is the subject of Volume 3.

- Chapter 7 (Consequence Modeling) describes the modeling system that is used to calculate consequences of scenarios. The Latin hypercube sampling technique that is used to generate the sample for Monte Carlo analysis is described elsewhere (Helton et al., 1991) and is not repeated. This chapter focuses on the 1992 modeling system through which uncertainty is propagated for the uncertainty and sensitivity analysis. Each major module of this system is described in terms of governing equations and modeling assumptions. More detailed code descriptions are contained in the four appendices as follows:

Appendix A. A repository and shaft seal module is used that simulates two-phase (gas and brine) flow through the repository, shaft seals, and surrounding environs (BRAGFLO) with an equilibrium-mixing cell for calculating radionuclide concentrations in the brine phase (PANEL). These codes were used in the 1991 PA.

Appendix B. A module (SANCHO) for simulating quasistatic, large-deformation, inelastic response of the halite is used to provide waste porosity as a function of time. These calculations incorporate the effect of creep closure and of halite response to waste-generated gas into the PA; they are performed outside the Monte Carlo analysis. Only the waste porosity functions are used during

consequence calculations. This is the first year that the effects of halite creep have been included in PA calculations.

Appendix C. Groundwater flow and transport models (SECO-2DH and SECO-TP) are used to calculate subsurface transport through the Culebra Dolomite Member of the Rustler Formation to the land-withdrawal boundary. First, the groundwater flow is calculated for a single-porosity, matrix-only, porous medium (dolomite). The flow calculation is performed first on a regional scale and second on a local scale with boundary conditions derived from the regional-scale distribution. Climate variability enters through time-varying boundary conditions that are based on a simple precipitation/recharge conceptualization. Spatial variability enters by drawing one field from a set of multiple, plausible transmissivity fields that are generated outside the Monte Carlo analysis (GRASP-INV). SECO-2DH was used in the 1991 PA.

Second, the flow field is used for a radionuclide-transport simulation. The transport simulator SECO-TP was used for the first time in 1992. It models single- or dual-porosity transport through an idealized, fractured medium. Retardation in pore volume of the dolomite matrix and/or the fracture-lining clay can be included simultaneously or separately. SECO-TP is a further improvement over previous capability in that it is more accurate and numerically efficient, allowing higher-resolution, higher-accuracy simulations in the same time.

Appendix D. A module (GRASP-INV) for generating multiple, plausible transmissivity fields to be used by SECO2-DH is used for the first time in 1992. This module is an improvement over previous capability in that it produces transmissivity fields that reproduce the measured values of transmissivity at well locations and that are calibrated, i.e., flow calculations with these fields reproduce (to within a pre-selected criterion) steady-state and transient pressure data at the well locations. Therefore, each field is a plausible realization of the true but unknown transmissivity field. One entire field is drawn and used for a single consequence calculation during the Monte Carlo analysis.

## 1.3 Code Linkage and Data Flow

The complexity of the compliance-assessment modeling system for the WIPP requires that calculations be controlled by an executive program (Rechard, 1989; Rechard et al., 1989; Rechard, 1992). CAMCON (Compliance Assessment Methodology CONtroller) controls code linkage and data flow during lengthy and iterative consequence analyses, minimizes analyst intervention during data transfer, and automatically handles quality assurance during the calculations. CAMCON currently consists of about 75 codes and FORTRAN object libraries; it includes approximately 293,000 lines of FORTRAN software written specifically for the WIPP Project and another 175,000 lines of software adapted from other applications.

The controller allows easy examination of intermediate diagnostics and final results. Computer modules within the executive program can be easily replaced for model comparisons. CAMCON modularizes tasks so computer programs for a particular module are interchangeable. CAMCON is fully described in Rechard (1992).

### 1.3.1 Data Bases

Three data bases, primary, secondary, and computational, are included in CAMCON. The primary data base contains measured field and laboratory data gathered during the disposal-system and regional characterization. Because the analysis can be no better than these data, the data base should contain all necessary data for the compliance assessment and repository design, have as little subjective interpretation as possible, and be quality assured. Data base structure must be flexible to accommodate different organizations and unforeseen types of data. Practical experience suggests that a relational data base is best.

The secondary data base contains interpreted data, usually interpolated onto a regular grid, and incorporates information that comprises the conceptual model of the disposal system. Levels of interpretation can vary from objective interpolation of data combined with subjective judgments to totally subjective extrapolations of data; all interpretations are well documented to ensure the secondary data is reproducible by others. Data from literature or professional judgment are used to fill knowledge gaps to complete the conceptual model. The secondary data base must be accessible to both the analyst and the executive package controlling the system.

The computational data base is CAMDAT (Compliance Assessment Methodology DATa). CAMDAT uses a neutral-file format so that a series of computer programs can be linked by a "zig-zag" connection rather than the usual serial connection. The file format chosen for CAMDAT was based on GENESIS (Taylor et al., 1987) and EXODUS and their associated data manipulation and plotting programs (Gilkey, 1986a,b, 1988; Gilkey and Flanagan, 1987). CAMDAT is fully described in Rechard (1992).

### 1.3.2 Program Linkage and Model Applications

Program linkage and data flow through CAMDAT are controlled by CAMCON. Computer programs that make up the CAMCON system are major program modules, support program modules, and translators. Major program modules refer to programs that represent major tasks of the consequence modeling. Support program modules refer to programs such as interpolators that are necessary to facilitate use of major program modules. Translator program modules refer to programs that translate data either into or out of the computational data base. Figure 1-1 shows how programs are used in the 1992 PA to evaluate human-intrusion scenarios. BRAGFLO, GRASP-INV, SECO-TP, and CUTTINGS were run outside of CAMCON, with manual data transfer. GENII-S was not used because a safety assessment was not included in the 1992 PA. All other codes were used within CAMCON as shown (Figure 1-1).

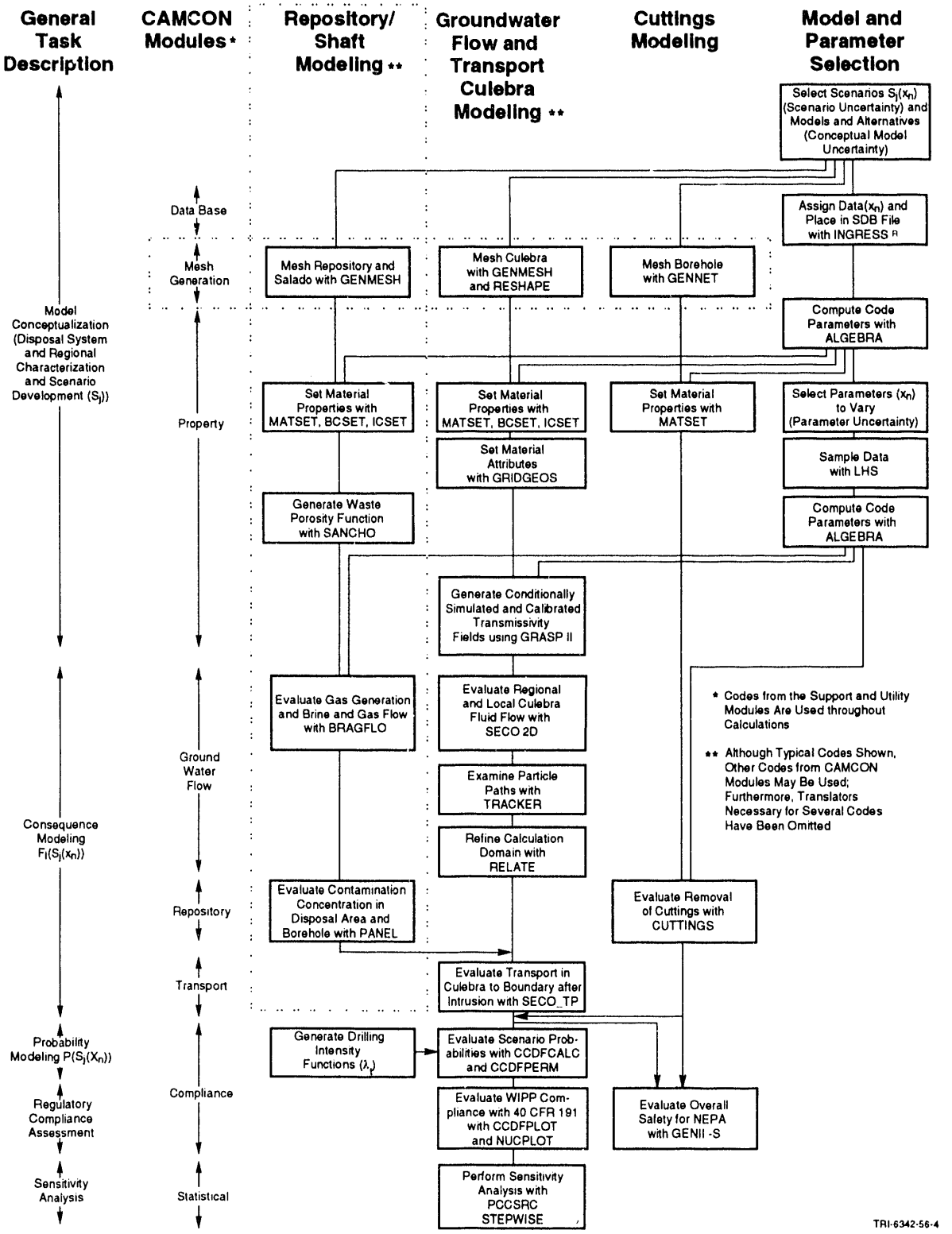


Figure 1-1. 1992 Organization of Programs in CAMCON (after Rechard, 1992).

# 2. CONCEPTUAL BASIS FOR CONSEQUENCE MODELING

## 2.1 Introduction

### 2.1.1 Conceptual Models

This chapter describes the conceptual basis for modeling the performance of the WIPP repository, the waste it contains, and the surrounding geology and hydrology, and summarizes the available knowledge of the site and the physical processes that operate there. This knowledge forms the framework for the preferred conceptual model used in WIPP PA (i.e., the model believed by the WIPP PA Department to be the most realistic representation for the behavior of the disposal system), and for alternative conceptual models. Conceptual model and alternative conceptual models are defined as follows (Gallegos et al., 1992; NEA, 1992):

- Conceptual model: A set of qualitative assumptions used to describe a system or subsystem for a given purpose. At a minimum, these assumptions concern the geometry and dimensionality of the system, initial and boundary conditions, time dependence, and the nature of the relevant physical and chemical processes. The assumptions should be consistent with one another and with existing information within the context of the given purpose.

- Alternative conceptual models: Alternative sets of assumptions that describe the same system for the same purpose, where each set of assumptions is consistent with the existing information.

Each alternative conceptual model identifies the processes that the mathematical models must characterize and provides the context within which the mathematical models must operate.

As an example of the role alternative conceptual models play in performance assessment, Volume 1 of the 1992 WIPP PA documents the use of three alternative conceptual models for the subsurface transport of radionuclides in the Culebra Dolomite Member of the Rustler Formation. (See Section 2.2 for an explanation of the regional geohydrology, Section 4.2 for an explanation of the transport pathway, and Section 7.6 for a discussion of the transport model. See Section 5.1 of Volume 1 of this report for a comparison of disposal-system performance estimated using each of the three conceptual models. See Volume 4 of this report for additional analysis of these and other alternative conceptual models.) In the first conceptual model, transport occurs only in clay-lined fractures in a single-porosity medium, and chemical retardation does not occur. In the second conceptual model, transport occurs in a dual-porosity medium (clay-lined fractures and matrix); radionuclides may diffuse into the pore volume of both the clay linings and the rock matrix. Chemical retardation does not occur. In the third conceptual model, believed by the WIPP PA Department to be the most realistic representation for the behavior of the system, transport occurs in a dual-porosity medium, as in the second conceptual model, except that chemical retardation does occur as a result of sorption of radionuclides in both clay linings and rock matrix.

The first of these three alternative conceptual models is not supported by available information (see Section 2.2.4), and is included in the analysis as an unrealistic, but known, endpoint of a continuum on which a realistic endpoint is unknown. As such, it provides useful guidance on the largest releases that may be anticipated as a result of groundwater transport in the Culebra. Comparison of all three conceptual models provides insight into the uncertainty in performance estimates resulting from an incomplete understanding of the dual-porosity behavior of the Culebra and the lack of defensible data describing chemical retardation of radionuclides (see Section 2.2.4).

Other major aspects of the conceptual model for the WIPP used in the 1992 PA include the following: generation of gas in the waste-emplacement panels by degradation of waste and containers; closure and re-expansion of the panels by salt creep; the release of radionuclides at the ground surface and into the Culebra as a result of borehole intrusion during exploratory drilling; changes in groundwater flow resulting from future climatic changes; and the effect of passive marker systems on intrusion rates.

### 2.1.2 Chapter Organization

The WIPP and surrounding environment provide multiple barriers to radionuclide migration. This chapter explains the WIPP PA's present understanding of the conceptual basis of these barriers. The chapter is organized into two major parts:

- natural barrier system (Section 2.2)—the regional geology and hydrology surrounding the WIPP (Section 2.2.1); the stratigraphy below and above the repository (Section 2.2.2); climate, water balance, and groundwater flow in the WIPP vicinity (Section 2.2.3); and radionuclide transport in the Culebra Dolomite (Section 2.2.4)

- engineered barrier system (Section 2.3)— the repository and seal design (Section 2.3.2); the waste itself (Section 2.3.3); the radionuclide source term (Section 2.3.4); and closure, flow, and room/waste interactions (Section 2.3.5)

## 2.2 Natural Barrier System

### 2.2.1 Regional Geology

The geology of the WIPP and the surrounding area has been introduced briefly in Chapter 2 of Volume 1, and is described elsewhere in detail (e.g., Hiss, 1975; Powers et al., 1978a,b; Cheeseman, 1978; Williamson, 1978; Hills, 1984; Ward et al., 1986; Harms and Williamson, 1988; Holt and Powers, 1988, 1990; Beauheim and Holt, 1990; Brinster, 1991). The brief review presented here describes regional structural features and introduces the major stratigraphic units. Specific geologic features that affect compliance-assessment modeling are described in subsequent sections of this chapter.

The WIPP is located near the northern end of the Delaware Basin, a structural depression that formed during the Late Pennsylvanian and Permian Periods, approximately 300 to 245 million years ago (Figures 2-1 and 2-2). Sedimentation within the subsiding basin resulted in the deposition of up to 4,000 m (13,000 ft) of marine strata. Organic activity at the basin margins produced massive carbonate reefs that separated deep-water facies from the shallow-water shelf sediments deposited landward.

Permian-age rocks of importance to WIPP performance-assessment modeling are those of the Guadalupian and Ochoan Series, deposited between approximately 265 and 245 million years ago (Figure 2-3). During this time subsidence in the Delaware Basin was initially rapid, resulting in deposition of deep-water shales, sandstones, and limestones of the Delaware Mountain Group. Intermittent connection with the open ocean and a decrease in clastic sediment supply, possibly in response to regional tectonic adjustments, led to the deposition of a thick evaporite sequence. Anhydrites and halites of the Castile Formation are limited to the structurally deeper portion of the basin, enclosed within the reef-facies rocks of the Capitan Limestone. Subsidence within the basin slowed in Late Permian time, and the halites of the Salado Formation, which include the host strata for the WIPP, extend outward from the basin center over the Capitan Reef and the shallow-water shelf facies. Latest Permian-age evaporites, carbonates, and clastic rocks of the Rustler Formation and the Dewey Lake Red Beds record the end of regional subsidence and include the last marine rocks deposited in southeastern New Mexico during the Paleozoic. The overlying sandstones of the Triassic-age Dockum Group reflect continental deposition and mark the onset of a period of regional tectonic stability that lasted approximately 240 million years, until late in the Tertiary Period.

Permian-age strata of the Delaware Basin now dip gently (generally less than $1^{o}$) to the east, and erosion has exposed progressively older units toward the western edge of the basin (Figures 2-1 and 2-4). This tilting reflects the Late Pliocene and early Pleistocene (approximately 3.5 million to 1 million years ago) uplift of the Capitan Reef to form the Guadalupe Mountains more than 60 km (37 miles) west of the WIPP (Figures 2-1, 2-4). Field evidence suggests that additional uplift may have occurred during the late Pleistocene and Holocene, and some faults of the Guadalupe Mountains may have been active within the last 1,000 years (Powers et al., 1978a,b). North and east of the WIPP, the Capitan Reef has not been uplifted and remains in the subsurface (Figure 2-5).

The present landscape of the Delaware Basin has been influenced by near-surface dissolution of the evaporites (Bachman, 1984, 1987). Karst features created by dissolution include sinkholes, subsidence valleys, and breccia pipes. Most of these features formed during wetter climates of the Pleistocene, although active dissolution is still occurring wherever evaporites are exposed at the surface. Some dissolution may also be occurring in the subsurface where circulating groundwater comes in contact with evaporites: for example, modern subsidence in San Simon Swale east of the WIPP (Figure 2-6) may be related to localized dissolution of the Salado Formation (Anderson, 1981; Bachman, 1984; Brinster, 1991). Nash Draw, which formed during the Pleistocene by dissolution and subsidence, is the most prominent karst feature near the WIPP. As discussed again in Section 2.2.2.6 following, evaporites in the Rustler Formation have been affected by dissolution near Nash Draw.

The largest karst feature in the Delaware Basin is the Balmorhea-Loving Trough, south of the WIPP along the axis of the basin (Figure 2-6). Dissolution of evaporites, perhaps along the course of a predecessor of the modern Pecos River, resulted in subsidence and the deposition of Cenozoic alluvium up to 300 m (984 ft) thick in south-

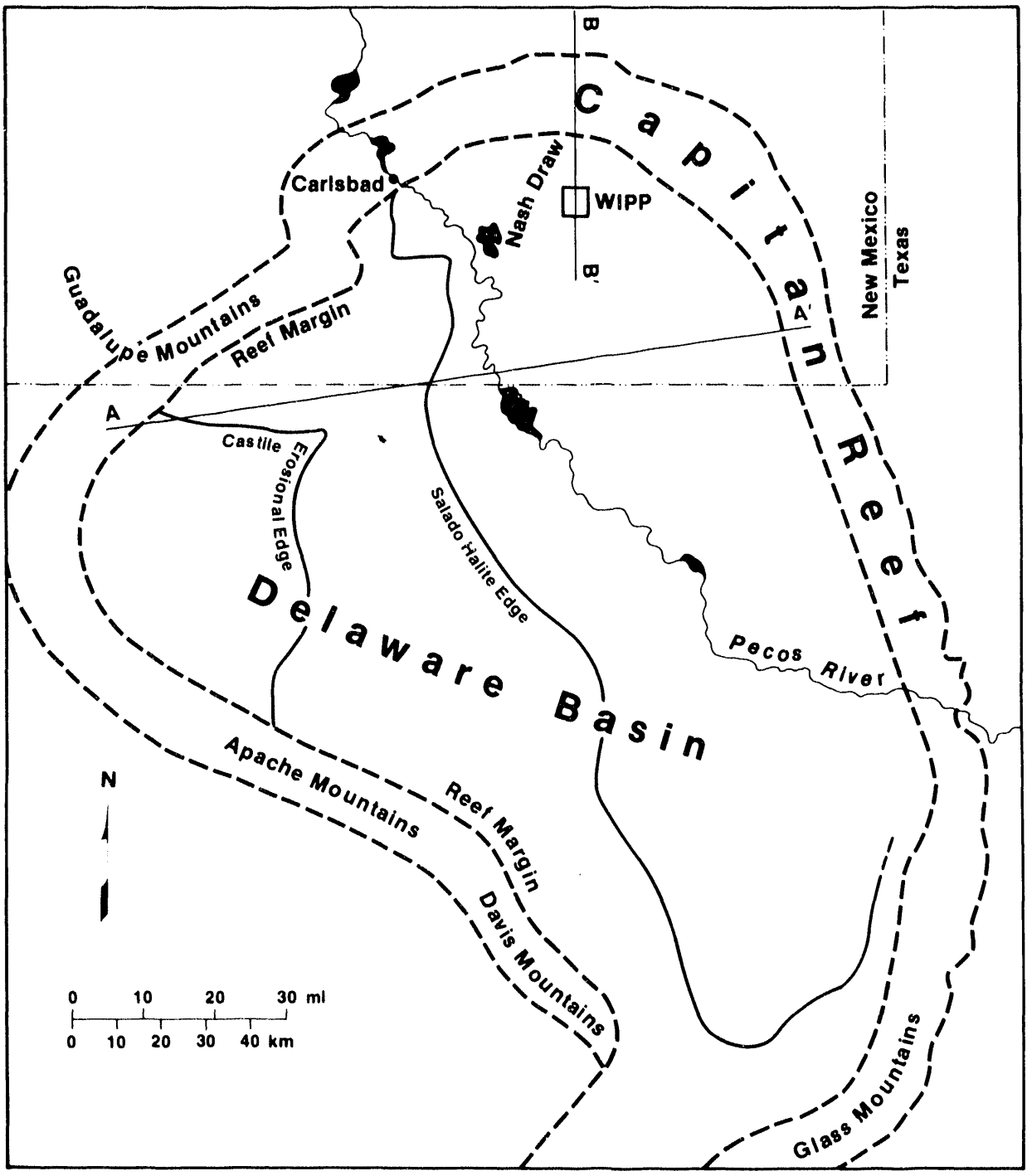


TRI-6342-237-4

Figure 2-1. Generalized geology of the Delaware Basin, showing the location of the Capitan Reef and the erosional limits of the basinal formations (Lappin, 1988).

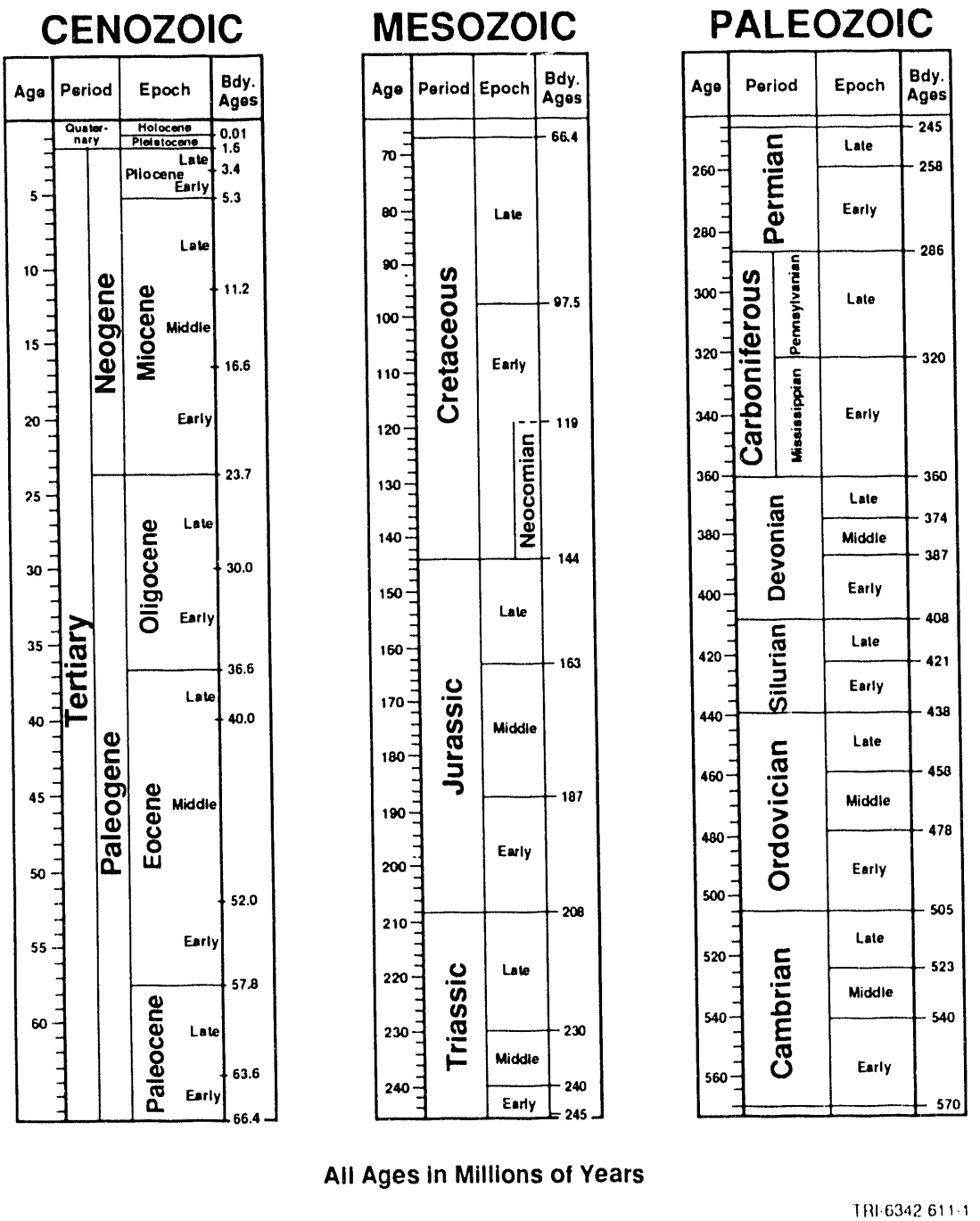


Figure 2-2. Geologic time scale (simplified from Geological Society of America, 1984).

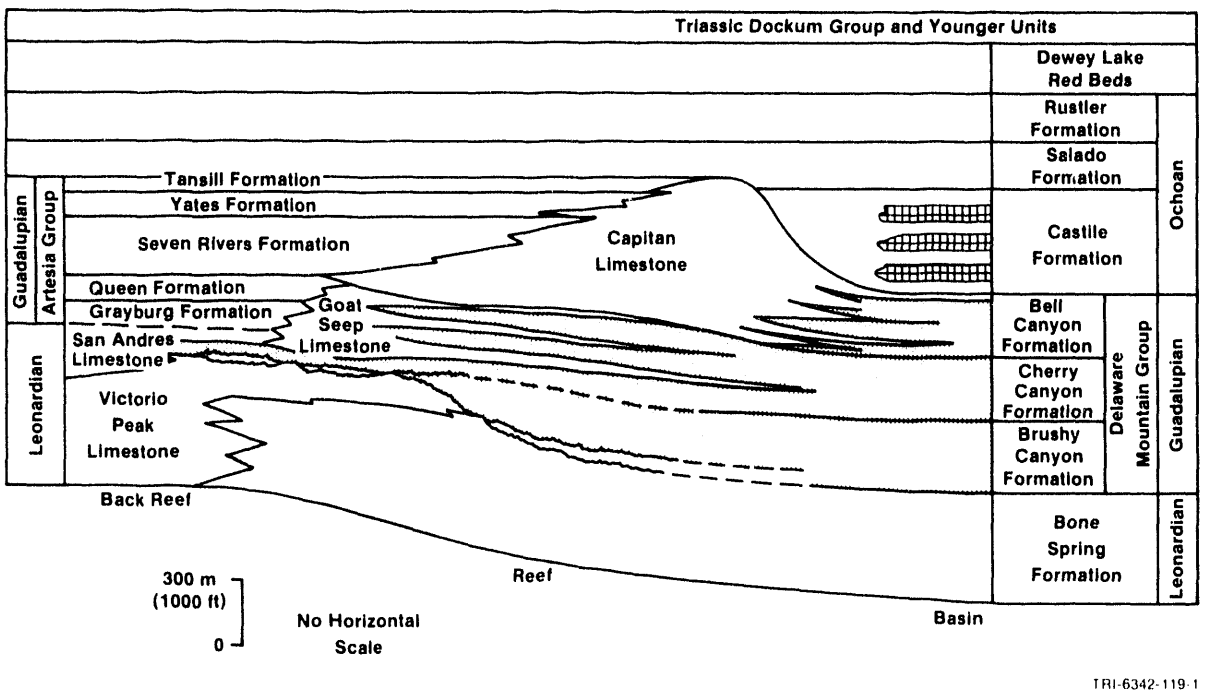


Figure 2-3. Stratigraphy of the Delaware Basin (modified from Mercer, 1983; Brinster, 1991)

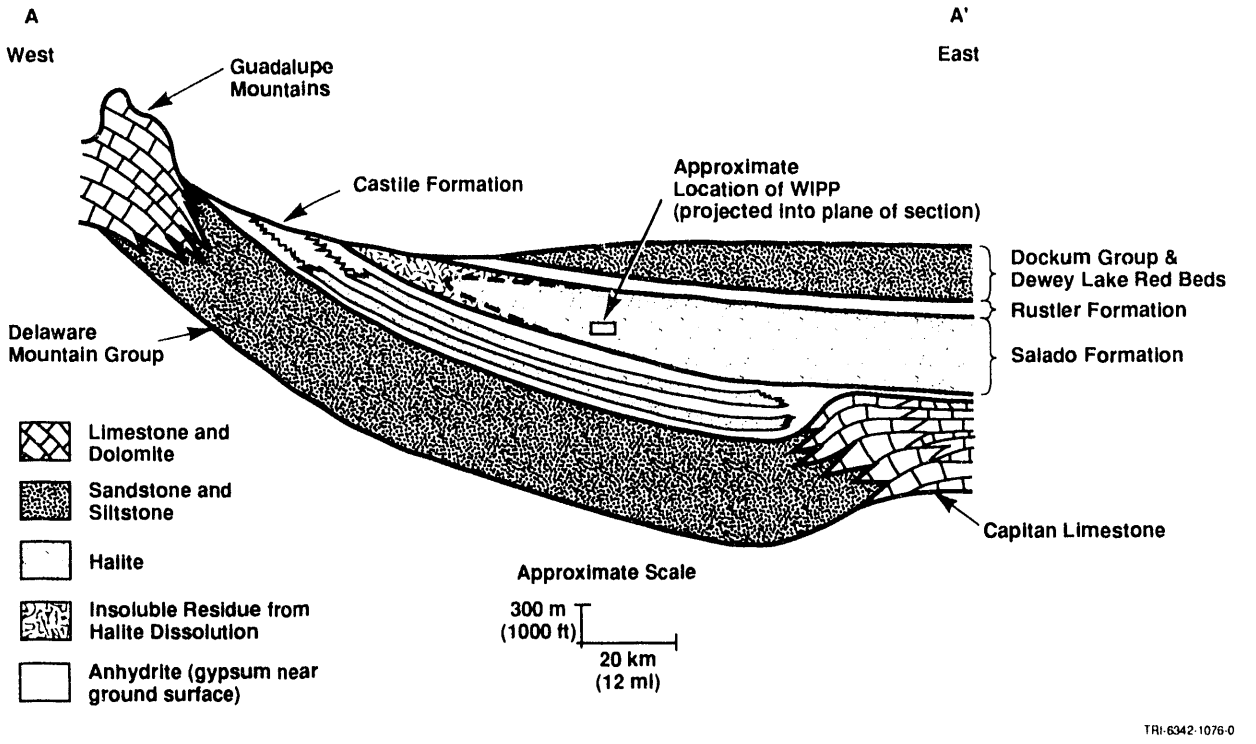


Figure 2-4. Schematic east-west cross section through the northern Delaware Basin (modified from Davies, 1984). Note extreme vertical exaggeration. Approximate location of line of section shown on Figure 2-1.

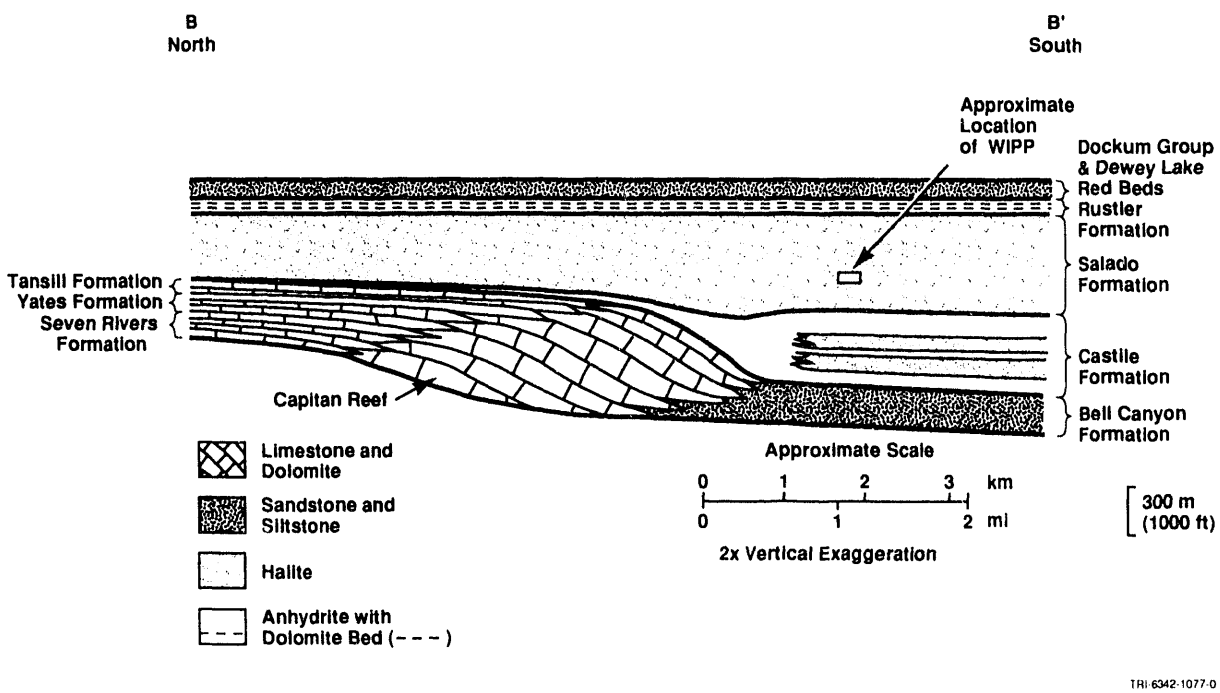


Figure 2-5. Schematic north-south cross section through the Northern Delaware Basin (modified from Davies, 1984). Note extreme vertical exaggeration. Approximate location of line of section shown on Figure 2-1.

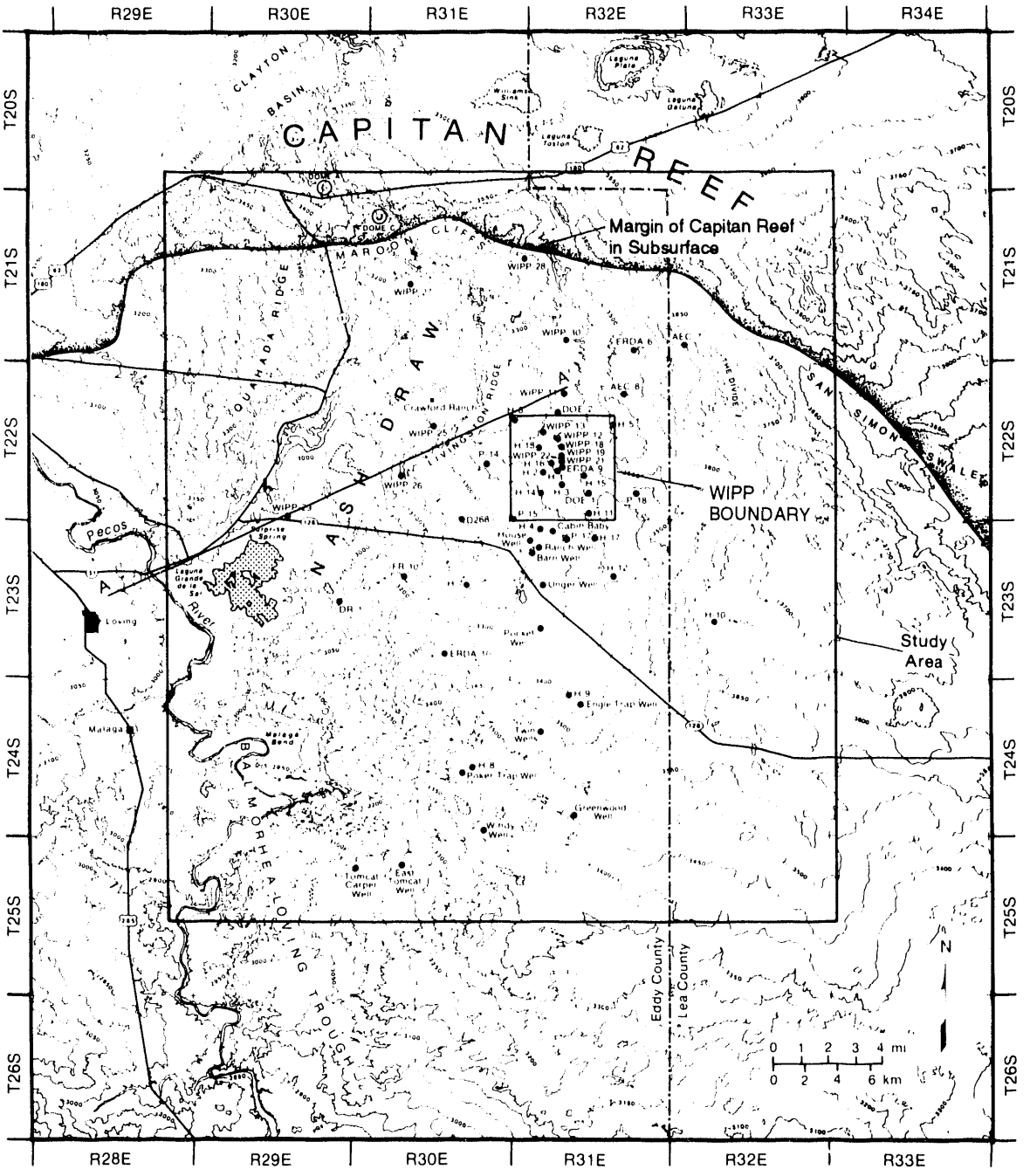


Figure 2-6. Map of the WIPP vicinity showing the land-withdrawal area (labeled "WIPP Boundary"), the study area of Brinster (1991), and the location of observation wells (Haug et al., 1987; Brinster, 1991).

ern Eddy County, and up to almost 600 m (1970 ft) thick across the state line in Texas (Bachman, 1984, 1987; Brinster, 1991).

## 2.2.2 Stratigraphy

This review is based primarily on the summary presented by Brinster (1991), and is limited to those units that may have an important role in future performance of the disposal system. Hydrologic data about the units have been summarized by Brinster (1991), and are, in general, not repeated here. Stratigraphic relationships between the units are shown in Figure 2-3. Figure 2-6 shows the region examined in detail by Brinster (1991) and the location of wells that provide basic data.

### 2.2.2.1 BELL CANYON FORMATION

The Bell Canyon Formation consists of 210 to 260 m (690 to 850 ft) of sandstones and siltstones with minor limestones, dolomites, and conglomerates (Williamson, 1978; Mercer, 1983; Harms and Williamson, 1988). Sandstones within the upper portion of the Bell Canyon Formation occur as long, sinuous channels separated by siltstones, reflecting their deposition by density currents that flowed into the deep basin from the Capitan Reef (Harms and Williamson, 1988). These sandstones have been targets for hydrocarbon exploration elsewhere in the Delaware Basin and are also of interest for the WIPP performance assessment because they are the first aquifers below the evaporite sequence that hosts the repository.

Simulations of undisturbed repository performance do not include the Bell Canyon Formation because a thick sequence of evaporites with very low permeability separates the formation from the overlying units. Simulations of human intrusion scenarios do not include a borehole pathway for fluid migration between the Bell Canyon Formation (or deeper units) and the repository. Relatively little is known about the head gradient that would drive flow along this pathway, but data from five wells in the Bell Canyon Formation suggest that flow would be slight, and, in an uncased hole, downward because of brine density effects (Mercer, 1983; Beauheim, 1986; Lappin et al., 1989).

### 2.2.2.2 CAPITAN LIMESTONE

The Capitan Limestone is not present at the WIPP, but is a time-stratigraphic equivalent of the Bell Canyon Formation to the west, north, and east (Figures 2-1, 2-3). The unit is a massive limestone ranging from 76 to 230 m (250 to 750 ft) thick. Dissolution and fracturing have enhanced effective porosity, and the Capitan is a major aquifer in the region, providing the principal water supply for the city of Carlsbad. Upward flow of groundwater from the Capitan aquifer may be a factor in dissolution of overlying halite and the formation of breccia pipes. Existing breccia pipes are limited to the vicinity of the reef, as is the active subsidence in San Simon Swale (Figure 2-6) (Brinster, 1991).

### 2.2.2.3 CASTILE FORMATION

The Castile Formation is approximately 470 m (1540 ft) thick at the WIPP and contains anhydrites with intercalated limestones near the base and halite layers in the upper portions. Primary porosity and permeability in the Castile Formation are extremely low. However, approximately 18 wells in the region have encountered brine reservoirs in fractured anhydrite in the Castile Formation (Brinster, 1991). Hydrologic and geochemical data have been interpreted as indicating that these brine occurrences are hydraulically isolated (Lambert and Mercer, 1978; Lappin, 1988). Fluid may have been derived from interstitial entrapment of connate water after deposition (Popielak et al., 1983), dehydration of the original gypsum to anhydrite (Popielak et al., 1983), or intermittent movement of meteoric waters from the Capitan aquifer into the fractured anhydrites between 360,000 and 880,000 years ago (Lambert and Carter, 1984). Pressures within these brine reservoirs are greater than those at comparable depths in other relatively permeable units in the region and range from 7 to 17.4 MPa (Lappin et al., 1989).

Pressurized brine in the Castile Formation is of concern for performance assessment because occurrences have been found at WIPP-12 within the WIPP land-withdrawal area and at ERDA-6 and other wells in the vicinity. The WIPP-12 reservoir is at a depth of 918 m (3012 ft), about 250 m (820 ft) below the repository horizon, and is estimated to contain $2.7\times10^{6}$ $m^3$ ($1.7\times10^{7}$ barrels) of brine at a pressure of 12.7 MPa (Lappin et al., 1989). This pressure is greater than the nominal freshwater hydrostatic pressure at that depth (9 MPa) and is slightly greater than the nominal hydrostatic pressure for a column of equivalent brine at that depth (11.1 MPa). The brine is saturated, or nearly so, with respect to halite, and has little or no potential to dissolve the overlying salt (Lappin et al., 1989). Brine could, however, reach the repository, overlying strata, and the ground surface through an intrusion borehole.

Early geophysical surveys mapped a structurally disturbed zone in the vicinity of the WIPP that may correlate with fracturing or development of secondary porosity within the Castile Formation; this zone could possibly contain pressurized brine (Borns et al., 1983). Later electromagnetic surveys indicated that the brine present at WIPP-12 could underlie part of the waste panels (Earth Technology Corporation, 1988). WIPP-12 data are therefore used to develop a conceptual model of the brine reservoir for analyzing scenarios that include the penetration of pressurized brine. Data describing the Castile Formation brine reservoir are summarized in Volume 3, Section 4.3 of this report.

### 2.2.2.4 SALADO FORMATION

The Salado Formation is about 600 m (1970 ft) thick at the WIPP and contains halite interbedded with anhydrite, polyhalite, glauberite, and some thin mudstones (Adams, 1944; Bachman, 1981; Mercer, 1983). Unlike the underlying Castile Formation, the Salado Formation overlaps the Capitan Limestone and extends eastward beyond the reef for many kilometers into west Texas (Figure 2-3). Erosion has removed the Salado Formation from the western portion of the basin (Figure 2-1).

Where the Salado Formation is intact and unaffected by dissolution, natural groundwater flow is negligible because primary porosity and open fractures are lacking in the plastic salt (Mercer, 1983; Brinster, 1991). The formation is not dry, however. Interstitial brine seeps into the repository at rates up to approximately 0.01

ℓ/day/for each m (in length) of excavation (Bredehoeft, 1988; Nowak et al., 1988), and the Salado is assumed to be saturated (Brinster, 1991). Porosity is estimated to be approximately 0.01 (expressed as void volume per unit volume of rock). Permeability of the formation is very low but measurable, with an average value of 0.05 microdarcies ($5\times10^{-20}$ $m^2$) reported by Powers et al. (1978a,b) from well tests. This value corresponds approximately to a hydraulic conductivity $5\times10^{-13}$ m/s ($1\times10^{-7}$ ft/d) (Freeze and Cherry, 1979, Table 2.3). In situ testing of halite in the repository indicates lower permeabilities ranging from 1 to 100 nanodarcies ($10^{-22}$ to $10^{-20}$ $m^2$) (Stormont et al., 1987; Beauheim et al., 1991). Additional information about the geology of the Salado Formation at the repository is provided in Section 2.3.1, and in Volume 3, Section 2.3 of this report.

#### 2.2.2.5 RUSTLER-SALADO CONTACT ZONE

In the vicinity of Nash Draw, the contact between the Rustler and Salado Formations is an unstructured residuum of gypsum, clay, and sandstone created by dissolution of halite. The residuum becomes thinner to the east and intertongues with clayey halite of the unnamed lower member of the Rustler Formation. Mercer (1983) concluded, on the basis of brecciation at the contact, that dissolution in Nash Draw occurred after deposition of the Rustler Formation. In shafts excavated at the WIPP, the residuum shows evidence of channeling and filling, fossils, and bioturbation, indicating that some dissolution occurred before Rustler deposition (Holt and Powers, 1988).

The residuum ranges in thickness in the vicinity of the WIPP from 2.4 m (7.9 ft) in P-14 east of Nash Draw to 33 m (108 ft) in WIPP-29 within Nash Draw (Mercer, 1983). Measured hydraulic conductivity values for the residuum are highest at Nash Draw (up to $10^{-6}$ m/s [$10^{-1}$ ft/d]), and three to six orders of magnitude lower to the east (Brinster, 1991). Porosity estimates range from 0.15 to 0.33 (Robinson and Lang, 1938; Hale and Clebsch, 1958; Geohydrology Associates, Inc., 1979; Mercer, 1983).

#### 2.2.2.6 RUSTLER FORMATION

The Rustler Formation is of particular importance for WIPP PA because it contains the most transmissive units above the repository and therefore provides the most likely pathway for the subsurface transport of radionuclides to the accessible environment.

The Rustler Formation is 95 m (312 ft) thick at the WIPP (as measured in ERDA-9) and ranges in the area from a minimum of 8.5 m (28 ft) where thinned by dissolution and erosion west of the repository to a maximum of 216 m (709 ft) to the east (Brinster, 1991). Overall, the formation is composed of about 40 percent anhydrite, 30 percent halite, 20 percent siltstone and sandstone, and 10 percent anhydritic dolomite (Lambert, 1983). On the basis of outcrops in Nash Draw west of the WIPP, the formation is divided into four formally named members and a lower unnamed member (Vine, 1963). These five units (Vine, 1963; Mercer, 1983) are, in ascending order, the unnamed lower member (oldest), the Culebra Dolomite Member, the Tamarisk Member, the Magenta Dolomite Member, and the Forty-niner Member (youngest) (Figure 2-7, Table 2-1).

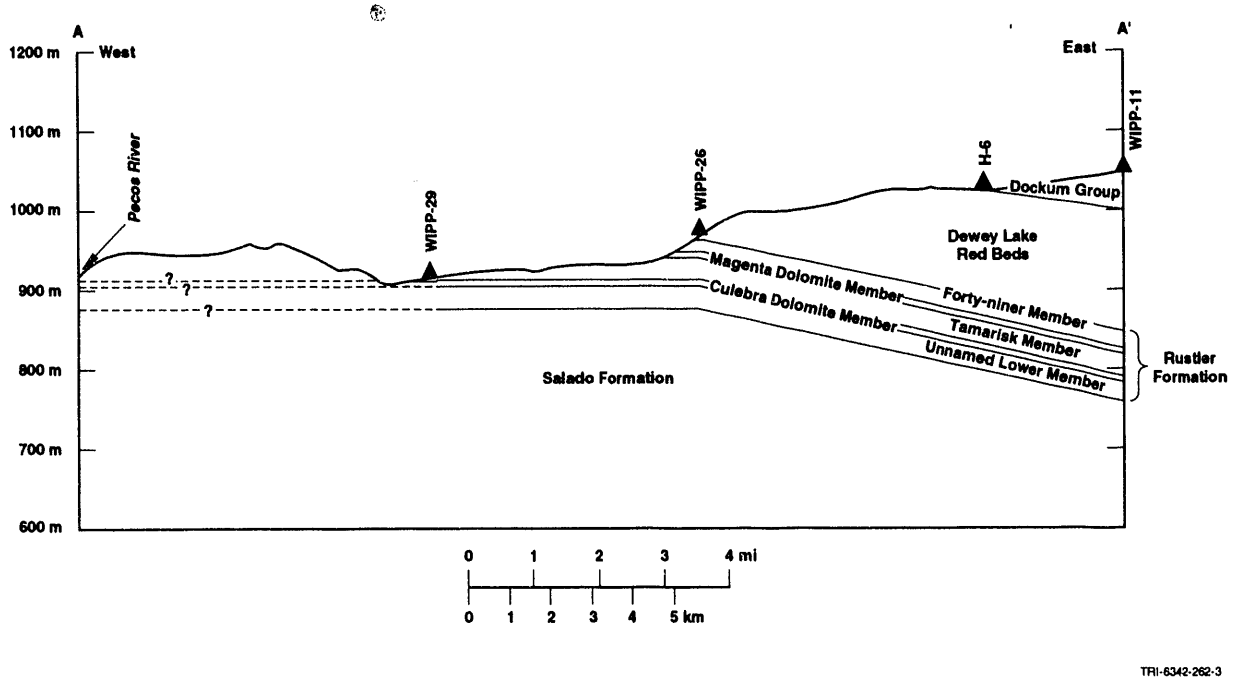


Figure 2-7. East-west cross section showing stratigraphy of the Rustler Formation and the Dewey Lake Red Beds (modified from Brinster, 1991). Note vertical exaggeration. Location of cross section is shown on Figure 2-6.

Table 2-1. Properties of the Rustler Formation Units and Rustler-Salado Contact Zone. (Sources for data provided in text.)

| Member Name | Thickness (max/min) (m) | Hydraulic Conductivity (max/min) (m/s) | Porosity (max/min) |
|---|---|---|---|
| Forty-niner | 20 | $5.0\times10^{-9}$<br>$5.0\times10^{-10}$ | — |
| Magenta | 8<br>4 | $5.0\times10^{-5}$<br>$5.0\times10^{-10}$ | — |
| Tamarisk | 84<br>8 | | — |
| Culebra | 11.6<br>4 | $1\times10^{-4}$<br>$2\times10^{-10}$ | 0.30<br>0.03 |
| Unnamed | 36 | $1\times10^{-11}$<br>$6\times10^{-15}$ | — |
| Rustler-Salado Contact Zone | 33<br>2.4 | $1\times10^{-6}$<br>$1\times10^{-12}$ | 0.33<br>0.15 |

## The Unnamed Lower Member

The unnamed lower member is about 36 m (118 ft) thick at the WIPP and thickens slightly to the east. The unit is composed mostly of fine-grained silty sandstones and siltstones interbedded with anhydrite (converted to gypsum at Nash Draw) west of the WIPP. Increasing amounts of halite are present to the east. Halite is present over the WIPP (Figure 2-8), but is absent north and south of the WIPP where the topographic expression of Nash Draw extends eastward. Distribution of halite within this and other members of the Rustler Formation is significant because, as is discussed in the following section, an apparent correlation exists between the absence of halite and increased transmissivity in the Culebra Dolomite Member.

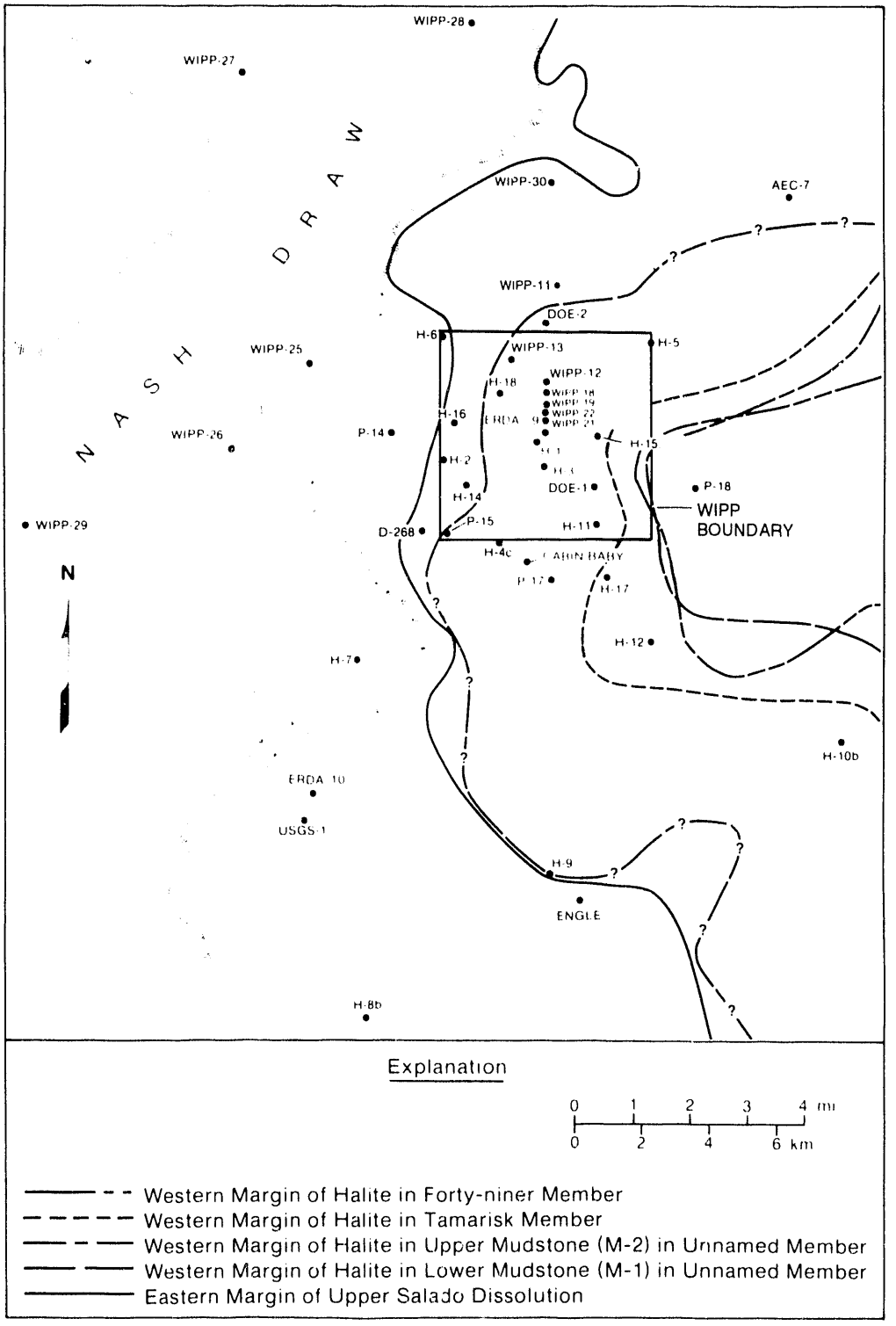


TRI-6330-94-3

Figure 2-8. Rustler Formation halite around the WIPP (Lappin et al., 1989).

The basal interval of the unnamed lower member contains siltstone and sandstone of sufficient transmissivity to allow groundwater flow. Transmissivities of $2.9\times10^{-10}$ $m^2/s$ ($2.7\times10^{-4}$ $ft^2/d$) and $2.4\times10^{-10}$ $m^2/s$ ($2.2\times10^{-4}$ $ft^2/d$) were calculated from tests at H-16 that included this interval (Beauheim, 1987a). Assuming all flow in the 34-m (112-ft) test interval came from the 20 m (64 ft) of the basal interval, these transmissivity values correspond to hydraulic conductivities of $1.5\times10^{-11}$ m/s ($4.2\times10^{-6}$ ft/d) and $1.2\times10^{-11}$ ms ($3.4\times10^{-6}$ ft/d). Hydraulic conductivity in the lower portion of the unnamed member is believed to increase to the west in and near Nash Draw, where dissolution in the underlying Rustler-Salado contact zone has caused subsidence and fracturing of the sandstone and siltstone (Beauheim and Holt, 1990).

The remainder of the unnamed lower member contains mudstones, anhydrite, and variable amounts of halite. Hydraulic conductivity of these lithologies is extremely low: tests of mudstones and claystones in the waste-handling shaft gave hydraulic conductivity values ranging from $6\times10^{-15}$ m/s ($2\times10^{-9}$ ft/d) to $1\times10^{-13}$ m/s ($3\times10^{-8}$ ft/d) (Saulnier and Avis, 1988; Brinster, 1991).

### Culebra Dolomite Member

The Culebra Dolomite Member of the Rustler Formation is microcrystalline dolomite or dolomitic limestone with solution cavities (Vine, 1963). In the vicinity of the WIPP, it ranges in thickness from 4 to 11.6 m (13 to 38.3 ft) and has a mean thickness of about 7 m (23 ft). Outcrops of the Culebra Dolomite occur in the southern part of Nash Draw and along the Pecos River.

The Culebra Dolomite has been identified as the most likely pathway for release of radionuclides to the accessible environment because of its relatively high hydraulic conductivity near the WIPP, and hydrologic research has concentrated on the unit for over a decade (Mercer and Orr, 1977, 1979; Mercer, 1983; Mercer et al., 1987; Beauheim, 1987a,b; LaVenue et al., 1988, 1990; Davies, 1989; Cauffman et al., 1990). Hydraulic data are available from 41 well locations in the WIPP vicinity (Cauffman et al., 1990).

Hydraulic conductivity of the Culebra varies six orders of magnitude from east to west in the vicinity of the WIPP (Figure 2-9), ranging from $2\times10^{-10}$ m/s ($6\times10^{-5}$ ft/d) at P-18 east of the WIPP to $1\times10^{-4}$ m/s ($6\times10^{1}$ ft/d) at H-7 in Nash Draw (Brinster, 1991). Present understanding of the geologic controls on this variation in conductivity is based primarily on studies of core samples from 17 boreholes, exposures in the walls of three shafts excavated at the WIPP, and approximately 600 geophysical logs from boreholes throughout the vicinity (Figure 2-10) (Holt and Powers, 1988; Powers and Holt, 1990; Beauheim and Holt, 1990).

Measured matrix porosities of the Culebra Dolomite range from 0.03 to 0.30 (Lappin et al., 1989; Kelley and Saulnier, 1990). Fracture porosity values have not been measured directly, but interpreted values from tracer tests at the H-3 and H-11 hydropads are $2\times10^{-3}$ and $1\times10^{-3}$, respectively (Kelley and Pickens, 1986). Data are insufficient to map spatial variability of porosity.

Variations in hydraulic conductivity in the Culebra are believed to be controlled by the relative abundance of open fractures (Snyder, 1985; Beauheim and Holt, 1990; Brinster, 1991) rather than by primary (i.e., depositional) features of the unit. Lateral variations in depositional environments were small within the mapped region, and

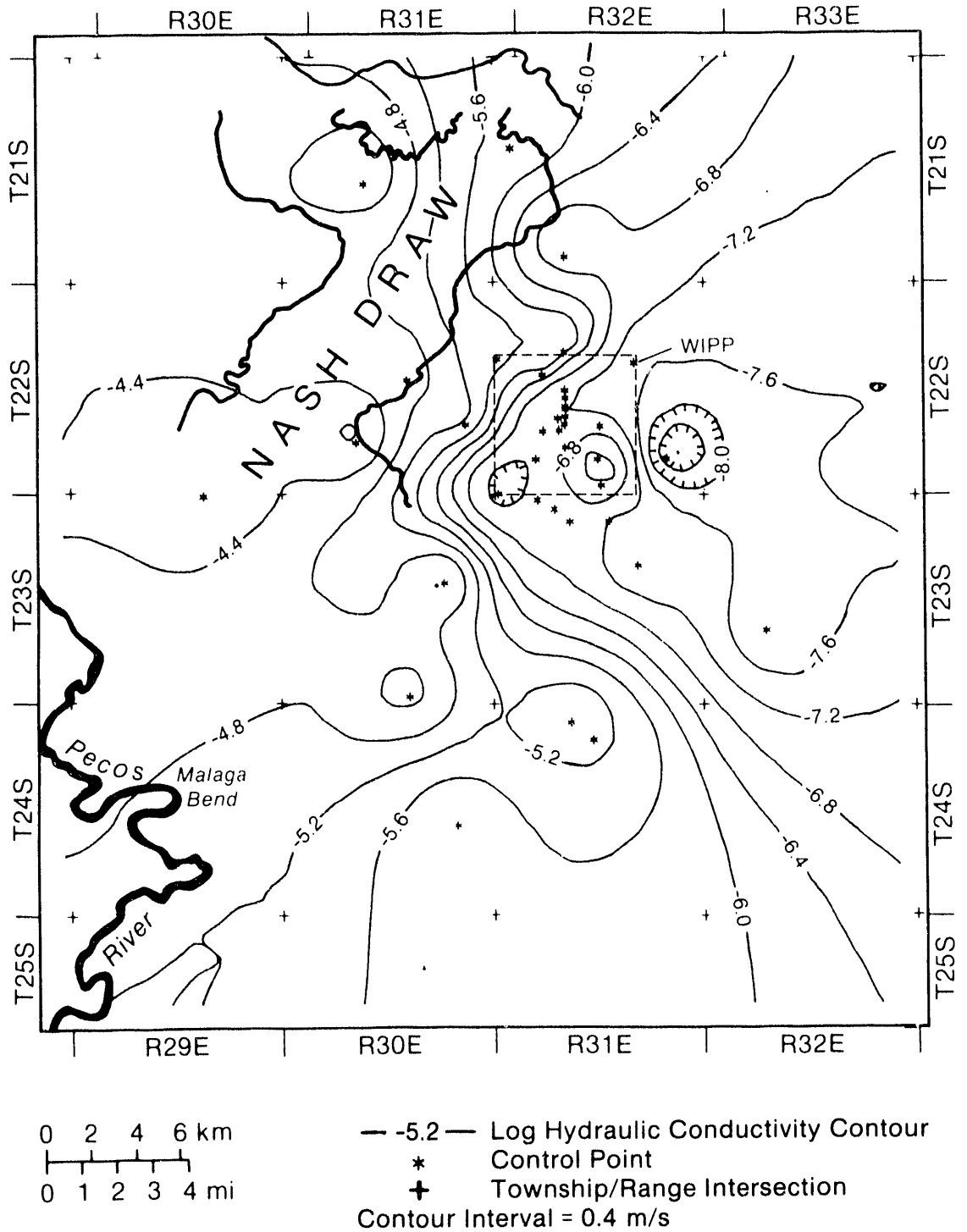


Figure 2-9. Log hydraulic conductivities (measured in m/s) of the Culebra Dolomite Member of the Rustler Formation (Brinster, 1991).

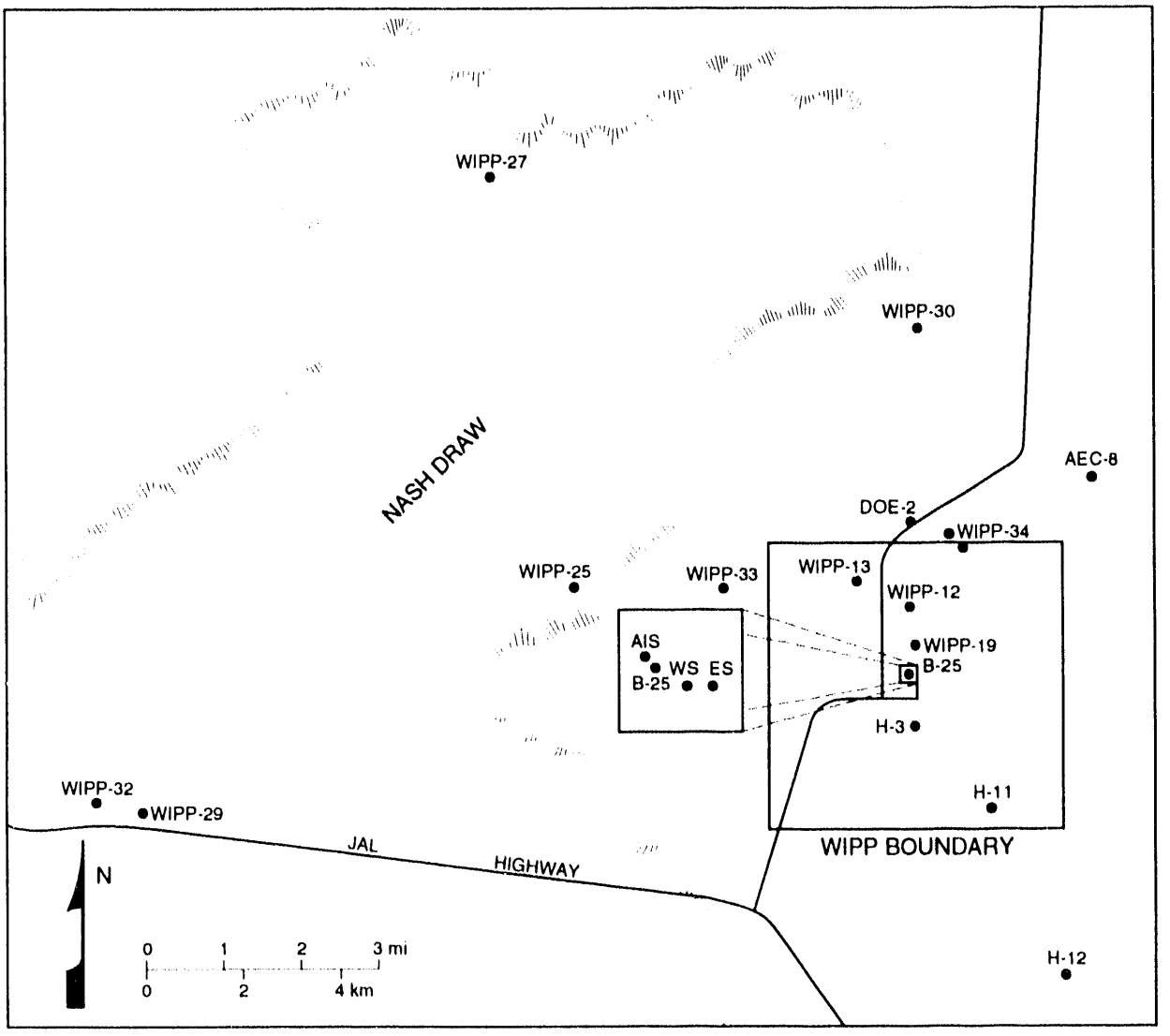


Figure 2-10. Sources of geologic information about the Culebra Dolomite, including boreholes from which core samples are available, and shafts studied during excavation. AIS, ES, and WS refer to the air intake, exhaust, and waste shafts, respectively.

primary features of the Culebra show little map-scale spatial variability (Holt and Powers, 1988). Direct measurements of the density of open fractures are not available from core samples because of incomplete recovery and fracturing during drilling, but comparisons between highly fractured outcrops of the Culebra in southern Nash Draw and the relatively unfractured exposures in the WIPP shafts suggests that density of open fractures in the Culebra decreases to the east. Qualitative correlations have been noted between hydraulic conductivity and several geologic features possibly related to open-fracture density, including (1) the distribution of overburden above the Culebra (Figure 2-11) (Holt and Powers, 1988; Beauheim and Holt, 1990); (2) the distribution of halite in other members of the Rustler Formation (compare Figures 2-8 and 2-9) (Snyder, 1985); (3) the dissolution of halite in the upper portion of the Salado Formation (Figure 2-12) (Beauheim and Holt, 1990); and (4) the distribution of gypsum fillings in fractures in the Culebra (Figure 2-13) (Beauheim and Holt, 1990).

Regional tilting of the Delaware Basin during the Late Pliocene and early Pleistocene (see Section 2.2.1) and subsequent erosion have resulted in a westward decrease in overburden above the Culebra (Figure 2-13). The decrease in confining stress during erosional unloading may have caused fracturing in the Culebra (Beauheim and Holt, 1990), and may also have controlled the degree to which fractures opened. Locally, however, variations in conductivity do not correlate precisely with variations in overburden thickness, and other geologic phenomena must contribute (Beauheim and Holt, 1990).

Where the present distribution of halite in the Rustler Formation (Figure 2-8) results from post-depositional dissolution, subsidence over areas of dissolution may have caused fracturing in the Culebra (Snyder, 1985). Mapping of depositional environments in the Rustler Formation indicates, however, that the present limits of halite in the formation coincide, in general, with a depositional transition from evaporites to mudstones near the margins of a saline pan (Holt and Powers, 1988; Powers and Holt, 1990). Dissolution of the upper portion of the Salado Formation (Figure 2-12), as inferred from stratigraphic thinning observed in geophysical logs, may also have caused subsidence and fracturing in the Culebra (Beauheim and Holt, 1990).

Detailed examination of core samples from the Culebra shows that the percentage of fractures that are filled with post-depositional gypsum crystals increases eastward across the site (Figure 2-13) (Beauheim and Holt, 1990). Furthermore, the crystalline structure of the fracture fillings changes across the site, suggesting that the present conductivity distribution may reflect spatial variability in the processes that formed fracture fillings. East of the WIPP, fracture-filling crystals have predominantly incremental growth forms, indicating gradual growth as the fractures opened and no subsequent dissolution. Fractures with incremental fillings probably have had relatively small apertures and little groundwater flow through them throughout their history. From the WIPP west, fracture fillings, where present, are predominantly passive gypsum crystals that grew in pre-existing void spaces. By implication, any early, incremental fillings in these fractures must have been dissolved at some time in the past, and the fractures may have had relatively large groundwater flow through them before passive crystal growth. In places where early, incremental fillings have been removed by dissolution and passive crystal growth have not formed, or where they have been removed by further dissolution, conductivity is high. In places where either passive or incremental crystals fill most fractures, conductivity is low.

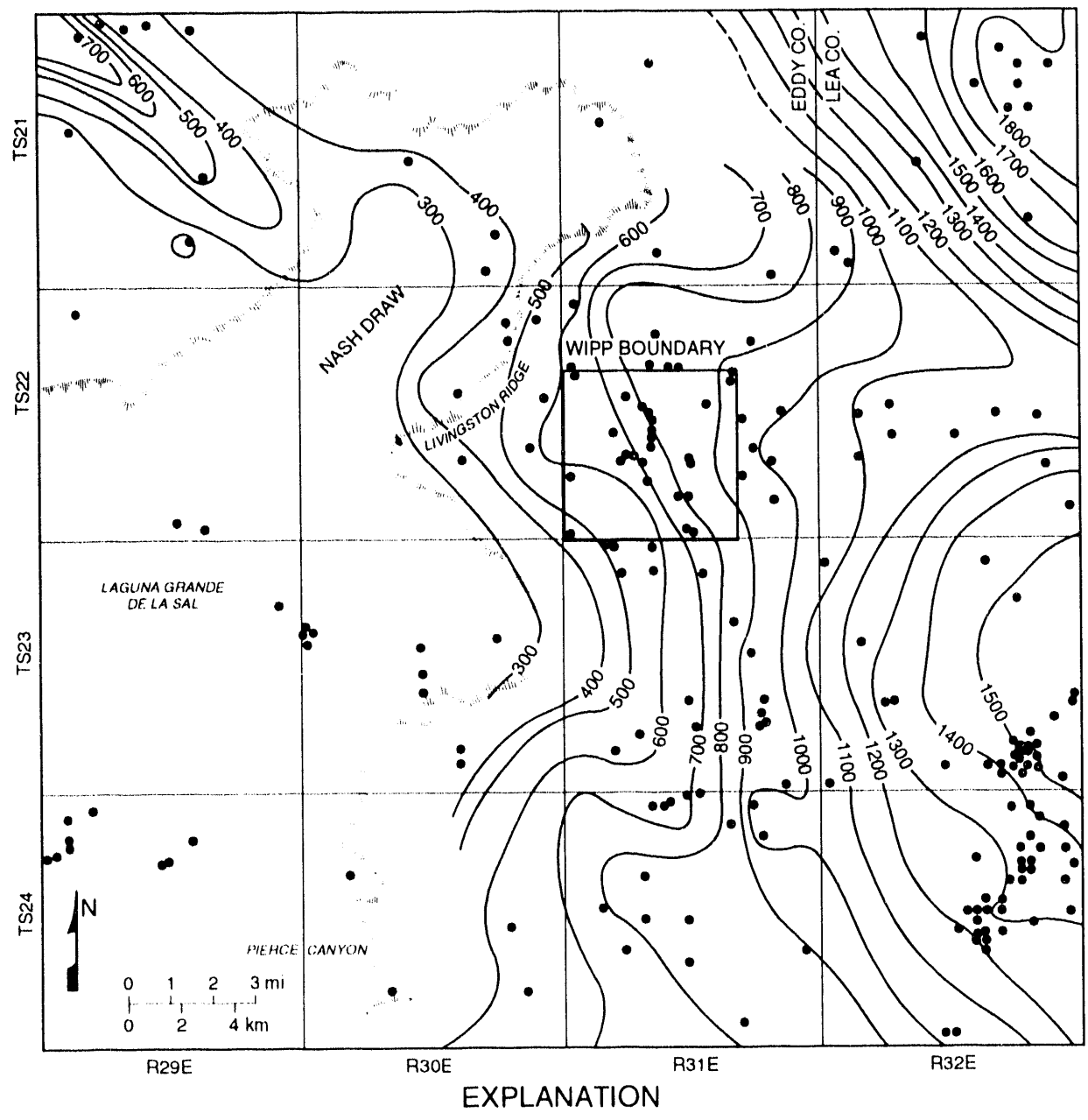


Figure 2-11. Isopach of overburden for the Culebra Dolomite Member (Beauheim and Holt, 1990).

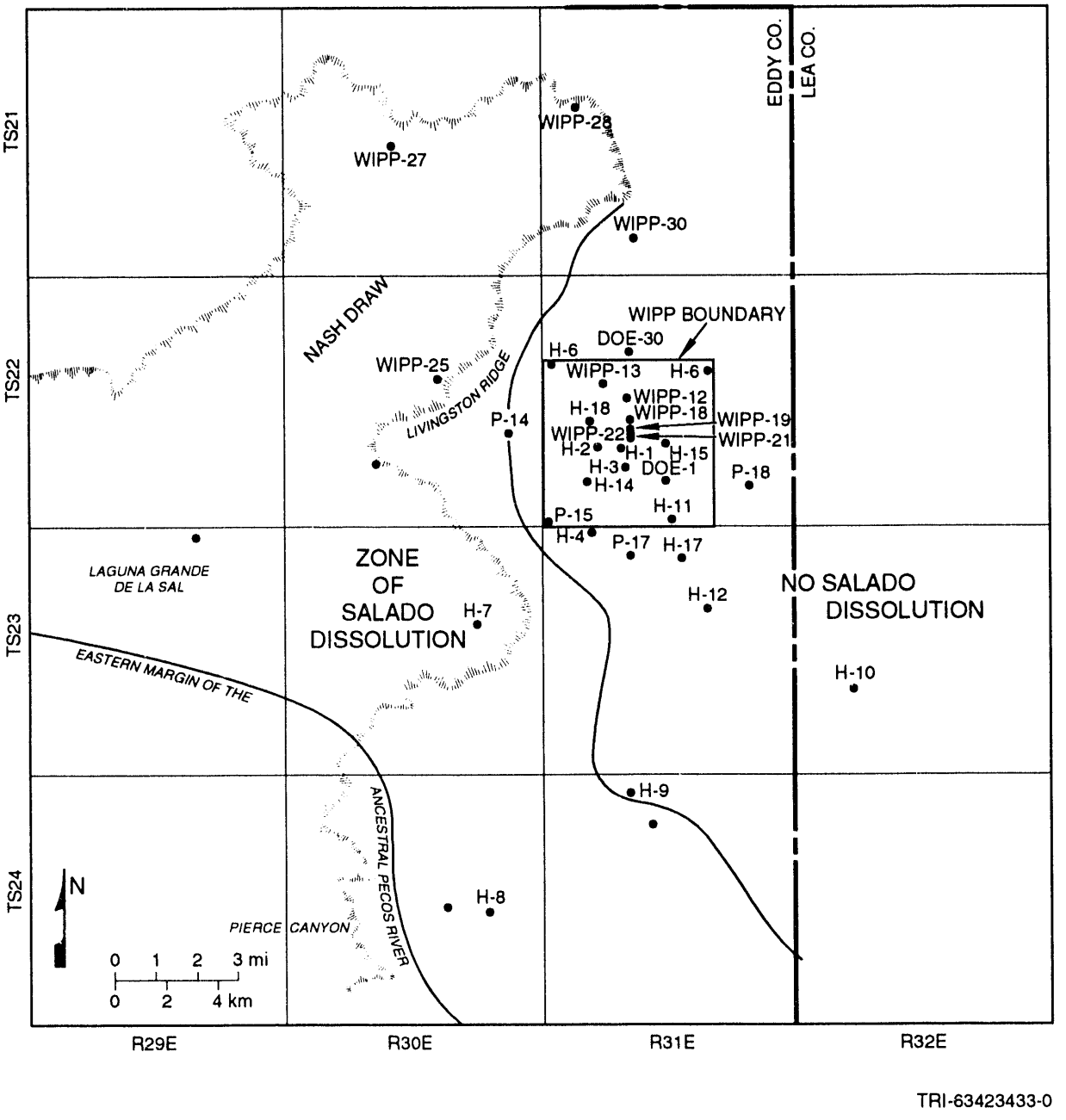


TRI-63423433-0

Figure 2-12. Interpreted extent of Salado dissolution (Beauheim and Holt, 1990).

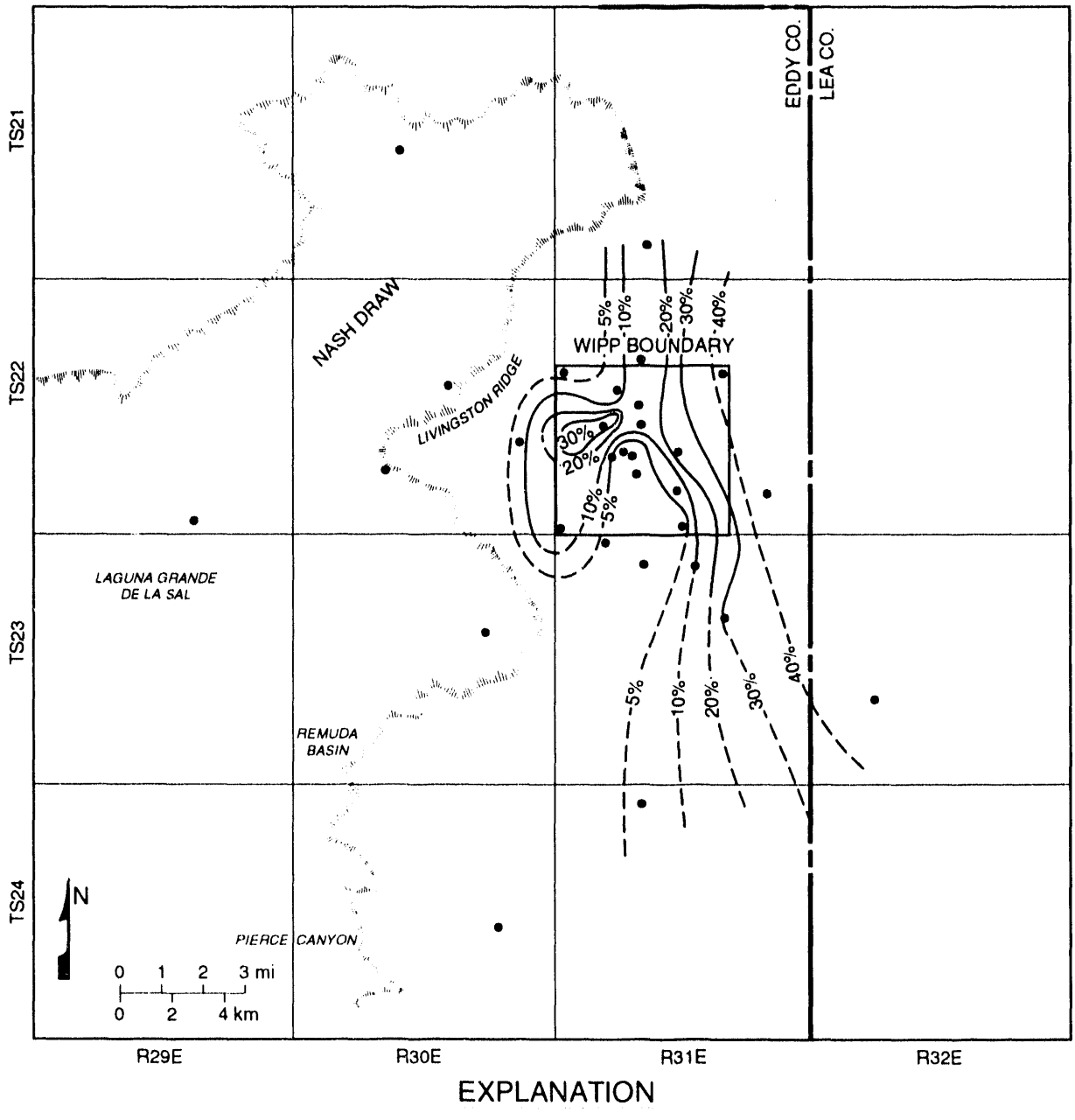


Figure 2-13. Percentage of natural fractures in the Culebra Dolomite Member filled with gypsum (Beauheim and Holt, 1990).

As observed in core samples from the Culebra, clay minerals commonly occur on the surfaces of subhorizontal fractures in dolomite (Sewards, 1991; Sewards et al., 1991a,b). Present distribution and composition of clay in the Culebra (and other members of the Rustler Formation) reflect both depositional and diagenetic processes (Sewards et al., 1992). Clays are most abundant in horizontal layers that represent original bedding planes in the evaporite sequences. These clay-rich layers are found within the Culebra throughout the WIPP vicinity. Because they are less competent than the dolomite above and below, clay-rich layers are preferentially opened during fracturing, creating clay-lined subhorizontal fractures. Clay minerals identified by x-ray diffraction analysis include corrensite (ordered mixed-layer chlorite/saponite) and illite, with minor amounts of serpentine and chlorite. Corrensite is the most abundant of the clay minerals, usually constituting about 50 percent of the clay assemblage (Sewards et al., 1991a). Original detrital clays were illite and smectite; alternation of smectite into corrensite occurred during early diagenesis as magnesium-rich pore waters migrated through the formation (Sewards et al., 1992). Isotopic analyses (Rb/Sr) indicate that clay minerals reached their present composition during the Late Permian (Brookins et al., 1990).

Because the cation exchange capacity of clay minerals in general and corrensite in particular is higher than that of dolomite or gypsum, clay fracture-linings may play an important role in the chemical retardation of radionuclides during potential transport (Siegel et al., 1990; Sewards et al., 1992). Clay fracture-linings may also affect physical retardation of radionuclides by diffusion into the pore volume of both dolomite matrix and the clay linings during transport (Section 7.6.2 of this volume; Volume 3, Section 2.6 of this report; memorandum by Novak et al. in Volume 3, Appendix A of this report).

### Tamarisk Member

Where present in southeastern New Mexico, the Tamarisk Member ranges in thickness from 8 to 84 m (26 to 276 ft) in southeastern New Mexico, and is about 36 m (118 ft) thick at the WIPP. The Tamarisk consists of mostly anhydrite or gypsum interbedded with thin layers of claystone and siltstone. Near Nash Draw, dissolution has removed evaporites from the Tamarisk Member, and the Magenta and Culebra Dolomites are separated only by a few meters of residue (Brinster, 1991).

Unsuccessful attempts were made in two wells, H-14 and H-16, to test a 2.4-m (7.9-ft) sequence of the Tamarisk Member that consists of claystone, mudstone, and siltstone overlain and underlain by anhydrite. Permeability was too low to measure in either well within the time allowed for testing, but Beauheim (1987a) estimated the transmissivity of the claystone sequence to be one or more orders of magnitude less than that of the tested interval in the unnamed lower member, which yielded transmissivity values of $2.9\times10^{-10}$ $m^2/s$ ($2.7\times10^{-4}$ $ft^2/d$) and $2.4\times10^{-10}$ $m^2/s$ ($2.2\times10^{-4}$ $ft^2/d$), corresponding to hydraulic conductivities in the basal siltstone of the unnamed lower member of $1.5\times10^{-11}$ m/s ($4.2\times10^{-6}$ ft/d) and $1.2\times10^{-11}$ m/s ($3.4\times10^{-6}$ ft/d).

### Magenta Dolomite Member

The Magenta Dolomite Member of the Rustler Formation is a fine-grained dolomite that ranges in thickness from 4 to 8 m (13 to 26 ft) and is about 6 m (19 ft) thick at the WIPP. The Magenta is saturated except near

outcrops along Nash Draw, and hydraulic data are available from 14 wells. Hydraulic conductivity ranges over five orders of magnitude from $5.0\times10^{-10}$ to $5.0\times10^{-5}$ m/s ($1\times10^{-4}$ to $1\times10^{1}$ ft/d).

A contour map of log hydraulic conductivities of the Magenta Dolomite Member based on sparse data (Figure 2-14) shows a decrease in conductivity from west to east, with slight indentations of the contours north and south of the WIPP that correspond to the topographic expression of Nash Draw (Brinster, 1991). Comparison of Figures 2-9 and 2-14 show that in most locations conductivity of the Magenta is one to two orders of magnitude less than that of the Culebra.

No porosity measurements have been made on the Magenta Dolomite Member. Beauheim (1987a) assumed a representative dolomite porosity of 0.20 for interpretations of well tests.

#### Forty-niner Member

The uppermost member of the Rustler Formation, the Forty-niner Member, is about 20 m (66 ft) thick throughout the WIPP area and consists of low-permeability anhydrite and siltstone. Tests in H-14 and H-16 yielded hydraulic conductivities of about $5\times10^{-9}$ m/s ($1\times10^{-3}$ ft/d) and $5\times10^{-10}$ m/s ($1\times10^{-4}$ ft/d) respectively (Beauheim, 1987a).

### 2.2.2.7 SUPRA-RUSTLER ROCKS

Strata above the Rustler Formation are not believed to represent a significant pathway for the migration of radionuclides from the repository to the accessible environment because of relatively low transmissivities within the saturated zone. These units are important to performance assessment, however, because vertical flux through them may play an important role in the inflow and outflow of water from the Rustler Formation. Available models of groundwater flow in the Culebra do not incorporate the effects of vertical flux.

Where present, the supra-Rustler units collectively range in thickness from 4 to 536 m (13 to 1758 ft). Regionally, the supra-Rustler units thicken to the east and form a uniform wedge of overburden across the region (Brinster, 1991). Fine-grained sandstones and siltstones of the Dewey Lake Red Beds (Pierce Canyon Red Beds of Vine, 1963) conformably overlie the Rustler Formation at the WIPP and are the uppermost Permian rocks in the region. The unit is absent in Nash Draw, is as much as 60 m (196 ft) thick where present west of the WIPP, and can be over 200 m (656 ft) thick east of the WIPP (Figures 2-4, 2-7). East of the WIPP, the Dewey Lake Red Beds are unconformably overlain by Mesozoic rocks of the Triassic Dockum Group. These rocks are absent west of the repository and reach a thickness of over 100 m (328 ft) in western Lea County. East of the WIPP, Triassic and, in some locations, Cretaceous rocks are unconformably overlain by the Pliocene Ogallala Formation. At the WIPP, Permian strata are overlain by 8 m (25 ft) of the Triassic Dockum Group, discontinuous sands and gravels of the Pleistocene Gatuña Formation, the informally named Pleistocene Mescalero caliche, and Holocene soils (Holt and Powers, 1990).

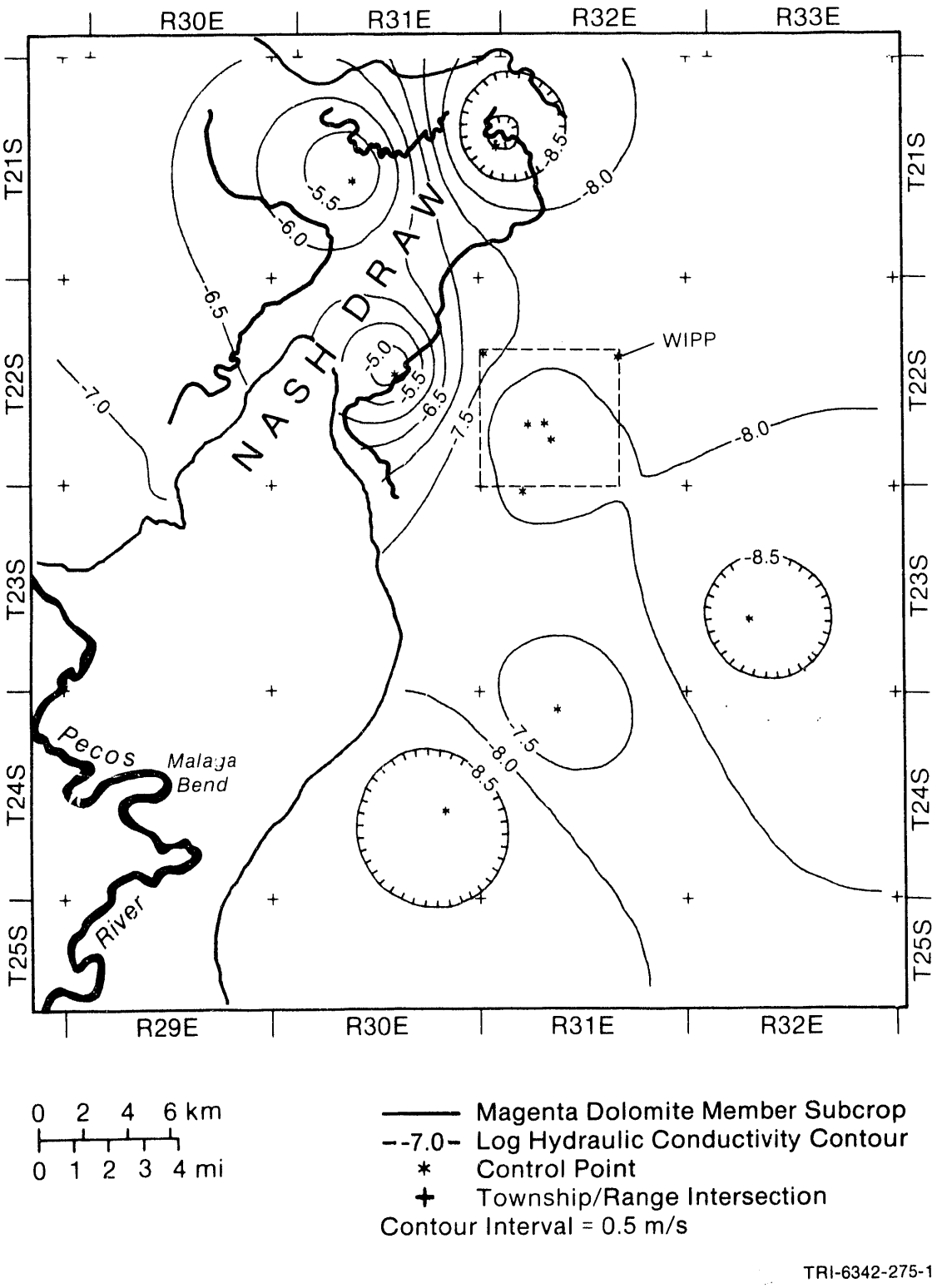


Figure 2-14. Log hydraulic conductivities (measured in m/s) of the Magenta Dolomite Member of the Rustler Formation (Brinster, 1991).

Drilling in the Dewey Lake Red Beds has not identified a continuous zone of saturation. Some localized zones of relatively high permeability were identified by loss of drilling fluids at DOE-2 and H-3d (Mercer, 1983; Beauheim, 1987a). Thin and apparently discontinuous saturated sandstones were identified in the upper Dewey Lake Red Beds at H-1, H-2, and H-3 (Mercer and Orr, 1979; Mercer, 1983). Several wells operated by the J. C. Mills Ranch (James Ranch) south of the WIPP produce sufficient quantities of water from the Dewey Lake Red Beds to supply livestock (Brinster, 1991).

Hydrologic properties of supra-Rustler rocks are relatively poorly understood because of the lack of long-term hydraulic tests and the difficulty of making those measurements. Hydraulic conductivity of the Dewey Lake Red Beds, assuming saturation, is estimated to be $10^{-8}$ m/s ($10^{-3}$ ft/d), corresponding to the hydraulic conductivity of fine-grained sandstone and siltstone (Mercer, 1983; Davies, 1989). Porosity is estimated to be about 0.20, which is representative of fine-grained sandstone (Brinster, 1991).

## 2.2.3 Hydrology

### 2.2.3.1 PRESENT CLIMATE

The present climate of southeastern New Mexico is arid to semi-arid (Swift, 1992). Annual precipitation is dominated by a late summer monsoon, when solar warming of the continent creates an atmospheric pressure gradient that draws moist air inland from the Gulf of Mexico (Cole, 1975). Winters are cool and generally dry.

Mean annual precipitation at the WIPP has been estimated to be between 28 and 34 cm/yr (10.9 and 13.5 in/yr) (Hunter, 1985). At Carlsbad, 42 km (26 mi) west of the WIPP and 100 m (330 ft) lower in elevation, 53-year (1931-1983) annual means for precipitation and temperature are 32 cm/yr (12.6 in/yr) and 17.1°C (63°F) (University of New Mexico, 1989). Freshwater pan evaporation in the region is estimated to be 280 cm/yr (110 in/yr) (U.S. DOE, 1980).

Short-term climatic variability can be considerable in the region. For example, the 105-year (1878 to 1982) precipitation record from Roswell, 135 km (84 mi) northwest of the WIPP and 60 m (200 ft) higher in elevation, shows an annual mean of 27 cm/yr (10.6 in/yr) with a maximum of 84 cm/yr (32.9 in/yr) and a minimum of 11 cm/yr (4.4 in/yr) (Hunter, 1985).

### 2.2.3.2 PALEOCLIMATES AND CLIMATIC VARIABILITY

Based on the past record, it is reasonable to assume that climate will change at the WIPP during the next 10,000 years, and the performance-assessment hydrologic model must allow for climatic variability. Presently available long-term climate models are incapable of resolution on the spatial scales required for numerical predictions of future climates at the WIPP (e.g., Hansen et al., 1988; Mitchell, 1989; Houghton et al., 1990), and simulations using these models are of limited value beyond several hundreds of years into the future. Direct modeling of climates during the next 10,000 years has not been attempted for WIPP performance assessment.

Instead, performance-assessment modeling uses past climates to set limits for future variability (Swift, 1991, 1992). The extent to which unprecedented climatic changes caused by human-induced changes in the composition of the Earth's atmosphere may invalidate this assumption is uncertain. Presently available models of climatic response to an enhanced greenhouse effect (e.g., Mitchell, 1989; Houghton et al., 1990) do not predict changes of a larger magnitude than those of the Pleistocene (although predicted rates of change are greater), suggesting the choice of a Pleistocene analog for future climatic extremes will remain appropriate.

Geologic data from the American Southwest show repeated alternations of wetter and drier climates throughout the Pleistocene, which correspond to global cycles of glaciation and deglaciation (Swift, 1992). Climates in southeastern New Mexico have been coolest and wettest during glacial maxima, when the North American ice sheet reached its southern limit roughly 1200 km (750 mi) north of the WIPP. Mean annual precipitation at these extremes was approximately twice that of the present. Mean annual temperatures may have been as much as 5°C (9°F) cooler than at present. Modeling of global circulation patterns suggests these changes resulted from the disruption and southward displacement of the winter jet stream by the ice sheet, causing an increase in the frequency and intensity of winter storms throughout the Southwest (COHMAP Members, 1988).

Data from plant and animal remains and paleo-lake levels permit quantitative reconstructions of precipitation in southeastern New Mexico during the advance and retreat of the last major ice sheet in North America. Figure 2-15 shows estimated mean annual precipitation for the WIPP for the last 30,000 years, based on an estimated present precipitation of 30 cm/yr (11.8 in/yr). The precipitation maximum coincides with the maximum advance of the ice sheet 22,000 to 18,000 years ago. Since the final retreat of the ice sheet approximately 10,000 years ago, conditions have been generally dry, with intermittent and relatively brief periods when precipitation may have approached glacial levels. Causes of these Holocene fluctuations are uncertain (Swift, 1992).

Glacial periodicities have been stable for the last 800,000 years, with major peaks occurring at intervals of 19,000, 23,000, 41,000 and 100,000 years, corresponding to variations in the Earth's orbit (Milankovitch, 1941; Hays et al., 1976; Imbrie et al., 1984; Imbrie, 1985). Barring anthropogenic changes in the Earth's climate, relatively simple modeling of the nonlinear climatic response to astronomically controlled changes in the amount of solar energy reaching the Earth suggests that the next glacial maximum will occur in approximately 60,000 years (Imbrie and Imbrie, 1980). Regardless of anthropogenic effects, short-term, non-glacial climatic fluctuations comparable to those of the last 10,000 years are probable during the next 10,000 years and must be included in performance-assessment modeling.

Climatic variability will be incorporated into the modeling system conceptually by varying groundwater flow into the Culebra Dolomite Member of the Rustler Formation as a scaled function of precipitation (Swift, 1991). Short-term variability in precipitation is approximated with a periodic function that generates peaks of twice present precipitation three times during the next 10,000 years and with a future climate that is wetter than that of the present approximately one half of the time. Long-term, glacial increase in precipitation is approximated with a periodic function that reaches a maximum of twice present precipitation in 60,000 years. For this performance assessment, climatic variability has been included in the consequence analysis by varying boundary conditions of the Culebra groundwater-flow model as a scaled function of future precipitation. Potentiometric heads along a portion of the northern boundaries of the regional model domain were varied between present elevation and approximately the ground surface, reaching maximum elevations at times of maximum precipitation.

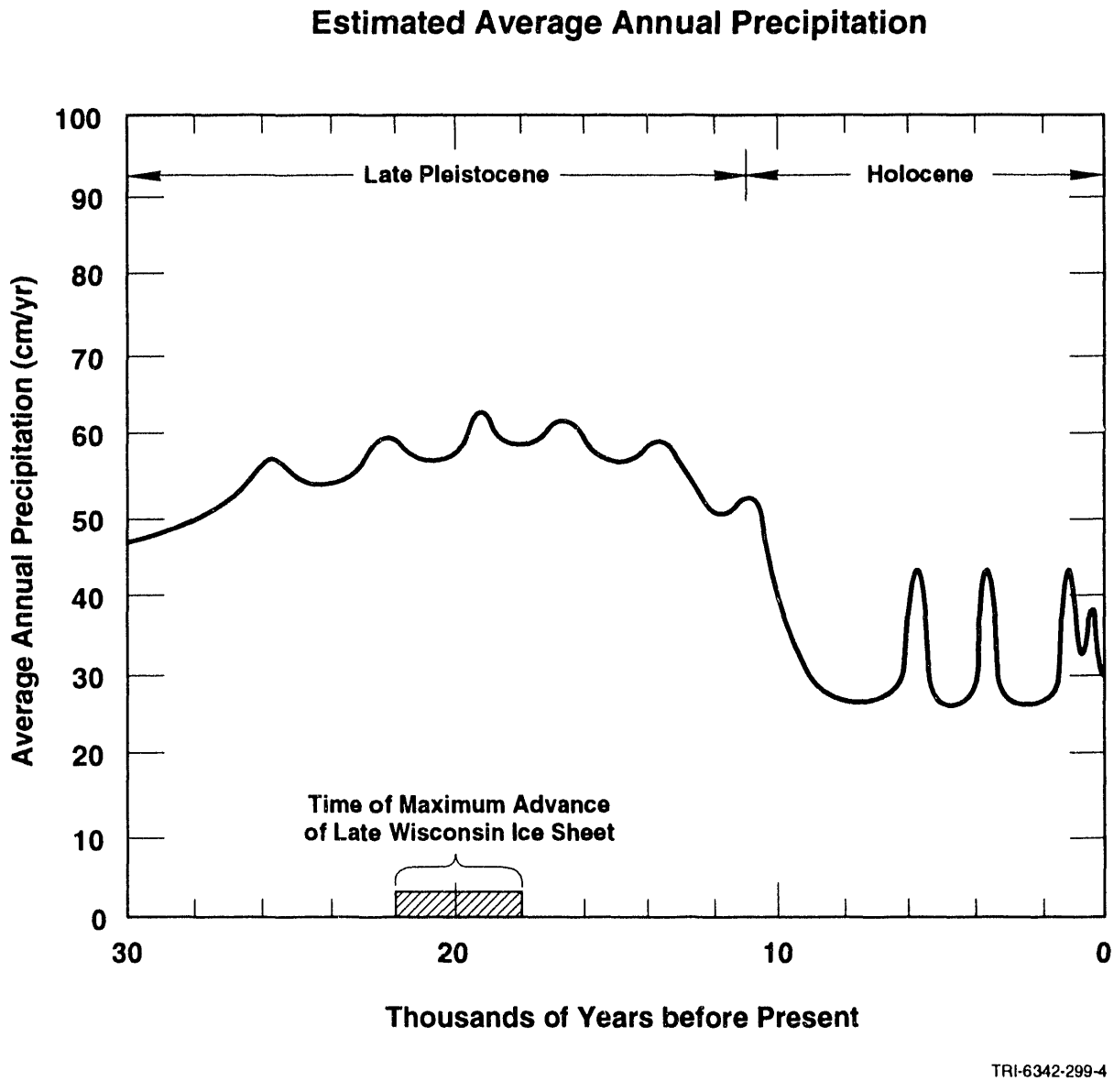


Figure 2-15. Estimated mean annual precipitation at the WIPP during the Late Pleistocene and Holocene (modified from Swift, 1992).

### 2.2.3.3 SURFACE WATER

The Pecos River, the principal surface-water feature in southeastern New Mexico, flows southeastward in Eddy County approximately parallel to the axis of the Delaware Basin (Figure 2-1) and drains into the Rio Grande in western Texas. In the vicinity of the WIPP, the drainage system includes small ephemeral creeks and draws and has a drainage area of about 50,000 $km^2$ (20,000 $mi^2$). At its closest point, the Pecos River is about 20 km (12 mi) southwest of the WIPP (Brinster, 1991).

Very little, if any, of the surface water from Nash Draw reaches the Pecos River (Robinson and Lang, 1938; Lambert, 1983). Several shallow, saline lakes in Nash Draw cover an area of about 16 $km^2$ (6 $mi^2$) southwest of the WIPP (Figure 2-6) and collect precipitation, surface drainage, and groundwater discharge from springs and seeps. The largest lake, Laguna Grande de la Sal, has existed throughout historic time. Since 1942, smaller, intermittent, saline lakes have formed in closed depressions north of Laguna Grande de la Sal as a result of effluent from potash mining and oil-well development in the area (Hunter, 1985). Effluent has also enlarged Laguna Grande de la Sal.

### 2.2.3.4 THE WATER TABLE

No maps of the water table are available for the vicinity of the WIPP. Outside of the immediate vicinity of the Pecos River, where water is pumped for irrigation from an unconfined aquifer in the alluvium, near-surface rocks are either unsaturated or of low permeability and do not produce water in wells. Tests of the lower Dewey Lake Red Beds in H-14 that were intended to provide information about the location of the water table proved inconclusive because of low transmissivities (Beauheim, 1987a). Livestock wells completed south of the WIPP in the Dewey Lake Red Beds at the J. C. Mills Ranch (James Ranch) may produce from perched aquifers (Mercer, 1983; Lappin et al., 1989), or they may produce from transmissive zones in a continuously saturated zone that is elsewhere unproductive because of low transmissivities.

Regionally, water-table conditions can be inferred for the more permeable units where they are close to the surface and saturated. The Culebra Dolomite may be under water-table conditions in and near Nash Draw and near regions of the Rustler Formation outcrop in Bear Grass Draw and Clayton Basin north of the WIPP (Figure 2-6). The Magenta Dolomite is unsaturated and presumably above the water table at WIPP-28 and H-7 near Nash Draw. Water-table conditions exist in the Rustler-Salado contact zone near where it discharges into the Pecos River at Malaga Bend (Brinster, 1991).

### 2.2.3.5 REGIONAL WATER BALANCE

Hunter (1985) examined the overall water budget of approximately 5180 $km^2$ (2000 $mi^2$) surrounding the WIPP. Water inflow to the area comes from precipitation, surface-water flow in the Pecos River, groundwater flow across the boundaries of the region, and water imported to the region for human use. Outflow from the water-budget model occurs as stream-water flow in the Pecos River, groundwater flow, and evapotranspiration. Volumes of water gained by precipitation and lost by evapotranspiration are more than one order of magnitude larger than volumes gained or lost by other means.

Uncertainties about precipitation, evapotranspiration, and water storage within the system limit the usefulness of estimates of groundwater recharge based on water-budget analyses. Regionally, Hunter (1985) concluded that approximately 96 percent of precipitation was lost directly to evapotranspiration, without entering the surface or groundwater flow systems. Within the 1000 $km^2$ (386 $mi^2$) immediately around the WIPP, where no surface runoff occurs and all precipitation not lost to evapotranspiration must recharge groundwater, a separate analysis suggested evapotranspiration may be as high as 98 to 99.5 percent (Hunter, 1985). Direct measurements of infiltration rates are not available from the WIPP vicinity.

#### 2.2.3.6 GROUNDWATER FLOW ABOVE THE SALADO FORMATION

Well tests indicate that the three most permeable units in the vicinity of the WIPP above the Salado Formation are the Culebra Dolomite and Magenta Dolomite Members of the Rustler Formation and the residuum at the Rustler-Salado contact zone. The vertical permeabilities of the strata separating these units are not known, but lithologies and the potentiometric and geochemical data summarized below suggest that for most of the region, vertical flow between the units is very slow. Although preliminary hydrologic modeling indicates that some component of vertical flow between units can be compatible with observed conditions (Haug et al., 1987; Davies, 1989), the Culebra is assumed to be perfectly confined for the 1992 performance-assessment calculations.

##### Potentiometric Surfaces

Mercer (1983) and Brinster (1991) have constructed potentiometric-surface maps for the Rustler-Salado residuum, the Culebra Dolomite, and the Magenta Dolomite; Brinster's (1991) maps are reproduced here (Figures 2-16, 2-17, and 2-18). These maps show the elevation above sea level to which fresh water would rise in a well open to each unit. Contours are based on measured heads (water elevations in wells) that have been adjusted to freshwater-equivalent heads (the level to which fresh water would rise in the same well). Maps for the Culebra and the Magenta Dolomites are based on data from 31 and 16 wells, respectively. The map for the Rustler-Salado residuum includes data from 14 wells and water elevations in the Pecos River, reflecting an assumption that water-table conditions exist in the unit near the river.

Because the data used to construct the potentiometric maps are sparse and unevenly distributed, interpretations must be made with caution. For example, the "bull's-eye" patterns visible in all three maps are controlled by single data points, and would probably disappear from the maps if sufficient data were available. Contours are most reliable where data are closely spaced, particularly in the immediate vicinity of the WIPP, and are least reliable where they have been extrapolated into areas of no data, such as the southeast portion of the mapped area. With these caveats noted, however, the potentiometric maps can be useful in drawing conclusions about flow both within and between the three units.

Flow of a constant-density liquid within an isotropic medium would be perpendicular to the potentiometric contours. Near the WIPP, localized regions have been identified where variations in brine density result in non-uniform gravitational driving forces and anomalous flow directions (Davies, 1989), and the effects of anisotropy on flow patterns are not fully understood. In general, however, flow in the Rustler-Salado contact zone is from

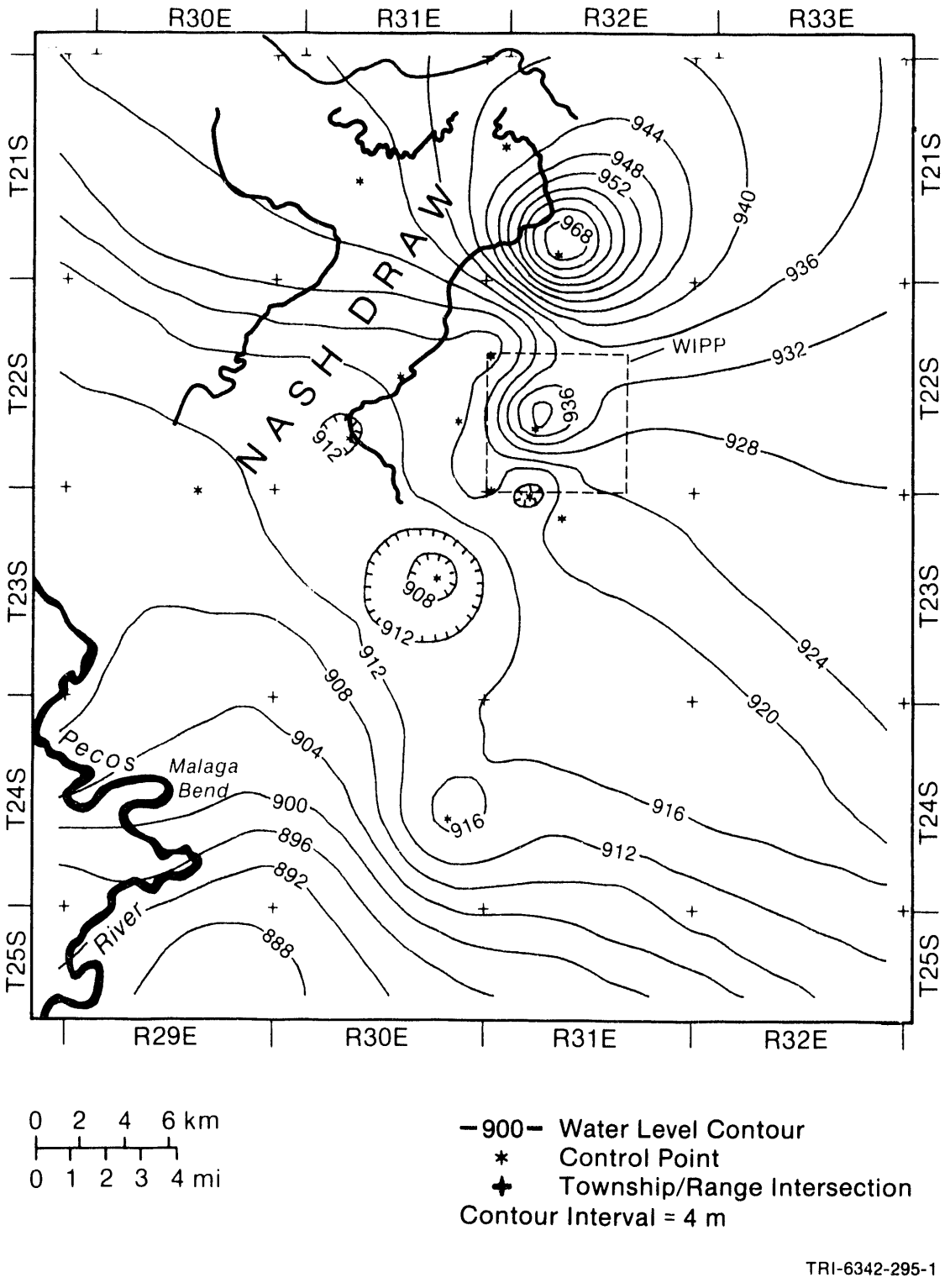


Figure 2-16. Adjusted potentiometric surface of the Rustler-Salado contact zone in the WIPP vicinity (Brinster, 1991). Contours based on head data from indicated wells and water elevations in the Pecos River.

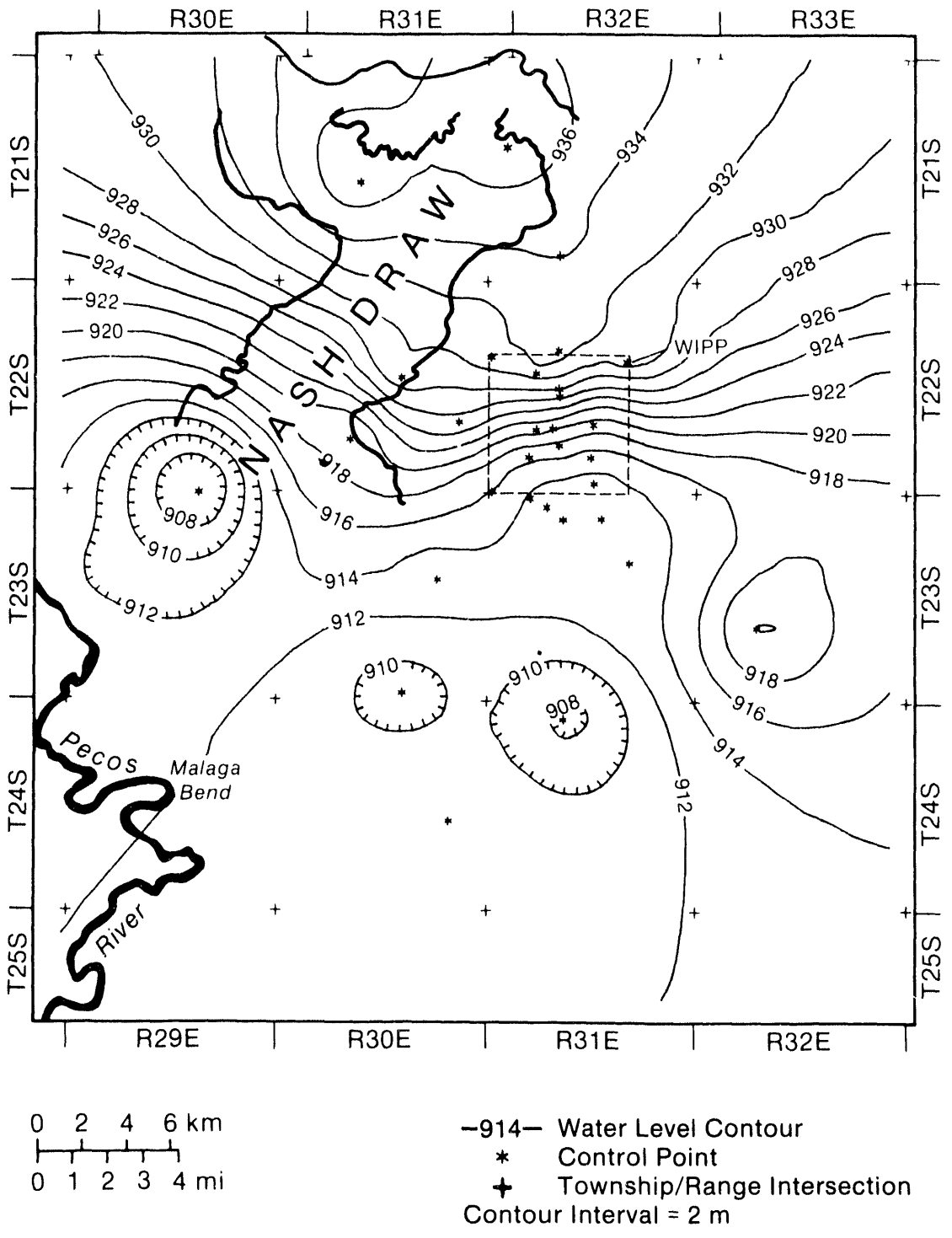


Figure 2-17. Adjusted potentiometric surface of the Culebra Dolomite Member of the Rustler Formation in the WIPP vicinity (Brinster, 1991). Contours based on head data from indicated wells.

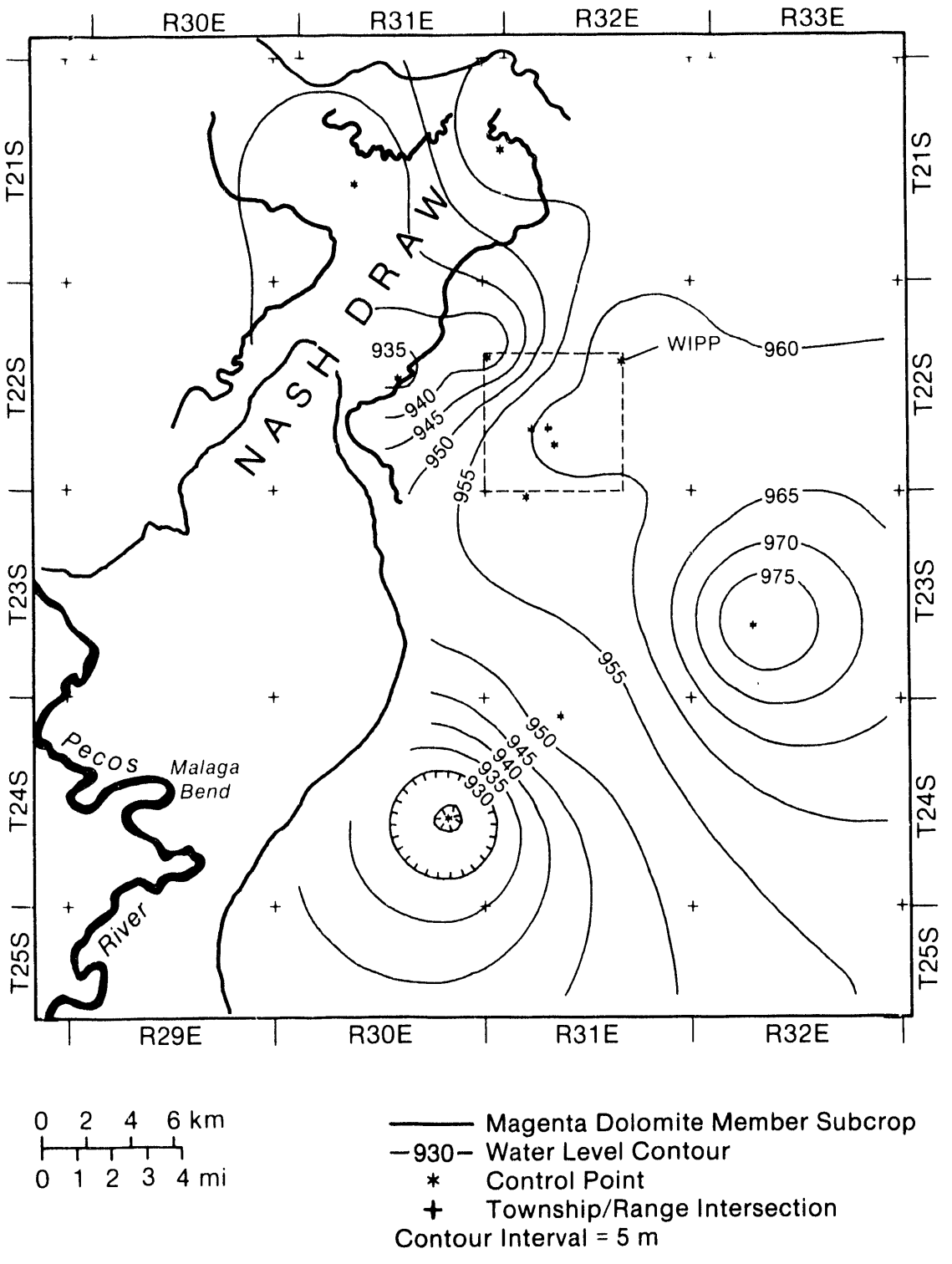


Figure 2-18. Adjusted potentiometric surface of the Magenta Dolomite Member of the Rustler Formation in the WIPP vicinity (Brinster, 1991). Contours based on head data from indicated wells.

northeast to southwest. Flow in the Culebra is from north to south, and flow in the Magenta is from east to west in that portion of the study area where data are sufficient to permit interpretation (i.e., near the WIPP). Differences in flow directions may reflect long-term transient conditions (see "Recharge and Discharge" in Section 2.2.3.6) and indicate low permeability of the strata separating the three units; that is, if the three functioned as a single aquifer, potentiometric maps would be similar.

Flow between units also is a function of hydraulic gradient and can be interpreted qualitatively from the potentiometric maps. Like lateral flow within units, vertical flow between units is from higher potentiometric levels to lower levels. Differences between the elevations of the potentiometric surfaces reflect low permeabilities of the intervening strata and slow rates of vertical leakage relative to rates of flow within the aquifers. Brinster (1991), and Beauheim (1987a) present analyses of vertical hydraulic gradients on a well-by-well basis. These analyses suggest that, if flow occurs, the direction of flow between the Magenta and the Culebra is downward throughout the WIPP area. Directly above the repository, flow may be upward from the Rustler-Salado residuum to the Culebra Dolomite. Elsewhere in the region, both upward and downward flow directions exist between the two units.

### Groundwater Geochemistry

Major solute geochemical data are available for groundwater from the Rustler-Salado contact zone from 20 wells, from the Culebra Dolomite from 32 wells, and from the Magenta Dolomite from 12 wells (Siegel et al., 1991). Groundwater quality in all three units is poor, with total dissolved solids (TDS) exceeding 10,000 mg/L (the concentration specified for regulation by the Individual Protection Requirements of 40 CFR 191B) in most locations.

Waters from the Rustler-Salado contact zone have the highest TDS concentrations of any groundwaters in the WIPP area. The lowest concentration reported from the unit is 70,000 mg/L from H-7c southwest of the WIPP, and the highest is 410,000 mg/L from H-5 at the northeast corner of the land-withdrawal area (Siegel et al., 1991).

Waters from the Magenta Dolomite are the least saline of those in the confined units. Within the land-withdrawal area, TDS concentrations range from approximately 4000 to 25,000 mg/L. Higher values are reported from H-10 southeast of the WIPP, where the sample is of uncertain quality, and from WIPP 27 in Nash Draw, where groundwater chemistry has been altered by dumping of effluent from potash mines (Siegel et al., 1991).

Groundwater chemistry is variable in the Culebra Dolomite. A maximum TDS concentration of 324,100 mg/L is reported from WIPP-29 west of the repository in Nash Draw, and a minimum value of 2830 mg/L is reported from H-8, 14 km (9 mi) southwest of the repository. Three other wells (H-7, H-9, and the Engle well), all south of the WIPP, also contain water with less than 10,000 mg/L TDS (Siegel et al., 1991).

Relative concentrations of major ions vary spatially within the Culebra Dolomite. Siegel et al. (1991) recognized four zones containing distinct hydrochemical facies (Figure 2-19) and related water chemistry to the distribution of halite in the Rustler Formation. Zone A contains a saline (about 2 to 3 molal) sodium chloride brine with a magnesium/calcium molar ratio greater than 1.2. Zone A waters occur eastward from the repository,

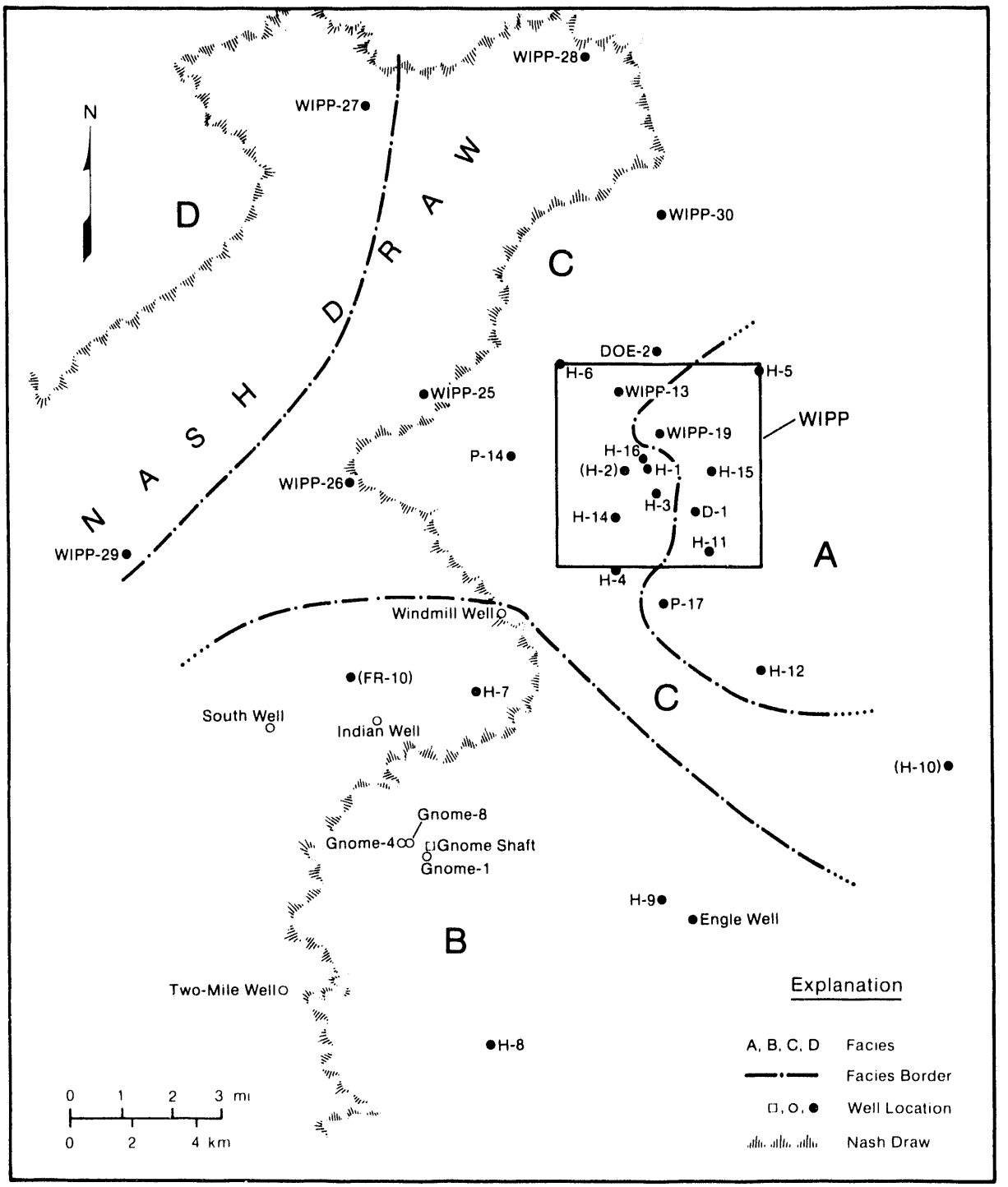


TRI-6331-78-0

Figure 2-19. Hydrochemical facies in the Culebra Dolomite Member of the Rustler Formation (Siegel et al., 1991).

in a region that corresponds roughly with the area of lowest transmissivity in the Culebra Dolomite. Halite is present in the unnamed lower member of the Rustler Formation throughout Zone A, and in the eastern portion of the region halite occurs in the upper members as well. Zone B is an area of dilute, calcium sulfate-rich water (ionic strength less than 0.1 molal) south of the repository. This region generally has high transmissivity in the Culebra Dolomite, and halite is absent from all members of the Rustler Formation. Zone C, extending from the repository west to Nash Draw, contains waters of variable composition with low to moderate ionic strength (0.3 to 1.6 molal), with magnesium/calcium molar ratios less than 1.2. Transmissivity is variable in this region, and halite is present in the Rustler Formation only to the east, in the unnamed lower member. Salinities are highest near the eastern edge of the zone. Zone D waters, found only in two wells in Nash Draw, are anomalously saline (3 to 6 molal) and have high potassium/sodium ratios that reflect contamination by effluent from potash mines.

Distribution of the hydrochemical facies may not be consistent with the inferred north-to-south flow of groundwater in the Culebra Dolomite. Specifically, less saline waters of Zone B are down-gradient from more saline waters in Zones A and C. Chapman (1988) suggested that direct recharge of fresh water from the surface could account for the characteristics of Zone B. As discussed in more detail below ("Recharge and Discharge" section), the inconsistency between chemical and potentiometric data could also result from a change in location and amount of recharge since the wetter climate of the last glacial maximum (Lambert, 1991). Present flow in the Culebra could be transient, reflecting gradual drainage of a groundwater reservoir filled during the Pleistocene (Lambert and Carter, 1987; Davies; 1989; Lambert, 1991). Regional hydrochemical facies may not have equilibrated with the modern flow regime and instead may reflect geographic distribution of halite during a past flow regime (Siegel and Lambert, 1991).

## Recharge and Discharge

The only documented points of naturally occurring groundwater discharge in the vicinity of the WIPP are the saline lakes in Nash Draw and the Pecos River, primarily near Malaga Bend (Hunter, 1985; Brinster, 1991). Discharge into the lakes from Surprise Spring was measured at a rate of less than 0.01 $m^3/s$ (0.35 $ft^3/s$) in 1942 (Hunter, 1985). Estimated total groundwater discharge into the lakes is 0.67 $m^3/s$ (24 $ft^3/s$) (Hunter, 1985). Based on chemical and potentiometric data, Mercer (1983) concluded that discharge from the spring was from fractured and more transmissive portions of the Tamarisk Member of the Rustler Formation, and that the lakes were hydraulically isolated from the Culebra Dolomite and lower units. Lambert and Harvey's (1987) analysis of stable isotopes in water from Surprise Spring supports the conclusion that Surprise Spring and Laguna Grande de la Sal are not discharge points for the Culebra Dolomite.

Groundwater discharge into the Pecos River is larger than discharge into the saline lakes. Based on 1980 stream-flow gage data, Hunter (1985) estimated that groundwater discharge into the Pecos River between Avalon Dam north of Carlsbad and a point south of Malaga Bend was no more than approximately 0.92 $m^3/s$ (33 $ft^3/s$). Most of this gain in stream flow occurs near Malaga Bend and is the result of groundwater discharge from the residuum at the Rustler-Salado contact zone (Hale et al., 1954; Kunkler, 1980; Hunter, 1985; Brinster, 1991).

The only documented point of groundwater recharge is also near Malaga Bend, where an almost immediate water-level rise has been reported in a Rustler-Salado residuum well following a heavy rainstorm (Hale et al.,

1954). This location is hydraulically down-gradient from the repository, and recharge here has little relevance to flow near the WIPP. Examination of the potentiometric-surface map for the Rustler-Salado contact zone (Figure 2-16) indicates that some inflow may occur north of the WIPP, where freshwater-equivalent heads are highest. Additional inflow to the contact zone may occur as leakage from overlying units, particularly where the units are close to the surface and under water-table conditions. Brinster (1991) proposed that inflow to the contact zone (and other units in the Rustler Formation) could also come from below, upward through breccia pipes from the Capitan aquifer north and east of the repository.

No direct evidence exists for the location of either recharge to or discharge from the Culebra Dolomite. The potentiometric-surface map (Figure 2-17) implies inflow from the north and outflow to the south. Mercer (1983) suggested that recharge from the surface probably occurred 15 to 30 km (9 to 19 mi) northwest of the WIPP in and north of Clayton Basin (Figure 2-6), where the Rustler Formation crops out. An undetermined amount of inflow may also occur as leakage from overlying units throughout the region.

The potentiometric-surface map (Figure 2-17) indicates that flow in the Culebra Dolomite is toward the south. Some of this southerly flow may enter the Rustler-Salado contact zone under water-table conditions near Malaga Bend and ultimately discharge into the Pecos River. Additional flow may discharge directly into the Pecos River or into alluvium in the Balmorhea-Loving Trough to the south (Figure 2-6) (Brinster, 1991).

Recharge to the Magenta Dolomite may also occur north of the WIPP in Bear Grass Draw and Clayton Basin (Mercer, 1983). The potentiometric-surface map indicates that discharge is toward the west in the vicinity of the WIPP, probably into the Tamarisk Member and the Culebra Dolomite near Nash Draw. Some discharge from the Magenta Dolomite may ultimately reach the saline lakes in Nash Draw. Additional discharge probably reaches the Pecos River at Malaga Bend or alluvium in the Balmorhea-Loving Trough (Brinster, 1991).

Isotopic data from groundwater samples suggest that groundwater travel time from the surface to the Dewey Lake Red Beds and the Rustler Formation is long and rates of flow are extremely slow. Low tritium levels in all WIPP-area samples indicate minimal contributions from the atmosphere since 1950 (Lambert and Harvey, 1987). Four modeled radiocarbon ages from Rustler Formation and Dewey Lake Red Beds groundwater are between 12,000 and 16,000 years (Lambert, 1987). Observed uranium isotope activity ratios require a conservative minimum residence time in the Culebra Dolomite of several thousands of years and more probably reflect minimum ages of 10,000 to 30,000 years (Lambert and Carter, 1987). Stable-isotope data are more ambiguous: Lambert and Harvey (1987) concluded that compositions are distinct from modern surface values and that the contribution of modern recharge to the system is slight, whereas Chapman (1986, 1988) concluded that available stable-isotope data do not permit interpretations of groundwater age. Additional stable-isotope research is in progress and may resolve some uncertainty about groundwater age.

Potentiometric data from four wells support the conclusion that little infiltration from the surface reaches the transmissive units of the Rustler Formation. Hydraulic head data are available for a claystone in the Forty-niner Member from DOE-2, H-3, H-4, H-5, and H-6. Comparison of these heads to Magenta heads in surrounding wells shows that flow between the units at all four wells may be upward (Beauheim, 1987a). This observation offers no insight into the possibility of infiltration reaching the Forty-niner Member, but it rules out the possibility of infiltration reaching the Magenta Dolomite or any deeper units at these locations.

Location and amount of groundwater recharge and discharge in the area may have been substantially different during wetter climates of the Pleistocene. Gypsiferous spring deposits on the east side of Nash Draw are of late Pleistocene age and reflect discharge from an active water table in the Rustler Formation (Bachman, 1981, 1987; Davies, 1989; Brinster, 1991). Coarse sands and gravels in the Pleistocene Gatuña Formation indicate deposition in high-energy, through-going drainage systems unlike those presently found in the Nash Draw area (Bachman, 1987). Citing isotopic evidence for a Pleistocene age for Rustler Formation groundwater, Lambert and Carter (1987) and Lambert (1991) have speculated that during the late Pleistocene, Nash Draw may have been a principal recharge area, and flow in the vicinity of the WIPP may have been eastward. In this interpretation, there is essentially no recharge at the present, and the modern groundwater-flow fields reflect the gradual draining of the strata. Preliminary modeling of long-term transient flow in a two-dimensional, east-west cross section indicates that, although the concept remains unproven, it is not incompatible with observed hydraulic properties (Davies, 1989). As the performance-assessment groundwater-flow model is further developed and refined, the potential significance of uncertainty in the location and amount of future recharge will be re-evaluated.

### 2.2.4 Radionuclide Transport in the Culebra Dolomite

Hydraulic tests using nonreactive tracers have been conducted in the Culebra Dolomite Member of the Rustler Formation near the WIPP at the H-2, H-3, H-4, H-6, and H-11 hydropad well locations (Kelley and Pickens, 1986; Saulnier, 1987; Beauheim, 1987b,c; Jones et al., 1992) (see Figures 2-6 and 2-8 for well locations). At the H-2 and H-4 hydropads, transmissivity in the Culebra is low, and tracer test results are best explained by characterizing the Culebra as a single-porosity, matrix-only medium in which interconnected open fractures are not present (see Section 2.2.2.6 for a discussion of fractures in the Culebra). At the H-3, H-6, and H-11 hydropads, a dual-porosity, fracture-plus-matrix model for transport provides the best agreement with the tracer test data. Neither a single-porosity, fracture-only nor a single-porosity, matrix-only model provides a suitable interpretation of the tracer test data at these locations (Jones et al., 1992). The H-3 and H-11 hydropad locations lie south and southeast of the waste panels, within the predicted flow paths from the panels (LaVenue and RamaRao, 1992), and the WIPP PA Department therefore believes that a dual-porosity transport model provides the most realistic estimate of subsurface releases at the accessible environment boundary. Alternative conceptual models for both single-porosity, fracture-only transport (believed to be an unrealistic but known endpoint of a continuum of models on which a realistic endpoint is uncertain) and dual-porosity, matrix-plus-fracture transport (believed to be realistic) were used in the 1992 PA. Results are compared in Volume 1, Chapter 5 of this report.

Unlike the nonreactive materials used in tracer tests, radionuclides may be retarded during transport by chemical interactions with the rock. Distribution coefficients ($K_d$s, mL/g), defined for a given element as the concentration sorbed per gram of rock divided by the concentration per a milliliter of solution, are used to describe the partitioning of radionuclides between groundwater and rock. As described in Section 7.6, $K_d$s are then used to derive retardation factors, defined as mean fluid velocity divided by mean radionuclide velocity, which take into account pore space geometry and the thickness of clay linings that line pores and fractures as well as $K_d$ values. Distribution coefficients may be determined experimentally for individual radionuclides in specific water/rock systems (e.g., Lappin et al., 1989), but because values are strongly dependent on water chemistry and rock mineralogy and the nature of the flow system, experimental data cannot be extrapolated directly to a complex natural system. For the 1992 (and 1991) preliminary performance assessments, cumulative distribution functions

(cdfs) for $K_d$s were based on judgment elicited from an expert panel as described in the following section. In keeping with the agreement between the DOE and the State of New Mexico (U.S. DOE and the State of New Mexico, 1981, as modified), $K_d$s used in final compliance evaluations will be based on experimentally justified data.

Sensitivity analyses performed as part of the 1990 PA indicated that, conditional on the models and distributions used in the 1990 calculations, variability in distribution coefficients was one of the most important contributors to overall variability in cumulative releases through groundwater transport (Helton et al., 1991), and that overall performance was sensitive to the choice of conceptual model (single porosity versus dual porosity) for transport (Bertram-Howery et al., 1990). Sensitivity analyses performed as part of the 1991 PA confirmed the importance of both chemical retardation and physical retardation (Helton et al., 1992). The potential impact of uncertainty in the conceptual model for transport is examined again in the 1992 PA.

#### 2.2.4.1 EXPERT JUDGMENT ELICITATION FOR $K_d$s

Unlike other expert panels organized for WIPP performance assessment, which consisted of experts with no formal affiliation with SNL (e.g., the future intrusion and markers panels discussed in Chapter 5 of this volume and the source term panel discussed later in this chapter), the Radionuclide Retardation Expert Panel consisted of SNL staff members who are currently working or have worked on retardation in the Culebra. In other regards, procedures for the presentation of the issues and the elicitation of results were as suggested by Hora and Iman (1989) and Bonano et al. (1990).

The Radionuclide Retardation Expert Panel was requested to provide probability distributions for distribution (sorption) coefficients for eight elements (americium, curium, uranium, neptunium, plutonium, radium, thorium, and lead) that represent a spatial average over the total area of concern (from a hypothetical intrusion borehole to the boundary of the accessible environment). This was to be done for two separate cases: (1) the coefficients that result from the clay that lines the fractures in the Culebra Dolomite, and (2) the coefficients that result from the matrix pore space of the Culebra Dolomite. During the meetings, the panelists decided to further break down the problem by examining the coefficients that would result from the particular rock species and two different transport fluids: (1) transport fluid that is predominantly relatively low-salinity Culebra brine, or (2) transport fluid that is predominantly high-salinity Salado brine. Probability distributions were thus provided for four situations for each radionuclide.

Two short meetings were held in April 1991 to discuss the physical situation and the issue statement. The period between the second and third meetings (approximately one month) was available for the panelists to examine the existing data base and discuss the results with each other. The third meeting, held at the end of May 1991, involved the expert judgment elicitation training, a discussion among the panelists as to the cases and assumptions to be used during the elicitation, and the actual elicitation sessions. At the request of one of the panelists, judgments were elicited separately from the experts. Each panelist provided distributions where they were able. Incompleteness resulted in some cases from a lack of knowledge about a particular radionuclide. Specific distributions provided by each panelist are presented in Volume 3 of the 1991 edition of this report

(Section 2.6.10 of WIPP PA Division [1991c]). The composite distributions used in the 1992 performance-assessment calculations are provided in Volume 3 of this report (Section 2.6.4).

The panelists judgments were based on a body of data generated largely by experiments with rock samples taken from boreholes in the vicinity of the WIPP (Trauth et al., 1992):

- plutonium $K_d$s (Dosch and Lynch, 1978; Lynch and Dosch, 1980; Dosch, 1980; Nowak, 1980; Serne et al., 1977; Tien et al., 1983)
- americium $K_d$s (Dosch and Lynch, 1978; Lynch and Dosch, 1980; Nowak, 1980; Serne et al., 1977; Tien et al., 1983)
- curium $K_d$s (Dosch and Lynch, 1978; Serne et al., 1977; Tien et al., 1983)
- neptunium $K_d$s (Dosch and Lynch, 1978; Serne et al., 1977; Tien et al., 1983)
- uranium $K_d$s (Dosch, 1981; Dosch, 1980; Serne et al., 1977; Tien et al., 1983)
- strontium $K_d$s (as analog for radium) (Dosch and Lynch, 1978; Lynch and Dosch, 1980; Dosch, 1980; Serne et al., 1977)
- radium and lead $K_d$s (Tien et al., 1983)
- thorium $K_d$s (Tien et al., 1983).

The $K_d$ values reported in these references were calculated by indirect means: Measurements were not taken of the activity sorbed to the rock. Rather, measurements were taken as to the activity lost from the solution contacting the rock.

Tien et al. (1983) differed in their experimental approach from the other experimenters cited above. Tien et al. (1983) compiled experimental distribution coefficients from open literature that might be applicable to investigations of a potential repository site in bedded salt in the Palo Duro Basin of Texas.

### 2.2.4.2 PLANNED AND ONGOING EXPERIMENTAL WORK RELATED TO RADIONUCLIDE TRANSPORT IN THE CULEBRA

The WIPP Test Phase Plan (U.S. DOE, 1990a, currently in revision) contains experimental programs that will provide additional information on both chemical and physical retardation.

Chemical retardation will be addressed through laboratory experiments that will measure adsorption of radionuclides as a function of water composition to characterize adsorption in the wide range of groundwater compositions expected in the Culebra. Batch sorption experiments, in which crushed Culebra rock will be placed

in a brine solution containing the radionuclides of interest, will provide $K_d$ values for many different conditions, but will provide little information about retardation in natural fractures. $K_d$s based on these experiments will provide an upper bound on the amount of sorption that can be expected. A set of column-flow experiments is therefore in progress that will measure radionuclide sorption in columns of intact Culebra rock (core samples from the Air Intake Shaft at the WIPP), thus providing a more direct determination of natural (both chemical and physical) retardation in the Culebra (see U.S. DOE, 1992, and references cited therein for additional information about these experiments).

Retardation could also be addressed through tracer tests at a proposed new seven-well hydropad, to be called H-19 (Beauheim and Davies, 1992). The test may be conducted at the site of an existing well (e.g., H-3), or a new location may be selected. In either case H-19 will be in a region of relatively high transmissivity south or southeast of the waste panels, within the envelope of predicted flow paths to the accessible environment. Tests with both conservative and reactive (but not radioactive) tracers will examine transport along various paths between a central well and six outer wells drilled at different radii from the central location. Specific objectives of these tests are to: address questions about vertical heterogeneity in the Culebra (tests will isolate specific horizontal layers within the Culebra in different wells to examine vertical flow and transport between layers); to provide data to allow evaluation of alternative conceptual models for transport in the Culebra, including anisotropic, heterogeneous, and channeling models; to provide information about chemical retardation processes on a field scale; to provide additional evidence that matrix diffusion is an important process in retardation; and to provide core samples for additional laboratory tests from the region of predicted flow paths to the accessible environment. Results of the field tracer tests are anticipated to be available for use in performance assessment beginning in 1995 (Beauheim and Davies, 1992).

## 2.3 Engineered Barrier System

The WIPP disposal system includes engineered barriers that minimize the rate at which radionuclides may migrate through the hydrogeologic setting to the accessible environment. As presently designed, the repository relies on seals in panels, drifts, and shafts to prevent migration through the excavated openings. If performance assessments indicate additional barriers are needed to reduce potential radionuclide transport up an intrusion borehole, modifications can be made to the form of the waste and backfill or to the design of the waste-emplacement areas that will enhance long-term performance. Section 2.3 contains descriptions of the repository and seal design, the waste, the radionuclide source term, and the room/waste interactions. Because the performance of engineered barriers is dependent on the properties of the surrounding strata, Section 2.3 also contains additional information about the Salado Formation at the repository horizon.

### 2.3.1 The Salado Formation at the Repository Horizon

Depositional processes that created the Salado Formation were laterally persistent over large areas, and individual stratigraphic horizons within the formation can be recognized in potash mines and boreholes throughout the WIPP region (Lowenstein, 1988). Forty-four anhydrite and polyhalite "marker beds" in the Salado Formation have been identified and numbered within the approximately 2700 $km^2$ (1050 $mi^2$) of the Carlsbad potash mining

district (Jones et al., 1960). Thinner interbeds of anhydrite, clay, and polyhalite occur throughout the formation, and are also laterally persistent.

Lithologic layers in the Salado Formation dip less than 1° to the southeast at the WIPP, and the waste-emplacement area is being excavated at a constant stratigraphic horizon rather than at a constant elevation so that all waste panels will share the same local stratigraphy. This slight slope of the repository will result in a difference in floor elevation between the highest and lowest panels of less than 10 m.

Panels are excavated entirely within a 7.3-m (24-ft) thick section of halite and polyhalite between anhydrite marker beds 138 (MB138) and 139 (MB139), approximately 380 m (1250 ft) below the top of the Salado Formation (Figure 2-20a). Waste-emplacement panels are excavated in the lower portion of this section, approximately 1.4 m (4.6 ft) above MB139 (Figure 2-20b). Excavation has penetrated MB139 in sumps of all four shafts, and in other locations. Experimental rooms, located in a separate part of the repository north of the waste-emplacement area (see Section 2.3.2), have been excavated at a stratigraphic level higher than that of the waste-emplacement panels, in part, so that borehole tests can be conducted beneath the room floors in undisturbed strata of the waste-emplacement horizon.

Anhydrite interbeds are of importance for performance assessment because they are more permeable than the halite layer containing the disposal room, and therefore provide the dominant pathway for fluid migration. As discussed in more detail in Volume 3, presently available WIPP test data indicate undisturbed permeabilities ranging between $10^{-16}$ and $10^{-21}$ $m^2$ for anhydrite and between $10^{-19}$ and $10^{-24}$ $m^2$ for halite (Gorham et al. memo in Volume 3, Appendix A of this report). Interbeds included in the 1992 performance assessment are MB139, and anhydrites A and B and MB138 located above the waste-emplacement panels (Figures 2-20a and 2-20b).

Excavation of the repository and the consequent release of lithostatic stress has created a disturbed rock zone (DRZ) around the underground openings. The DRZ at the WIPP has been confirmed by borehole observations, geophysical surveys, and gas-flow tests, and varies in extent from 1 to 5 m (3.3 to 16.4 ft) (Stormont et al., 1987; Peterson et al., 1987; Lappin et al., 1989). Fractures and microfractures within the DRZ have increased porosity and permeability of the rock and increased brine flow from the DRZ to the excavated openings (Borns and Stormont, 1988, 1989). Fracturing has occurred in MB139 below the waste-emplacement panels and in both anhydrites A and B above the waste-emplacement panels. It is not known how far fracturing in the anhydrite interbeds extends laterally from the excavations at this time, nor is the ultimate extent of the DRZ known. Most deformation related to development of the DRZ is believed to occur in the first five years after excavation (Lappin et al., 1989).

Fracturing in the DRZ, particularly in the anhydrite interbeds, may provide an enhanced pathway for fluid migration out of the repository and possibly around panel and drift seals. Characterization of fracture-related permeability in these layers is essential to modeling of two-phase (gas and brine) fluid flow into and out of the repository. Work is in progress on modeling the possible pressure dependency of fracture permeability in anhydrite interbeds, and results will be incorporated in future PAs.

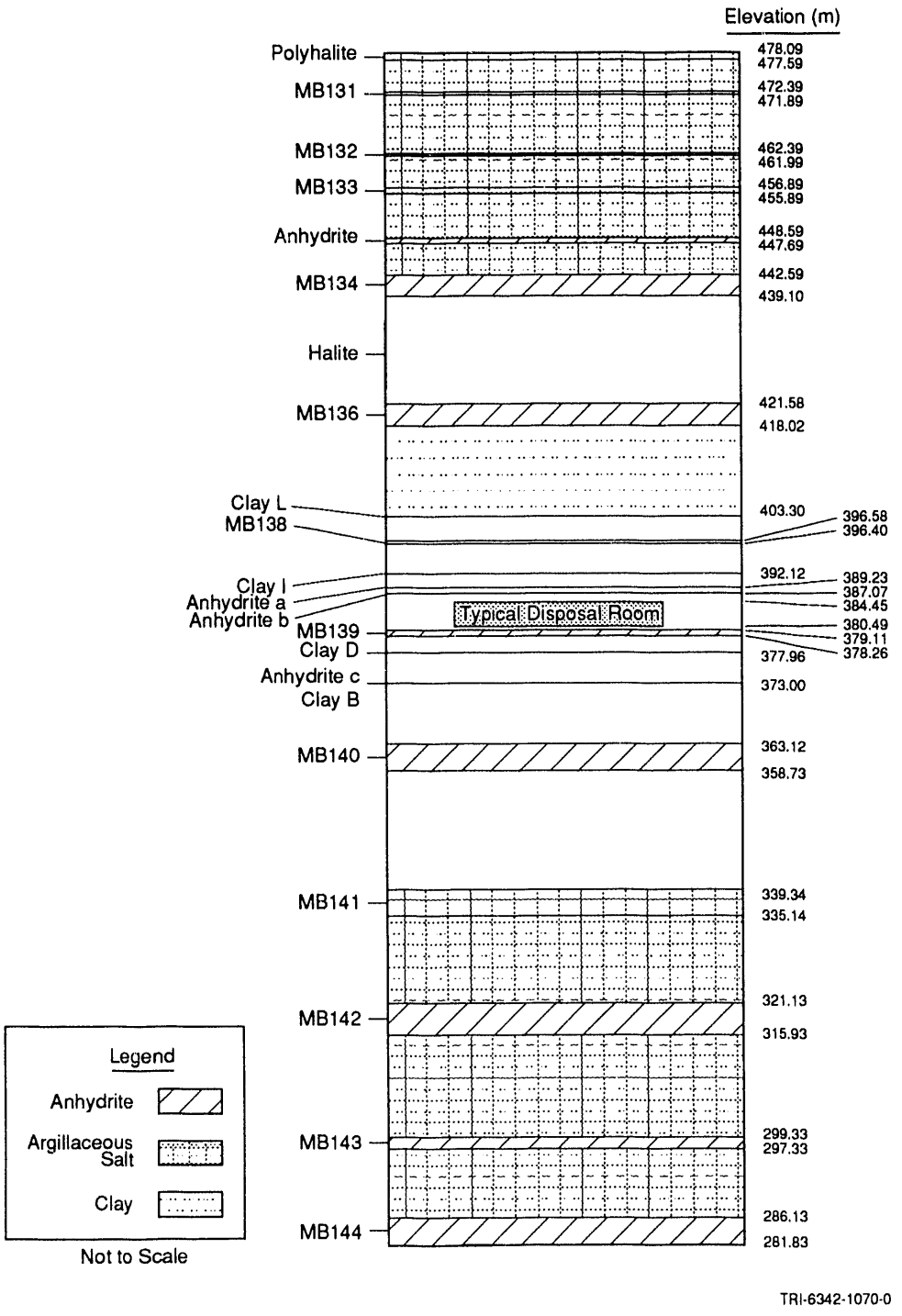


Figure 2-20a. Reference local stratigraphy near repository (after Munson et al., 1989a, Figure 3-3).

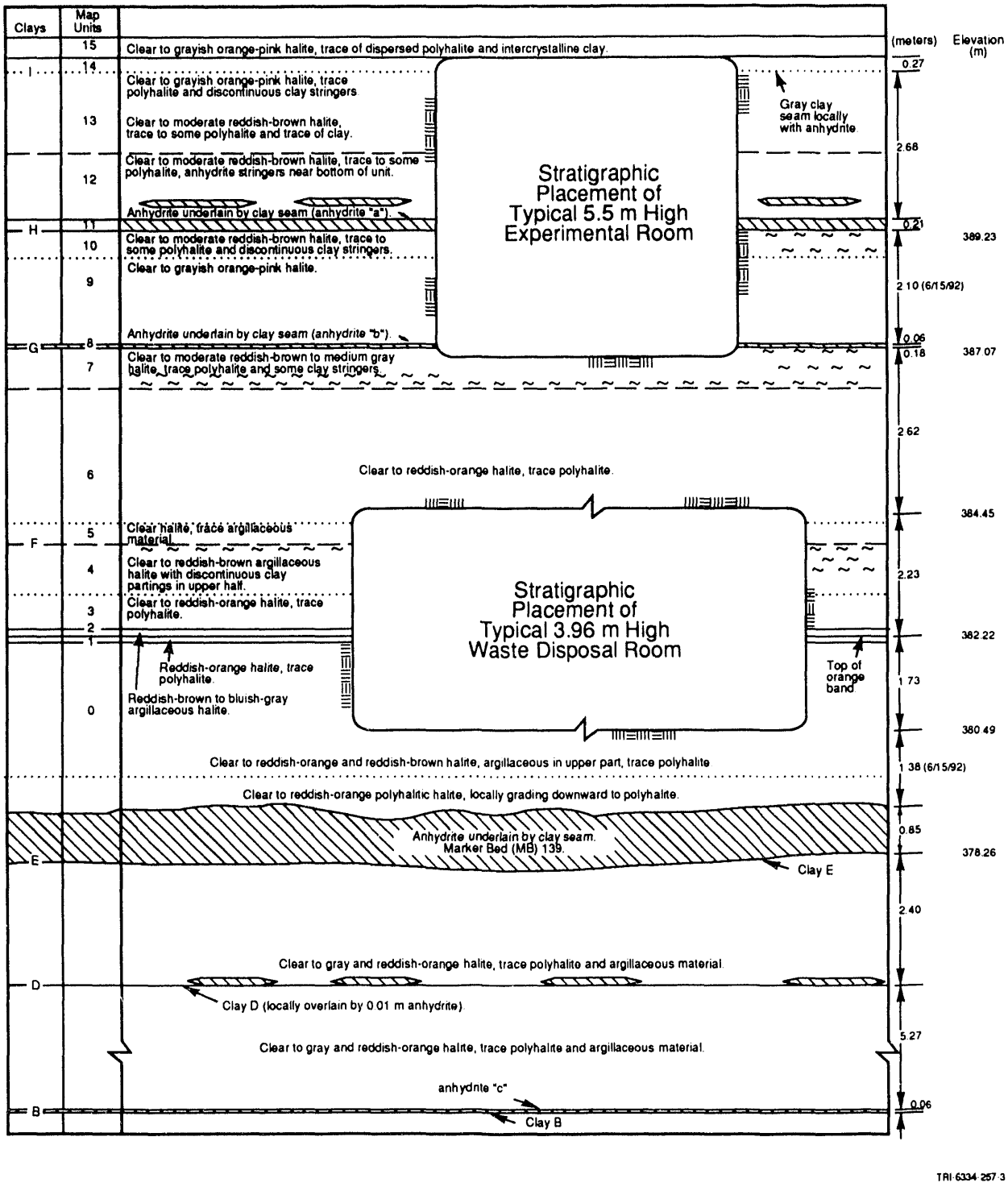


Figure 2-20b. Stratigraphy at the repository horizon (after Bechtel National, Inc., 1986, Figures 6-2, 6-3, and Lappin et al., 1989, Figure 4-12). Units in the disposal area dip slightly to the south, but disposal excavations are always centered about the orange marked band (reddish-orange halite).

Borehole observations of pore-fluid pressure and permeability suggest that there may be a transition zone extending outward beyond the DRZ. Within this transition zone pore-fluid pressures have dropped from their undisturbed, pre-excavation level, apparently without irreversible rock damage and large permeability changes (Gorham et al. memo in Volume 3, Appendix A of this report). The full extent of the transition zone is uncertain, as are its material properties. Properties of the transition zone used in the 1992 PA calculations are discussed in a memorandum of July 14, 1992 by Davies et al. in Volume 3, Appendix A of this report.

## 2.3.2 Repository and Seal Design

Major components of repository design that affect performance assessment are the waste itself, the underground waste-emplacement area and its access drifts and shafts, and the seals that will be used to isolate the emplacement area when the repository is decommissioned. The underground workings will ultimately consist of eight waste-emplacement panels, access drifts and shafts, and an experimental area (Figure 2-21). Drifts in the central portion of the repository will also be used for waste emplacement, providing the equivalent of an additional two panels for waste emplacement. A more detailed discussion of repository design is available in Volume 3 of this report.

All underground horizontal openings are rectangular in cross section. The emplacement area drifts are 4.0 m (13 ft) high by 7.6 m (25 ft) wide; the disposal rooms are 4.0 m (13 ft) high, 10.1 m (33 ft) wide, and 91.4 m (300 ft) long. Pillars between rooms are 30.5 m (100 ft) wide. The eight waste-emplacement panels will each have an initial volume of 46,000 $m^3$ ($1.6\times10^6$ $ft^3$). The northern drift emplace area will have an initial volume of 34,000 $m^3$ ($1.2\times10^6$ $ft^3$), and the southern drift emplacement area will have an initial volume of 33,000 $m^3$ ($1.2\times10^6$ $ft^3$) (Rechard et al., 1990a). Overall, the waste-emplacement areas will have an initial volume of about 435,000 $m^3$ ($1.5\times10^7$ $ft^3$).

The four vertical access shafts are cylindrical and range in diameter from 5.8 m (19 ft) to 3.0 m (10 ft). Shafts are lined in the units above the Salado Formation to prevent groundwater inflow and provide stability; they are unlined in the salt.

Excavation of the first waste-emplacement panel is complete; the remaining panels will be excavated as needed. Waste will be emplaced within the panels in drums or metal boxes, and panels will be backfilled and sealed as they are filled. Seals will be installed in panels, drifts, and the vertical shafts before the repository is decommissioned. Waste, backfill, and seals will be consolidated by creep closure after decommissioning.

### 2.3.2.1 WASTE CHARACTERIZATION

The waste that will be emplaced in the WIPP must meet the Waste Acceptance Criteria for the Waste Isolation Pilot Plant (U.S. DOE, 1991a) as explained in Volume 1 of this report (Chapter 3). These acceptance criteria specify that waste material containing particulates in certain size and quantity ranges will be immobilized,

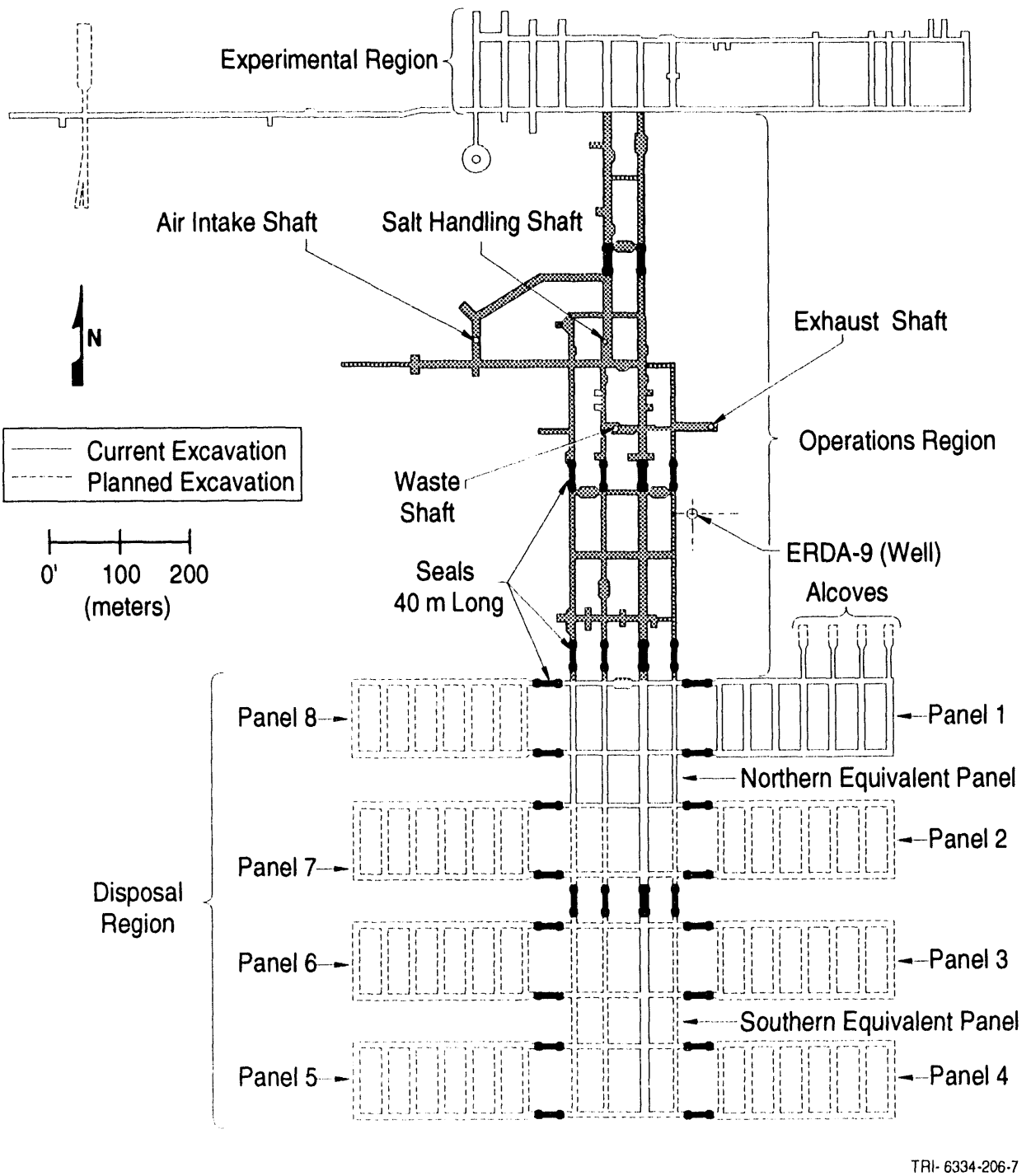


Figure 2-21. Plan view of waste-disposal horizon showing shaft, drift, and panel seal locations (after Nowak et al., 1990).

that waste liquid content be restricted to that remaining in well-drained containers and be less than one volume percent of the waste container, and that radionuclides in phyrophoric form be limited to less than one percent by weight of the external container. The requirements also prohibit disposal at the WIPP of wastes containing explosives, compressed gases, and ignitable, corrosive or reactive materials.

The current design of the WIPP has a total emplacement volume for contact-handled transuranic (CH-TRU) waste of $6.2\times10^6$ ft$^3$ (approximately 175,600 m$^3$) (U.S. DOE, 1980; Public Law 102-579, 1992). The estimated volume of CH-TRU waste supplied by the 10 waste-generator and/or storage sites for the 1991 Integrated Data Base (IDB, US DOE 1991b) was approximately 53,700 m$^3$ of stored waste and an additional 42,800 m$^3$ of waste to be generated by 2013. Estimates of the volume of waste to be generated may change in the future. Rather than revise the volume of waste emplaced in the WIPP each year, the current performance-assessment calculations are based on an initial CH-TRU-waste volume of approximately 175,600 m$^3$, the design volume. This is mostly for modeling convenience and will not have a significant effect on comparisons to 40 CFR 191B.

The current estimate of the stored and projected waste total about 96,500 m$^3$. Therefore, an additional 79,000 m$^3$ of waste could be emplaced in the WIPP. The characteristics of the additional 79,000 m$^3$ of waste were estimated from the characteristics of the projected waste of the five largest future generators. Because of changes that are occurring in weapons production and waste processing the waste that has not been generated cannot be characterized precisely. Estimates of waste characterization currently used in performance assessment have the potential for a large uncertainty. As discussed in Section 3.3.5 of Volume 3 of this report, uncertainty in the constituents that affect gas generation from corrosion of iron-based materials and from biodegradation of cellulosics and rubbers have been included in the 1992 preliminary performance assessment.

Characterization of the CH-TRU waste for the current performance-assessment calculations was based on a scale-up of masses estimated from expanded waste-characterization information. Based on 175,600 m$^3$ of CH-TRU waste emplaced in the WIPP, estimates of a total of about 12,000,000 kg of combustibles, 20,000,000 kg of metals and glass, and 25,000,000 kg of sludges were calculated. The total masses of iron-based metals, cellulosics, and rubbers were also calculated, and are provided in the memorandum by Peterson in Volume 3, Appendix A of this report. The masses of these materials are required for performance assessment because they influence gas generation and potential radionuclide transport.

The weight of the waste containers, drums and boxes, and of container liners were estimated because they also effect gas-generation potential. It was assumed in the estimation of the container weights that only steel 55-gallon drums and standard waste boxes (SWBs) will be emplaced in the WIPP. Other than test bins, these are the only containers that can currently be transported in a TRUPACT-II (NuPac, 1989). Based on emplacing 175,600 m$^3$ of CH-TRU-waste in drums and SWBs, it was estimated that about 518,000 drums and 35,600 SWBs would be disposed of in the WIPP. The total weight of the low-carbon steel in the drums and SWBs is larger that the estimated weight of corrodible iron-based materials in the waste.

The estimates of the total weight of the metals and glass and combustibles were nearly the same as were estimated for the 1991 PA analyses (WIPP PA Division, 1991a). The weight of sludge decreased significantly from the 1991 estimate. The weight of sludge in 1991 was based on the total weight of waste and average

weights of combustibles and metals and glass. The current estimate of the weight of sludge was based on expanded input from the sites. The estimates of the weights of iron-based corrodible metals and biodegradable materials were slightly decreased from the 1991 estimates.

### 2.3.2.2 SEALS

Seals will be emplaced in the entrance to each panel, in two locations within the drifts between the panels and the vertical shafts in the drifts between the experimental area and the vertical shafts, and in each of the four vertical shafts (Figure 2-21, 2-22) (Nowak et al., 1990). Design of these seals reflects specific functions for each type of seal. Seals in the upper portion of the shafts must prevent groundwater flow from the transmissive units of the Rustler Formation from reaching the lower portions of the shafts and the waste-emplacement areas. Seals in the lower portion of the shafts must provide a long-term, low-permeability barrier that will prevent Salado Formation brine and gas from migrating up the shaft. Panel seals (and drift seals) will inhibit long-term migration of radionuclide-contaminated brine through the drifts to the base of the shafts and must also provide safe isolation of radionuclides during the operational phase of the repository.

The primary long-term component of both lower shaft and panel seals will be crushed salt, confined between short-term rigid bulkheads until creep closure reconsolidates it to properties comparable to those of the intact Salado Formation. The short-term seals will be concrete in the panels and drifts, and composite barriers of concrete, bentonite, and consolidated crushed salt in the shafts. Crushed salt in the long-term portion of the seals will be preconsolidated to approximately 80% of the density of the intact formation and will compact further to approximately 95% of initial density within 100 years, at which time permeabilities are expected to be comparable to those of the undisturbed rock (Nowak and Stormont, 1987). Panel seals will be 40 m (131 ft) long, with 20 m (66 ft) of preconsolidated crushed salt between two 10-m (33-ft) concrete barriers. Shaft-seal systems will extend from the repository horizon in the Salado Formation to the surface, and will include composite barriers at the appropriate depths for individual lithologic units, including the Culebra Dolomite Member of the Rustler Formation (Nowak et al., 1990). Additional information about seal design is presented in Volume 3 of this report.

Marker Bed 139 will be sealed below each panel and drift seal by grouting, either with crushed-salt-based grout, cementitious material, bitumen, or other appropriate materials. Other anhydrite layers will be sealed similarly. Salt creep is expected to close fractures in halite in the DRZ over time, and engineered seals are not planned for the DRZ outside of MB139 and other interbeds.

### 2.3.2.3 BACKFILL

Void space between waste containers and elsewhere in the underground workings will be backfilled before sealing and decommissioning (Tyler et al., 1988; Lappin et al., 1989). The primary function of backfill will be to reduce initial void space in the excavated regions and to accelerate the entombment of the waste by creep closure. Consolidation of backfill by salt creep may reduce permeability in the waste-emplacement regions and limit brine flow through the waste; long-term properties of the backfill are uncertain, however, and will depend on

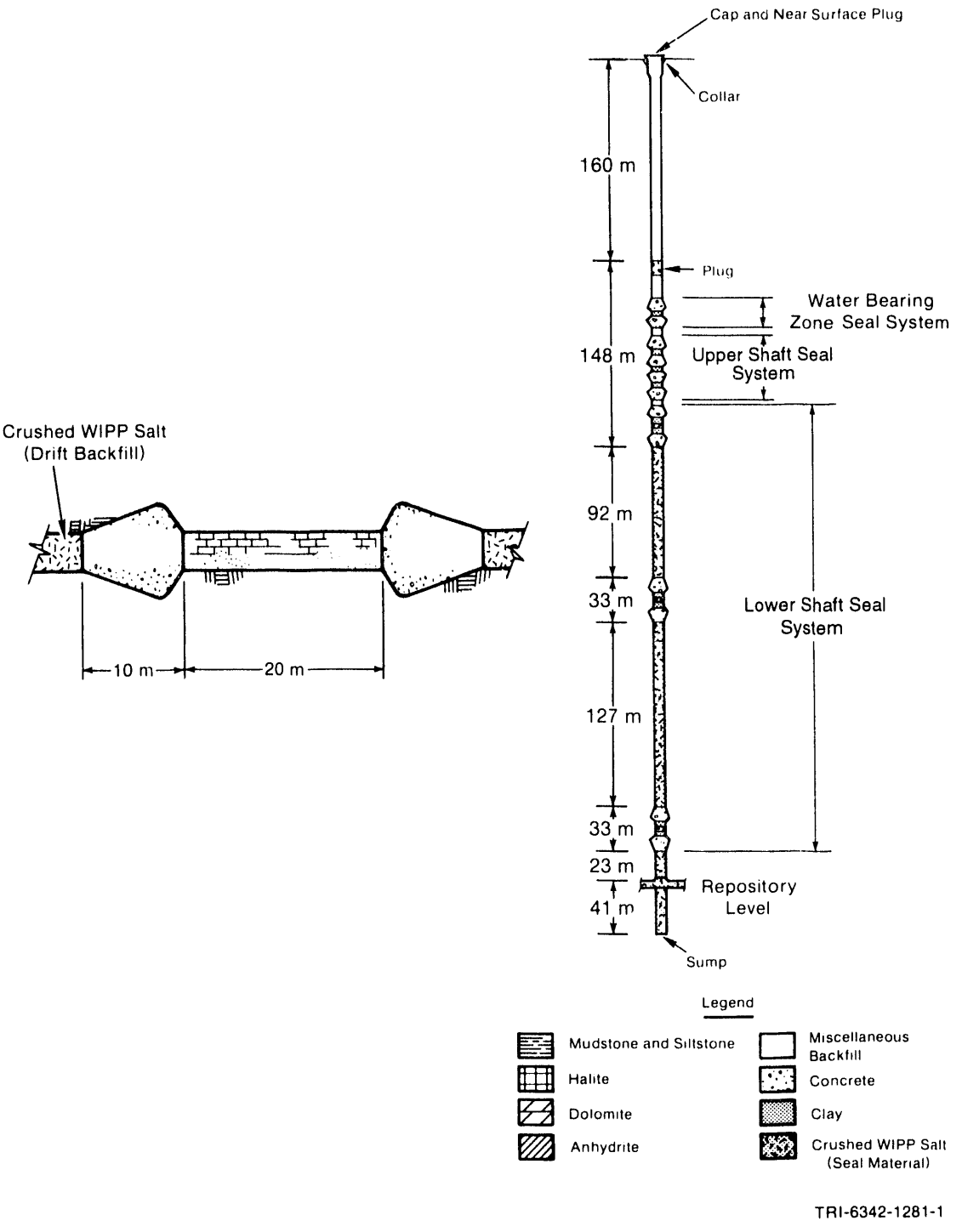


Figure 2-22. Representative shaft and plug seals (after Nowak et al., 1990). Vertical distances based on stratigraphy in ERDA-9.

fluid pressures within the panels. As discussed in Section 2.3.5, the pressure history of the repository will depend on the complexly coupled processes of salt creep, gas generation within the waste, and brine inflow from the surrounding Salado Formation. Performance-assessment calculations for 1992 assume a backfill of pure, unconsolidated crushed salt, with a relatively high permeability that provides little resistance to fluid flow. Pure salt will not sorb radionuclides, and retardation of radionuclides within the repository environment is not simulated. Design alternatives for backfill that contains bentonite as an additional barrier to retard radionuclides have been examined (U.S. DOE, 1990b, 1991c; Butcher et al., 1991; Pfeifle and Brodsky, 1991; Brodsky and Pfeifle, 1992) and will be available if needed.

#### 2.3.2.4 ENGINEERED ALTERNATIVES

The WIPP has been designed to dispose of waste in the form in which it is shipped from the TRU-waste-generator and/or storage sites. Preliminary performance-assessment calculations indicate that modifications to the waste form that limit dissolution of radionuclides in brine have the potential to improve predicted performance of the repository (Marietta et al., 1989; Bertram-Howery and Swift, 1990). Modifications to the backfill and design of the room could also reduce radionuclide releases. Modifications could also, if needed, mitigate the effects of gas generated within the repository. Present performance assessments are not complete enough to determine whether or not such modifications will be needed for regulatory compliance, but the DOE has investigated engineered alternatives to waste form and repository design so that alternatives will be available if needed (U.S. DOE, 1990b). The Engineered Alternatives Task Force (EATF) has identified 19 possible modifications to waste form, backfill, and room design that merit additional investigation (U.S. DOE, 1990b, 1991c). The 1992 performance-assessment calculations do not include simulations of these alternatives. Selected alternatives may be examined in future performance-assessment calculations, however, to provide guidance to DOE on possible effectiveness of modifications.

## 2.3.3 Radionuclide Inventory

As described in additional detail in Volume 3, Chapter 3 of this report, the radionuclide inventory for the 1992 performance assessment is estimated from input to the 1991 Integrated Data Base (IDB, U.S. DOE, 1991b). The 1991 IDB inventory of contact-handled transuranic (CH-TRU) waste (defined as transuranic waste with a surface dose rate not greater than 200 mrem/hr [Public Law 102-579, 1992]) identifies approximately 53,700 $m^3$ of waste as currently stored at generator sites, and projects an additional volume of 42,800 $m^3$ that will be generated in the future. The design volume of the WIPP (175,600 $m^3$) will accommodate an additional approximately 79,100 $m^3$ of waste that is not described in the IDB. Performance assessments use an inventory in which the amount of CH-TRU is scaled up from the IDB volume to the design volume. CH-TRU activity of the initial design-volume inventory, expressed in curies, is estimated by scaling the curie inventory of the projected CH-TRU waste from each of the five sites that will generate the most waste in the future by a factor of 1.89 (the ratio of design volume to IDB volume) (Volume 3, Sections 3.3 and 3.4 of this report). This scaling of the inventory to a standard volume is done for modeling convenience, primarily to ensure the commensurability of analysis results from one iteration of performance assessment to the next. Because the releases allowed by the EPA are normalized using a waste unit factor based on the total inventory of transuranic waste (U.S. EPA, 1985; see Volume 1, Appendix A,

and Volume 3, Section 3.3.4 of this report), scaling of the inventory does not have a proportional effect on the location of the CCDF used for preliminary comparison with 40 CFR 191.13 (Volume 1, Section 5.1 of this report).

The initial design-volume inventory of CH-TRU waste used in the 1992 performance assessment contains $8.2\times10^6$ Ci (memorandum by Peterson in Volume 3, Appendix A of this report). Uncertainty in this inventory is large, particularly given the potential changes in the sources of CH waste due to changes in weapons production. Existing legislation, regulations, and agreements do not limit the total curie inventory of CH-TRU waste that may be emplaced, but do limit the total volume of waste that may be emplaced in the WIPP ($6.2\times10^6$ $ft^3$, or 175,600 $m^3$) (Public Law 102-579, 1992).

Remotely-handled transuranic waste (RH-TRU), defined to have a surface dose rate greater than 200 mrem/hr but less than 1,000 rem/hr, will also be emplaced in the WIPP. The total RH-TRU inventory is limited to $5.1\times10^6$ Ci; no more than five percent of the RH-TRU canisters emplaced at the WIPP may have surface dose rates that exceed 100 rem/hr, and the activity of the RH-TRU waste shall not exceed 23 Ci/liter averaged over the volume of a canister (Public Law 102-579, 1992). Existing and projected RH-TRU waste in the IDB (US DOE, 1991b) has a volume of 6,667 $m^3$. This is slightly less than the WIPP design volume for RH-TRU waste (7080 $m^3$), but is predicted by the IDB to require 8071 canisters, somewhat more than the design capacity of 7950 canisters. The discrepancy occurs because the volume of waste placed in each canister differs depending on the generator site, and not all canisters will be filled to the capacity assumed for the WIPP design criteria. The 1991 IDB also indicates that there may be a considerable volume of uncharacterized waste that will probably be classified as RH-TRU. Given these uncertainties, the RH-TRU inventory is not scaled to design volume, and is used in the 1992 PA as reported in the 1991 IDB. The total remotely-handled inventory for 1992 is approximately $3.5\times10^6$ Ci, of which $1.8\times10^6$ Ci result from transuranic radionuclides and isotopes of uranium (i.e., radionuclides with atomic number greater than or equal to 92) (memorandum from Peterson, Volume 3, Appendix A of this report).

Radioactive decay within the repository is simulated with a simplified set of decay chains, provided in Volume 3, Section 3.3.3 of this report. Of the 70 radionuclides identified as present either in the initial WIPP inventory or as decay products, 26 are considered explicitly in PA analyses of direct releases from the repository to the ground surface. (See Section 4.2 of this volume for a discussion of human intrusion scenarios and Section 7.7 of this volume for a discussion of modeling of releases during drilling.) Radionuclides omitted from the simplified decay chains are those that have very short half-lives, very low activities, or both. Subsurface transport within the Culebra Dolomite Member of the Rustler Formation (see Sections 4.2 and 7.6 of this volume) is simulated for the nine most important radionuclides, identified in Volume 3, Section 3.3.3 of this report.

The only radioactive gas expected in the repository is radon-222, created from decay of radium-226. Decay of thorium-230 will cause the activity of radium-226 in a panel to increase from about 0 Ci at the time of emplacement to 8 Ci at 10,000 years. Because radon-222, with a half-life of only 3.8 days, will exist in secular equilibrium (equal activity) with radium-226, with a half-life of 1600 years, its activity will also be insignificant throughout the 10,000-year period. At 100,000 years the activity of radium-226 would increase to about 58 Ci in a panel, and the activity of radon-222 would still not be significant. Not including release of volatile radionuclides does not significantly affect the total radionuclide release.

## 2.3.4 Radionuclide Solubility and the Source Term for Transport Calculations

Before 1991, WIPP performance assessments calculated the source term for transport modeling* using the same estimated range and distribution (loguniform from $10^{-9}$ to $10^{-3}$ M) for the solubility limit of all radionuclide species in repository brine (Lappin et al., 1989; Brush and Anderson, 1989a). A fixed distribution was applied to all radionuclides for PA calculations before 1991 because, as is explained below, the state of knowledge at that time did not allow for the differentiation of radionuclides.

During the first meeting of the WIPP PA Source Term Group (in June of 1988), Choppin reported that estimates of the speciation and solubilities of americium, neptunium, plutonium, uranium, and thorium in both the Salado and Castile brines for expected concentrations of organic ligands were not possible because there are no thermodynamic data (solubility products for solid phases, or stability constants for dissolved organic or inorganic complexes) for these elements in solutions with ionic strengths equal to those of the Salado and Castile brines (Brush and Anderson, 1989b). In addition, Choppin observed that data reported by different groups using different experimental techniques are often contradictory, making the use of subjective expert judgment necessary for preliminary data selection for PA use until data from WIPP-specific experimental programs are available (see Section 2.3.4.2).

In lieu of data from laboratory experiments, the Source Term Group recommended a "best estimate" of $10^{-6}$ M for the concentration of plutonium and americium in any brine that resaturates the WIPP disposal rooms (Brush and Anderson, 1989a). This is the intermediate value (on a logarithmic scale) of the range of dissolved radionuclide concentrations ($10^{-9}$ to $10^{-3}$ M) that have been used for sensitivity studies of the source term. Because the PA calculations require the input of a probability distribution, the entire range discussed above was used as a loguniform distribution. Because of the lack of applicable experimental data, there was no differentiation between the concentrations of various radionuclides in the 1989 PA. The 1990 estimated range in effective radionuclide solubilities was intended to include the effects of possible colloid formation within the repository (Rechard et al., 1990a). The conservative assumption was that colloidal materials would be completely transportable (i.e., that they would not be sorbed or precipitated within the repository).

### 2.3.4.1 EXPERT JUDGMENT ELICITATION

Since the beginning of the WIPP PA effort, it has been recognized that assuming a fixed solubility distribution for all radionuclides does not adequately capture the considerable uncertainty in radionuclide concentrations expected in the repository. The need for a better understanding of the source term was further highlighted by sensitivity analyses performed as part of the 1990 preliminary performance assessment. These sensitivity analyses indicated that, conditional on the models and distributions used in the 1990 calculations, uncertainty in the solubility limit was the most important single contributor to variability in total cumulative releases to the accessible environment resulting from groundwater transport (Helton et al., 1991).

* The source term for transport modeling for the PA is based on analytical model that calculates the equilibrium concentration of the radionuclide species in the repository brine. See Section 7.4 and Appendix A.

Because of the paucity of experimental data for the conditions and solutions expected specifically at the WIPP, a panel of experts external to the WIPP Project, called the Source Term Expert Panel, was convened in the spring of 1991 to provide the performance-assessment team with judgment about both dissolved and suspended radionuclides* for specific elements under variable Eh and pH conditions. Their judgments have been used to develop radionuclide solubilities that vary by radionuclide and type of brine solution. The resulting solubility ranges have been used in the 1991 and 1992 PA calculations.

Selection of the Source Term Expert Panel and elicitation of their judgment on solubility limits followed the procedure suggested by Hora and Iman (1989). Candidates for the expert panel on source term were gathered by a two-tiered nomination process. Initial nominations were solicited from an SNL staff member and an external consultant, as well as from members of the Performance Assessment Peer Review Panel and the National Research Council's WIPP Panel. Additional nominations were requested from all those contacted. Curricula vitae from those who were interested in participating in such a panel and available during the entire study period were reviewed by a two-member selection committee external to SNL. Some individuals removed themselves from consideration because of prior time commitments, current contracts with SNL, a self-determined lack of expertise, or involvement in an oversight organization. Nominees were evaluated on the basis of expertise and professional reputation; four experts were selected whose complementary areas of specialization provided the needed breadth and balance to the panel.**

During the first meeting of the Source Term Expert Panel (March 1991), the Panel members were presented with published papers and reports identified from a comprehensive literature search that focused on radionuclide solubility in high-ionic-strength solutions in salt formations, covering the United States repository program as well as experiments conducted in Germany, Canada, Finland, Sweden, and at the Commission of the European Communities, Joint Research Center at Ispra, Italy. Other issues discussed in these publications were speciation, colloids, the leaching of radionuclides from high-level waste (HLW) glass, and the impact of backfill materials.

A summary of the expert judgment elicitation procedure and results, presented in detail in Trauth et al. (1992), follows. A final report on this effort by the members the Source Term Expert Panel will be available in 1993.

As stated above, the Source Term Expert Panel was selected to include a balance in the required areas of expertise (experience in actinide chemistry and with high-ionic-strength solutions). At the first meeting, the panelists divided the problem into areas of specific responsibility and provided a structure for assembling the individual judgments to obtain a single distribution codifying the collective judgment of the panel. In addition, the group of experts decided to be elicited together to produce one set of results. A consequence of the group elicitation is that the uncertainty expressed by specific experts could not be assessed. However, many of the inter-expert differences were captured during the elicitation process resulting in more widely dispersed probability functions.

* Because of the limited state of knowledge regarding colloids, the Source Term Expert Panel chose to limit their judgments to dissoloved radionuclides (solubility).

** In the case of the Source Term Expert Panel, expertise was required in actinide chemistry and high-ionic-strength chemistry. Therefore, experts from both these disciplines were selected. These individuals used their complementary expertise to arrive at judgments that satisfy all the pertinent constraints of the solubility problem.

In addition to a literature review (discussed above), preparation for elicitation involved computer calculations by the panel members using a standard brine that simulates the brine in the Salado Formation (the solvent (WIPP Brine A) (Lappin et al., 1989). These efforts resulted in the determination of the oxidation state(s) in which the radionuclides would exist in the WIPP rooms and drifts. Moreover, the solution and solid species that would coexist with that particular oxidation state were identified using two regimes: (1) one regime based on solid species with the highest solubility and therefore highest radionuclide concentration, and (2) another regime based on solid species with the lowest solubility and therefore lowest radionuclide concentration. Which regime predominates depends on the chemical properties within the repository, which in turn may depend on pH and ionic strength of the brine and the presence of carbonates and/or sulfates. Furthermore, the factors controlling each regime may differ for different radionuclides.

The experts' judgments on the solubility distributions were elicited at the second meeting (in April of 1991). The assessment for each distribution began by establishing the upper and lower solubility regimes and the calculated solubility of each radionuclide within each regime. The resulting probability distributions for the radionuclides used in the 1992 calculations are presented in Volume 3 of this report (Section 3.3.5). Because the calculated solubility is a single number that does not incorporate any uncertainty, it was necessary to account for uncertainty in both the calculated value and the underlying conditions, such as pH.

Typically, the calculated value would be used to establish a fractile, often either the 0.10 or 0.90 fractile, of the distribution. The absolute lower limit of the distribution was obtained by considering the sensitivity of solubility to the underlying brine chemistry. The interior fractiles were obtained after the 0.10 and 0.90 fractiles and the endpoints were established. Where possible, concentration data from well water from the Nevada Yucca Mountain site (J-13) was used with a correction for the ionic-strength difference between the J-13 water and the WIPP Brine A to determine the 0.50 fractile. For the determination of the 0.25 and 0.75 fractiles, one speciation was thought in some cases to be more likely, resulting in a skewed distribution. In other cases, both speciations were thought to be likely, resulting in a more symmetrical distribution.

The Source Term Expert Panel had considerable difficulty dealing with colloids because of a lack of experimental data and limited knowledge of the physical principles governing their formation. Some diversity of opinion existed about the significance of colloids. The panel did not believe that they could make judgments about suspended-solids concentrations at the present time. They planned to include recommendations for future experiments related specifically to colloids in a final panel report. Transport of radionuclides in colloids has not been included in the 1992 PA.

Correlations between the concentrations assigned to the radionuclides were discussed briefly by the panel. The consensus was that correlations do exist, possibly between americium(III) and curium(III), and between neptunium(IV) and plutonium(IV). The panel is expected to address this issue in a forthcoming report on their findings.

### 2.3.4.2 EXPERIMENTAL WORK

Future WIPP performance assessments will rely increasingly on data from planned solubility tests of actual waste. These tests will complement the laboratory studies of radionuclide chemistry. The laboratory program is currently determining solubilities and sorption coefficients of plutonium and its oxidation state analogues in synthetic brines under various conditions of pH, and will soon examine actinide speciation and measure stability constants for complex ions (Brush, 1990). As currently planned, the actinide source-term program will involve filling test containers with a mixture of natural and synthetic brines with compositions chemically similar to those of intergranular brines found in the Salado Formation. Container size will depend on waste homogeneity; heterogeneous waste types such as combustibles will use "drum scale" vessels of 210 L volume, while more homogeneous types such as process sludges will use "liter scale" test containers. The containers will permit regular brine sampling, and gas monitoring and venting.

## 2.3.5 Creep Closure, Fluid Flow, and Room/Waste Interactions

When the repository is decommissioned, free brine initially will not be present within the emplacement area, and void space above the backfilled waste will be air-filled. Brine seepage from the Salado Formation will have filled fractures in anhydrite interbeds above and below the emplacement area (Lappin et al., 1989; Rechard et al., 1990b).

Following excavation salt creep will begin to close the repository. In the absence of elevated gas pressures within the repository, modeling of salt creep indicates that consolidation of the waste in unreinforced rooms would be largely complete within 100 years (Tyler et al., 1988; Munson et al., 1989a,b). Brine will seep into the emplacement area from the surrounding salt, however, and gas will be generated in the humid environment by corrosion of metals, radiolysis of brine, and microbial decomposition of organic material. Some gas will disperse into the surrounding anhydrite layers. Continued gas generation could increase pressure within the repository sufficiently to reverse brine inflow and partially or completely desaturate the waste-emplacement area. Pressure may be high enough to open fractures in the anhydrite interbeds above and below the repository, allowing additional lateral migration of gas from the waste-emplacement area. High pressure may also halt and partially reverse closure by salt creep. In the undisturbed final state, the emplacement area could be incompletely consolidated and gas-filled rather than brine-filled.

All of the major processes active in the waste-emplacement area are linked, and all are rate- and time-dependent. For example, creep closure will be, in part, a function of pressure within the repository. Pressure will be in turn a function of the amount of gas generated and the volume available within the repository and the surrounding Salado Formation for gas storage. Gas-storage volume will be a function of closure rate and time, with storage volume decreasing as consolidation continues. Time and rate of gas generation, therefore, will strongly influence repository pressurization and closure. Gas-generation rates will be dependent on specific reaction rates and the availability of reactants, including water. Some water can be generated by microbial activity (Brush and Anderson, 1989b). Additional water will be provided by brine inflow, which, is assumed to occur according to two-phase immiscible flow through a porous medium and which will depend in large part on repository pressure, so that some gas-generation reactions could be partially self-buffering.

Responses of the disposal system to human intrusion are equally complicated. Consequences will depend on the time of intrusion, the degree to which the repository has closed, and the amount of gas generated. If intrusion occurs into a fully pressurized, dry, and partially unconsolidated waste-emplacement area, venting of gas up the borehole will permit brine to resaturate available void space. Following eventual deterioration of plugs in an intrusion borehole, brine may flow from the emplacement area into the borehole, transporting radionuclides upward toward the accessible environment. Upward flow from a pressurized brine pocket in the Castile Formation may contribute to flow and radionuclide transport.

# 3. PERFORMANCE ASSESSMENT METHODOLOGY

This chapter contains an overview of WIPP performance-assessment methodology. Additional information about this subject is provided in other published sources (Helton et al., 1991; WIPP PA Division, 1991a).

## 3.1 Conceptualization of Risk for the WIPP Performance Assessment

The WIPP performance assessment uses a conceptualization for risk similar to that developed for risk assessments for nuclear power plants. This conceptualization characterizes risk in terms of what can go wrong, how likely things are to go wrong, and what the consequences are of things going wrong. This description provides a structure on which both the representation and calculation of risk can be based.

Kaplan and Garrick (1981) have presented this representation of risk as a set of ordered triples. The WIPP performance assessment uses their representation, and defines risk to be a set $\mathcal{R}$ of the form

$$\mathcal{R} = \left\{ \left( S_i, pS_i, \mathbf{cS}_i \right), \; i = 1, \ldots, nS \right\}, \tag{3-1}$$

where

$S_i$ = a set of similar occurrences,

$pS_i$ = probability that an occurrence in set $S_i$ will take place,

$\mathbf{cS}_i$ = a vector of consequences associated with $S_i$,

$nS$ = number of sets selected for consideration,

and the sets $S_i$ have no occurrences in common (i.e., the $S_i$ are disjoint sets). This representation formally decomposes risk into what can happen (the $S_i$), how likely things are to happen (the $pS_i$), and the consequences of what can happen (the $\mathbf{cS}_i$). The $S_i$ are scenarios in the WIPP performance assessment, the $pS_i$ are scenario probabilities, and the vector $\mathbf{cS}_i$ contains the normalized EPA releases and other performance measures associated with scenario $S_i$. Other performance measures of interest are dose and health effects for safety assessments, and concentrations of heavy metals and volatile organic compounds (VOCs) for hazardous waste assessments.

Risk results in $\mathcal{R}$ can be summarized with complementary cumulative distribution functions (CCDFs). These functions provide a display of the information contained in the probabilities $pS_i$ and the consequences $\mathbf{cS}_i$. With the assumption that a particular consequence result $cS$ in the vector $\mathbf{cS}$ has been ordered so that $cS_i \le cS_{i+1}$ for $i = 1, \ldots, nS$, the CCDF for this consequence result is the function $F$ defined by

$F(x)$ = probability that $cS$ exceeds a specific consequence value $x$

$$= \sum_{j=i}^{nS} pS_j \tag{3-2}$$

where $i$ is the smallest integer such that $\mathbf{cS}_i > x$. As illustrated in Figure 3-1, $F$ is a step function that represents the probabilities that consequence values on the abscissa will be exceeded. To avoid a broken appearance, CCDFs are usually plotted with vertical lines added at the discontinuities.

The steps in the CCDFs shown in Figure 3-1 result from the discretization of all possible occurrences into the sets $S_i,\ldots S_{nS}$. Unless the underlying processes are inherently disjoint, the use of more sets $S_i$ will tend to reduce the size of these Ssteps and, in the limit, will lead to a smooth curve.

### 3.1.1 Calculation of Risk

The calculation of risk and its associated uncertainty begins with the determination of the sets $S_i$, which are the scenarios to be analyzed. Once these sets are determined, their probabilities $pS_i$ and associated consequences $\mathbf{cS}_i$ must be determined. In practice, development of the $S_i$ is an iterative process that must take into account the procedures required to determine the probabilities $pS_i$ and the consequences $\mathbf{cS}_i$. For the WIPP performance assessment, the overall process is organized so that $pS_i$ and $\mathbf{cS}_i$ are calculated by various models, the configuration of which depends on the individual $S_i$.

Use of these models requires values for imprecisely known variables that can be represented by a vector

$$\mathbf{x} = [x_1, x_2, \ldots, x_{nV}], \tag{3-3}$$

where each $x_j$ is an imprecisely known input required in the analysis and $nV$ is the total number of such inputs. If the analysis has been developed so that each $x_j$ is a real-valued quantity for which the overall analysis requires a single value, the representation for risk in Equation 3-1 can be restated as a function of $\mathbf{x}$:

$$\mathcal{R}(\mathbf{x}) = \left\{\left[S_i(\mathbf{x}), pS_i(\mathbf{x}), \mathbf{cS}_i(\mathbf{x})\right],\ i = 1,\ldots,nS(\mathbf{x})\right\} \tag{3-4}$$

As $\mathbf{x}$ changes, so will $\mathcal{R}(\mathbf{x})$ and all summary measures that can be derived from $\mathcal{R}(\mathbf{x})$. Thus, rather than a single CCDF for each consequence contained in the vector $\mathbf{cS}$ shown in Equation 3-1, a distribution of CCDFs results from the possible values that $\mathbf{x}$ can represent (Figure 3-2).

The distribution assigned to the individual variables $x_j$ in $\mathbf{x}$ reflect uncertainty in the modeling system. Factors that affect uncertainty in risk results can be subdivided into those that affect imprecisely known variables, those related to the selection of conceptual and computational models, and those related to scenario selection. Factors related to scenario selection can be further subdivided into completeness, aggregation, and stochastic

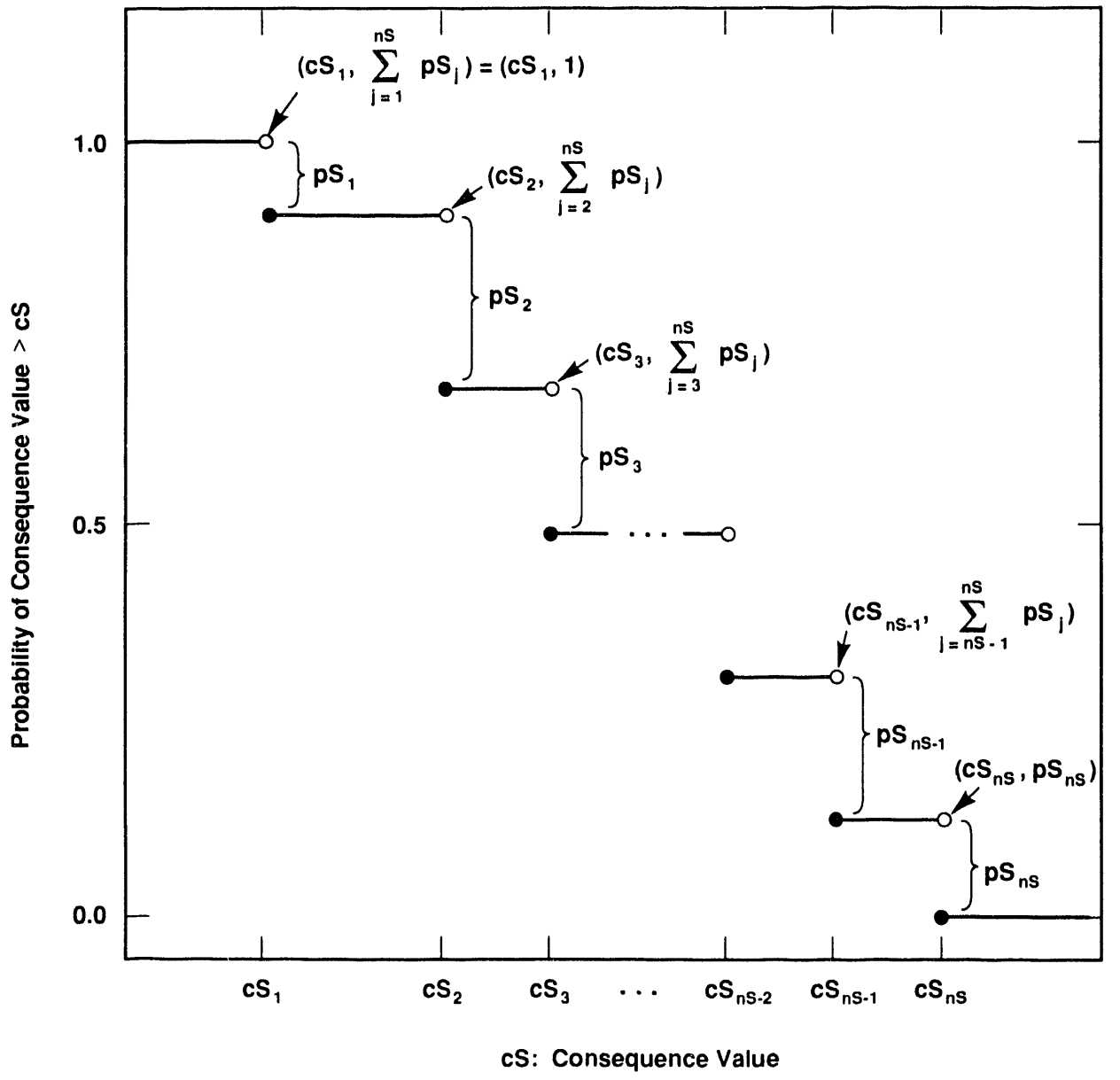


TRI-6342-730-5

Figure 3-1. Estimated CCDF for consequence result **cS** (Helton et al., 1991; Helton, in press). The open and solid circles at the discontinuities indicate the points included on (solid circles) and excluded from (open circles)the CCDF.

variation. Uncertainty about imprecisely known variables may result from incomplete data or measurement uncertainty, and can affect all three elements of the triple introduced in Equation 3-1. Uncertainty about the appropriate choices of models can affect both $pS_i$ and $\mathbf{cS}_i$. Due to the complex nature of risk assessments, model selection can also affect the definition of the $S_i$. Completeness refers to the extent that a performance assessment includes all possible occurrences for the system under consideration. In terms of the risk representation in Equation 3-1, completeness deals with whether or not all possible occurrences are included in the union of the sets $S_i$. Aggregation refers to the division of the possible occurrences into the sets $S_i$. Resolution is lost if the $S_i$ are defined too coarsely (e.g., $nS$ is too small) or in some other inappropriate manner. Computational efficiency is lost if $nS$ is too large. Model selection refers to the actual choice of the models used in a risk assessment. Uncertainty about the appropriate model choice can affect both $pS_i$ and $\mathbf{cS}_i$. Due to the complex nature of risk assessments, model selection can also affect the definition of the $S_i$. Uncertainty about imprecisely known variables, which may result from incomplete data or measurement uncertainty, can also affect all three elements of the risk triple. Stochastic variation is represented by the probabilities $pS_i$, which are functions of the many factors that affect the occurrence of the individual sets $S_i$.

Individual variables $x_j$ may relate to each of these different types of uncertainty. For example, individual variables might relate to completeness uncertainty (e.g., the value for a cutoff used to drop low-probability occurrences from the analysis), aggregation uncertainty (e.g., a bound on the value for $nS$), model uncertainty (e.g., a 0-1 variable that indicates which of two alternative models should be used), variable uncertainty (e.g., a solubility limit or a retardation for a specific element), or stochastic uncertainty (e.g., a variable that helps define the probabilities for the individual $S_i$).

### 3.1.2 Characterization of Uncertainty in Risk

Characterization of the uncertainty in the results of a performance assessment requires characterization of the uncertainty in $\mathbf{x}$, the vector of imprecisely known variables. This uncertainty can be described with a sequence of probability distributions

$$D_1, D_2, \ldots, D_{nV}, \tag{3-5}$$

where $D_j$ is the distribution developed for the variable $x_j$, $j=1, 2, \ldots, nV$, contained in $\mathbf{x}$. The definition of these distributions may also be accompanied by the specification of correlations and various restrictions that further define the possible relations among the $x_j$. These distributions and other restrictions probabilistically characterize where the appropriate input to use in the performance assessment might fall, given that the analysis is structured so that only one value can be used for each variable under consideration.

Once the distributions in Equation 3-5 have been developed, Monte Carlo techniques can be used to determine the uncertainty in $\mathcal{R}(\mathbf{x})$ from the uncertainty in $\mathbf{x}$. First, a sample

$$\mathbf{x}_k = \left[x_{k1}, x_{k2}, \ldots, x_{k,nV}\right], \; k = 1, \ldots, nK \tag{3-6}$$

is generated according to the specified distributions and restrictions, where $nK$ is the size of the sample. Performance-assessment calculations are then performed for each sample element $\mathbf{x}_k$, which yields a sequence of risk results of the form

$$\mathcal{R}(\mathbf{x}_k) = \left\{\left[S_i(\mathbf{x}_k), pS_i(\mathbf{x}_k), \mathbf{cS}_i(\mathbf{x}_k)\right],\ i = 1, \ldots, nS(\mathbf{x}_k)\right\}, \tag{3-7}$$

for $k = 1, \ldots, nK$. Each set $\mathcal{R}(\mathbf{x}_k)$ is the result of one complete set of calculations performed with a set of inputs (i.e., $\mathbf{x}_k$) that the review process producing the distributions in Equation 3-5 concluded was possible. Further, associated with each risk result $\mathcal{R}(\mathbf{x}_k)$ in Equation 3-7 is a probability or weight* that can be used in making probabilistic statements about the distribution of $\mathcal{R}(\mathbf{x})$.

A single CCDF can be produced for each set $\mathcal{R}(\mathbf{x}_k)$ of results shown in Equation 3-7, yielding a family of CCDFs of the form shown in Figure 3-2. This distribution of CCDFs can be summarized by plotting the mean value and selected percentile values of the exceedance probabilities shown on the ordinate for each consequence value on the abscissa. For example, the mean plus the 10th, 50th (i.e., median), and 90th percentile values might be used (Figure 3-3). The mean and percentile values can be obtained from the exceedance probabilities associated with the individual consequence values and the weights or "probabilities" associated with the individual sample elements.

Consideration of a family of CCDFs allows a distinction between the uncertainty that controls the shape of a single CCDF and the uncertainty that results in a distribution of CCDFs. The stepwise shape of a single CCDF reflects the fact that a number of different occurrences have a real possibility of taking place. This type of uncertainty is referred to as stochastic variation in this report. A family of CCDFs arises from the fact that fixed, but unknown, quantities are needed in the estimation of a CCDF. The distributions that characterize what the values for these fixed quantities might be lead to a distribution of CCDFs, with each single CCDF reflecting a specific sample element $\mathbf{x}_k$.

Both Kaplan and Garrick (1981) and the International Atomic Energy Agency (IAEA, 1989) distinguish between these two types of uncertainty. Specifically, Kaplan and Garrick distinguish between probabilities derived from frequencies and probabilities that characterize degrees of belief. Probabilities derived from frequencies correspond to the probabilities $pS_i$ in Equation 3-1, while probabilities that characterize degrees of belief (i.e., subjective probabilities) correspond to the distributions indicated in Equation 3-5. The IAEA report distinguishes between what it calls Type-A uncertainty and Type-B uncertainty. The IAEA report defines Type-A uncertainty to be stochastic variation; as such, this uncertainty corresponds to the frequency-based probability of Kaplan and Garrick and the $pS_i$ of Equation 3-1. Type-B uncertainty is defined to be uncertainty that is due to lack of knowledge about fixed quantities; thus, this uncertainty corresponds to the subjective probability of Kaplan and

* In random or Latin hypercube sampling, this weight is the reciprocal of the sample size (i.e., $1/nK$) and can be used in estimating means, cumulative distribution functions, and other statistical properties. This weight is often referred to as the probability for each observation (i.e., sample $\mathbf{x}_k$). However, this association is not technically correct. If continuous distributions are involved, the actual probability of each observation is zero.

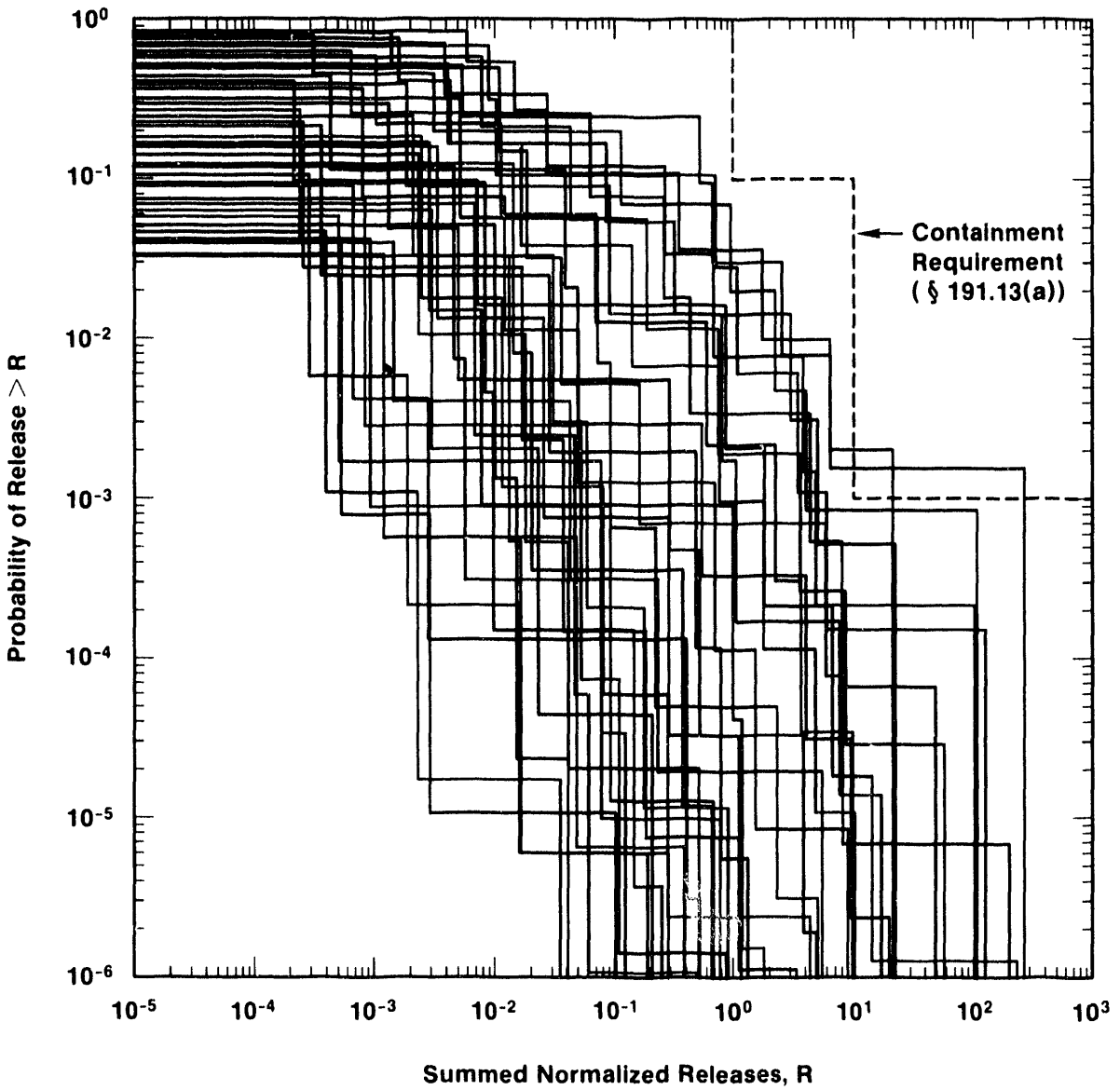


Figure 3-2. Example distribution of CCDFs obtained by sampling imprecisely known variables.

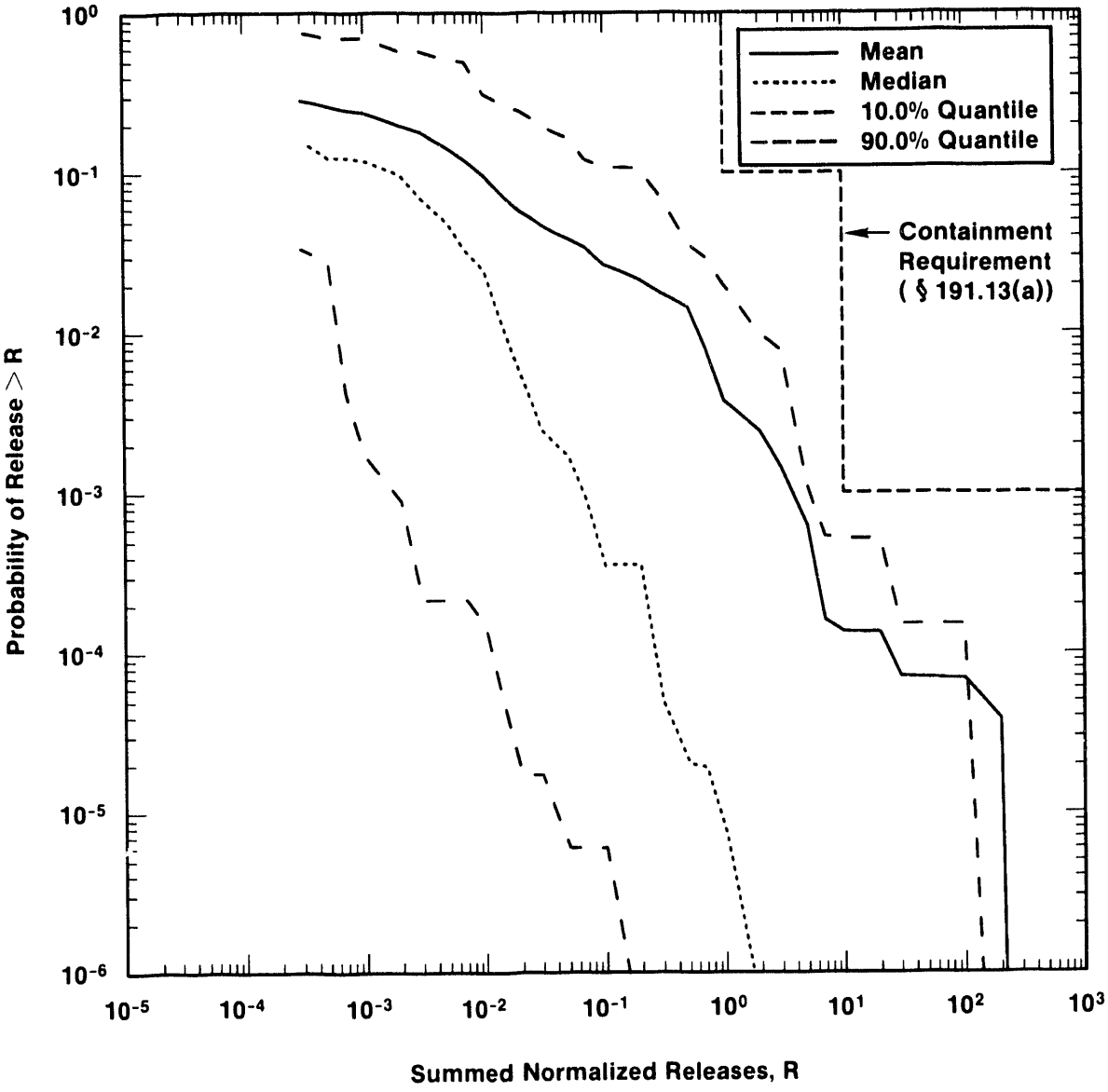


TRI-6342-1501-0

Figure 3-3. Example summary curves derived from an estimated distribution of CCDFs. The curves in this figure were obtained by calculating the mean and the indicated percentiles for each consequence value on the abscissa in Figure 3-2. The 90th-percentile curve crosses the mean curve due to the highly skewed distributions for exceedance probability. This skewness also results in the mean curve being above the median curve.

Garrick and the distributions indicated in Equation 3-5. This distinction has also been made by other authors, including Vesely and Rasmuson (1984), Paté-Cornell (1986), and Parry (1988).

For a given conceptual model in the WIPP performance assessment, subjective uncertainty enters the analysis due to lack of knowledge about quantities such as solubility limits, retardation factors, and flow fields. Stochastic uncertainty enters the analysis through the assumption that future exploratory drilling will be random in time and space (i.e., follows a Poisson process). However, the rate constant $\lambda$ in the definition of this Poisson process is assumed to be imprecisely known. Thus, subjective uncertainty exists in a quantity used to characterize stochastic uncertainty.

### 3.1.3 Risk and the EPA Limits

The EPA expressly identifies the need to consider the impact of uncertainties in calculations performed to show compliance with the Containment Requirements. Specifically, Appendix B of 40 CFR 191 suggests that

> ...whenever practicable, the implementing agency will assemble all of the results of the performance assessments to determine compliance with § 191.13 into a "complementary cumulative distribution function" that indicates the probability of exceeding various levels of cumulative release. When the uncertainties in parameters are considered in a performance assessment, the effects of the uncertainties considered can be incorporated into a single such distribution function for each disposal system considered. The Agency assumes that a disposal system can be considered to be in compliance with [section] 191.13 if this single distribution function meets the requirements of [section] 191.13(a) (U.S. EPA, 1985, p. 38088).

The representation for risk in Equation 3-1 provides a conceptual basis for the calculation of the complementary cumulative distribution function (CCDF) for normalized releases specified in 40 CFR 191B. Further, this representation provides a structure that can be used for both the incorporation of uncertainties and the representation of the effects of uncertainties.

Each CCDF in the family of CCDFs that results from Eq. 3-7 would be the appropriate choice for comparison against the EPA requirements, *if* $\mathbf{x}_k$ contained the correct variable values for use in determining the $pS_i$ and $\mathbf{cS}_i$ *and if* the assumed conceptual models correctly characterize the disposal system. Increasing the sample size $nK$ will, in general, produce a better approximation of the true distribution of CCDFs, but will not alter the fact that the distribution of CCDFs is conditional on the assumptions of the analysis.

If $nK$ is large, displays of the complete family of CCDFs can be difficult to interpret. As discussed in the previous section, mean and percentile curves can be used to summarize the information contained in the family. Appendix B of 40 CFR 191 suggests that "the effects of the uncertainties considered can be incorporated into a single [CCDF]" (U.S. EPA, 1985; p. 38088), but 40 CFR 191 does not contain specific guidance on which curve should be compared to the Containment Requirements. In previous work, the mean curve has generally been proposed for showing compliance with § 191.13(a) (e.g., Cranwell et al., 1987, 1990; Hunter et al., 1986). Only mean curves are shown in Volume 1 of this report. Complete families of curves and the associated summary curves are presented in Volume 4 of this report.

Whenever a distribution of curves is reduced to a single curve, information on uncertainty is lost. Replicated Monte Carlo analyses can characterize the uncertainty in an estimated mean CCDF or other summary curve. However, representing the uncertainty in an estimated value in this way is quite different from displaying the variability or uncertainty in the population from which the estimate is derived. For example, the uncertainty in the estimated mean curve in Figure 3-3 is less than the variability in the population of CCDFs that was averaged to obtain this mean. Therefore, results of the preliminary WIPP performance assessments are displayed as both complete families of CCDFs (as illustrated in Figure 3-2) and summary curves (as illustrated in Figure 3-3).

Because CCDFs are conditional on the assumptions of the analysis, no single curve or family of curves from a single analysis can display conceptual model uncertainty. The WIPP performance assessment examines conceptual model uncertainty by repeating the complete Monte Carlo analysis for each alternative conceptual model, and comparing mean CCDFs. Only those portions of the analysis specific to the alternative conceptual models (e.g., selected parameter values or computational models) are altered. All other models and parameter values are the same in each analysis, and the two conceptual models are thus compared *ceteris paribus* (all other things being equal). The shift in the location of the CCDF provides a measure of the uncertainty introduced by the existence of alternative conceptual models, and provides the Project guidance on which alternative conceptual models have the greatest potential to affect disposal-system performance.

## 3.2 Selection of Scenarios

40 CFR 191 does not include the term scenario in its definition of performance assessment, referring instead only to events and processes that might affect the disposal system during the next 10,000 years. Considering the consequences of isolated events and processes, however, is not sufficient; the various combinations of events and processes that define possible future states of the disposal system must be considered in a complete analysis. Combinations of events and processes are referred to as scenarios in Bertram-Howery and Hunter (1989), Marietta et al. (1989), Cranwell et al. (1990), Bertram-Howery et al. (1990), and WIPP PA Division (1991a).

### 3.2.1 Conceptual Basis for Scenario Development

The scenarios $S_i$ are obtained by subdividing a set $S$ (the sample space) that contains all possible 10,000-year time histories at the WIPP beginning at the decommissioning of the facility. Because resources for analysis are finite and the set $S$ has infinitely many elements, an important goal of scenario development is to recognize and remove from full consideration those scenarios for which the impact on compliance with 40 CFR 191B can be reasonably anticipated to be negligible due to low probability, low consequences, or regulatory exclusion.

Five subsets of $S$ provide a starting point for scenario development (Figure 3-4). The reasoning behind selecting these subsets is provided in Section 4.2.3 of this volume. First, the base-case subset $S_B$ consists of all elements in $S$ that fall within the bounds of what can be reasonably anticipated to occur at the WIPP over

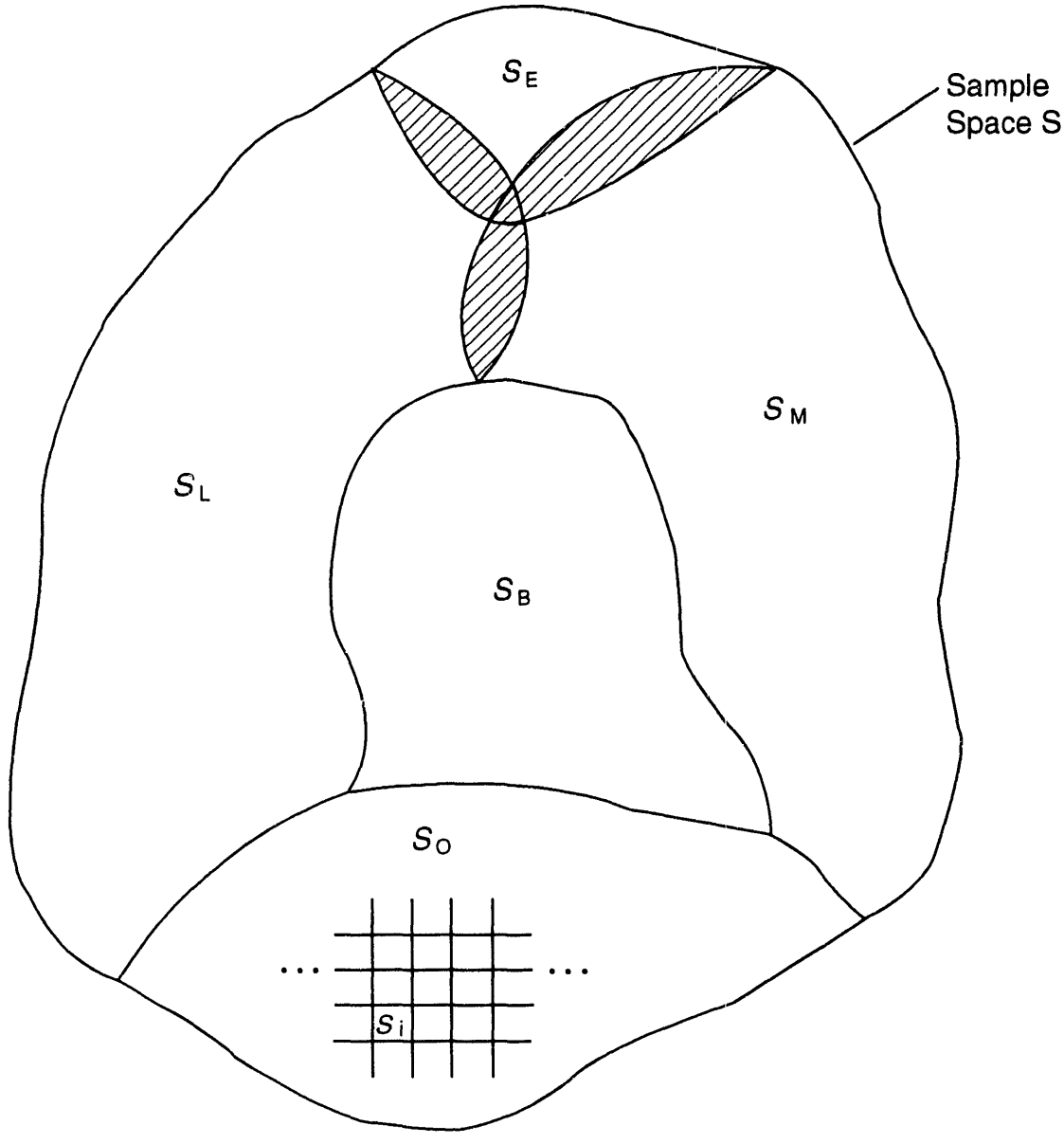


Figure 3-4. Decomposition of the sample space $S$ into high-level subsets, where $S_B$ designates the base-case subset, $S_M$ designates a minimal disruption subset, $S_E$ designates a regulatory exclusion subset, $S_L$ designates a low-probability subset, and $S_O$ designates $\left(S_B \cup S_M \cup S_E \cup S_L\right)^c$.

10,000 years, and represents the undisturbed performance of the disposal system. Second, a minimal disruption subset $S_M$ consists of all elements in $S$ that involve disruptions that result in no significant perturbation to the consequences associated with the corresponding elements in the base-case subset $S_B$. Third, a regulatory exclusion subset $S_E$ consists of all elements in $S$ that are excluded from consideration by regulatory directive (e.g., human intrusions more severe than the drilling of exploratory boreholes). Fourth, a low-probability subset $S_L$ consists of elements of $S$ not contained in $S_B$ whose collective probability is small (e.g., the probability of $S_L$ is less than 0.0001) regardless of their potential consequences. Everything that remains in $S$ after the identification of $S_B$, $S_M$, $S_E$, and $S_L$ now becomes a fifth subset $S_O$, where the subscript $O$ represents "Other." In set notation,

$$S_O=\left(S_B\cup S_M\cup S_E\cup S_L\right)^c \tag{3-8}$$

where the superscript $c$ is used to designate the complement of a set.

Evaluation of compliance with the Containment Requirements of 40 CFR 191B does not depend equally on each of the five subsets of $S$. By definition, elements of $S_E$ are excluded from consideration. The relative contributions of the other four subsets to a hypothetical CCDF for the WIPP are shown in Figure 3-5. Releases associated with the base case $S_B$ for the WIPP are zero for this analysis (see Chapter 5 of Volume 1 and references cited there), and the consequences of both $S_B$ and $S_M$ therefore plot well below the EPA limits, at the extreme upper left of the CCDF. Consequences of $S_L$ are by definition of sufficiently low probability (less than $10^{-4}$ in $10^4$ years) that they plot below the EPA limits. High-consequence elements of $S_L$ plot at the lower right of the CCDF. Compliance depends primarily therefore on the examination of $S_O$, and specifically on a set of additional scenarios $S_i$, $i$=1, ..., $nS$, obtained by further refining (i.e., subdividing) the subset $S_O$. $S_E$, $S_L$, and $S_M$ could be defined to be mutually exclusive, but this distinction is not important here so they are represented in Figure 3-4 with non-empty intersections. As described in Section 4.2.1, $S_B$ and $S_O$ are constructed to be mutually exclusive and to have empty intersections with $S_M$ and $S_L$.

Although the scenarios that affect compliance for the WIPP come from the set $S_i$, performance assessments must also include $S_B$. The overall pattern of Figure 3-5 can be seen in the results of the WIPP preliminary performance assessments, with $S_B$ determining the upper left of the CCDF and the remainder being determined by the $S_i$.

This analysis does not exclude $S_L$ from consideration in the comparison with the EPA release limits. The contribution from $S_L$ would always plot to the lower right of the CCDF, well below the EPA probability limits, and therefore would not matte. in a compliance decision. $S_M$ is not included in WIPP PA so the probability of $S_M$ is not accumulated as shown in Figure 3-5, i.e., only the probability of $S_B$ is included. The net effect of excluding $S_M$ is to raise the CCDF toward the probability limits; therefore, including $S_M$ would not negate a compliance decision.

Consequences of $S_M$ cannot be seen on the CCDF for the WIPP because releases from $S_B$ are zero. Consequences of $S_L$, which, if calculated, would appear as an extension on the extreme lower right of the CCDF, are also not displayed directly in the results of the WIPP performance assessments.

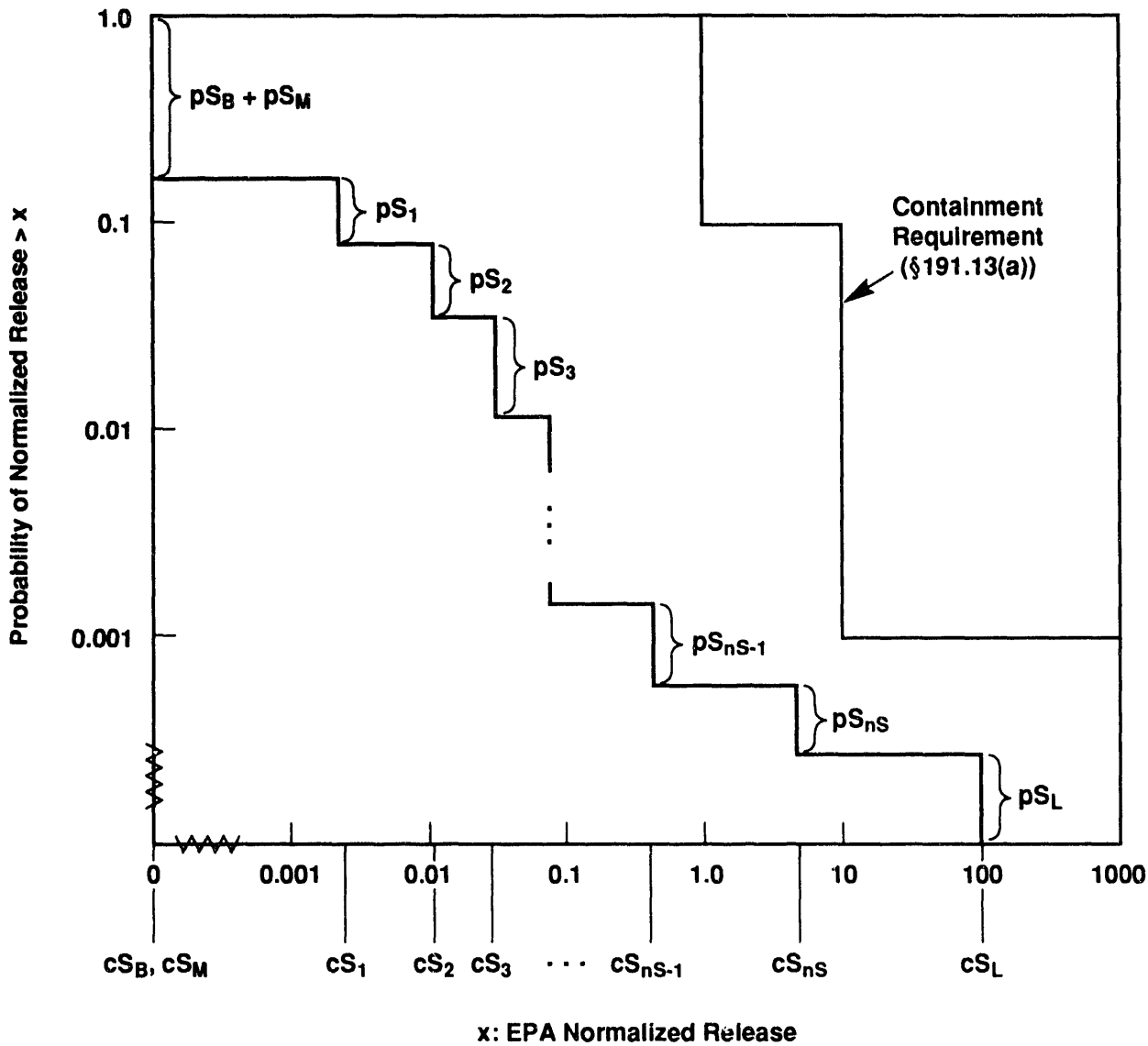


Notation: $pS_B, pS_M, pS_1, pS_2, \ldots, pS_{nS}, pS_L$ probability for corresponding scenario

$cS_B, cS_M, cS_1, cS_2, \ldots, cS_{nS}, cS_L$ consequence for corresponding scenario

$S_1, S_2, \ldots, S_{nS}$ assumed to be ordered so that $cS_1 \leq cS_2 \leq \ldots \leq cS_{nS}$

TRI-6342-1278-0

Figure 3-5. Construction of a CCDF for comparison with the EPA release limits. Note that the location of $cS_B$ at the lower left of the plot is correct for the WIPP—where no releases are predicted from the undisturbed base case—but is not a generic requirement for all sites.

The WIPP performance assessment does not follow the exact EPA guidance in defining $S_L$. Appendix B of 40 CFR 191 suggests that "... performance assessments need not consider categories of events or processes that are estimated to have less than one chance in 10,000 of occurring over 10,000 years" (U.S. EPA, 1985, p. 38088). By suitably defining the events and processes selected for consideration (i.e., by making $nS$ sufficiently large), all probabilities can theoretically be made less than the specified bound. Conceptually, the WIPP performance assessment avoids the potential problems raised by the wording of the guidance by placing a bound on the total probability of all occurrences that are removed from detailed consideration (i.e., the probability $pS_L$ for $S_L$) rather than the individual probabilities for a number of different scenarios. In practice, the distinction has little impact because, as discussed later in Chapter 4 of this volume, probabilities estimated for elements of $S_L$ are substantially below the suggested cutoff.

### 3.2.2 WIPP Performance-Assessment Approach to Scenario Development

Recognition of the five subsets of $S$ provides the basis for the WIPP performance assessment's approach to scenario development. Because $S_B$, $S_E$, $S_L$, and $S_M$ may account for a large part of the sample space $S$ and also have readily predicted effects on the CCDF used for comparison with the EPA release limits, $S_B$, $S_E$, $S_L$, and $S_M$ are determined in the first stage of development before $S_O$ is subdivided into the scenarios $S_i$ shown in Figure 3-4.

The WIPP performance assessment uses a two-stage procedure for scenario development and the determination of scenario probabilities. The purpose of the first stage is to develop a comprehensive set of scenarios that includes all occurrences that might reasonably take place at the WIPP, and to determine the probabilities of these scenarios. The result of this stage is a set of scenarios that summarize what might happen at the WIPP. These scenarios provide a basis for discussing the future behavior of the WIPP and a starting point for the second stage of the procedure, which is the definition of scenarios $S_i$ and the determination of the probabilities $pS_i$ at a level of detail that is appropriate for use with the conceptual and computational models employed in the performance assessment.

The first stage of the analysis focuses on the determination of the sample space $S$ and the subsets $S_B$, $S_E$, $S_L$, $S_M$ and $S_O$. Major groupings of scenarios within $S_O$ are also recognized at this time, and defined for reference purposes as summary scenarios. This stage of the analysis uses a scenario-selection procedure suggested by Cranwell et al. (1990) that consists of the following five steps: (1) compiling or adopting a "comprehensive" list of events and processes that potentially could affect the disposal system, (2) classifying the events and processes to aid in completeness arguments, (3) screening the events and processes to identify those that can be eliminated from consideration in the performance assessment, (4) developing scenarios by combining the events and processes that remain after screening, and (5) screening scenarios to identify those that have little or no effect on the shape or location of the mean CCDF.

The purpose of the first step is to develop the sample space $S$, which consists of all possible 10,000-year time histories that involve the identified events and processes. The sample space $S$ is subdivided into the subsets $S_B$, $S_E$, $S_L$, $S_M$, and $S_O$ in Steps 2 and 3. The screening associated with Steps 2 and 3 also removes time

histories from $S$ that are physically unreasonable. In Step 4, a preliminary subdivision of the subset $S_O$ into additional summary scenarios is accomplished through a two-part process. In the first part, subsets of $S_O$ (i.e., scenarios) are defined that involve specific events or processes. However, these scenarios are not mutually exclusive. In the second part, a subdivision of $S_O$ into mutually exclusive scenarios $S_i$ is accomplished by forming all possible intersections of the single event/process scenarios and their complements. The fifth and final step in the process is a screening of the scenarios $S_i$ on the basis of probability, consequence, and physical reasonableness. The purpose of this screening is to determine if some of the $S_i$ can be removed from the analysis.

A second stage of scenario development is necessary because the summary scenarios developed in the first stage are, in general, not defined at sufficiently fine levels of resolution for use in the construction of a CCDF that adequately displays the effects of stochastic, or Type-A, uncertainty (Section 3.1.2). The computational scenarios described in Section 4.4 of this volume represent a substantially finer subdivision of $S_O$ than that used to construct the summary scenarios, but they are based on the same screening of events and processes conducted during the first stage of scenario development. As in previous scenario construction for preliminary performance assessments of the WIPP, inadvertent intrusion into the repository during exploratory drilling is the only disruptive event considered in the 1992 assessment, and the computational scenarios reflect subdivisions based on time and number of intrusion, the activity of the waste intersected, and whether or not pressurized brine is encountered in the Castile Formation below the repository.

The determination of both scenarios and scenario probabilities is a complex process with significant uncertainties. To help assure that the WIPP performance assessment brings a broad perspective to this task, expert panels have been formed to provide a diversity of views with respect to possible futures at the WIPP and the probability of human intrusion. The formation of these panels and the results obtained from their deliberations are documented in Hora et al. (1991) and the memorandum by Hora in Volume 3, Appendix A of this report.

No inherently correct grouping exists of the possible time histories into scenarios; the probabilities associated with individual scenarios $S_i$ can always be reduced by using a finer grouping. As long as low-probability $S_i$ are not discarded, the use of more but lower probability $S_i$ will improve the resolution in the estimated CCDF shown in Figure 3-1. Because a consequence must be calculated for each scenario $S_i$, the use of more $S_i$ results in more detailed specification of the calculations that must be performed for each scenario.

For example, a scenario $S_i$ for the WIPP might be defined by

$$S_i = \{x : x \text{ a single 10,000-year time history beginning at decommissioning of the facility under consideration in which a single borehole occurs}\}. \quad (3\text{-}9)$$

A more refined definition would be

$S_{ik} = \{x : x$ a 10,000-year history at the WIPP beginning at decommissioning in which a single borehole occurs between $(i-1)\times 10^3$ and $i \times 10^3$ years and no boreholes occur during any other time interval$\}$. (3-10)

Then,

$$S_{ik} \subset S_i, i = 1,\ldots,10, \text{ and } S_i = \bigcup_{k=1}^{10} S_{ik} \quad (3\text{-}11)$$

Thus, $S_i$ and $\cup_k S_{ik}$ contain the same set of time histories. However, the individual $S_{ik}$ are smaller sets of time histories that are included in the larger set $S_i$. In terms of performance assessment, each $S_{ik}$ describes a more specific set of conditions that must be modeled than does $S_i$. The estimated CCDF in Figure 3-1 could be constructed with either $S_i$ or the $S_{ik}$, although the use of the $S_{ik}$ would result in less aggregation error, and thus, provide better resolution in the resultant CCDF.

The $S_i$ appearing in the definition of risk in Equation 3-1 should be developed to a level of resolution at which it is possible to view the analysis for each $S_i$ as requiring a fixed, but possibly imprecisely known, vector $\mathbf{x}$ of variable values. When a set $S_i$ is appropriately defined, it should be possible to use the same model or models and the same vector of variable values to represent every occurrence (e.g., a 10,000-year time history for the WIPP) in $S_i$. Scenario definition must permit the consequences $\mathbf{cS}_i$ appearing in Equation 3-1 to be calculated with reasonable efficiency, while holding the amount of aggregation error that enters the analysis to a reasonable level. Thus, although subdivision of $S$ into a large number of $S_i$ (e.g., on the basis of time of intrusion) may result in increased resolution in the estimate of $\mathbf{cS}$, it may also result in a computationally impractical analysis. Performance assessments must balance these competing requirements.

## 3.3 Determination of Scenario Probabilities

The second element of the ordered triples shown in Equation 3-1 is the scenario probability $pS_i$. As with scenario definition, the probabilities $pS_i$ have been developed at two levels of detail.

Preliminary probabilities for the summary scenarios have been developed by Marietta et al. (1989) and Guzowski (1991). Apostolakis et al. (1991) provide an additional discussion of techniques for determining probabilities in the context of performance assessment for radioactive-waste disposal.

Probabilities for the computational scenarios used in the construction of CCDFs are discussed in Chapter 5 of this volume, and are based on the assumption that the occurrence of boreholes through the repository follows a Poisson process (i.e., are random in time and space) with a rate constant $\lambda$. Formulas for determining $pS_i$ dependent on this assumption are derived in Chapter 5. The derivations are general and include both the stationary (i.e., constant $\lambda$) and nonstationary (i.e., time-dependent $\lambda$) cases. The 1992 performance assessment estimates consequences using both constant values for $\lambda$ and time-dependent values derived from expert judgment.

## 3.4 Calculation of Scenario Consequences

The third element of the ordered triples shown in Equation 3-1 is the scenario consequence, $\mathbf{cS}_i$. Estimation of $\mathbf{cS}_i$ is done using a linked system of computational models described in greater detail in Chapters 7 and 8 of this volume.

The models used in the WIPP performance assessment, as in other complex analyses, exist at four different levels. First, conceptual models provide a framework in which information about the disposal system can be organized and linked to processes that can be simulated with quantitative models. An adequate conceptual model is essential for both the development of the sample space $S_O$ appearing in Equation 3-8 and the division of $S_O$ into the scenarios $S_i$ appearing in Equation 3-1. As defined in Chapter 2, alternative conceptual models may exist that are equally consistent with the available information. Consequences for each scenario must be estimated separately for each alternative conceptual model included in the analysis.

Second, mathematical models are developed to represent the processes at the site. The conceptual models provide the context within which these mathematical models must operate and define the processes they must characterize. The mathematical models are predictive in the sense that, given known properties of the system and possible perturbations to the system, they predict the response of the system. Among the processes represented by these mathematical models are fluid flow, mechanical deformation, radionuclide transport in groundwater, removal of waste through intruding boreholes, and human exposure to radionuclides released to the surface environment. Mathematical models for these processes, and others, are described in Chapter 7 of this volume.

Third, numerical models are developed to approximate the mathematical models. Most mathematical models do not have closed-form solutions, and numerical procedures must be developed to provide approximations to the solutions of the mathematical models. In essence, these approximations provide "numerical models" that calculate results that are close to the solutions of the original mathematical models. For example, Runge-Kutta procedures are often used to solve ordinary differential equations, and finite difference and finite element methods are used to solve partial differential equations. In practice, it is unusual for a mathematical model to have a solution that can be determined without the use of an intermediate numerical model. Numerical models used in the WIPP performance assessment are described in appendices to this volume.

Fourth, the complexity of the system requires the use of computer codes to implement the numerical models. Figure 3-6 illustrates the sequence of linked codes used in the 1992 WIPP performance assessment. Each of the models appearing in this figure is briefly described in Table 3-1; more information is available in Chapter 7 and appendices to this volume, and in references cited there.

## 3.5 Monte Carlo Analysis Techniques

As discussed in more detail by Helton et al. (1991) and in Volume 4 of this report, the WIPP performance assessment uses Monte Carlo techniques for uncertainty and sensitivity analyses. In the context of this report, uncertainty analyses evaluate uncertainty in performance estimates that results both from the existence of alternative conceptual models and from the uncertainty about imprecisely known input variables. Sensitivity anal-

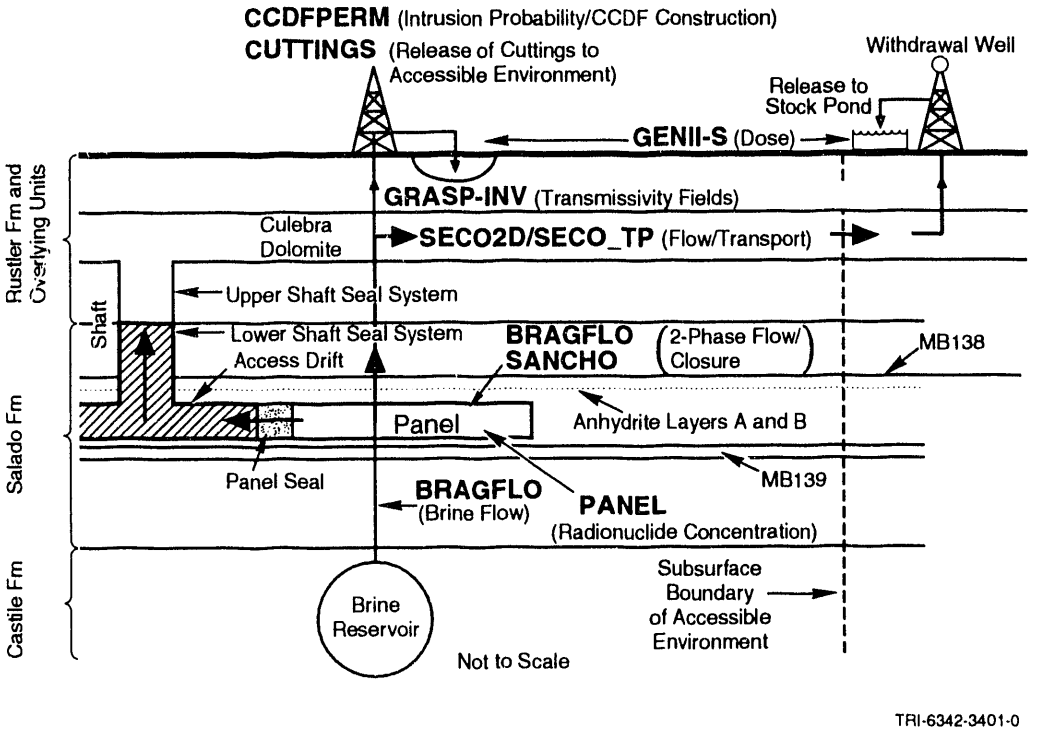


Figure 3-6. Models used in 1992 WIPP performance assessment. The names for computer models (i.e., computer codes) are shown in capital letters.

Table 3-1. Summary of Computer Models Used in the 1992 WIPP Performance Assessment

| Model | Description |
|---|---|
| BRAGFLO | Describes the multiphase flow of gas and brine through a porous, heterogenous reservoir. BRAGFLO solves simultaneously the coupled partial differential equations that describe the mass conservation of gas and brine along with appropriate constraint equations, initial conditions, and boundary conditions (Chapter 7). |
| CCDFPERM | Constructs probabilities for various computational scenarios associated with human intrusion by exploratory drilling (Section 1.4.2 of Volume 3). |
| CUTTINGS | Calculates the quantity of radioactive material (in curies) brought to the surface as cuttings and cavings generated by an exploratory drilling operation that penetrates a waste panel (Chapter 7). |
| GENII-S | Estimates potential radiation doses to humans from radionuclides in the environment (Leigh et al., in review). |
| GRASP-INV | Automatically generates simulations of transmissivity fields (estimates of transmissivity values) conditioned on measured transmissivity values and calibrated to steady-state and transient pressure data at well locations using an adjoint sensitivity and pilot-point technique (LaVenue and RamaRao, 1992). |
| PANEL | Calculates rate of discharge and cumulative discharge of radionuclides from a repository panel through an intrusion borehole. Discharge is a function of fluid flow rate, nuclide solubility, and remaining inventory (Chapter 7). |
| SANCHO | Finite element program that solves quasistatic, large deformation, inelastic response of two-dimensional solids (Stone et al., 1985). Used in the 1992 performance assessment to determine porosity of the waste as a function of time and moles of gas generated (Section 1.4.7 of Volume 3). |
| SECO2D | Calculates single-phase Darcy flow for groundwater-flow problems in two dimensions. The formulation is based on a single partial differential equation for hydraulic head using fully implicit time differencing (Chapter 7). |
| SECOTP | Simulates fluid flow and transport of radionuclides in fractured porous media (Chapter 7). |

yses determine the contribution of individual input variables to the uncertainty in model predictions. As used here, both these types of analyses provide information about the effects of subjective, or Type-B, uncertainty. The effects of stochastic, or Type-A, uncertainty are incorporated into the performance assessment through the scenario probabilities $pS_i$ appearing in Equation 3-1.

Monte Carlo analyses involve five steps: (1) selection of the variables to be examined and the ranges and distributions for their possible values; (2) generation of the samples to be analyzed; (3) propagation of the samples through the analysis; (4) uncertainty analysis; and (5) sensitivity analysis. These steps are described briefly in the following sections. A more complete discussion can be found in Helton et al. (1991).

### 3.5.1 Selection of Variables and Their Ranges and Distributions

Monte Carlo analyses use a probabilistic procedure for the selection of model input. Therefore, the first step in a Monte Carlo analysis is the selection of uncertain variables and of ranges and distributions that characterize the uncertainty in their possible values. These variables are typically input parameters to computer models, and the impact of the assigned ranges and distributions can be great: analysis results are controlled in large part by the choice of input. Results of uncertainty and sensitivity analyses, in particular, strongly reflect the characterization of uncertainty in the input data.

As discussed in detail in Volume 3 of this report, information about the ranges and distributions of possible values is drawn from a variety of sources, including field data, laboratory data, literature, and, in instances where significant uncertainty exists and site-specific information is unavailable or insufficient at the time of the analyses, subjective expert judgement. In general, data from these sources cannot be examined statistically and incorporated directly in performance-assessment analyses, because data are rarely gathered with the specific model application in mind. Spatial and temporal scales over which the data are valid often do not match those of the models' applications, and in many cases, real site-specific data are simply not available. Data may be sparse or unavailable because measurements are infeasible (e.g., drilling sufficient boreholes to determine the regional heterogeneity of transmissivity in overlying aquifers), because direct measurements would in themselves create risk (e.g., drilling of boreholes through the repository to determine the extent of an underlying brine reservoir), because measurements are impossible (e.g., measuring future drilling technology), or for other reasons.

The review process that leads from the available data to the construction of the cumulative distribution functions (cdfs) used in the performance-assessment analyses is described in detail in Volume 3 of this report. Because of the nature of the available data and the type of analysis, this review process is unavoidably subjective, and involves the expert judgment of the investigators and performance-assessment analysts.

The ultimate outcome of the review process is a distribution function $F(x)$ of the form shown in Figure 3-7 for each independent variable of interest. For a particular variable $x_j$, the function $F$ is defined such that

$$\text{prob}\left(x < x_j \leq x + \Delta x\right) = F(x + \Delta x) - F(x) \tag{3-12}$$

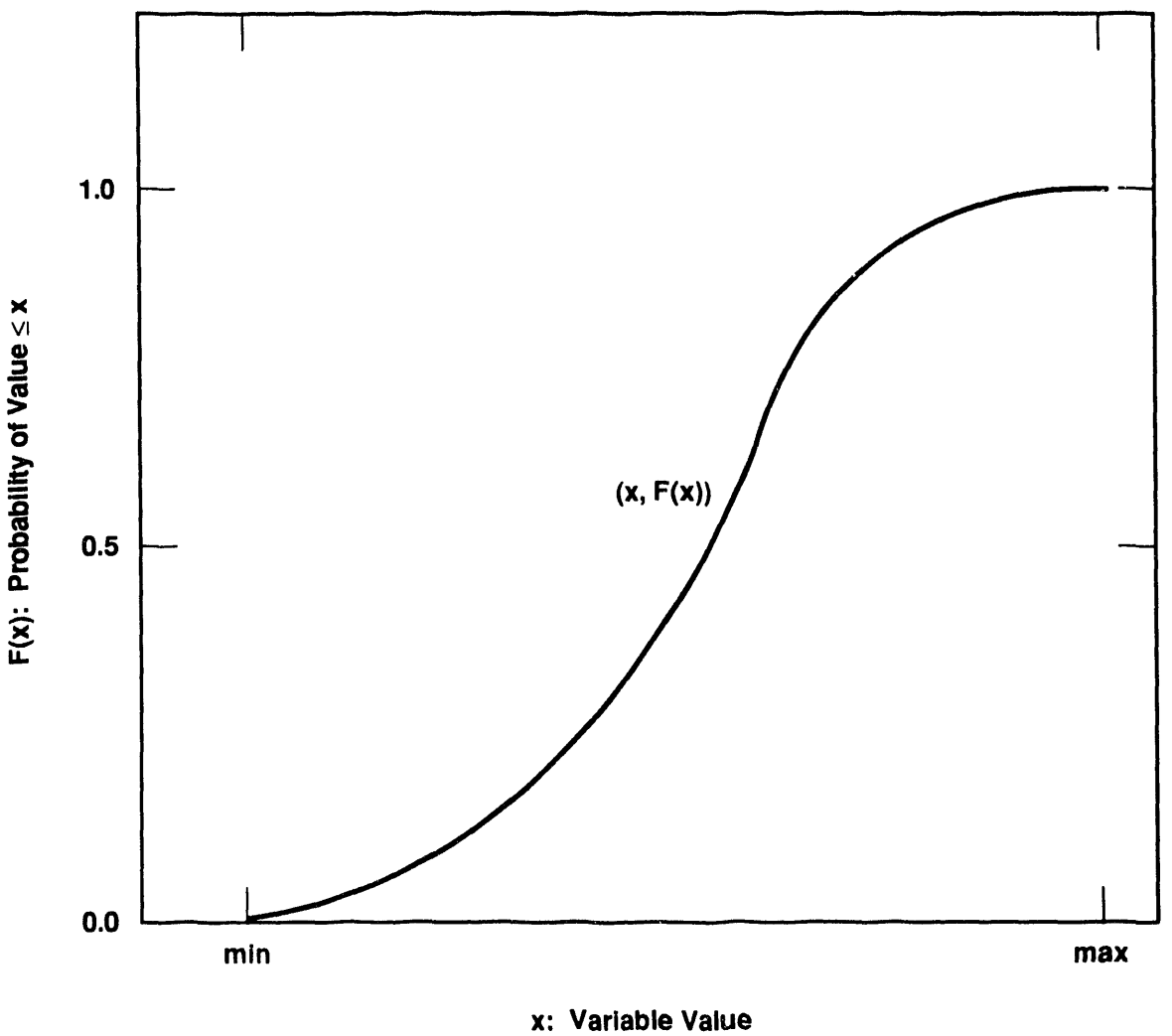


Figure 3-7. Distribution function for an imprecisely known analysis variable. For each value $x$ on the abscissa, the corresponding value $F(x)$ on the ordinate is the probability that the appropriate value to use in the analysis is less than or equal to $x$ (Helton et al., 1991).

That is, $F(x+\Delta x) - F(x)$ is equal to the probability that the appropriate value to use for $x_j$ in the particular analysis under consideration falls between $x$ and $(x + \Delta x)$.

### 3.5.2 Generation of the Sample

Various techniques are available for generating samples from the assigned distribution functions for the variables (McGrath et al., 1975; McGrath and Irving, 1975a,b), including random sampling, stratified sampling, and Latin hypercube sampling. As discussed in more detail in Helton et al. (1991), the WIPP performance assessment uses stratified sampling and Latin hypercube sampling.

Stratified sampling is a modification of random sampling in which a systematic coverage of the full range of possible values is forced by subdividing the sample space into strata with assigned probabilities. The decomposition of the subset $S_O$ shown in Equation 3-8 into scenarios $S_i$ as indicated in Equation 3-1 is a form of stratified sampling in which the scenario probabilities $pS_i$ are the strata probabilities. Stratified sampling forces the inclusion of low-probability, but possibly high-consequence, scenarios, and is used to incorporate stochastic, or Type-A, uncertainty into the WIPP performance assessment.

Latin hypercube sampling (McKay et al., 1979), in which the full range of each variable is subdivided into intervals of equal probability and samples are drawn from each interval, is used to incorporate subjective, or Type-B, uncertainty, into the WIPP performance assessment. Specifically, a Latin hypercube sample of size 70 was generated from the 49 variables in Tables 6.0-1, -2, and -3 in Volume 3 of this report. The restricted pairing technique of Iman and Conover (1982) was used to prevent spurious correlations within the sample. The resultant sample is listed in Volume 4 of this report.

### 3.5.3 Propagation of the Sample through the Analysis

The next step is the propagation of the sample through the analysis. Each element of the sample is supplied to the model as input, and the corresponding model predictions are saved for use in later uncertainty and sensitivity studies. The Compliance Assessment Methodology Controller (CAMCON) has been developed to facilitate the complex calculations and storage of the input and output files from each program (Rechard, 1989, 1992). This methodology incorporates data bases, sampling procedures, model evaluations, data storage, uncertainty and sensitivity analysis procedures, and plotting capabilities into a unified structure. The structure and operation of CAMCON is illustrated in Figure 1-1.

Additional information on CAMCON and its use in the 1992 WIPP performance assessment is given in Chapter 1 of this volume and in Rechard (1992).

## 3.5.4 Uncertainty Analysis

Once a sample has been generated and propagated through a model, uncertainty in the model predictions can be interpreted directly from the CCDF. Stochastic, or Type-A, uncertainty, is represented by the steps in an individual CCDF. Subjective, or Type-B, uncertainty, can be represented either with a family of CCDFs or with a summary diagram showing mean and quantile curves, as shown in Figures 3-2 and 3-3.

Uncertainty in a predicted performance measure can be characterized with an estimated distribution function, which can be displayed either as the above CCDF, a density function, a cumulative distribution function, or as box plots (Iman and Conover, 1982), as shown in Figure 3-8. The endpoints of the boxes in Figure 3-8 are formed by the lower and upper quartiles of the data, that is, $x_{.25}$ and $x_{.75}$. The vertical line within the box represents the median, $x_{.50}$. The sample mean is identified by the large dot. The bar on the right of the box extends to the minimum of $x_{.75} + 1.5(x_{.75} - x_{.25})$ and the maximum observation. In a similar manner, the bar on the left of the box extends to the maximum of $x_{.25} - 1.5(x_{.75} - x_{.25})$ and the minimum observation. The observations falling outside of these bars are shown with $x$'s. Box plots display the same information as a distribution function in a reduced form (without explicit probabilities). They are convenient for presenting and comparing different distributions in a single figure, especially for displaying outliers (high consequence values).

## 3.5.5 Sensitivity Analysis

The final step in a Monte Carlo study is sensitivity analysis, which provides information about the sensitivity of the modeling system to uncertainty in specific input parameters. Sensitivity analyses can identify those parameters for which reductions in uncertainty (i.e., narrowing of the range of values from which the sample used in the Monte Carlo analysis is drawn) have the greatest potential to increase confidence in the estimate of disposal-system performance. Identification of sensitive parameters can help set priorities for additional research; however, because results of these analyses are inherently conditional on the models, data distributions, and techniques used to generate them, the analyses cannot provide insight about the correctness of the conceptual models and data distributions used. Qualitative judgment about the modeling system must be used in conjunction with sensitivity analyses to set priorities for performance-assessment data acquisition and model development.

Sensitivity analysis techniques used in the WIPP performance assessment include scatterplots and regression analysis, and are described in detail by Helton et al. (1991). Results of the 1992 sensitivity analyses are presented in Volume 4 of this report.

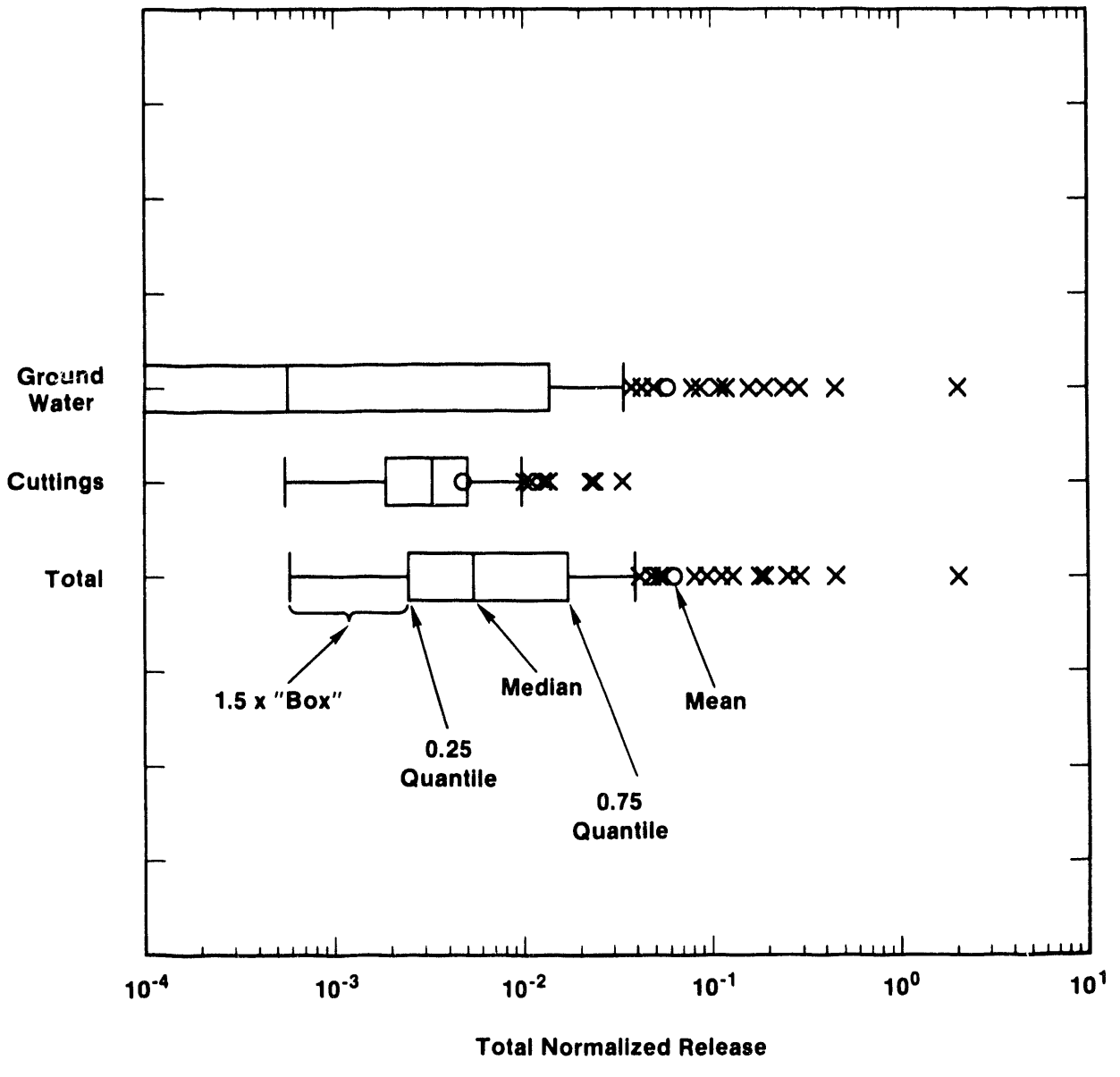


Figure 3-8. Example of box plots (hypothetical results).

# 4. SCENARIO CONSTRUCTION

## 4.1 Evaluation of Events and Processes

The selection of scenarios for consideration in WIPP PA is based on the formal five-step procedure described by Cranwell et al. (1990). The five steps are (1) compiling or adopting a comprehensive set of events and processes* that potentially could affect the disposal system, (2) classifying the events and processes to aid in completeness arguments, (3) screening the events and processes to identify those that can be eliminated from consideration in the PA, (4) developing scenarios by combining the events and processes that remain after screening, and (5) screening scenarios to identify those that have little or no effect on the shape or location of the CCDFs. Section 4.1 summarizes work done on the first three of these steps: the identification, classification, and screening of events and processes, referred to jointly as "evaluation of events and processes." Evaluation of events and processes has not been significantly revised since 1991, and more complete discussions of specific events and processes are available elsewhere (Guzowski, 1990; WIPP PA Division, 1991a). Additional work is in progress on evaluation of events and processes in response to reviewers' comments (e.g., Appendix B of Volume 1 of this report), and will be incorporated in future PAs.

### 4.1.1 Identifying Events and Processes

The WIPP PA uses the list of potentially disruptive events and processes provided by Cranwell et al. (1990) as a starting point for scenario development (Table 4-1). This list was developed by a panel of experts that met in 1976 and again in 1977 under the auspices of the U.S. Nuclear Regulatory Commission to identify events and processes that could compromise the performance of an engineered disposal system for nuclear waste constructed in deep geologic media.** Concerns raised during the development of the WIPP have led to the inclusion of three additional events and processes not identified by the panel: gas generation by the degradation of the waste, waste-related explosions, and nuclear criticality.

---

* Note that classification of a phenomenon as an event rather than a process, or vice versa, has no affect on scenario development. The distinction in terminology is based on 40 CFR 191B (§191.13(a)), and has been interpreted to describe the time interval over which a phenomenon occurs relative to the time interval of interest. Events are relatively brief whereas processes may occur during a large portion of the time interval of interest. The distinction is not rigid, however, and the terms are functionally interchangeable in scenario development.

** As listed in Cranwell et al. (1990), the Scenario Identification Panel Members and their affiliations were William S. Twenhofel, United States Geological Survey (USGS), Denver, CO; William W. Dudley, USGS, Denver, Co; Randolph Stone, Lawrence Livermore National Laboratory, Livermore, CA; Frederick J. Pearson, USGS, Reston, VA; Herbert R. Shaw, USGS, Menlo Park, CA; Donald Caldwell, United States Nuclear Regulatory Commission (USNRC), Washington, DC; Ben Ross, The Analytical Sciences Corp., Reading, MA; Edward Hawkins, USNRC, Washington, DC; and Martin Tierney, Sandia National Laboratories, Albuquerque, NM. Working sessions of this panel were held on December 7-8, 1976, at Grand Canyon, AZ, and again on April 13, 1977, in Carlsbad, NM.

Table 4-1. Potentially Disruptive Events and Processes

| | |
|---|---|
| **Natural Events and Processes** | |
| Celestial Bodies | Meteorite Impact |
| Surficial Events and Processes | Erosion/Sedimentation<br>Glaciation<br>Pluvial Periods<br>Sea-Level Variations<br>Hurricanes<br>Seiches<br>Tsunamis<br>Regional Subsidence or Uplift<br>Mass Wasting<br>Flooding |
| Subsurface Events and Processes | Diapirism<br>Seismic Activity<br>Volcanic Activity<br>Magmatic Activity<br>Formation of Dissolution Cavities<br>Formation of Interconnected Fracture Systems<br>Faulting |
| **Human-Induced Events and Processes** | |
| Inadvertent Intrusions | Explosions<br>Drilling<br>Mining<br>Injection Wells<br>Withdrawal Wells |
| Hydrologic Stresses | Irrigation<br>Damming of Streams and Rivers |
| Repository- and Waste-Induced Events and Processes | Caving and Subsidence<br>Shaft and Borehole Seal Degradation<br>Thermally Induced Stress Fracturing in Host Rock<br>Excavation-Induced Stress Fracturing in Host Rock<br>Gas Generation<br>Explosions<br>Nuclear Criticality |

Source: Modified from Cranwell et al., 1990.

### 4.1.2 Classifying Events and Processes

This step is optional, and has not been carried out explicitly for WIPP PA. Cranwell et al. (1990) included classification in the procedure to assist in organizing the events and processes, to assist in completeness arguments, and to provide insights when developing conceptual models of the disposal system.

### 4.1.3 Screening Events and Processes

Events and processes are screened using three criteria developed by Cranwell et al. (1990): probability of occurrence, consequence, and physical reasonableness; and a fourth criteria specific to PAs conducted for 40 CFR 191B, regulatory requirements. All four are applied in the context of the 1985 version of 40 CFR 191B (U.S. EPA, 1985), and screening will be reexamined when the regulation is repromulgated.

The "probability of occurrence" and "consequence" criteria are based directly on guidance provided in Appendix B of 40 CFR 191:

> The [EPA] assumes that . . . performance assessments need not consider categories of events or processes that are estimated to have less than one chance in 10,000 of occurring over 10,000 years. Furthermore, the performance assessments need not evaluate in detail the releases from all events and processes estimated to have a greater likelihood of occurrence. Some of these events and processes may be omitted from the performance assessments if there is a reasonable expectation that the remaining probability distribution of cumulative releases would not be significantly changed by such omissions (U.S. EPA, 1985, p. 38088).

As interpreted by the WIPP PA Department, individual events and processes (as well as "categories of events and processes") that have a probability of more than 1 chance in 10,000 of occurring over 10,000 years will be retained for further evaluation. Lower-probability phenomena are identified but not considered further. Low-consequence phenomena (i.e., those that would not significantly change the CCDF) are identified qualitatively in the WIPP PA methodology and are eliminated regardless of probability (WIPP PA Division, 1991a). Consequences of these phenomena can be evaluated quantitatively if uncertainties warrant.

The final screening criterion described by Cranwell et al. (1990), "physical reasonableness," is not explicitly described in 40 CFR 191B. As used in WIPP PA, this criterion distinguishes between those phenomena to which a meaningful probability can be assigned (e.g., meteorite impacts) and those phenomena for which scientific understanding is insufficient to assign meaningful and defensible quantitative probabilities (e.g., the occurrence of volcanic activity in a geologic setting where such an event is unprecedented). The distinction between "physical reasonableness" and "probability of occurrence" is not rigid, and phenomena identified as "physically unreasonable" could also be eliminated on the basis of extremely low probability.

The "regulatory requirements" criterion is used only to screen events related to human activities, and is based directly on guidance in Appendix B of 40 CFR 191:

> . . . inadvertent and intermittent intrusion by exploratory drilling for resources (other than any provided by the disposal system itself) can be the most severe intrusion scenario assumed by the implementing agencies (U.S. EPA, 1985, p. 38089).

As interpreted by the WIPP PA Department, this allows the exclusion of all deliberate human activities that disrupt the repository, as well as those inadvertent human activities that could result in consequences (e.g., EPA normalized cumulative releases to the accessible environment, or other performance measures) greater than those of exploratory drilling. Specifically, this criterion is used to screen acts of war, direct mining of the waste, systematic drilling of multiple boreholes for resource production or other purposes, and modes of intrusion other than exploratory drilling identified by an expert panel on inadvertent human intrusion into the WIPP (Hora et al., 1991; memorandum by Hora in Volume 3, Appendix A of this report).

### 4.1.4 Summary of Screened Events and Processes

The following summary is taken from the 1991 PA (WIPP PA Division, 1991a), where each of the events and processes listed in Table 4-1 are described in detail. As shown in Table 4-2, events and processes are either retained for consideration in PA or screened out on the basis of the four criteria described in the previous section. Events and processes retained for consideration are either included in the base-case scenario for the system or used for developing scenarios describing disturbed performance.

All of the natural events and processes listed in Table 4-1 that have been retained are part of the undisturbed performance of the system, and none are included in the development of disturbed-performance scenarios. Phenomena such as erosion, sedimentation, climatic change (pluvial periods), seismic activity, and some shallow dissolution are certain to occur during the next 10,000 years, and are part of the conceptual model for the base-case scenario. Several other listed events (i.e., sea-level variations, hurricanes, seiches, and tsunamis) are restricted to coastal areas, and are physically unreasonable at the WIPP location. Surficial geologic events, including regional subsidence or uplift, mass wasting, glaciation, and flooding, and all subsurface events except seismic activity and shallow dissolution of the Rustler-Salado contact are screened out as physically unreasonable or of low probability.

Of the human-induced events and processes, inadvertent explosions at the location of the waste panels are excluded by regulatory requirements; inadvertent explosions near the waste panels during warfare and nuclear testing are screened out on the basis of low probability. Irrigation and damming of valleys close enough to the WIPP to have an impact are low-probability events because of poor water and soil quality and limited water supplies. Based on the geologic setting and previous resource evaluations, both exploratory drilling for resources and the drilling of injection wells are realistic events for the WIPP, and are retained for scenario development. Intrusion of injection wells into the waste-emplacement region is not modeled explicitly in PA, because drilling technology and therefore consequences are assumed to be the same as for exploratory drilling. Expert judgment on the probability of intrusion by injection wells is not available (Hora, memo in Appendix A of Volume 3). Injection wells that do not penetrate the repository are screened out on the basis of low consequence.

Table 4-2. Summary of Screened Events and Processes (from WIPP PA Division, 1991a)

| Events and Processes | RETAINED | | SCREENED OUT | | | |
|---|---|---|---|---|---|---|
| | Base-Case Conditions | For Scenario Development | Low Probability | Physically Unreasonable | Low Consequence | Regulatory Requirements |
| Natural | | | | | | |
| Meteorite Impact | | | × | | | |
| Erosion/Sedimentation | × | | | | | |
| Glaciation | | | | × | | |
| Pluvial Periods (Climate Change) | × | | | | | |
| Sea-Level Variations | | | | × | | |
| Hurricanes | | | | × | | |
| Seiches | | | | × | | |
| Tsunamis | | | | | | |
| "Conventional" | | | | × | | |
| Meteorite Impact | | | × | | | |
| Regional Subsidence or Uplift | | | | × | | |
| Mass Wasting | | | | × | | |
| Flooding | | | | × | | |
| Diapirism | | | | × | | |
| Seismic Activity | × | | | | | |
| Volcanic Activity | | | | × | | |
| Magmatic Activity | | | | × | | |
| Formation of Dissolution Cavities | | | | | | |
| Deep Dissolution | | | | × | | |
| Shallow Dissolution | | | | | | |
| Rustler-Salado Contact | × | | | | | |
| Nash Draw* | | | × | × | | |
| Formation of Interconnected Fracture Systems | | | | × | | |
| Faulting | | | | × | | |

*Screening criterion depends on which possible mechanisms considered for origin of Nash Draw

Table 4-2. Summary of Screened Events and Processes (from WIPP PA Division, 1991a) (continued)

| Events and Processes | RETAINED | | SCREENED OUT | | | |
|---|---|---|---|---|---|---|
| | Base-Case Conditions | For Scenario Development | Low Probability | Physically Unreasonable | Low Consequence | Regulatory Requirements |
| Human-Induced | | | | | | |
| Explosions | | | | | | |
| At Waste-Panels Location | | | | | | × |
| Near Waste-Panels Location | | | | | | |
| At Surface/Warfare | | | × | | | |
| Deep Testing | | | × | | | |
| Drilling (Exploratory) | | × | | | | |
| Mining | | | | | | |
| At Waste-Panels Location | | | | | | × |
| Near Waste-Panels Location | | × | | | | |
| Injection Wells | | | | | × | |
| Withdrawal Wells | | | | | | |
| Water Wells | | × | | | | |
| Oil and Gas Wells | | | | | | |
| At Waste-Panels Location | | | | | | × |
| Near Waste-Panels Location | | | | | × | |
| Geothermal Wells | | | | | × | |
| Irrigation | | | × | | | |
| Damming of Streams and Rivers | | | | | | |
| At Pecos River | | | | | × | |
| Near Nash Draw | | | × | | | |
| Repository- and Waste-Induced | | | | | | |
| Subsidence and Caving | | | | | × | |
| Shaft & Borehole Seal Degradation | × | | | | | |
| Thermally Induced Fractures | | | | × | | |
| Excavation-Induced Fractures | × | | | | | |
| Gas Generation | × | | | | | |
| Explosions (Gas Ignition) | | | | | × | |
| Near Criticality | | | | | | |
| Critical Mass (Explosion) | | | × | | | |
| Sustained Reaction** | | | | | | |

** Retained for additional evaluation

In the category of waste- and repository-induced events and processes, gas generation and shaft-seal degradation are part of the conceptual model of the base-case scenario. Borehole seal degradation is addressed through parameter uncertainty during modeling. Excavation-induced fracturing in the host rock is handled by including the disturbed zone surrounding mined openings in the conceptual model of the base-case scenario. Caving into the rooms or drifts may occur in the short term after decommissioning, but this process has no long-term consequences on performance because of the mechanical behavior of salt. Thermally induced fracturing of the host rock is not a physically reasonable phenomenon because of the low thermal output of WIPP waste. Subsidence caused by the mined openings and explosions caused by the ignition of gases created by waste degradation have no effect on the long-term performance of the disposal system and can be eliminated from scenario development. Nuclear criticality requires additional evaluation before a screening decision is made.

As shown in Table 4-2, a total of 10 events and processes are retained for consideration following screening. Seven of these are essentially certain to occur, and are included in the conceptual model for the base-case scenario (see Section 4.2.3.1). The other three—exploratory drilling, potash mining near the waste panels, and water wells—are used to develop summary scenarios describing disturbed performance of the system. Exploratory drilling is subdivided into two possibilities: drilling into a waste-filled room or drift and a brine reservoir in the underlying Castile Formation (Event E1), and drilling into a waste-filled room or drift without penetrating a brine reservoir (Event E2). Mining (Event TS) is limited to potash extraction by either conventional or solution methods in areas beyond the boundaries of the waste panels; drilling of withdrawal wells (Event E3) is limited to water wells in areas where water quantity and quality will permit water use. Both mining and water wells will be evaluated in future performance assessments for their effects on groundwater flow in the WIPP area.

## 4.2 Summary Scenarios

### 4.2.1 Development of Summary Scenarios

As explained in the 1991 PA documentation (WIPP PA, 1991a, Section 4.1.7), logic diagrams based on the approach defined by Cranwell et al. (1990) are used to combine events and processes that remain after screening into summary scenarios. As the logic diagram for the WIPP performance assessment (Figure 4-1) shows, no temporal relationship between events and processes is implied by their sequence across the top of the diagram; at each junction within the diagram a yes/no decision is made as to whether the next event or process is added to the scenario. As a result, each scenario consists of a combination of occurrence and nonoccurrence of all events and processes that survive screening (Cranwell et al., 1990). To simplify scenario notation, only the events and processes that occur are used to identify the scenario. Based on the assumption that the events and processes remaining after screening define all possible futures of the disposal system that are important for a probabilistic assessment, the logic diagram produces scenarios that are comprehensive and mutually exclusive because all possible combinations of events and processes are developed, and each scenario is a unique set of events and processes.

Figure 4-1 shows all of the scenarios (the possible combinations of the four events) that survived the screening process for the WIPP (Section 4.1.4):

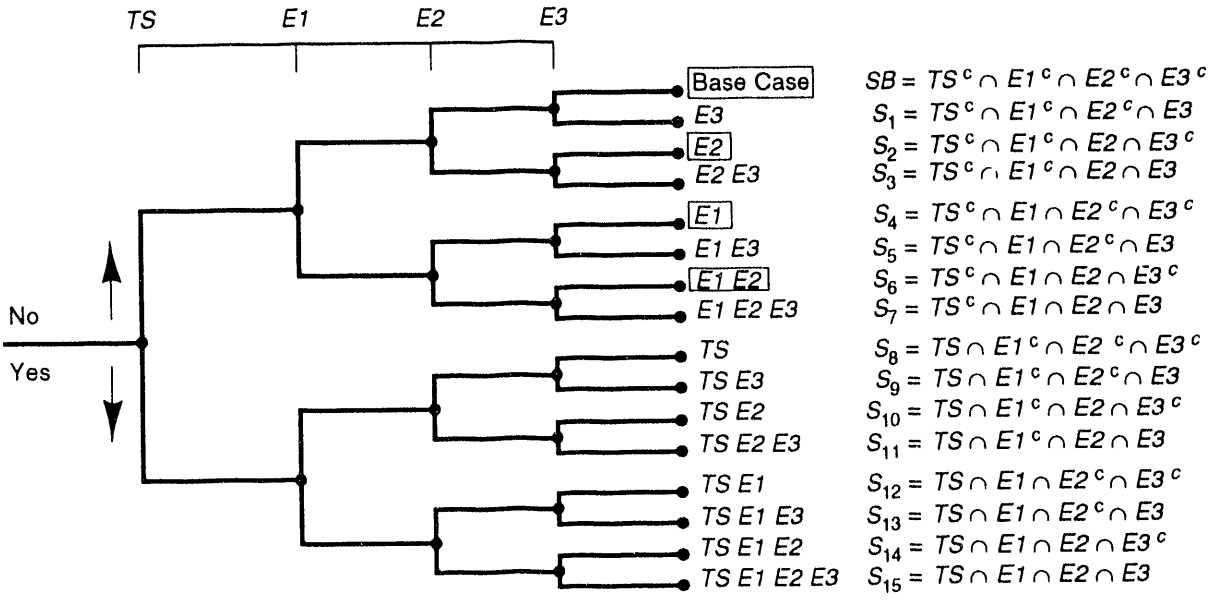


x = 10,000 yr Time History

*TS* = {x: Subsidence Resulting from Solution Mining of Potash}

*E1* = {x: One or More Boreholes Pass Through a Waste Panel and into a Brine Pocket}

*E2* = {x: One or More Boreholes Pass Through a Waste Panel Without Penetrating a Brine Pocket}

*E3* = {x: One or More Withdrawal Wells near Repository Where Water Quality Will Permit Water Use}

Superscript c (e.g., $TS^c$) Denotes Set Complement

TRI-6342-3436-0

Figure 4-1. Potential scenarios for the WIPP disposal system.

- E1, the inadvertent drilling of an exploratory borehole into a waste-filled room or drift and a brine reservoir in the underlying Castile Formation,

- E2, the inadvertent drilling of an exploratory borehole into a waste-filled room or drift that does not intersect a brine reservoir in the underlying Castile Formation,

- E3, drilling of water withdrawal wells in areas where water quality will permit water use, and

- TS, mining for potash by either conventional or solution methods in areas beyond the boundaries of the waste panels.

For the 1992 PA calculations, only the base-case scenario and scenarios containing the E1 and E2 events were considered; therefore, only four summary scenarios were evaluated this year: the base case (expected behavior of the disposal system without disruption by human intrusion), E1, E2, and E1E2. The TS event will be added to later PA calculations for 40 CFR 191B. The E3 event will be evaluated in safety assessments because it provides a potential pathway through which human doses could occur.

### 4.2.2 Screening of Summary Scenarios

The purpose of scenario screening is to identify those scenarios that will have no or a minimal impact on the shape and/or location of the mean CCDF. The criteria used to screen combinations of events and processes (scenarios) are similar to those criteria used to screen individual events and processes (Section 4.1.3). These criteria are physical reasonableness of the combinations of events and processes, probability of occurrence of the scenario, and consequence.

The probability of occurrence for a scenario is determined by combining the probabilities of occurrence and nonoccurrence from the events and processes that make up the scenario. A mechanical approach to determining scenario probabilities can be implemented by assigning the probability of occurrence and nonoccurrence for each event and process to the appropriate "yes" and "no" legs at each bifurcation in the logic diagram (Figure 4-1). The probability of a scenario is the product of the probabilities along the pathway through the logic diagram that defines that scenario. Based on the probability criterion in Appendix B of 40 CFR 191 for screening out individual events and processes, scenarios with probabilities of occurrence of less than 1 chance in 10,000 in 10,000 years need not be considered in determining compliance with 40 CFR 191B, and therefore, consequence calculations are not necessary.

Consequence in this step of the procedure means integrated discharge to the accessible environment for 10,000 years. By inferring that the guidance in Appendix B of 40 CFR 191 for individual events and processes also applies to scenarios, scenarios whose probability of occurrence is greater than the cutoff in Appendix B can be eliminated from further consideration if their omission would not significantly change the remaining probability distribution of cumulative releases. Because the degree to which the mean CCDF will be affected by omitting such scenarios is difficult to estimate prior to constructing CCDFs, only those scenarios that have no releases or very small, low-probability releases should be screened out from additional consequence calculations. If

significant changes are made to the data base, the conceptual models, or mathematical models of the disposal system, the omitted scenarios should be rescreened.

In implementing this step of the procedure for this preliminary WIPP performance assessment, no scenarios were screened out. Because parameter values did not define the events, all combinations of events in the scenarios are physically reasonable. Because final scenario probabilities have not been estimated, no scenarios were screened out on the basis of low probability of occurrence. Final calculations of consequences have not been completed, so no scenarios were screened out on the basis of this criterion.

## 4.2.3 Retained Summary Scenarios

This section describes the scenarios retained for consequence analysis that are considered in the 1992 PA calculations.

### 4.2.3.1 UNDISTURBED SUMMARY SCENARIO ($S_B$)

#### Guidance from 40 CFR 191

The Individual Protection Requirements of 40 CFR 191B (§191.15) call for a reasonable expectation that the disposal system will limit annual doses to individuals for 1,000 years after disposal, assuming undisturbed performance of the disposal system. Undisturbed performance is defined in 40 CFR 191B to mean "the predicted behavior of a disposal system, including consideration of the uncertainties in predicted behavior, if the disposal system is not disrupted by human intrusion or the occurrence of unlikely natural events" (§191.12(p)). Duration of this performance is not limited by the definition.

Although undisturbed performance is not mentioned in the Containment Requirements (§191.13), undisturbed performance is not precluded from the containment calculations and, for the WIPP, is the base case of the scenario-development methodology (Cranwell et al., 1990; Guzowski, 1990). The base-case scenario describes the disposal system from the time of decommissioning and incorporates all expected changes in the system and associated uncertainties for the 10,000 years of concern for §191.13. Subpart B of 40 CFR 191 does not provide a definition of unlikely natural events to be excluded from undisturbed performance nor, by implication, likely natural events to be included. Because of the relative stability of the natural systems within the region of the WIPP disposal system, all naturally occurring events and processes that will occur are part of the base-case scenario and are nondisruptive. These conditions represent undisturbed performance (Marietta et al., 1989; Bertram-Howery et al., 1990). They include the events and processes retained for undisturbed conditions, which are listed in Table 4-2.

## Base-Case Description

After the repository is filled with waste, the disposal rooms and drifts in the panels are backfilled and seals are emplaced in the shafts and access drifts to the panels (Figure 4-2). While excavations are open, the salt creeps inward because of the decrease in confining pressure on the salt around the rooms. Portions of the access drifts and the lower parts of shafts are filled with preconsolidated, crushed salt (Stormont et al., 1987; Borns and Stormont, 1988; Nowak et al., 1990). Because of the high lithostatic pressures at the repository depth, salt creep is expected to exert sufficient pressure on the crushed salt to consolidate the material into low-conductivity seals with properties similar to those of the host rock. Portions of the upper parts of the shafts are also filled with salt, but pressure is not expected to be sufficient here to cause the same degree of consolidation as is expected in lower portions of the shafts.

Gas generation is an important process for the undisturbed case. Some waste and some waste containers will be composed of organic material. Because microbes transported into the repository with the waste are expected to be viable under sealed-repository conditions (Brush and Anderson, 1989b), organic material in the repository will biodegrade with concomitant generation of gases. In addition, moisture in the repository, either brought in with waste or seeping in from the Salado Formation, can corrode metals in the waste and metallic waste containers themselves, with gas generated as a by-product. Radiolysis also will generate gases.

Sufficient quantities of gas will be generated to result in elevated pressures in the repository, approaching and perhaps exceeding lithostatic pressure (approximately 15 MPa). Elevated pressures may open fractures in anhydrite layers above and below the waste-disposal panels, which are relatively more brittle than the plastic halite.

Two potential pathways for groundwater flow and radionuclide transport dominate the undisturbed disposal system (Figure 4-2):

- In the first path, the pressure gradient between the waste-disposal panels and the Culebra causes brine and radionuclides to migrate from the waste-disposal panels to the base of the shafts and up the shafts toward the Culebra. This migration may occur directly through panel seals and the backfill in access drifts, but is more likely to occur through anhydrite interbeds (primarily MB139 below the panels, but possibly also MB138 and interbeds A and B above the panels). Contaminated brine may enter the interbeds either through fractures in salt in the DRZ, or directly as a result of rooms and drifts intersecting the interbeds during construction or room closure. Migration to the base of the shafts could then occur in fractures in the anhydrite layers. Migration up the shafts occurs through the shaft-seal system.

- The second major path for brine and radionuclide migration from the undisturbed repository is laterally through anhydrite interbeds toward the subsurface boundary of the accessible environment in the Salado Formation. Brine enters the interbeds as described for the first path, and is driven outward from the panels by elevated pressures in the waste resulting from gas generation.

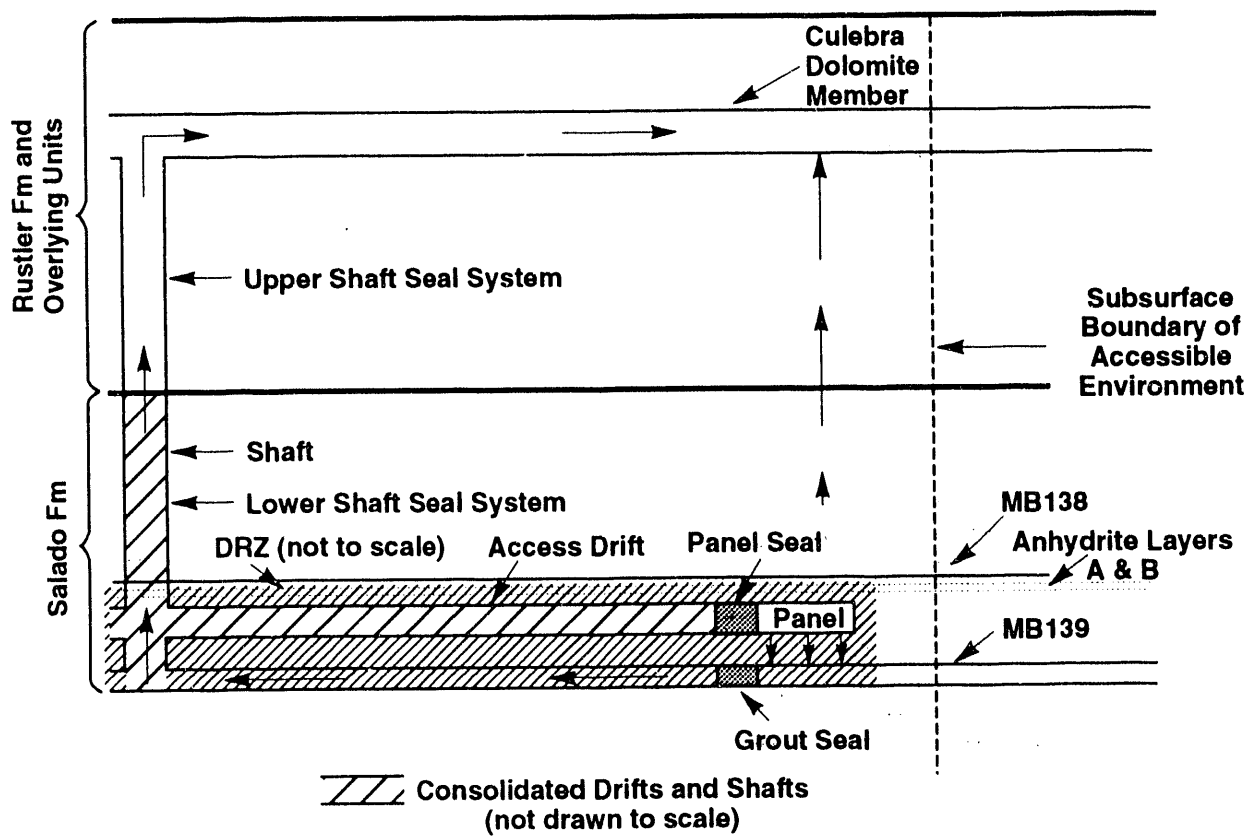


Figure 4-2. Conceptual model used in simulating undisturbed performance.

A third pathway for radionuclide transport from the undisturbed disposal system was considered in previous analyses (Lappin et al., 1989), in which brine migrated vertically from the panels through the intact Salado Formation toward the Culebra. Although this pathway has a larger pressure decline over the shortest distance than either of those discussed above, and also has the largest cross-sectional area through which migration could occur, low permeabilities of the intact halite result in extremely long travel times (400,000 years for the first arrival of radionuclides at the Culebra, as calculated by Lappin et al. [1989]). Because of the improbability of developing interconnected, vertical fractures in the plastic halite, this pathway is not modeled in performance assessment.

### 4.2.3.2 HUMAN-INTRUSION SUMMARY SCENARIOS

#### Guidance from 40 CFR 191

Appendix B of 40 CFR 191 provides guidance on a number of factors concerning human intrusion. Active controls cannot be assumed to prevent or reduce radionuclide releases for more than 100 years after disposal (U.S. EPA, 1985, p. 38088). Passive institutional controls can be assumed to deter systematic and persistent exploitation and to reduce the likelihood of inadvertent intrusion, but these controls cannot eliminate the chance of inadvertent intrusion. As discussed in Section 4.1.3, Appendix B (U.S. EPA, 1985, p. 38088) also suggests that exploratory drilling for resources can be the most severe form of human intrusion considered, and that the likelihood and consequence of drilling should be based on site-specific factors. In keeping with the guidance, this assessment includes scenarios that contain human-intrusion events.

#### Intrusion Borehole through a Room or Drift into Pressurized Brine in the Castile Formation (Summary Scenario E1)

Scenario E1 (Figure 4-3) consists of one or more boreholes that penetrate through a waste-filled room or drift and continue into or through a brine reservoir in the underlying Castile Formation in which brine pressure is between hydrostatic and lithostatic for that depth (Marietta et al., 1989). Radionuclides may be released to the accessible environment in two ways: some radionuclides will be brought to the ground surface during drilling as particulate material entrained in drilling fluid; additional radionuclides may reach the subsurface boundary of the accessible environment following long-term groundwater transport up the borehole and laterally down a potentiometric gradient in the Culebra Dolomite Member of the Rustler Formation.

Radionuclides released during drilling result from the drill bit directly intersecting waste. Material ground up by the drill bit (cuttings) is transported to the surface by the circulating drilling fluid. Additional material may be eroded from the walls of the borehole by the circulating drilling fluid (cavings) or by the spalling of solid material into the hole as the panel depressurizes. Cuttings, cavings, and spallings are collectively referred to as cuttings in performance-assessment documentation.

After drilling is complete, the hole is assumed to be plugged and abandoned. All borehole plugs and drilling mud remaining in the borehole, except for a plug above the Culebra, are assumed to degrade into material with

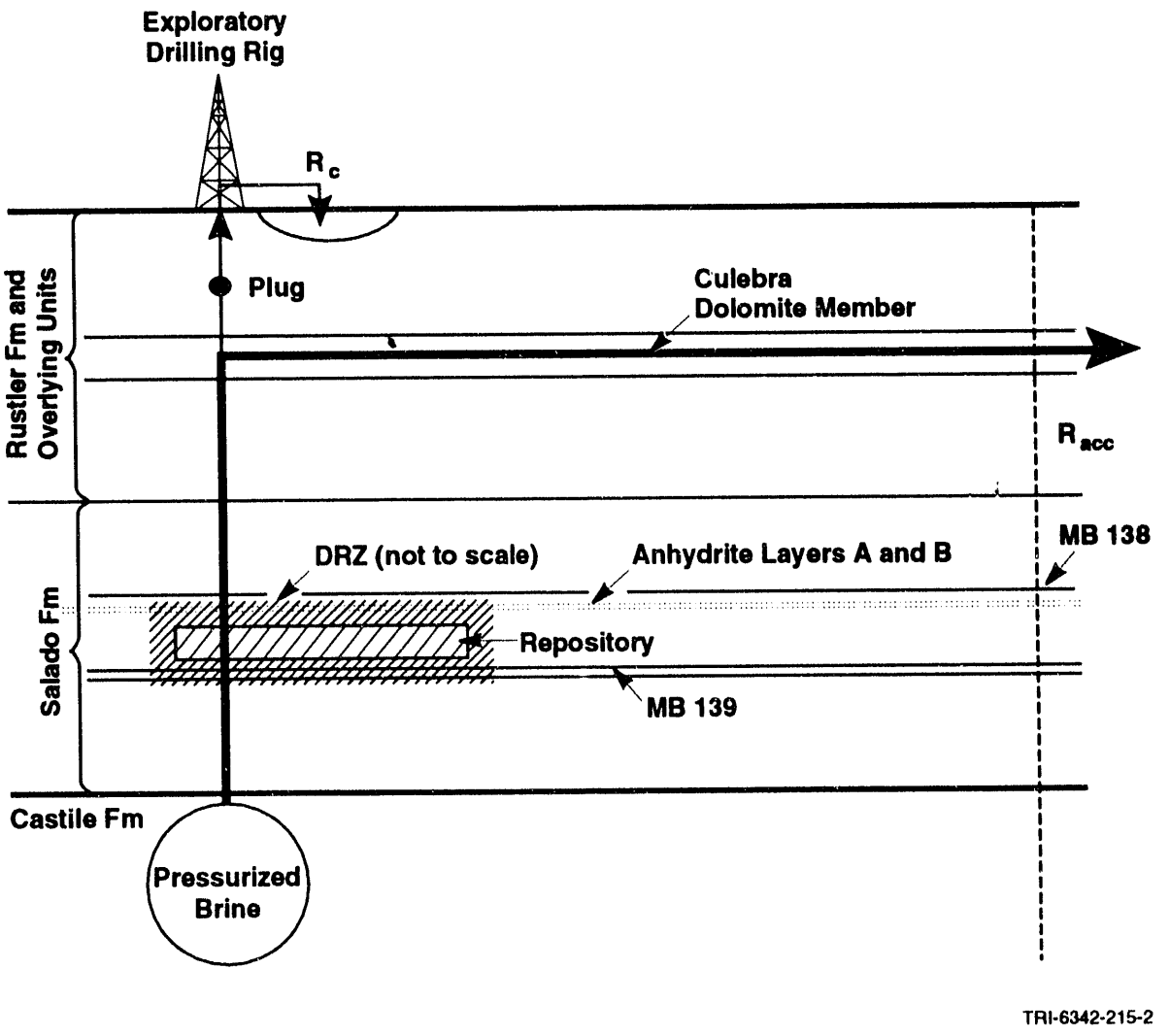


Figure 4-3. Conceptual model for scenario E1. Arrows indicate assumed direction of flow. Exploratory borehole penetrates pressurized brine below the repository horizon. $R_c$ is the release of material directly from the drilling operation. $R_{acc}$ is the release at the subsurface boundary of the accessible environment. A plug above the Culebra Dolomite Member is assumed to remain intact for 10,000 years.

properties similar to those of silty sand. Plug degradation is in keeping with guidance provided by Appendix B of 40 CFR 191: "consequences of ... inadvertent drilling need not be more severe than ... creation of a groundwater flow path with a permeability typical of a borehole filled by the soil or gravel that would normally settle into an open hole over time—not the permeability of a carefully sealed borehole" (U.S. EPA, 1985, p. 38089). The borehole is assumed to remain propped open by the material filling it, preventing closure of the hole by salt creep in the Salado Formation. A single plug above the Culebra is assumed to remain intact for Scenario E1, diverting all upward flow into the Culebra and maximizing radionuclide transport into that unit and toward the subsurface boundary of the accessible environment. Rate of flow depends on the head difference between the Culebra and the injected brine and on the hydraulic properties of the borehole fill. Radionuclides from the room may be incorporated into the Castile brine if it circulates through the waste adjacent to the borehole.

### Intrusion Borehole into a Room or Drift (Summary Scenario E2)

Scenario E2, like Scenario E1 (described above), also consists of one or more boreholes that penetrate to or through a waste-filled room or drift (Figure 4-4). Unlike Scenario E1, however, the borehole does not intersect pressurized brine or any other important source of water (Marietta et al., 1989). Releases of cuttings at the ground surface during drilling are identical to those described for Scenario E1, as are the assumptions about borehole plugging. Rate of flow into the Culebra is determined in Scenario E2 by the head gradient between the repository and the Culebra and the hydraulic properties of the borehole fill.

### Intrusion Borehole through a Room or Drift into Pressurized Brine in the Castile Formation and Another Intrusion Borehole into the Same Panel (Summary Scenario E1E2)

Scenario E1E2 consists of exactly two boreholes that penetrate waste-filled rooms or drifts in the same panel (Figure 4-5) (Marietta et al., 1989). One borehole also penetrates pressurized brine in the Castile Formation, whereas the other borehole does not. Assumptions about the degradation of borehole plugs are the same as those described for Scenarios E1 and E2, except that in this case specific plugs are assumed to remain intact so as to maximize flow from the Castile brine reservoir through the waste and into the Culebra. The borehole that penetrates the pressurized brine (the E1-type borehole) remains plugged between the waste and the Culebra; the other borehole (the E2-type borehole) remains plugged above the Culebra. Brine flow in Scenario E1E2 is driven by the head difference between the Castile brine reservoir and the Culebra.

Radionuclides are released directly to the surface during drilling of the two holes as described with E1 and E2; additional releases from this system are dependent on the sequence in which the holes are drilled. The plug in the borehole that penetrates the pressurized brine reservoir allows brine flowing up the hole to enter the repository but not leave the repository until the second hole penetrates the same panel. Once the second hole is drilled, a pathway is formed for brine and gas from the pressurized brine reservoir to flow through waste panels and nearby members to this new hole and up to the Culebra Dolomite Member. If the hole that does not penetrate pressurized brine is drilled first, gas and/or fluid pressure is relieved; this is followed by brine flow and radionuclide transport up the hole as a result of brine inflow into the panel from the host rock, possibly enhanced by creep

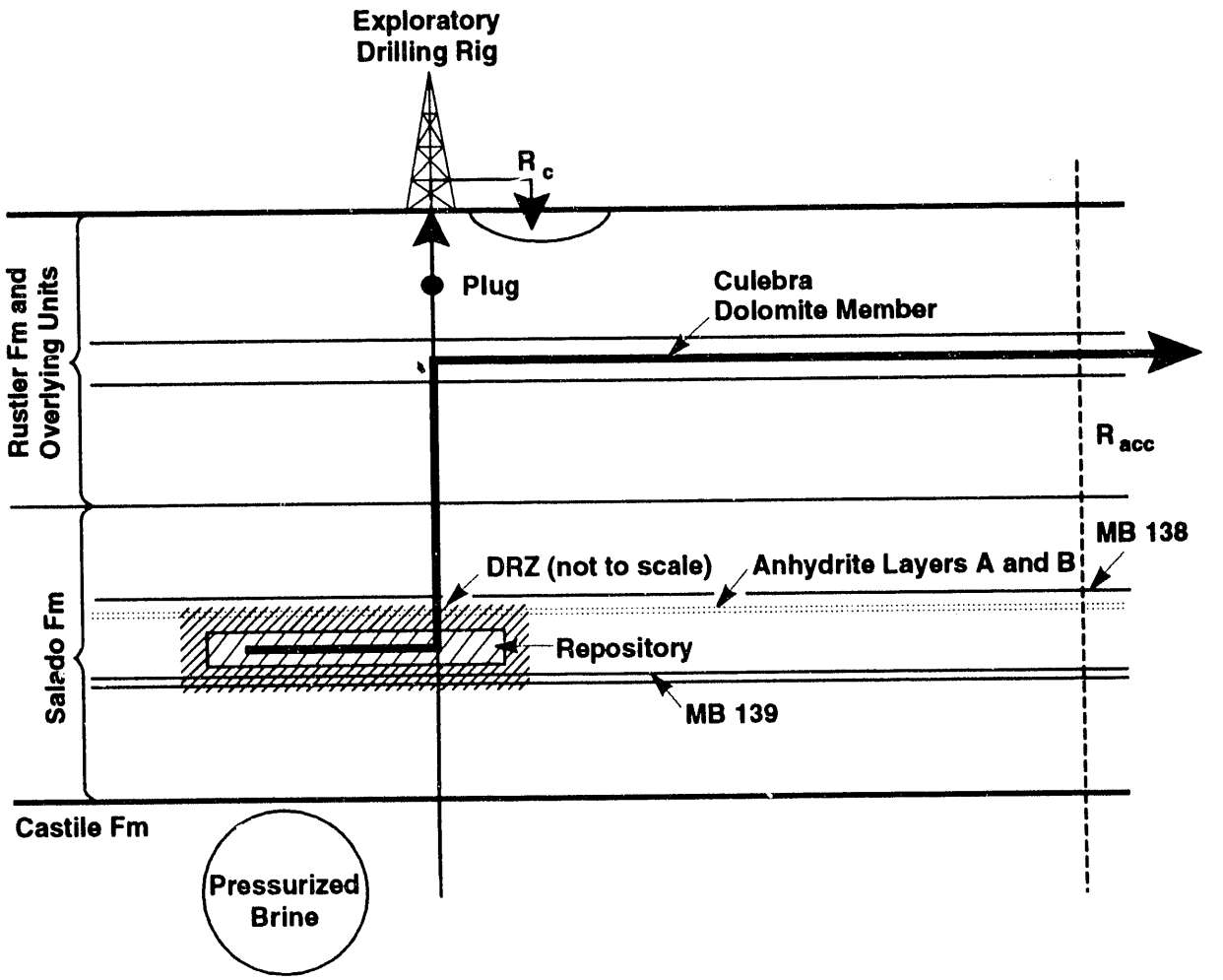


Figure 4-4. Conceptual model for scenario E2. Arrows indicate assumed direction of flow. Exploratory borehole does not penetrate pressurized brine below the repository horizon. $R_c$ is the release of material directly from the drilling operation. $R_{acc}$ is the release at the subsurface boundary of the accessible environment. A plug above the Culebra Dolomite Member is assumed to remain intact for 10,000 years.

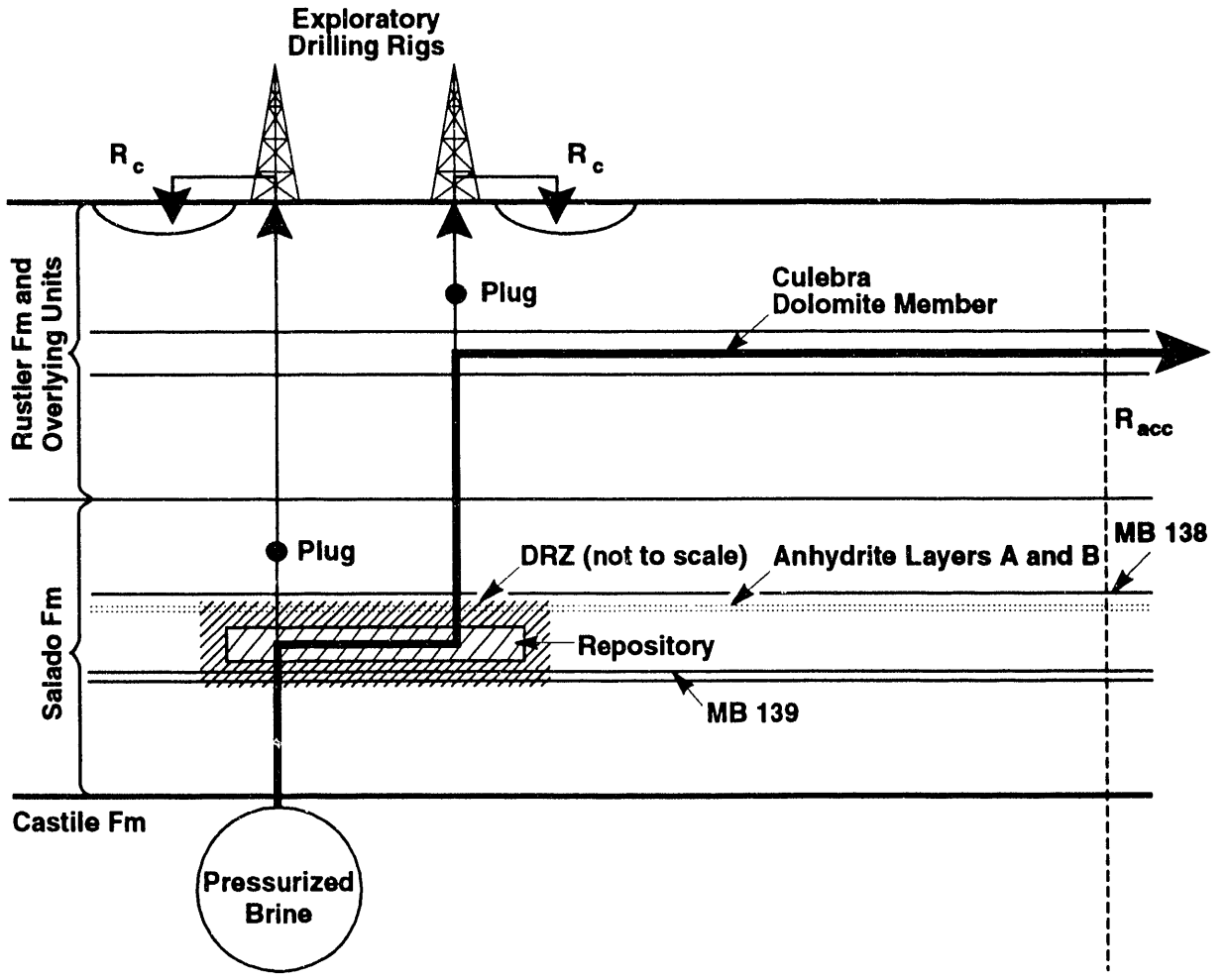


Figure 4-5. Conceptual model for scenario E1E2. Arrows indicate assumed direction of flow. One exploratory borehole penetrates pressurized brine below the repository horizon a plug between the repository and the Culebra Dolomite Member is assumed to remain intact for 10,000 years. The second borehole does not penetrate pressurized brine below the repository; a plug above the Culebra Dolomite Member is assumed to remain intact for 10,000 years. $R_c$ is the release of material directly from the drilling operation. $R_{acc}$ is the release at the subsurface boundary of the accessible environment.

closure of rooms and drifts. Flow is diverted into the Culebra by the plug located above this unit. The subsequent drilling and plugging of the borehole that penetrates the pressurized brine reservoir results in flow through the repository and up the other borehole. If driving pressure is depleted, Scenario E1E2 reverts to Scenario E2, because the borehole that penetrates the pressurized brine no longer contributes to flow and transport (Marietta et al., 1989). For modeling convenience, analyses of Scenario E1E2 assume that both boreholes are drilled at or close to the same time.

### 4.2.4 Computational Approximations of Scenarios E1, E2, and E1E2

The 1992 PA calculations use the same conceptual approximations for Scenarios E1, E2, and E1E2 that were used in the 1991 calculations (WIPP PA Division, 1991b, Sections 5.1.1 and 5.1.2). E2-type intrusions are simulated explicitly using the BRAGFLO, SANCHO, and PANEL codes (Sections 7.2, 7.3, and 7.4, and Appendices A and B of this volume).

E1E2-type intrusions are not simulated explicitly because the axisymmetric cylindrical geometry used for BRAGFLO cannot readily accommodate two intrusion boreholes (WIPP PA Division, 1991b, Section 5.1.1). E1E2-type boreholes are simulated therefore using a single borehole and the assumption that all brine in the panel mixes with all Castile brine flowing up the borehole. This assumption duplicates the primary feature of Scenario E1E2—all radionuclides in a single panel are potentially available for transport up the borehole. Because the flow path between the two boreholes is omitted, the simplification may somewhat overestimate both the amount of waste dissolved and the rate at which flow occurs through the waste and up the borehole.

E1-type intrusions are also not simulated explicitly, in this case for computational efficiency. Consequences of E1-type intrusions are instead assumed to be the same as the consequences for E2-type intrusions occurring at the same time. Probabilities are determined separately for the two types of intrusions (Section 5.3 of this volume); the contributions of Scenarios E1 and E2 to the overall CCDF are therefore not identical.

Justification for this approximation is based on the assumption that brine flowing up the E1 borehole from the Castile reservoir does not circulate through the waste. All radionuclides entering the borehole are assumed to be dissolved in brine that entered the waste from the far field of the Salado Formation or that was initially present in the panels. Comparison in the 1991 PA (WIPP PA Division, 1991b, Section 5.1.2) of the consequences of E1- and E2-type intrusions for 60 realizations indicates that cumulative flow of brine from the panel into the borehole is in most (but not all) realizations greater for the E2 borehole than for the E1 borehole. Larger brine flows from the waste (and therefore larger potential radionuclide releases) occur for the E2 borehole because the elevated Castile brine pressure present in the E1 borehole retards brine inflow into the waste from the far field of the Salado Formation. Brine flows from the waste into the E1 borehole exceed those into the E2 borehole only for those realizations in which total flow is small because the panel was not brine-saturated at the time of intrusion. These small total flows make only a small contribution to the total radionuclide release, and do not invalidate the approximation.

# 5. DRILLING INTRUSION PROBABILITIES

## 5.1 Introduction

Representation of a performance assessment as a set of ordered triples and the construction of CCDFs (Section 3.1) both involve the idea of scenario probabilities; in turn, the idea of scenario probabilities makes sense only if an underlying sample space is defined. Current performance assessments that address the EPA release limits use a sample space $S$ defined by

$$S = \{x : x \text{ a single 10,000-year history of the facility under consideration, beginning at decommissioning}\}. \quad (5\text{-}1a)$$

Each history, x, is assumed to be complete in the sense that it provides a full specification, including time of occurrence, for everything of importance to performance assessment. The summary scenarios (base case, E1, E2, and E1E2) are then defined as subsets of $S$. Specifically,

$$E1 = \{x : x \text{ a single 10,000-year history in which at least one borehole penetrates a waste-filled room or drift } \textit{and} \text{ a pressurized brine reservoir}\}, \quad (5\text{-}1b)$$

$$E2 = \{x : x \text{ a single 10,000-year history in which at least one borehole penetrates a waste-filled room or drift without penetrating a pressurized brine reservoir}\}, \text{ and} \quad (5\text{-}1c)$$

$$E1E2 = \{x : x \text{ a single 10,000-year history in which at least one pair of boreholes penetrates waste-filled rooms or drifts in the same panel; one of the boreholes in this pair penetrates a pressurized brine reservoir while the other does not}\}. \quad (5\text{-}1d)$$

Each summary scenario is further divided into disjoint subset $S_i$ called computational scenarios. For example,

$$E1 \triangleq \bigcup_i S_i, \quad (5\text{-}2)$$

where the $S_i$ appear in the ordered-triple representation in Equation (3-1). In the terminology of probability theory, the $S_i$ are events (as are the summary scenarios: base case, E1, E2, and E1E2), and the $pS_i$ are probabilities for these events. However, to avoid confusion engendered by the different disciplines' use of the word "event," the $S_i$ will be called scenarios and the $pS_i$s will simply be called probabilities. The purpose of this chapter is to show how the $pS_i$s are calculated in the 1992 performance-assessment exercise; but before proceeding, it is important to recognize several properties of the $S_i$s (computational scenarios) and the $pS_i$s (computational scenario probabilities).

It is the discretization of the sample space $S_i$ into the sets $\mathcal{S}_i$ that leads to the steps in the estimated CCDFs (Section 3.2). To construct CCDFs of the form shown in Section 3.2, the time histories associated with a given summary scenario must be sorted into disjoint sets such that

- each $\mathcal{S}_i$ is sufficiently homogeneous that it is reasonable to use the same consequence result $\mathbf{cS}_i$ for all elements of $\mathcal{S}_i$
- a probability $pS_i$ can be determined for each $\mathcal{S}_i$
- the computational costs for estimation of $pS_i$s and $\mathbf{cS}_i$s are acceptable.

## 5.2 Probability Computations

This section describes a decomposition of summary scenarios involving drilling intrusions into computational scenarios on the basis of number of intrusions and their times of occurrence and derives formulas necessary to convert from drilling rates to scenario probabilities. For these derivations, the occurrence of individual drilling intrusions is assumed to be random in time and space, although the drilling rate need not be assumed constant or, for that matter, continuous through time.

The symbol $\mathcal{S}_k(a,b)$ will be used to denote subsets of the sample space defined by

$$\mathcal{S}_k(a,b)=\{x: x \text{ an element of } \mathcal{S} \text{ that involves exactly k drilling intrusions in the time interval } [a,b]\}. \tag{5-3}$$

One objective of this section is to present the probability $p[\mathcal{S}_k(a,b)]$ for $\mathcal{S}_k(a,b)$. Membership in $\mathcal{S}_k(a,b)$ only places a restriction on intrusions in the time interval $[a,b]$ and thus does not preclude intrusions in other time intervals. As a result, an additional objective will be to present the probability $p\left[\bigcap_{i=1}^{n}\mathcal{S}_{n(i)}(t_{i-1},t_i)\right]$ for the set $\bigcap_{i=1}^{n}\mathcal{S}_{n(i)}(t_{i-1},t_i)$, where $t_0 < t_1 < \cdots < t_n$ and each $n(i)$, $i=1,2,\ldots,n$, is a nonnegative integer. This corresponds to determining the present of a scenario in which exactly $n(1)$ intrusions occur in time interval $[t_0,t_1]$, exactly $n(2)$ intrusions occur in time interval $[t_1,t_2]$, and so on. Helton (in press) has suggested a general form for these intrusion probabilities; the core of ideas behind his suggestion is outlined below.

The probability of having exactly one intrusion in the time interval $[u,v]$ is approximated by a function F such that

$$p[\mathcal{S}_1(u,v)] = F(u,v) + O\left[(v-u)^2\right], \tag{5-4}$$

where the preceding notation is a shorthand for the statement that the ratio

$$\frac{p[\mathcal{S}_1(u,v)] - F(u,v)}{(v-u)^2} \tag{5-5}$$

is bounded as $v-u$ approaches zero. More precisely, the statement in Equation 5-4 is satisfied on a time interval $[a,b]$ if there exists a number B and a sequence of times $a=t_0<t_1<\cdots<t_n=b$ such that, if $1\le i\le n$ and $t_{i-1}\le u<v\le b$, then

$$\left|\frac{p[S_1(u,v)]-F(u,v)}{(v-u)^2}\right|<B. \tag{5-6}$$

The expressions in Equations 5-4 and 5-6 are providing a mathematical form for the statement "$F(u,v)$ is a good approximation to $p[S_1(u,v)]$ when $v-u$ is small."

The function F in Equation 5-4 can be defined in a number of ways. The simplest definition is

$$F(u,v)=\lambda(v-u). \tag{5-7}$$

In this case, F corresponds to a Poisson process with a time-independent rate constant $\lambda$ (i.e., a homogeneous Poisson process) and

$$p[S_k(a,b)]=\frac{[\lambda(b-a)]^k}{k!}\exp[-\lambda(b-a)]. \tag{5-8}$$

The probability of intrusion by drilling was modeled as a homogeneous Poisson process in the 1991 series of PA calculations. The constant $\lambda$ was taken as an imprecisely known parameter with upper bound equal to the maximum drilling rate required by EPA standards; i.e., $\lambda$ was uniformly distributed between zero and $\lambda_{max}$, with

$$\begin{aligned}\lambda_{max}&=\left(\frac{30}{\text{km}^2\bullet 10{,}000\text{ yr}}\right)\bullet(\text{area of waste panels})\\&=3.28\times10^{-4}\text{ yr}^{-1}\end{aligned} \tag{5-9}$$

The next step in generalizing beyond Equation 5-7 is

$$F(u,v)=\lambda(u)(v-u), \tag{5-10}$$

in which case F corresponds to a Poisson process with a time-dependent rate constant (i.e., a nonhomogeneous Poisson process) and

$$p[S_k(a,b)]=\frac{1}{k!}\left(\int_a^b\lambda(s)ds\right)^k\exp\left[-\int_a^b\lambda(s)ds\right]. \tag{5-11}$$

This result can be used to compute the probability of a general scenario in which exactly $n(1)$ intrusions occur in time interval $[t_0, t_1]$, exactly $n(2)$ intrusions occur in time interval $[t_1, t_2]$, and so on. If this general scenario is denoted by $S(\mathbf{n})$, where

$$\mathbf{n} = [n(1), n(2), ..., n(n)] \text{ and } t_0 = a, t_n = b,$$

then

$$p[S(\mathbf{n})] = \prod_{i=1}^{n} \left[ \frac{1}{n(i)!} \left( \int_{t_{i-1}}^{t_i} \lambda(s) ds \right)^{n(i)} \right] \exp\left[ -\int_a^b \lambda(s) ds \right] . \tag{5-12}$$

Computational scenarios and corresponding probabilities for summary scenarios E1 and E2 can be generated by specification of the time intervals $[t_{i-1}, t_i]$ and the $n(i)$ appearing in Equation 5-12, and by suitably defining the function $\lambda(t)$ appearing in that equation.

In the preferred conceptual model for the 1992 series of PA calculations, probability of intrusion by drilling is modeled as an inhomogeneous Poisson process using Equations 5-11 and 5-12; for comparison, the 1992 PA also uses a homogeneous Poisson process (Equation 5-9) as an alternative conceptual model for drilling intrusions. For the preferred conceptual model, the time-dependent drilling rates, $\lambda(t)$, are calculated with an algorithm proposed by Hora (see Section 5.2; also Hora's memo in Appendix A of Volume 3 of this report) using information obtained in an expert judgment process concerning effects of human intrusion into the WIPP. Note that Hora's algorithm gives drilling rates in units of

$$\frac{\text{number of boreholes}}{\text{km}^2 \bullet 10{,}000\,\text{yr}}$$

and the time-dependent drilling rates used in Equations 5-11 and 5-12 are scaled from Hora's values by multiplying by area of the waste panels (Equation 5-9). As stated above, $\lambda(t)$ may also have to be scaled to reflect, for example, the fraction of the area of waste panels that overlaps brine pockets.

Computational scenarios for the E1E2 summary scenario can be defined in a manner similar to the ones employed for the E1 and E2 scenarios. Once defined, the probabilities of these computational scenarios are best calculated using the basic result in Equation 5-11 together with the scenario

$$BP^{+-}(t_{i-1}, t_i) = \{x : x \text{ an element of } S \text{ in which a waste panel is penetrated by one or more boreholes that pass through a pressurized brine pocket in the time interval } (t_{i-1}, t_i) \text{ and by one or more boreholes that do not pass through a pressurized brine pocket in the time interval } (t_{i-1}, t_i)\}.$$

Then, in extension of the derivations on pages 2-23 to 2-27 of the 1991 Volume 2 (WIPP PA Division, 1991b),

$$p\left[\mathcal{BP}^{+-}(t_{i-1}, t_i)\right] \doteq \sum_{\ell=1}^{nP}\left\{1-\exp\int_{t_{i-1}}^{t_i}\lambda_\ell^+(t)dt\right\}\left\{1-\exp\int_{t_{i-1}}^{t_i}\lambda_\ell^-(t)dt\right\}, \tag{5-13}$$

where

$nP$ = the number of waste panels

$$\lambda_\ell^+(t) = \left(\frac{aBP}{nP \bullet aTOT}\right)\lambda(t)$$

$$\lambda_\ell^-(t) = \left(\frac{aTOT(\ell) - aBP/nP}{aTOT}\right)\lambda(t)$$

$aBP$ = area of pressurized brine pocket under waste panels ($m^2$)

$aTOT(\ell)$ = area of $\ell^{th}$ waste panel ($m^2$)

$aTOT$ = total area of waste panels ($m^2$).

Variable activity loading in the repository was described using the same representation used in the 1991 PA (Helton et al., 1992, Chapter 2). Intrusion probabilities were calculated using the code CCDFPERM (Volume 3, Section 1.4.2 of this report).

## 5.3 Lambda Function Generation

The 1992 performance assessment is the first to incorporate the judgments of experts on possible future modes of intrusion into the WIPP and on how markers may mitigate the effects of these intrusions; 40 CFR 191, Subpart B, (U.S. EPA, 1985) requires consideration of both these questions. Specifically, 40 CFR 191, Subpart B, indicates that the DOE "should consider the effects of each particular disposal system's site, design, and passive institutional controls in judging the likelihood and consequence of . . . inadvertent human intrusion" (Appendix B of U.S. EPA, 1985). The discussion that follows in Sections 5.3.1, 5.3.2, and 5.3.3 describes WIPP PA's methodology for addressing the mitigating effect of passive markers. This approach may be refined and modified as the performance assessment process matures. The following material, largely excerpted from Hora (memo in Appendix A, Volume 3 of this report), is intended to give an overview of the expert-judgment processes and reasoning that entered into the construction of a probabilistic model of inadvertent intrusion by exploratory drilling.

### 5.3.1 The Expert Judgment Process

During 1990-1992, experts external to SNL were assembled to study the likelihood of potential inadvertent human intrusion into the WIPP. These experts formed two groups—one group (called the Futures Panel) studied

what future societies might be like and how they might inadvertently intrude into nuclear waste (Hora et al., 1991). The second group (called the Markers Panel), after considering the findings of the first group, studied how markers might be used to warn future societies about the presence and danger of the buried waste (memorandum by Hora in Volume 3, Appendix A of this report). Both groups provided probabilities and probability distributions for critical aspects of the human intrusion problem.

The Futures Panel was divided into four teams. Each team was composed of four experts from various fields of social and physical science. Each team was asked to address the same set of questions. The results of their work suggests that future societies may undertake activities that could lead to inadvertent intrusion into the WIPP. These teams judged that a number of factors (such as level of technology, demand for resources, population level, and ability to retain knowledge about nuclear waste) would influence the likelihood of inadvertent intrusion. Because the teams used different structures for analysis and considered different factors that would influence the likelihood of inadvertent intrusion, the results of their endeavors had to be interpreted individually in order to be used in the construction of Lambda Functions.

As the Futures Panel was completing its effort, the Markers Panel, consisting of 13 experts, was organized into two teams to study markers for the WIPP site. These markers may be incorporated into the repository design to serve as warnings to future societies about the presence of nuclear waste. Each team was asked to consider the findings of the Futures teams, to suggest design characteristics for a marker system, and to assess the efficacy of such a system of markers in deterring inadvertent human intrusion. Based on the assumption that the ability of a marker system to deter intrusions rests on the survival of the marker system over an extended period of time and the ability of potential intruders to detect the markers and to understand the messages that they carry, the Markers Panel members were asked to provide estimates of probabilities for several events:

- First, the probability that a marker and its message(s) would remain intact. (This first probability estimate was requested for various times in the future.)

- Second, if the marker and its messages remain intact, the probability that the potential intruders are able to understand the message and thus become forewarned of the inherent dangers of intrusion. (This second probability estimate was requested for several different types of intrusion.)

The above two probability estimates were made under various assumptions about the state of technology in the future.

As noted above, the Futures Panel posed several types of activities that could lead to inadvertent intrusion into the WIPP (drilling, mining, archaeological investigation); but on the basis of guidance in Appendix B of 40 CFR Part 191 (U.S. EPA, 1985), it was concluded that the preliminary performance assessment need not consider intrusion modes such as mining or archaeological investigation that may result in more severe consequences than exploratory drilling for resources. Moreover, the guidance also provides an upper bound for the drilling intensity to be used in the performance assessment. Three modes of exploratory drilling were identified by the experts examining human intrusion issues. These modes are exploratory drilling for mineral resources (primarily fossil fuels), drilling water wells, and drilling for injection disposal wells. Because the repository is well below the water table in an area where water quality is poor, drilling for water was judged to be an insignificant threat when

compared to drilling for mineral resources (see Section 4.1.3 of this volume). Drilling for disposal wells was identified as a possible threat by one of the four Futures teams, but probabilities were not provided. Thus, exploratory drilling for resources is the only mode of intrusion considered in the 1992 preliminary comparison.

## 5.3.2 Algorithm for Generating Lambda Functions

The time-dependent drilling rates, or lambda functions, that arise in modeling the probability of drilling (Section 5.2 of this volume) were calculated in the 1992 PA exercise using an algorithm constructed by Hora (memo in Volume 3, Appendix A of this report). The purpose of this algorithm was to assemble quantitative expert judgments concerning future human intrusion into the WIPP.

The existence of markers and the ability of a society to interpret the warnings left at the WIPP may depend upon the state of development of that society. In this exercise, the state of development of the society was represented by the level of the technological development of the society. The level of technological development (high, medium, or low) was randomly generated from probability distributions provided by the Futures teams. Prior to this step, however, the Futures team whose level of technology was to be sampled had to be chosen. This was necessary because the four teams studying potential futures developed analyses independently and in different ways and there was no simple way to combine their findings. For this reason, a team was randomly selected on each generation of a lambda function. The assessments from each team represent their collective judgment. In contrast, members of one of the Markers teams individually provided probability assessments while the other team provided a consensus set of probability distributions. Thus, when one of the two Markers teams was randomly chosen, it could also be necessary to select randomly one of the team members for that iteration. This procedure avoided making unfounded assumptions about how to combine disparate distributions.

Next, using a given level of technology, the frequency (f) at which attempted inadvertent intrusion occurs in the absence of markers or monuments was elicited from the Futures experts. This time-dependent frequency is called the raw drilling intensity; it does not take into account deterrence by markers. Thus, to gain an estimate of the effective drilling intensity $\lambda$, the raw drilling intensity was modified in the following way: For each of the several points in time that the raw drilling intensity was evaluated, the probability of the markers existing $(p_1)$ and the probability of the markers deterring an intrusion attempt given that the markers exist $(p_2)$ were evaluated. These two probabilities modify the raw drilling intensity to give the effective drilling intensity,

$$\lambda = f(1 - p_1 p_2).$$

The algorithm for generating inadvertent intrusion can then be succinctly described by the following steps:

1. Randomly select one of the four Futures teams.

The following steps use distributions conditional on the outcome of step 1:

2. Randomly select a level of technology in the future. When probabilities of levels of technology are time-dependent, a rank correlation of 1 will be used to generate the level of technology in the several time periods.

3. Generate a random variable to determine the intrusion intensity. When intrusion intensities vary with time periods, a rank correlation of 1 will be used to generate the intrusion intensities in the several time periods.

4. Randomly select one of the Markers teams and a Marker team member, if necessary.

5. For each time period generate the probability that markers are extant given the level of technology.

6. For each time period, generate the probability that the markers deter intrusion given that the markers are extant, the level of technology, and the mode of intrusion.

7. Compute the effective drilling intensity for each time period.

Note that in step 3, a single random number is used to select an intrusion intensity for all periods. This assumption results in the variability of the performance measure being maximized among the Monte Carlo iterations.

### 5.3.3 Use of the Lambda Functions

The effective drilling intensity, $\lambda(t)$, is used to generate probabilities of computational scenarios for human intrusion by drilling in the manner described in Section 5.2. However, the algorithm described in Section 5.3.2 does not provide direct input to sensitivity and uncertainty analyses; instead, the code implementing the algorithm is run many times in order to generate a family of equally likely realizations of the lambda functions, and it is this family of realizations that is sampled in the Monte Carlo calculations (see Section 5.2, Volume 3 of this report). A family of 70 realizations was generated for the 1992 series of calculations; one of these realizations is shown on Figure 5-1 and the remainder are displayed in Appendix D of Volume 3. The realizations of $\lambda(t)$ can be regarded as a random sample from an effectively infinite population of drilling intensities implicitly defined by the expert-judgment data and the reasoning that went into the construction of Hora's algorithm (Section 5.3.2). The variability shown by members of this artificial population (see Appendix D, Volume 3) represents the assessed uncertainty in future drilling intensities and the effectiveness of markers.

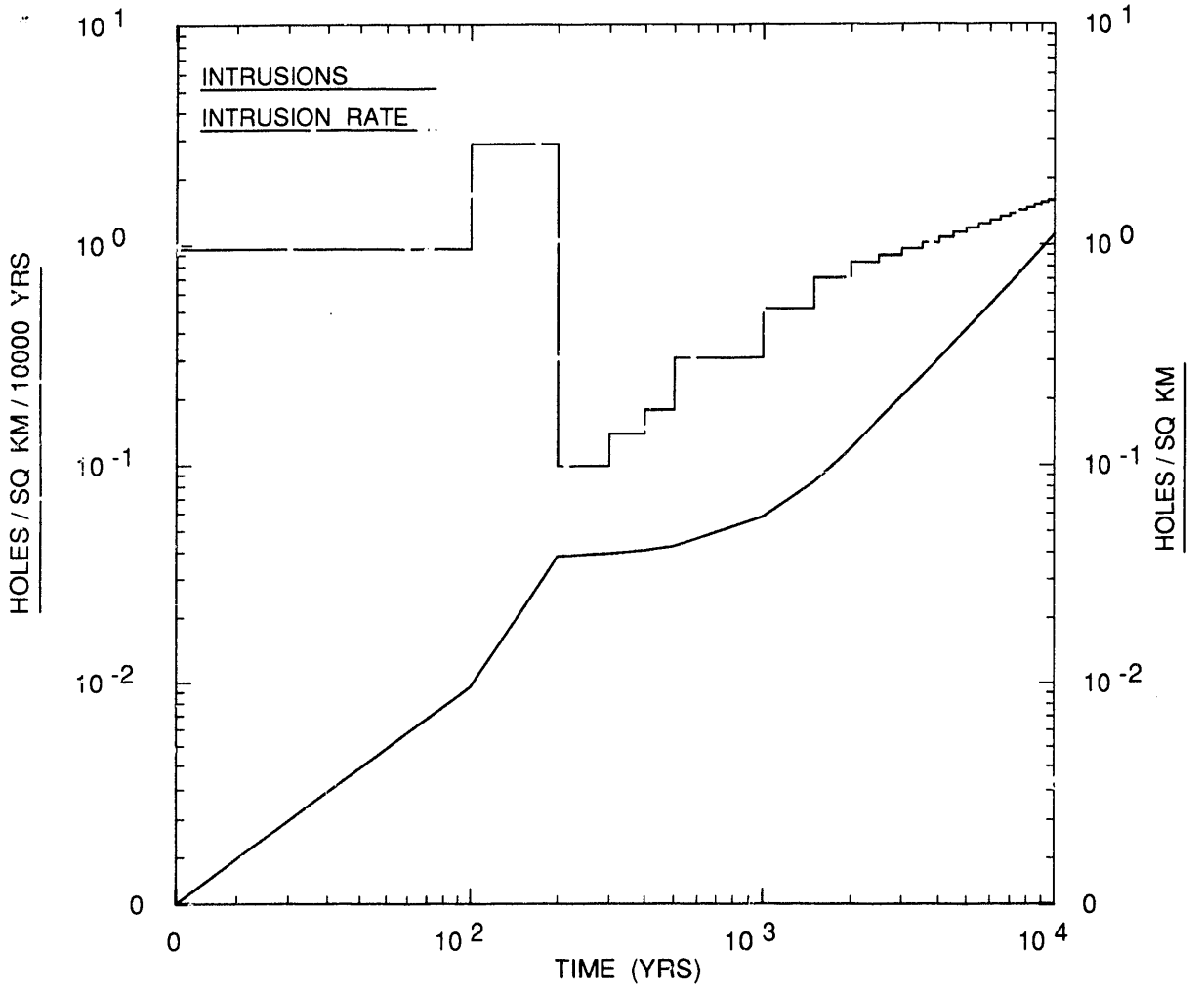


Figure 5-1. A realization of effective drilling intensity $\lambda(t)$ (dashed line) and its associated integrated effective drilling intensity (solid line) as functions of time. This is one of 70 realizations used in 1992 sensitivity and uncertainty analyses.

# 6. DATA AND CDFS

## 6.1. Conventions

Volume 3 of this report provides distribution functions for parameter values used as input to the 1992 PA calculations, and references for the primary data sources on which the distributions are based. Volume 3 uses standard terms of probability theory and statistics or nonstandard terms to characterize model parameters. Very brief explanations of these terms are provided below; more detailed explanations are provided in Section 1.2 of Volume 3.

### 6.1.1 Probability Distribution Functions

For a continuous, uncertain parameter, say X, the *probability density function* (pdf) is a function $f(x) \geq 0$ with the properties

$\int_a^b f(x)dx =$ probability that uncertain *parameter* X lies in interval $(a,b)$:

$$\int_{-\infty}^{+\infty} f(x)dx = 1$$

The *cumulative distribution function* (cdf) associated with $f(x)$ is defined by

$F(x) = \int_{-\infty}^{x} f(s)ds =$ probability that uncertain parameter X is less than or equal to x.

Uncertain parameters may also be called "imprecisely known parameters" elsewhere in this series of reports.

Probability density functions (pdfs) and cdfs can be similarly defined for uncertain parameters that take on a denumerable number of values, $x_i, i = 1, 2, \ldots$. The sequence $\{f_i\}, i = 1, 2, \ldots$, such that $f_i > 0$ and

$$\sum_i f_i = 1,$$

is the discrete analogue of the continuous pdf, and

$$F(x) = \sum_{all\ x_i < x} f_i$$

is the discrete analogue of the continuous cdf.

## 6.1.2 Empirical Distribution Functions

*Empirical cdfs* are histograms or piecewise-constant functions that are based on percentiles derived from a set of measurements (data), or a set of subjective estimates of experts. For independent measurements (data) of some quantity, the empirical cdf is an unbiased estimator of the unknown population cdf of that quantity (Blom, 1989, p. 216); this property does not always apply to empirical cdfs derived from subjective estimates of experts.

## 6.1.3 Range

The *range* of a distribution is denoted by $(a,b)$, the pair of numbers in which a and b are respectively the minimum and maximum values that can reasonably be taken by the uncertain parameter X.

## 6.1.4 Mean and Sample Mean

The mean value (or, simply, *mean*) of a distribution is one measure of the central tendency of a distribution; it is analogous to the arithmetic average of a series of numbers. The population mean, $\mu$, is defined by

$$\mu = \int_{-\infty}^{\infty} xf(x)dx \text{ for continuous distributions, or}$$

$$\sum_{\text{all } x_i} x_i f_i \text{ for discrete distributions.}$$

The sample mean, denoted by $\bar{x}$, is the arithmetic average of values in an empirical data set. A sample mean can also be assigned to empirical cdfs derived from subjective estimates of experts.

## 6.1.5 Median and Sample Median

The median value of a cdf is denoted by $x_{50}$ and is that value in the range at which 50% of all values lie above and below (i.e., the 0.5 quantile). Sample medians, here denoted by $\bar{x}_{50}$, can be obtained directly from empirical cdfs.

## 6.1.6 Variance and Coefficient of Variation

The *variance* of a distribution, $\sigma^2$, is the second moment of the distribution about its mean, i.e.,

$$\sigma^2 = \int_{-\infty}^{\infty} (x-\mu)^2 f(x)dx \text{ for continuous distributions, or}$$

$$\sum_{\text{all } x_i} (x_i - \mu)^2 f_i \text{ for discrete distributions.}$$

The *standard deviation*, $\sigma$, is the positive square root of the variance. The coefficient of variation, the ratio of standard deviation to mean, $\sigma/\mu$, is a convenient measure of the relative width of a distribution.

The *sample variance*, $S^2$, of a set of measurements of parameter X, say $X_1, X_2, \ldots, X_N$ is the sum

$$\frac{1}{N-1} \sum_{n=1}^{N} (X_n - \bar{x})^2 .$$

The sample variance of independent measurements of some quantity is an unbiased estimator of the population variance of that quantity (Blom, 1989, p. 197). (A variance can also be formally calculated for empirical cdfs derived from subjective estimates of experts; this is not a sample variance, however.)

## 6.1.7 Categories of Distributions

Distributions used in the 1992 PA are grouped into five categories:

- continuous, analytical distributions (normal, lognormal, uniform, or loguniform)
- discrete, analytical distributions (Poisson, binomial)
- constructed empirical distributions based on measurements
- constructed empirical distributions based on expert judgment
- miscellaneous categories (null distributions; i.e., constants and tabular functions).

### 6.1.7.1 CONTINUOUS DISTRIBUTIONS

Four continuous, analytical distributions are frequently used in the 1992 PA:

- **Normal.** Normal designates the normal pdf, a good approximation to the distribution of many physical parameters.
- **Lognormal.** Lognormal designates a lognormal pdf, a distribution of a variable whose logarithm follows a normal distribution.
- **Uniform.** Uniform designates a pdf that is constant in the interval $(a, b)$ and zero outside of that interval.

- **Loguniform.** Loguniform designates a loguniform pdf, a distribution of a variable whose logarithm follows a uniform distribution.

#### 6.1.7.2 DISCRETE DISTRIBUTIONS

A frequently used discrete distribution is the Poisson distribution. The Poisson pdf is often used to model processes taking place over continuous intervals of time such as the arrival of telephone calls at a switch station (queuing problem) or the number of imperfections per unit length produced in a bolt of cloth. The Poisson pdf was used in the 1991 probability model for human intrusion by exploratory drilling. The 1992 probability model for human intrusion incorporates effects of deterrence by markers; this model is based on generalized Poisson distributions.

#### 6.1.7.3 CONSTRUCTED DISTRIBUTIONS (DATA)

A *constructed distribution* of the *Data* type is simply an empirical cdf constructed from sets of measured data points in the data base. For intrinsically discrete data, the empirical cdf is a piecewise-constant function resembling a histogram. For intrinsically continuous data, the empirical cdf is always converted to a piecewise-linear function by joining the empirical percentile points with straight lines; this is done to ensure that, in Monte Carlo sampling, the distribution of sampled parameter values will cover all of the range of the distribution (Tierney, 1990, p. II-5).

In some cases, the PA Department may modify constructed distributions of the Data type by extending the range of the data set to include estimated 0.01 and 0.99 quantiles. Because the range of measurements in a data set may not reflect the true range of the random variable underlying the measurements, the PA Department may estimate the range by $\bar{x} + 2.33s$, where $\bar{x}$ is the sample mean and s is the sample standard deviation.

#### 6.1.7.4 CONSTRUCTED DISTRIBUTIONS (SUBJECTIVE)

*Constructed distributions* of the *Subjective* type are histograms based on subjective estimates of range (the 0 and 100 percentile) and at least one interior percentile point (usually the 50 percentile or median). The subjective estimates of percentile points are usually obtained directly from experts in the subject matter of the parameter of concern. Histograms for intrinsically continuous parameters are always converted to piecewise linear cdfs by joining the subjective percentile points with straight lines.

#### 6.1.7.5 MISCELLANEOUS CATEGORIES

*Null* categories of distributions are described below:

- **Constant.** When a distribution type is listed as constant, a distribution has not been assigned and a constant value is used in all PA calculations.

- **Spatial.** The spatial category indicates that the parameter varies spatially. This spatial variation is usually shown on an accompanying figure. The median value recorded is a typical value for simulations that use the parameter as a lumped parameter in a model; however, the value varies depending upon the scale of the model. The range of a spatially varying parameter is also scale dependent.

- **Table.** The table category indicates that the parameter varies with another property and the result is a tabulated value. For example, relative permeability varies with saturation; its distribution type is listed as table (also, the median value is not meaningful and is therefore omitted in the table).

## 6.2 Selection of Parameter Distributions

### 6.2.1 Requests for Data from Sandia Investigators and Analysts

The PA Department follows a well-defined procedure for acquiring and controlling the parameter distributions used in consequence and probability models:

- **Identify Necessary Data.** Each year, the PA Department identifies data that are necessary to construct parameter distributions for the preliminary performance assessment. Members of the department may compile data from published reports, personal communications with investigators, and other sources.

- **Request Median Value and Distribution.** The PA Department then requests that the investigators provide either new data or a median value and distribution for each parameter in a large subset of the parameters. Some model parameters are specific to the PA calculations and so individuals in the PA Department are considered the experts for these parameters (e.g., probability model parameters). Initially, Sandia investigators are responsible for providing data, or if data are unavailable, distributions for all parameters. As this procedure for acquiring data is repeated, a few parameters are evaluated through formal elicitation.

- **Update Secondary Data Base.** The PA Department enters the endorsed or elicited data for all parameters into the secondary data base. The PA Department then either constructs parameter distributions or uses distributions provided by the investigator; the PA Department selects a subset of these parameters to sample in each annual PA exercise, keeping all other values constant at their median values, unless specifically noted.

- **Perform Consequence Simulations and Sensitivity Analyses.** The PA Department runs consequence simulations and sensitivity analyses with selected subsets of parameters from the updated secondary data base. The sensitivity analysis evaluates the sensitivity of a parameter in determining variation of the result (i.e., CCDF).

- **Determine Whether Parameter Is Important in Analysis.** By means of the sensitivity analyses, the PA Department can determine whether the parameter as specified is significant in the calculations.

## 6.2.2 Construction of Distributions

The PA Department follows the five-step procedure outlined below to construct probability distributions (cdfs):

1. Determine whether site-specific data for the parameter in question exist. If data exist, go to step 3.

2. Request that the investigator supply a specific shape (e.g., normal, lognormal) and associated numerical parameters for the distribution of the parameter. If specific shape and distribution parameters cannot be supplied, go to step 4; otherwise go to step 5.

3. Determine the size of the combined data sets. Is sample size is sufficiently large, PA staff constructs distribution (go to step 5).

4. If sample size is small, or investigator cannot provide a specific distribution, request that the investigator provide subjective estimates of the range and details on the distribution of the parameter.

5. Assign distribution.

## 6.2.3 Some Limitations on Distributions

The major limitations on the validity of the probability distributions assigned to parameters in the 1992 PA are believed to be a consequence of two things:

- The equating of spatial variability with model parameter uncertainty, particularly for that class of parameters called material-property parameters.

- The neglect of correlations between model parameters.

These limitations are discussed in detail in Volume 3 (Section 1.3.3).

# 7. CONSEQUENCE MODELING

## 7.1 Radioactive Decay

The quantity of radioactive material that reaches the accessible environment depends in part on the growth and decay of the component radionuclides in the waste. The Bateman equations (Wehr et al., 1984) are used to calculate this decay within the repository. The Bateman equations in terms of activity are:

$$\frac{dN_i}{dt} = -\lambda_i N_i + \lambda_i N_{i-1}, \tag{7-1}$$

where $N_i$ is the activity of radionuclide $i$, $t$ is time, and $\lambda_i$ is the disintegration constant of radionuclide $i$.

For given initial inventories $N_i^{(0)}$, the solution can be written as

$$N_i(t) = \sum_{j=1}^{i} a_{i,j} e^{-\lambda_j t}, \tag{7-2}$$

where the coefficients $a_{i,j}$ are defined by the recurrence relations

$$a_{i,i} = N_i^{(0)} - \sum_{j=1}^{i-1} a_{i,j} \tag{7-3}$$

and

$$a_{i,j} = \frac{\lambda_i}{\lambda_i - \lambda_j} a_{i-1,j} \qquad i > j. \tag{7-4}$$

## 7.2 Multiphase Flow Through Porous Media

A computational model called BRAGFLO (BRine And Gas FLOw) that simulates two-phase fluid flow through porous, heterogeneous reservoirs has been developed for WIPP PA. As discussed in Appendix A of this volume, BRAGFLO uses finite-difference methods to solve the coupled nonlinear partial differential equations (PDEs) describing the mass conservation of the gas and brine components distributed between the gas and liquid phases.

The PA Department uses BRAGFLO in Monte Carlo consequence analyses to quantify the flow of brine and gas through the repository and surrounding strata for both the undisturbed, base-case scenario and human-intrusion scenarios. For the 1992 PA, the code is used to model fluid flow within the Salado Formation and the repository, including a representation of the shaft system for undisturbed performance. The Culebra Dolomite Member of the

Rustler Formation and a hypothetical pressurized brine reservoir in the Castile Formation are included in the model because of their potential roles as a sink and a source, respectively, for fluid flow.

### 7.2.1 Features and Capabilities of BRAGFLO

BRAGFLO is capable of describing three-phase (e.g., water, gas, and oil) fluid flow through porous media in one, two, or three dimensions. Only two phases (brine and gas) are modeled for WIPP PA; calculations to date have only been performed in one and two dimensions. The code uses spatially varying meshes and solves the coupled nonlinear PDEs using nonlinear Newton-Raphson iteration, automatic time-stepping, and direct or iterative solvers.

Additional features of BRAGFLO are the capability to incorporate the following: the effect of halite creep on waste porosity using output from the SANCHO code (see Section 7.3 and Appendix B of this volume); anisotropic permeabilities; nonideal gas behavior (Redlich-Kwong-Soave); rock compressibility; and kinetic or reactant-dependent gas generation as a function of fluid saturations.

Multiphase flow is simulated as simultaneous immiscible displacement in porous media. Regions within the model domain (e.g., waste, seals, and lithologic units) are represented as solid continua of interconnected void space, and porosity is expressed as the ratio of void volume to total volume for each region. Flow occurs according to heuristic extensions of Darcy's Law, in that the rate of flow of a homogeneous fluid through a porous medium is proportional to the hydraulic gradient and to the cross-sectional area normal to the direction of flow, and inversely proportional to fluid viscosity (see Appendix A of this volume for additional discussion). Permeability is the constant of proportionality in Darcy's law. Flow is assumed to be laminar, and fluids are viscous and Newtonian. Forces that affect fluid flow are those due to pressure, gravity, capillarity, and viscous shear. Fluid saturation is defined to be the ratio of fluid volume to void volume. At least one fluid phase is present at all times, and all void volume is occupied by fluid.

Effects of capillary pressure and relative permeability occur when two (or more) fluid phases are present in a porous medium. Curvature of the interface separating fluid phases and surface tension cause a capillary pressure difference across the interface. During fluid flow, interference between the phases deforms the interface. Relative permeability describes this interference on a macroscopic scale, and varies with fluid saturation. Relative permeability is expressed as the ratio of the permeability of the rock (or other material) with the fluid in question at a given saturation to the permeability of the rock when 100 percent saturated with the fluid.

Residual saturation of a fluid phase is defined as the smallest saturation of fluid required to form continuous pathways through the medium. It is the minimum saturation at which the phase will flow in response to a pressure gradient. Below residual brine saturation, brine exists as a thin film around rock grains or as isolated pockets, and gas is present in sufficient volume to form an interconnected pathway. The relative permeability for brine is zero. Above residual brine saturation and below residual gas saturation, both brine and gas form continuous pathways through the porous network, and relative permeabilities for both phases are greater than zero.

When brine saturation is sufficiently high that gas saturation falls below residual, gas exists only as isolated pockets surrounded by brine. Gas flow does not occur, and relative permeability for gas is zero.

### 7.2.2 Interaction of Important Repository Processes

The coupling of processes simulated by BRAGFLO is illustrated schematically in Figure 7-1. The material properties that describe the repository system are represented in the center of a triangle, the apices of which represent the physical processes that operate within the system. Arrows indicate the major interactions. Thus, the amount of brine present in the room is a function of two-phase flow, and is a contributing factor in the rate and amount of gas generation. The rate and amount of gas generation are contributing factors to two-phase flow, as is brine consumption by corrosion reactions that generate gas. Changes in waste porosity result from halite creep; it affects both two-phase flow and, therefore, gas generation through its influence on brine solubility. Completing the coupled interactions, both two-phase flow and gas generation affect halite creep (through their impact on pressure within the panels) and therefore have an effect on changes in waste porosity.

### 7.2.3 General Assumptions Used in 1992 PA Two-Phase Flow Modeling

The following is a list of major assumptions used in two-phase flow modeling for the 1992 PA:

- Rock permeabilities (1) varied with material type, (2) were uniform within a material, and (3) did not vary with time.

- Void volume of waste was estimated as a function of pressure using SANCHO (Section 7.3 of this volume).

- Gas potential was based on an extrapolation of inventory volume fractions of combustibles and metals/glasses to design capacity (Section 2.3.2.1 of this volume; Volume 3, Section 3.4 of this report).

- Gas generation occurs by corrosion of ferrous metals and biodegradation of combustible materials only, and the contribution of radiolysis is assumed to be negligible (Volume 3, Section 3.3 of this report; WIPP PA Division, 1991c, Section 3.3).

- All gas was assumed to have the physical properties of hydrogen, which will be a principal component resulting from corrosion of ferrous metals (Volume 3, section 1.4.1 of this report).

- As long as corrodible or biodegradable waste remains, gas generation is a function only of brine saturation (WIPP PA Division, 1991c, Section 3.3).

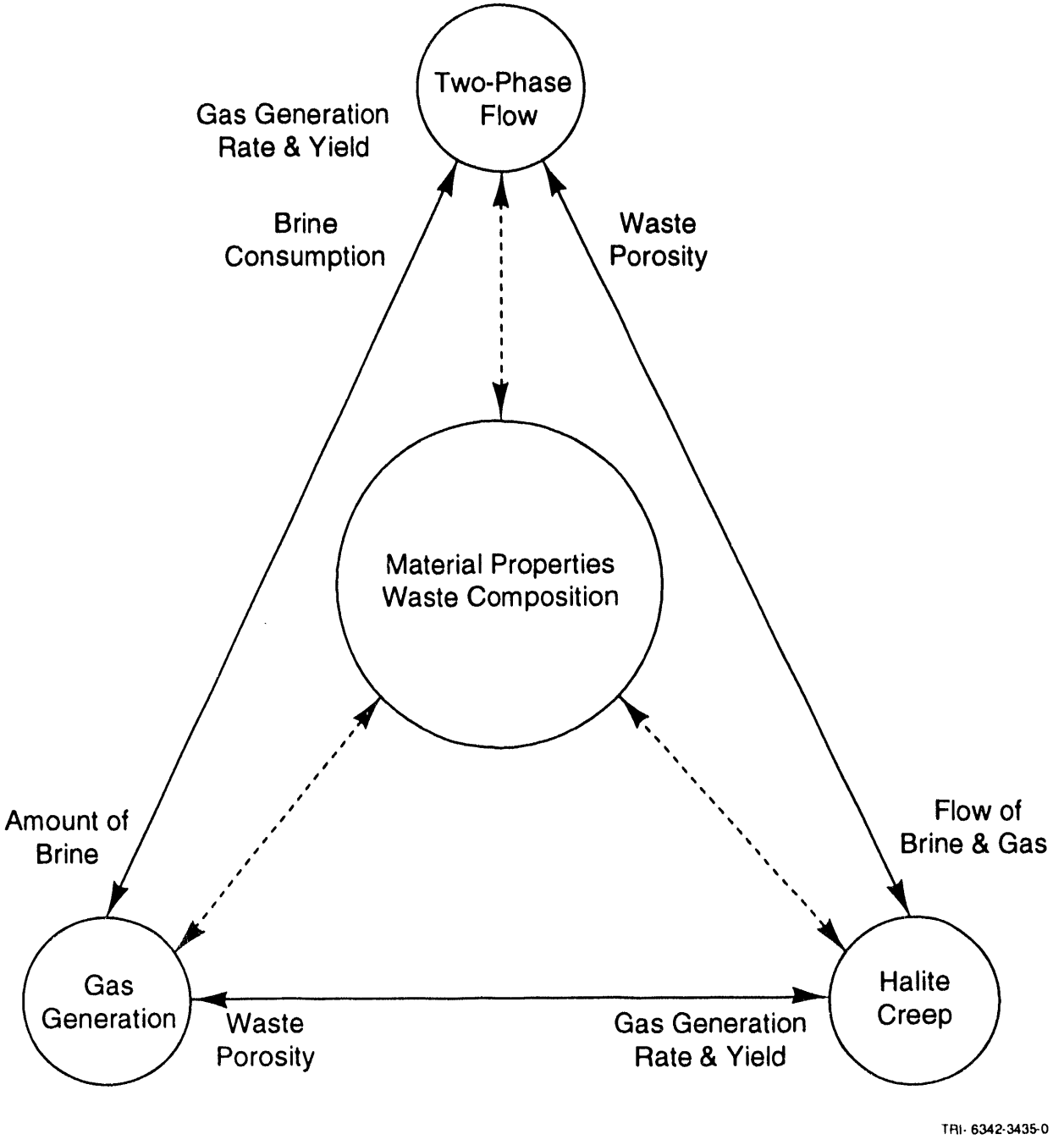


Figure 7-1. Interaction of some important repository processes.

- Water is consumed during corrosion of ferrous metals; biodegradation reactions require the presence of water to occur but have no effect on the net water balance (WIPP PA Division, 1991c, Section 3.3).
- No reactions affect gas after it is generated (WIPP PA Division, 1991c, Section 3.3).
- The solubility of gas in brine is assumed to be negligible.
- The Salado Formation is assumed to be initially 100 percent brine saturated.
- Initial pressures in the Salado Formation vary hydrostatically from a sampled pressure at the elevation of MB139 (Volume 3, Section 2.4.3 of this report).

## 7.3 Waste-Filled Room Deformation

Consequence models of multiphase flows within a waste-filled room (Section 7.2) require that the effective porosity and permeability of waste and backfill materials be specified. Realistic estimates of effective porosity and permeability must in turn account for three phenomena:

- waste-material composition (metallics, sludges, combustibles)
- geomechanical closure of the room
- backpressure of gases generated in the room by chemical and biological degradation of waste materials.

Thus, the ideal model of multiphase flow within a waste-filled room would couple the two-phase flow model described in Section 7.2 and Appendix A with a model that can simulate the geomechanical closure of the room.

This ideal model, however, is not practically achievable. Direct solution of the fully coupled equations of two-phase flow and geomechanical closure in the repetitive manner required by the PA methodology is unrealistic using present resources; the PA Department instead has chosen to examine the sensitivity of the system to closure using simplifications of the coupling that capture closure approximately while keeping calculations of two-phase flow manageable. In the 1991 series of PA calculations, a simple approximation was made: Effects of room closure and gas pressure were ignored and room material-property parameters were assigned time-independent values that were based on the assumed waste-material composition. (See Sections 3.4.7 and 3.4.8 of WIPP PA Division [1991c]).

The present (1992) series of calculations includes effects of room closure and gas generation in an indirect way. A *separate* (i.e., uncoupled) calculation of the effective porosity of a waste-filled room as a function of time and total moles of gas generated was made (Mendenhall and Lincoln, February 28, 1992, memo in Appendix A, Volume 3 of this report); data from this calculation were used to fit a porosity "surface" (Figure 7-2) that was then used as a constraint on room porosity in the equations of two-phase flow (see Appendix A on BRAGFLO).

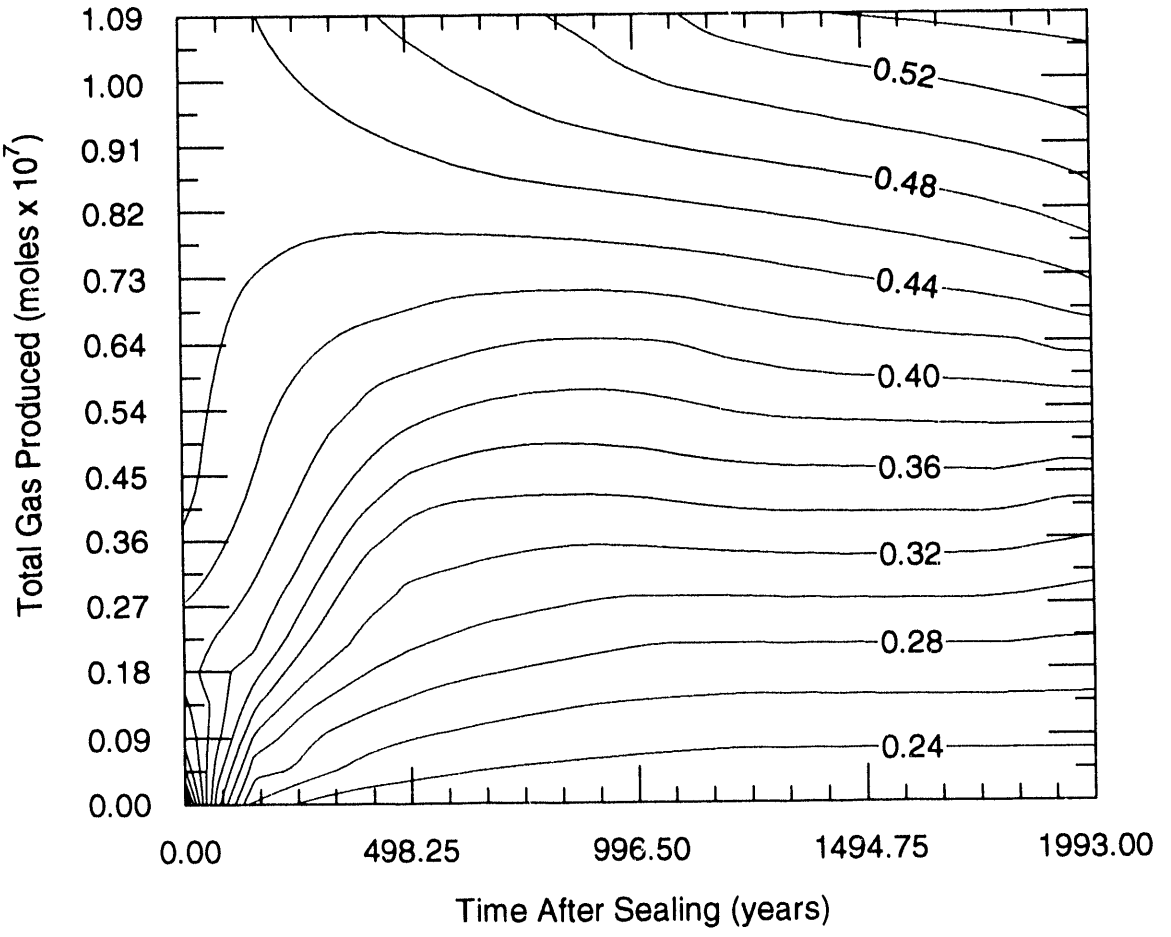


Figure 7-2. Surface giving porosity of waste-filled disposal room as a function of total volume of gas produced and time after sealing. Pore space is assumed to be fully saturated with gas. Porosity is expressed as void volume per unit volume of waste.

The room deformation component of the separate calculation was accomplished with SANCHO, a finite element computer program for simulating the quasistatic, large-deformation, inelastic response of two-dimensional solids; a brief description of the SANCHO code is provided in Appendix B. Details of room-deformation and gas-generation components of the separate calculation and values of mechanical and material-property parameters used in the separate calculation are provided in Volume 3 of this report.

## 7.4 Waste Mobilization

Following the occurrence of an E2 or E1E2 scenario (Section 4.2.3.2), flow of brine through a collapsed WIPP panel and up an intrusion borehole may result in mobilization of dissolved, radionuclide-bearing compounds and their transport towards the Culebra Dolomite Member of the Rustler Formation. The consequence model that simulates the process of waste mobilization is currently implemented in part of a computer code called PANEL. The mathematical model on which PANEL is based is described in Section 1.4.4 of Volume 3 of this series of reports, and represents an extreme simplification of a potentially complex situation that in reality involves a mixture of waste forms having widely varying physical and chemical compositions in contact with inhomogeneous flows of brine. The discussion that follows (1) details the assumptions that were made in order to arrive at the simplified mathematical model of waste mobilization (Section 7.4.1) and (2) briefly presents the simplified model of waste mobilization (Section 7.4.2).

### 7.4.1 Assumptions

Eight assumptions about panel geometry, waste and backfill composition, brine discharge, and brine-waste chemical reactions are implicit in the PA Department's current model of waste mobilization:

1. A collapsed WIPP panel (rooms and drifts) is idealized as a single, connected cavity of constant volume (Figure 7-3).

2. Waste and backfill within the collapsed WIPP panel (cavity) are treated as a homogeneous porous medium of constant porosity and infinite permeability; radionuclide-bearing compounds are uniformly distributed throughout the cavity.

3. The idealized panel (cavity) is connected to sources and sinks for brine by one or more discrete inlets or outlets (boreholes); brine may also flow across walls of the cavity (Figure 7-3).

4. Steady-state discharge of brine through the idealized panel is assumed to hold for all time; that is,

$$\sum Q_{in} = \sum Q_{out} = Q(t),$$

where the net discharge, $Q(t)$, is calculated with the model for multiphase flow (Section 7.2).

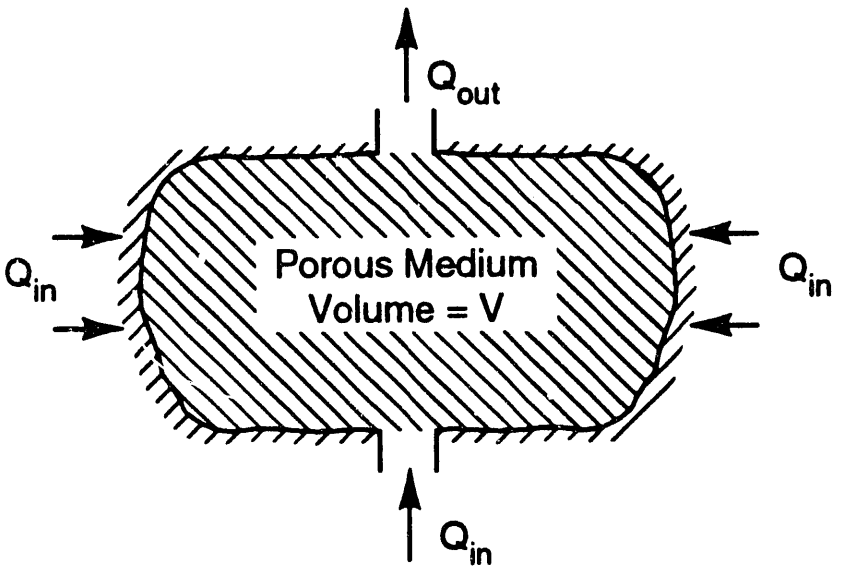


TRI-6342-1435-0

Figure 7-3. Idealized collapsed WIPP panel in PANEL model.

5. The pore spaces of the idealized panel are fully saturated with brine at all times; that is, mobilization of radionuclide-bearing compounds in the gas phase is ignored.

6. Chemical equilibrium and uniform mixing of liquid-phase compounds throughout the idealized panel are achieved on time scales that are much smaller than the mean residence time of the brine in the cavity.

7. The solubility limit for a given isotope (e.g., U-234) of a given element (e.g., uranium) is assumed to be proportional to the solubility limit of the element; the constant of proportionality is taken as the ratio of the mass of the isotope that currently remains in the cavity to the sum of the masses of all currently remaining isotopes of the element.

8. Mobilization is limited to dissolved radionuclides; suspended radionuclides (colloids) are not considered to be mobilized by the brine.

Assumptions 1 and 2 imply that the total pore space in the idealized, collapsed WIPP panel is constant and equal to $\epsilon V$, where $\epsilon$ is the constant porosity and V is the cavity volume; assumption 5 implies that the total pore space is filled with brine at all times. Assumptions 3 and 4 imply that the mean residence time of brine in the repository is given by

$$\tau = \frac{\epsilon V}{Q},$$

regardless of the stated time dependence of Q. Assumption 6 implies that characteristic times to reach chemical equilibrium and characteristic times for complete mixing of dissolved species by diffusion through cavity pore spaces are always much smaller than $\tau$. Because the rates of chemical reactions between dissolved and immobile species are unknown, the validity of assumption 6 cannot be tested at this time; times for complete mixing by diffusion can be estimated but have not yet been compared with mean residence times for brine.

Assumption 7 was made in order to simplify the equations that describe the masses of the various radioactive isotopes of an element that remain in the cavity at any time after occurrence of an E2 or E1E2 scenario (see Section 7.4.2 below and Section 1.4.4 of Volume 3). An alternative assumption would set isotope solubility limits equal to the element solubility limit.

## 7.4.2 Simplified Mathematical Model

The simplified mathematical model of waste mobilization is expressed as a system of coupled, ordinary differential equations, with each system applying to a radioactive decay chain:

$$\dot{M}_i = -S_i \left( \frac{M_i}{\sum_j M_j} \right) Q(t) - \lambda_i M_i + \left(\lambda_{i-1} M_{i-1}\right) \left( \frac{\text{atomic wt}_i}{\text{atomic wt}_{i-1}} \right), \tag{7-5}$$

where $i = 1, 2, \ldots, N$ numbers the N radionuclides in a given decay chain, a dot ($\bullet$) over a quantity means the time derivative, and

$M_i(t)$ = mass of $i^{th}$ radionuclide remaining in cavity at time $t > t_0$ (kg),

$Q(t)$ = discharge of brine through cavity at $t > t_0$ ($m^3/s$),

$S_i$ = solubility limit for *element* associated with $i^{th}$ radionuclide ($kg/m^3$),

$\lambda_i$ = decay constant for $i^{th}$ radionuclide ($s^{-1}$), and

$t_0$ = the time of initiation of a disruptive scenario (s).

In Equation 7-5, $\Sigma M_j$ signifies summation over the remaining masses of all radionuclides (including the $i^{th}$ radionuclide) associated with a given element. The initial conditions of Equation 7-5 are

$$M_i(t_0) = M_{i0}(t_0), \tag{7-6}$$

where $M_{i0}(t_0)$ is the initial ($t = 0$) inventory of the $i^{th}$ radionuclide (kg) aged by the Bateman equations (Section 7.1) to reflect mass remaining at $t_0 > 0$.

## 7.5 Groundwater Transmissivity Fields

The WIPP PA Department employs a multiple-realization technique to account for spatial variability of the transmissivity field within the Culebra Dolomite (LaVenue and RamaRao, 1992). The technique uses an automated inverse approach to calibrate a two-dimensional model to both steady-state and transient pressure data. The multiple-realization technique can be broken down into three steps:

1. **Unconditional Simulation.** An unconditional simulation of the WIPP transmissivity fields is generated. This is a random field that has the same spatial correlation structure as the transmissivity measurements, but does not necessarily match measured transmissivities at the location of their measurements.

2. **Conditional Simulation.** The random field produced in Step 1 is conditioned in this step so that it honors exactly the measured transmissivities at the locations of their measurements. The resulting field, called a "conditional simulation" of the transmissivity field, is used as the initial estimate of the Culebra transmissivity field.

3. **Automated Calibration.** The conditional simulation of the transmissivity field is then calibrated so that the pressures computed by the groundwater-flow model (both steady and transient state) agree closely (calibrated within the uncertainty in head measurements, i.e., between 1 and 2 m) with the measured pressures in a least-square sense. Calibration is achieved by placing synthetic transmissivity values (pilot points) automatically where the sensitivity of the difference between observed and calculated pressure to changes in the transmissivity field is greatest. When calibration is completed, a conditionally simulated transmissivity field is obtained that conforms with all head and transmissivity data at the WIPP site and may be regarded therefore as a plausible version of the true distribution of transmissivity.

This process is repeated to produce the desired number of calibrated, conditionally simulated fields. (Seventy of these fields were calculated in this manner for the 1992 PA calculations.) A description of this methodology, extracted from LaVenue and RamaRao (1992), follows. (A more complete discussion of the methodology is provided in Appendix D of this volume.)

### 7.5.1 Unconditional Simulation

The following methods have been used earlier in groundwater hydrology for generating unconditional simulations: nearest-neighbor method (Smith and Freeze, 1979; Smith and Schwartz, 1981), matrix decomposition (de Marsily, 1986), multidimensional spectral analysis (Shinozuka and Jan, 1972; Mejía and Rodríguez-Iturbe, 1974), turning-bands method (Matheron, 1971, 1973; Mantoglou and Wilson, 1982; Zimmerman and Wilson, 1990). Here the turning-bands method is used.

In the turning-bands method, a two-dimensional stochastic process is generated by the summation of a series of equivalent one-dimensional processes (Mantoglou and Wilson, 1982):

$$Z_s(N) = \frac{\sum_{i=1}^{L} Z_i\left(\zeta_{N_i}\right)}{\sqrt{L}}, \tag{7-7}$$

where $Z_s(N)$ is the two-dimensional field to be simulated, $Z_i\left(\zeta_{N_i}\right)$ is the one-dimensional process in the line interval (band) of line $i$ measured by $\zeta_i$ and containing $N_i$ (the projection of point $N$ onto line $i$), and $L$ is the number of lines selected. As in LaVenue et al. (1990), the 1992 calculations model the WIPP transmissivity data as a two-dimensional field with an intrinsic random function of order zero (IRF-0), making it possible to use the Weiner-Levy Process to generate the line process $Z_i\left(\zeta_{N_i}\right)$ in Equation 7-7.

## 7.5.2 Conditional Simulation

The procedure for conditioning is based on the following relationship:

$$Z(x) \approx Z_{ok}(x) + \left[Z_{uc}(x) - Z_{uk}(x)\right], \tag{7-8}$$

where $Z(x)$ is the true (but unknown) value of the field at point x, $Z_{ok}(x)$ is the kriged estimate of $Z$ at $x$ based on the observed values of Z at the locations of the observations, $Z_{uc}(x)$ is the unconditionally simulated value of the field at point $x$, and $Z_{uk}(x)$ is value of the kriged estimate at $x$ based on the unconditionally simulated values of $Z_{uc}$ at the locations of the observations. Equation 7-8 clarifies the conditioning step as one of adding a simulated kriging error on a kriged field using the measured data. This step involves kriging twice, once with the measured transmissivities and another time with the unconditionally simulated transmissivities, both at the location of the observations. The simulated kriging error is rendered zero at all observation points.

## 7.5.3 Automated Calibration

In the 1992 calculations, model calibration is done by an indirect approach. Synthetic transmissivity values, referred to as pilot points, are automatically placed in regions of the conditionally simulated transmissivity field where an objective function (Equation 7-9) is most sensitive to changes in the this transmissivity field. This objective function is defined as the weighted sum of the squared deviations between the model computed pressures and the observed pressures, with the summation being extended in the spatial and temporal domain where pressure measurements are taken:

$$J(\underline{u}) = \sum_{k=1}^{L} \underline{e}_p^T(k)\underline{\underline{R}}^{-1}(k)\underline{e}_p(k), \tag{7-9}$$

where $J(\underline{u})$ is the weighted least square (WLS) error criterion function, $\underline{u}$ is the vector of parameters ($Y_p = \log_{10} T_p$), $T_p$ is the pilot-point transmissivity, $\underline{e}_p$ is the difference between the computed and observed pressures, $\underline{\underline{R}}$ is the covariance matrix of errors in the observed pressure, $k$ is the time step number, $L$ is the number of time steps, and $T$ is the transpose.

Pilot points are added to the existing measured transmissivity data set during the course of calibration. After a pilot point is added to the transmissivity data set, the augmented data set is used to obtain a revised, conditionally simulated transmissivity field for a subsequent iteration in calibration. With the addition of a pilot point, the transmissivity distribution in the neighborhood of the pilot point gets modified with dominant modifications being closer to the pilot-point location.

Pilot points are placed at locations where their potential for reducing the objective function (Equation 7-9) is highest. This potential is quantified by the sensitivity coefficients ($dJ/dY$) of the objective function $J$ with respect to $Y$, the logarithm (to base 10) of pilot-point transmissivity. Coupled adjoint sensitivity analysis and kriging are used to compute the required derivatives (RamaRao and Reeves, 1990). The transmissivities at pilot points are assigned by an unconstrained optimization algorithm and a subsequent imposition of constraints. The optimization algorithm, which belongs to a class of iterative search algorithms, involves the repeated application of the following equation until convergence is achieved:

$$\underline{Y}_{i+1} = \underline{Y}_i + \beta_i \underline{d}_i, \tag{7-10}$$

where $i$ is the iteration index, $\underline{d}_i$ is the direction vector, $\beta_i$ is the step length (a scalar), and $\underline{Y}_i$ is a vector of parameters to be optimized (i.e., logarithms of pilot point transmissivities to base 10).

There are two levels of iteration used in the calibration process, designated as "inner" and "outer" iterations. An inner iteration relates to the iterations needed to optimize the transmissivities of the pilot points. When the convergence of an inner iteration is achieved, the pilot points are added to the transmissivity data set, and then the outer iteration may proceed. During the outer iteration, optimal location of the next set of pilot points is determined using coupled kriging and adjoint sensitivity analysis. Subsequently, their transmissivities are optimized by a sequence of inner iterations.

Convergence criteria for the inner iterations are as follows:

- The performance measure $J$ drops below a prescribed minimum value.
- The number of iterations equals a prescribed maximum for the inner iterations.
- The ratio of the norm of the gradient to the initial gradient norm reduces below a prescribed value.
- The gradient norm is less than a prescribed minimum.
- The relative change in the objective function falls below a prescribed value.

Outer iterations cease once the performance measure $J$ drops below a prescribed minimum value or the number of iterations equals a prescribed maximum for the outer iterations.

## 7.6 Groundwater Flow and Transport

Following the occurrence of an E2 or E1E2 scenario (Section 4.2.3.2), flow of brine through a collapsed WIPP panel may result in mobilization of dissolved, radionuclide-bearing compounds from waste (Section 7.4), the transport of these compounds up an intrusion borehole, and eventually their injection into the Culebra Dolomite Member of the Rustler Formation (Section 2.2.2.6). Dissolved compounds that reach the Culebra could then be carried to the accessible-environment boundary by advection and diffusion in groundwater flowing in the Culebra. Thus, to estimate consequences of certain disturbed-case scenarios, models of groundwater flow and solute transport through the Culebra are needed.

The consequence model that simulates groundwater flow in the Culebra is currently implemented by a computer code called SECO_2DH (Appendix C). The mathematical model on which SECO_2DH is based is described in Section 7.6.1 (below), which details assumptions that were made in order to arrive at the current model of groundwater flow; this section also contains discussions of modeling the effects of climate change on boundary conditions for the Culebra flow model.

Simulations of solute transport in groundwater flowing through the Culebra are currently implemented by a companion to the SECO_2DH code called SECO_TP (Appendix C). The mathematical model on which SECO_TP is based is described in Section 1.4.6 of Volume 3 of the present series of reports. Section 7.6.2 (following) contains discussion of the assumptions that were made in order to arrive at the current model of solute transport; it also contains discussion of the 1992 treatments of hydrodynamic dispersion (Section 7.6.2.1) and chemical sorption in fracture flows (Section 7.6.2.2).

The mathematical models of groundwater flow and solute transport are based on a common, highly simplified conceptual model of the Culebra Dolomite Member of the Rustler Formation: The Culebra Dolomite Member is imagined to be a sheet-like mass of rock having lateral dimensions of the order of tens of kilometers and uniform thickness of about 8 meters. Sets of planar fractures, all parallel to the plane of bedding, run continuously throughout the rock mass (Figure 7-4, top) and it is assumed that all water flow through the Culebra is sustained by the fracture sets, i.e., there is no flow through matrix blocks separating fractures (Figure 7-4, lower left) even though the matrix blocks are assumed to be saturated and have a finite kinematic porosity. The surfaces of fractures are assumed to be uniformly coated with layers of clay of constant thickness greater than or equal to 0 (Figure 7-4, lower right) that are never allowed to entirely fill the void space of a fracture; these clay layers are assumed to be saturated and to have finite kinematic porosity, but as in the matrix material, no advective flow is allowed through a clay layer.

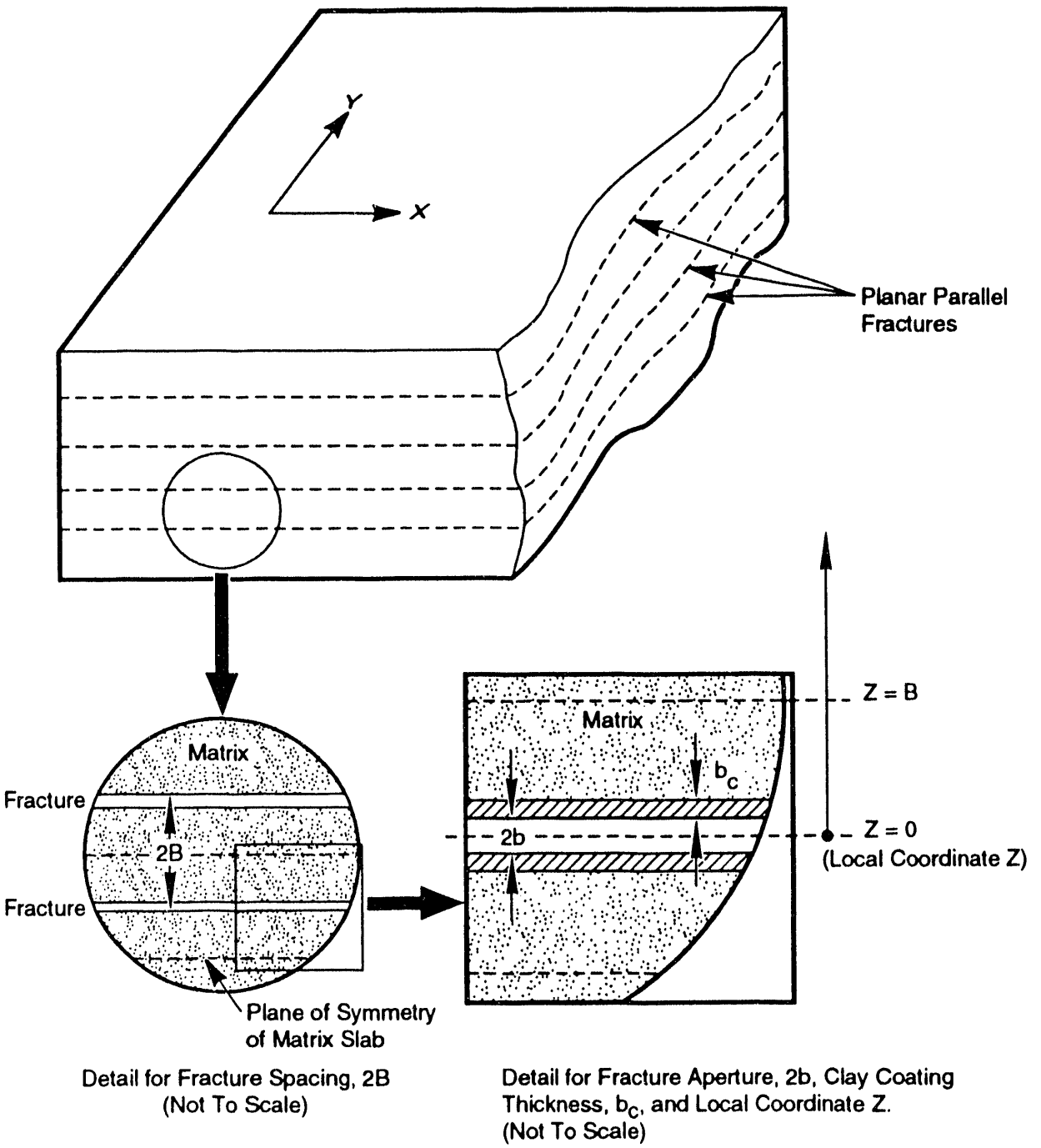


Figure 7-4. Conceptual hydrologic model of the Culebra Dolomite Member.

## 7.6.1 Groundwater Flow in the Culebra

Groundwater flow at regional and local scales within the Culebra Dolomite is simulated by solving the following partial differential equation in two dimensions $(x,y)$:

$$S_s \frac{\partial h}{\partial t} = \nabla \bullet \left( \overline{K} \bullet \nabla h \right) \tag{7-11}$$

where

$h$ = $h(x,y,t)$, the hydraulic head(m),

$S_s$ = $S_s(x,y,t)$, the specific storage of the Culebra ($m^{-1}$),

$\overline{K}$ = $\overline{K}(x,y,t)$, the hydraulic conductivity tensor (m/s).

The specific storage and hydraulic conductivity tensors are obtained from more directly measurable quantities.

$$S_s = \frac{S(x,y)}{\Delta Z}, \quad \overline{K} = \frac{\overline{T}(x,y)}{\Delta Z}, \tag{7-12}$$

where

$S(x,y)$ = storage coefficient in the Culebra (dimensionless),

$\Delta Z$ = $Z(x,y)$, Culebra thickness (m),

$\overline{T}(x,y)$ = one of a set of simulated transmissivity tensors (units: $m^2/s$). See Section 2.6.9 of Volume 3 for a discussion of how transmissivity fields are generated. Also see Section 7.5 of this report.

Given appropriate initial and boundary conditions, the SECO_2DH code is used to solve Equation 7-11 numerically to yield a potentiometric head field, $h(x,y,t)$, which may be used to compute specific discharge (or Darcy velocity) at any point in the Culebra:

$$\vec{q}(x,y,t) = -\overline{K} \bullet \nabla h \,(\mathrm{m/s}). \tag{7-13}$$

The storage coefficients $S(x,y)$, and the Culebra thickness $\Delta Z$ are treated as constants (as opposed to functions of position) in the 1992 series of calculations.

### 7.6.1.1 BOUNDARY CONDITIONS

Groundwater flow is modeled separately in regional and local grids (Figure 7-5) to provide increased resolution in the area of primary interest around the WIPP. In solving Equation (7-11), boundary conditions are specified on the outer edges of the regional grid; these boundary conditions may be a mix of the following kind, depending upon geological and hydrological conditions at a point on the regional boundary: (1) Dirichlet (specified $h$ on boundary); (2) inhomogeneous Neuman (specified gradients of $h$ on boundary); (3) Robin boundary conditions [a mixture of (1) and (2)]; and (4) adaptive boundary conditions, in which flux ($\vec{q}$) is specified at inflow boundaries and head ($h$) is specified at outflow boundaries. Boundary conditions for the local grid, in which radionuclide transport is modeled, are determined by the groundwater flow calculated for the regional grid. The actual problem geometry and specifications for boundary conditions that were used in the 1992 series of calculations can be found in Volume 4 of this report.

### 7.6.1.2 EFFECTS OF CLIMATE CHANGE

The effects of climate change are simulated through inclusion of time-dependent Dirichlet boundary conditions. Specifically, potentiometric heads on portions of the northwestern and northeastern edges of the regional grid (closest to the assumed recharge area for the Culebra) are set according to the formula (Swift, 1992, 1991)

$$h_f(x,y,t) = h_p(x,y)\left[\frac{3A_R+1}{4} - \left(\frac{A_R-1}{2}\right)\left(\cos\theta t - \sin\frac{\Phi}{2}t + \frac{1}{2}\cos\Phi t\right)\right] \tag{7-14}$$

where

$h_f$ = future potentiometric head (m)

$h_p$ = present potentiometric head (m)

$A_R$ = Recharge amplitude factor (dimensionless)

$\theta$ = Pleistocene glaciation frequency (Hz)

$\Phi$ = frequency of Holocene-type climatic fluctuations (Hz).

The recharge amplitude factor, $A_R$, is a number to be chosen between 1 and $\gamma > 1$. If $A_R = 1$, it is seen that there are no effects of climatic change. If $A_R > 1$, the maximum future head, $h_f$, will be greater than the present head. The constant $\gamma$ is a scaling factor that is chosen to ensure physically reasonable head values on the portion of the recharge boundary where boundary conditions are applied.

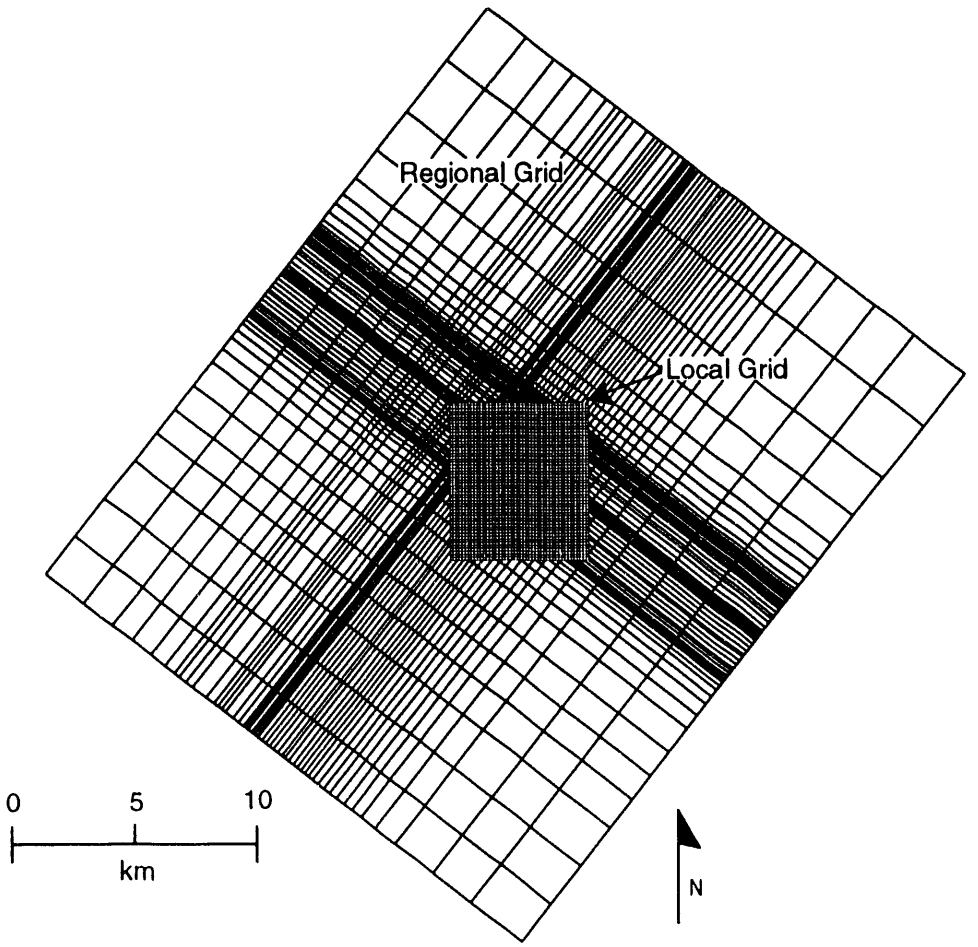


Figure 7-5. Example of regional and local grids used for disturbed fluid flow and transport calculations.



7-17

## 7.6.2 Solute Transport in the Culebra

The mathematical model of solute transport at the local scale is described in Section 1.4.6 of Volume 3 of the present series of reports. The physical assumptions and limitations of the 1992 version of the solute transport model are the same as those of the 1991 version (see 6.5.2.3 in WIPP PA Division, 1991b), namely:

1. The numerical solution is limited to two dimensions, reflecting the conceptual model of the Culebra Dolomite member (Figure 7-4).

2. Hydrodynamic dispersion is quantified with a Fick's law term.

3. Fracture flow is modeled as an equivalent porous medium of constant porosity.

4. No advective transport exists through the Culebra matrix; however, one-dimensional diffusion of solutes across fracture-matrix interfaces are allowed (Figure 7-4).

5. Adsorption of solutes on solid phases obeys a linear isotherm.

6. Local chemical equilibrium always exists between solutes and solid phases.

7. Material-property parameters are treated as constants over distinct material regions; in other words, intramaterial spatial variability is ignored.

The purpose of assumption 4 is to permit simple simulation of the phenomenon of dynamic solute storage within porous materials surrounding fractures. As solute concentration in fractures increases, solute will diffuse into and become immobilized within the matrix; if concentrations in fractures decreases with time, solute is returned to fractures by diffusion out of the matrix.

The major differences between the 1992 and 1991 versions of the solute transport model lie in the former's treatment of dispersivity parameters and adsorption effects in fracture flows. Details of changes in the way these important physical effects are implemented in the model are presented in the remainder of this section.

### 7.6.2.1 MODELING HYDRODYNAMIC DISPERSION

The components of the hydrodynamic dispersion tensor for the fracture system $D_{ij}$, are (Scheidegger, 1960)

$$D_{11} = \alpha_L \frac{(V_1)^2}{|V|} + \alpha_T \frac{(V_2)^2}{|V|} + D^*,$$

$$D_{22} = \alpha_L \frac{(V_2)^2}{|V|} + \alpha_T \frac{(V_1)^2}{|V|} + D^*,$$

$$D_{12} = D_{21} = (\alpha_L - \alpha_T)\frac{V_1 V_2}{|V|},$$

where $V_i$, $i$ = 1,2, are the components of the average linear velocity vector in the fracture system (m/s), $\alpha_L$ and $\alpha_T$ are respectively longitudinal and transverse dispersivities (m), $D^*$ is the molecular diffusion coefficient of the "average" solute species ($m^2/s$), and

$$|V| = \left(V_1^2 + V_2^2\right)^{1/2}$$

The dispersivities, $\alpha_L$ and $\alpha_T$, are measures of the dispersion of the true linear velocity vector about the average value. Ideally, these parameters would be estimated by fitting transport model calculations to results of tracer tests conducted in the Rustler Formation at an appropriate scale; but, in the absence of tracer-test results suitable for parameter estimation, the PA Department has had to rely on subjective judgments and results from stochastic transport theory to form the necessary estimates. In 1991, it was assumed that $\alpha_L$, $\alpha_T$ were imprecisely known constants (WIPP PA Division, 1991c, Section 2.6.2), with longitudinal dispersivity varying between 50 and 300 meters and transverse dispersivity varying between 5 and 30 meters (i.e., one-tenth of longitudinal dispersivity).

The treatment of Culebra dispersivity in the present (1992) series of PA calculations relies heavily on stochastic transport theory, exemplified by the universal scaling approach used by Neuman (1990) to investigate the compatibility of fractal transmissivity fields with the observed scale dependence of dispersivity. Neuman provides an expression that relates longitudinal dispersivity to the mean value of the variogram of ln $T$ variance at the scale $S$ and the travel distance $L$, namely

$$\alpha_L = C_o \, L \, \sigma_y^2(S), \tag{7-15}$$

where $C_o$ is a constant ~ 1 in isotropic media; and

$$\sigma_y^2(S) = \bar{\gamma}(v, v) \simeq \frac{1}{v^2} \int_v \int_v \gamma(\mathrm{x} - \mathrm{y}) \, \mathrm{dx} \, \mathrm{dy}, \tag{7-16}$$

where $\gamma(h)$ is the variogram of ln $T$, $h = |\mathrm{x}\text{-}\mathrm{y}|$, and each integration in the above expression is carried over a fixed area v, ~ $L^2$. In current (1992) PA calculations, $C_o$ = 1 and $L$ is taken to be the size of the model block in which $\alpha_L$ is being evaluated.

The variogram, $\gamma(h)$, is taken to be the one used in the "local" scale generation of the 1992 random transmissivity fields (Section 7.5 and Appendix D, Volume 3),

$$\gamma(h) = 1.2 \times 10^{-3}\, h\,. \tag{7-17}$$

Here, the "local" scale is defined as that appropriate for the transmissivity measurements, i.e., a scale length between slug tests radii of influence and pump tests radii of influence; such a scale length is of the order of 10 meters. Note that Equation (7-17) is a linear variogram, for which the concepts of "correlation length" and "integral scale" have no meaning.

The integral in Equation (7-16) has been evaluated by Journel and Huijlbregts (1978, p. 113) for a linear variogram $\gamma(h) = h$ and a rectangular mesh with dimensions $L$ and $\ell$. Their result is analytically messy, but in the case where $L = \ell$ ( v = area of a square of side $L$), their expression reduces to

$$\bar{\gamma}(v, v) = 0.5213\, L\,.$$

Multiplying this expression by the constant in Equation (7-17), $1.2 \times 10^{-3}$, and substituting for $\bar{\gamma}(v, v)$ in Equation (7-13) gives an expression for the longitudinal dispersivity in terms of the size of the model block in which $\alpha_L$ is being evaluated:

$$\alpha_L \simeq 6.2 \times 10^{-4}\, L^2 \text{ (m)}\,. \tag{7-18}$$

In practice, a value of 1.5 meters is added to the $\alpha_L$ obtained by Equation (7-18) in order to account for microscale dispersion that must occur below the "local" scale.

The ratio of longitudinal to transverse dispersivity does not seem to be scale dependent; data from Gelhar et al. (1992) suggest that this ratio is almost always between 10 and 50. In the present (1992) series of calculations, the fixed relation

$$\alpha_T = \frac{1}{10}\,\alpha_L \tag{7-19}$$

was adopted.

Note that using model block size as travel distance in obtaining Equation (7-18) is equivalent to the assumption that dispersivity reaches its asymptotic limit at the scale of a model block, and any other non-asymptotic behavior is taken care of by variability of the simulated transmissivity fields (Section 7.5 and Appendix D, Volume 3).

### 7.6.2.2 MODELING CHEMICAL SORPTION IN FRACTURE FLOWS

Chemical retardation of solutes by sorption on fracture surfaces was modelled in 1990-1991 PA calculations with a formula proposed by M. D. Siegel (1990). Siegel suggested that the effective solute velocity in a clay-lined fracture, $V_{eff}$, is related to the average linear velocity of groundwater in the fracture, $V$, by

$$\frac{V}{V_{eff}} = 1 + \rho_c \, K_{dc} \left( b_c / b \right), \tag{7-20}$$

where

$\rho_c$ = density of clay liner (kg/m$^3$),

$K_{dc}$ = partition coefficient of solute in clay (m$^3$/kg),

$2b_c$ = total thickness of clay layer in a fracture (m), and

$2b$ = fracture aperture (m).

The expression on the right side of Equation (7-20) is called $R$, the retardation factor; the partition coefficient $K_{dc}$ is also called the distribution coefficient.

Consideration of Equation (7-20) will show that it cannot generally describe retardation of solutes being transported through an *open*, saturated fracture; in this case, retardation of solute molecules must proceed by reactions between the mobilized species and stationary species located on the solid surface facing the fracture void space. In contrast, Equation (7-20) turns out to be a "thin-skin" approximation to retardation of mobile solutes *within* pore spaces of the clay layer, which is valid only after solute molecules have diffused or been advected into the clay layer and concentrational equilibrium is nearly established. In other words, Equation (7-20) is appropriate for concentrational equilibrium; note, however, that it may take a long time to reach concentrational equilibrium by diffusion of solute through highly sorbing clay and that, by assuming instantaneous equilibrium, the retardation of solutes in fracture flows may have been overestimated in the 1990-1991 calculations.

The PA Department abandoned use of Equation (7-20) in 1992 and, for reasons provided below, has set $R = 1$ in fracture flows (see Equation 1.4.6-1 in Section 1.4.6, Volume 3 of this report). An approximate, but physically motivated expression for the retardation of solutes in fracture flows is derived in the remainder of this subsection and used to justify the choice of $R = 1$.

Freeze and Cherry (1979, p. 411) give an expression for the retardation factor in solute transport through a planar fracture of aperture $2b$:

$$R = 1 + \frac{1}{b} K_a, \tag{7-21}$$

where

$$K_a = \frac{\text{mass of solute on solid phase per unit area of solid phase}}{\text{concentration of solute in solution}} \quad (\text{m}).$$

Equation (7-21) should be valid when time scales for (1) diffusion across a fracture aperture and (2) achievement of equilibrium in surficial chemical reactions are always much smaller than other problem time scales (e.g., time required to advect a solute molecule across a grid cell, time required to diffuse into clay layers).

The surficial distribution coefficient, $K_a$, can be related to the familiar mass-based distribution coefficient (Freeze and Cherry, 1979, p. 405),

$$K_d = \frac{\text{mass of solute on solid phase per unit mass of solid phase}}{\text{concentration of solute in solution}} \quad (\text{m}^3/\text{kg}).$$

by

$$K_a = K_d / \sigma_m ,$$

where $\sigma_m$ is the surface area per unit mass of the solid phase ($m^2$/kg). Obviously, $\sigma_m$ depends upon the physical nature of the solid phase, here a natural aggregation of clay grains on the surfaces of saturated fractures in the Culebra Dolomite. No measurements or estimates of $\sigma_m$ for these clays seem to be available, but an order-of-magnitude estimate of this quantity can be rapidly made if the clay is visualized as an aggregation of regularly packed spheres of radius $a$ (i.e., spheres centered on vertices of a cubic lattice of elemental size $2a$). To begin making this estimate, consider $M$ kg of bulk clay having *grain-density* $\rho_g$; then the number of spheres in this mass is

$$n_p \simeq (3M)/\left(4\pi a^3 \rho_g\right),$$

and the surface area of the solid phase that is presented to the pore space of the $M$ kg of clay is

$$A \simeq 4\pi a^2 n_p = \frac{3M}{a\rho_g}.$$

It follows that

$$\sigma_m = \frac{A}{M} \approx \frac{3}{a\rho_g}, \quad \text{and so } K_a \simeq \frac{a\rho_g K_d}{3}.$$

Substitution of this result in Equation (7-21) gives the promised order-of-magnitude estimate of the fracture retardation factor:

$$R \simeq 1 + \frac{\rho_g}{3} K_d \, (a/b). \tag{7-22}$$

Note the superficial similarity of expressions in Equations (7-20) and (7-22). Their relative magnitudes are nevertheless always different as can be seen by forming the ratio of ($R$-1)s from the respective formulas; for instance, the ratio of ($R$-1) for Equation (7-22) to ($R$-1) for Equation (7-20) is of the order of $a/b_c$, the ratio of clay particle size to clay layer thickness. In all but the narrowest of fracture apertures, $a/b_c$ should be of the order of $10^{-2}$ or less (take $a$ = 1 μm, $b$ = 100 μm). Thus, retardations computed from Equation (7-22) should be much less than retardations computed from Equation (7-20), justifying the earlier claim that retardation in fracture flows (i.e., "single porosity" model) may have been overestimated in the 1990-1991 series of PA calculations.

Clay layers on fracture surfaces actually played two roles in 1990-1991 PA models of solute transport in the Culebra Dolomite: (1) the role described above, i.e., as agents of retardation of solutes in fracture flows, and (2) as barriers to mass transfer of solutes across the matrix-fracture interface (the "matrix skin resistance" of Section 2.6.7 in WIPP PA Division, 1991c). The PA Department has also abandoned the second of these roles for clay linings in 1992 versions of the solute-transport models. Clay linings are now treated as extensions of the matrix and a single diffusion equation [Equation (1.4.6-5), Section 1.4.6, Volume 3 of this series] is used to model solute mass transport in an effective porous media comprised of Culebra matrix blocks and their adjacent clay linings.

## 7.7 Direct Removal of Waste

Of the possible pathways for release during the 10,000-year regulatory period, one of the most important is that caused by the direct removal of waste that would result when an exploratory drill bit inadvertently penetrates a waste storage room. To quantify the extent of radioactive release resulting from direct removal of waste, the model described below, extracted from Berglund (1992), has been developed. The current performance assessment model assumes that future drilling techniques will be similar to those in use today. This assumption is necessary to provide a basis on which predictions of release can be estimated.

In rotary drilling, a cutting bit attached to a series of hollow drill collars and drill pipes is rotated at a fixed angular velocity and is directed to cut downward through underlying strata. To remove the material loosened by the drilling action, a drilling fluid ("mud") is pumped down the drill pipe, through and around the drill bit, and up to the surface within the annulus formed by the drill pipe and the borehole wall (Figure 7-6).

If an exploratory drill bit penetrates a waste-filled room, waste resulting from three separate physical processes can mix with the drilling fluid and be transported to the surface:

- cuttings—waste contained in the cylindrical volume created by the cutting action of the drill bit through the waste,
- cavings—waste that erodes from the borehole in response to the upward-flowing drilling fluid within the annulus, and
- spallings—waste surrounding the eroded borehole that is transported by waste-generated gas escaping to the lower-pressure borehole.

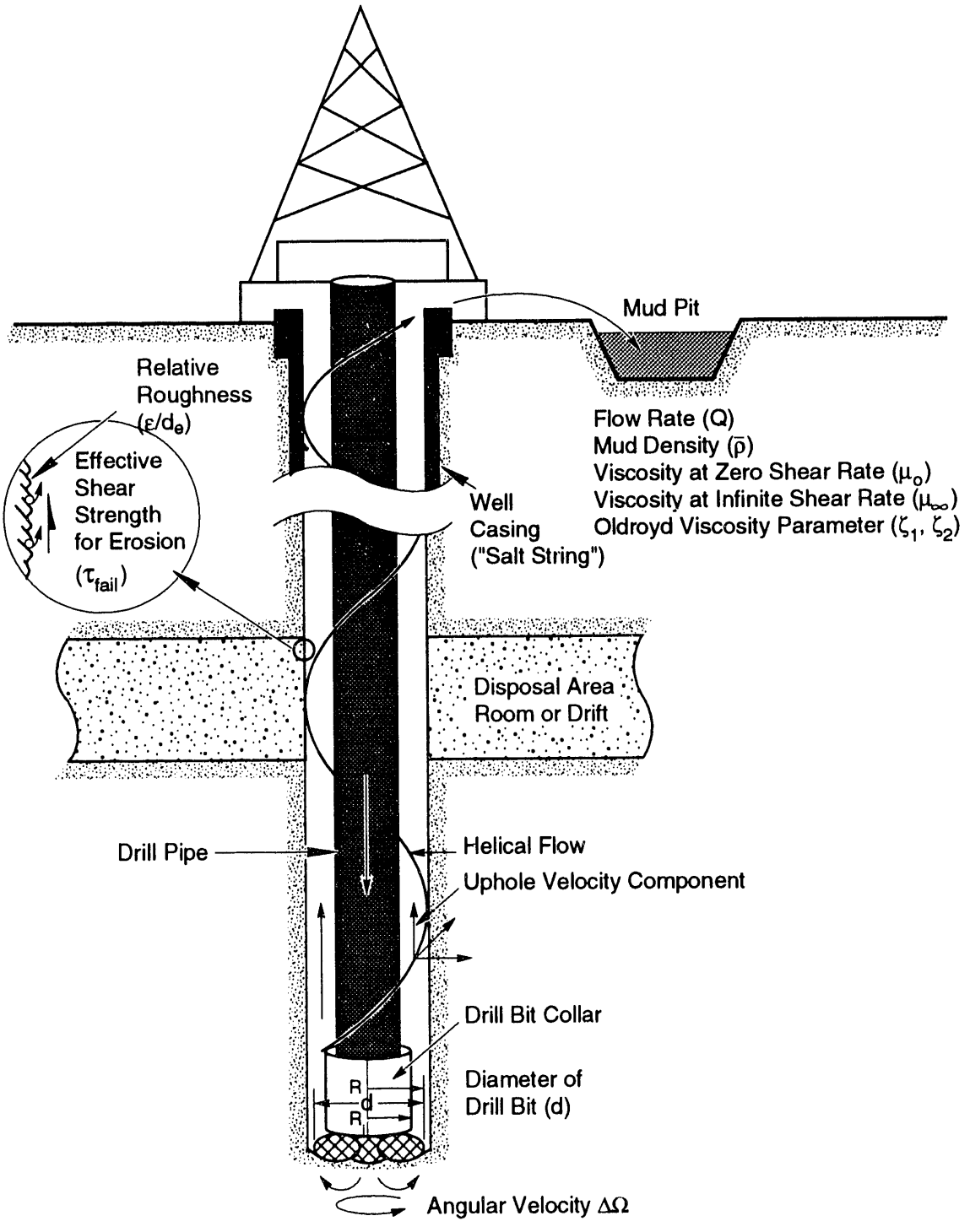


Figure 7-6. Rotary drilling.

A discussion of these three processes follows.

## 7.7.1 Cuttings

For a gauge borehole, the volume of cuttings removed and transported to the surface is equal to the product of the drill bit area and the drill depth. Thus, to estimate the total volume of waste removed due to the cutting action of the drill bit ($V$), it is only necessary to know the compacted repository height ($h$) and the drill-bit area ($A$):

$$V = Ah. \tag{7-23}$$

The cuttings volume calculated in this manner is a lower bound to the total quantity of waste removed by drilling.

## 7.7.2 Cavings

While a number of factors that influence drillhole wall erosion have been identified in the literature (Broc, 1982), industry opinion singles out fluid shear stress as the most important factor (Walker and Holman, 1971; Darley, 1969). This analysis therefore assumes that borehole erosion is caused primarily by the magnitude of fluid shear stress acting on the borehole wall. This analysis also assumes that erosion of wall material occurs when the fluid shear stress at the wall exceeds the effective shear strength for erosion of the wall material (the surrounding compacted repository wastes) and that the diameter of the bored hole increases until this condition no longer exists. In this process, it is assumed that sufficient time is available to complete the erosion process. All the eroded material is assumed to pass to the surface in the flowing drilling fluid.

Flow in the annulus between the drill pipe and borehole wall is usually laminar (Darley and Gray, 1988). Adjacent to the collars, however, the smaller annular volume created by the larger collar diameter (Figure 7-6) causes higher mud velocities, making flow either laminar or turbulent (Berglund, 1990; Pace, 1990). For laminar flow, the analysis lends itself to classical solution methods. Turbulent flow, where the flow is assumed to be axial with no rotational component, requires a more approximate approach.

### 7.7.2.1 LAMINAR FLOW

Below Reynolds numbers of about 2100 for Newtonian fluids and 2400 for some non-Newtonian fluids (Walker, 1976), experiments have shown that the flow of a fluid in a circular pipe or annulus is well behaved and can be described using a well-defined relationship between the velocity field and the fluid shear stress. This type of flow is called laminar. Drilling fluids exhibit non-Newtonian fluid behavior, making it necessary to choose a functional form for the variation of viscosity with shear rate for the fluid. Of the several different functional forms that can be used to account for the varying viscosity, this analysis uses a form chosen by Oldroyd (1958) and further developed by Savins and Wallick (1966).

Savins and Wallick (1966) have shown that the solution for laminar helical flow of a non-Newtonian fluid in an annulus could be written in terms of three nonlinear integral equations:

$$F_1 = \int_{\alpha}^{1} \left( \frac{\rho^2 - \lambda^2}{\rho} \right) \frac{d\rho}{\eta} = 0$$

$$F_2 = C \int_{\alpha}^{1} \frac{d\rho}{\rho^3 \eta} - \Delta\Omega = 0$$

$$F_3 = \frac{4Q}{\pi R^3} + 4\left( \frac{RJ}{2} \right) \int_{\alpha}^{1} \left( \frac{\alpha^2 - \rho^2}{\eta} \right) \left( \frac{\rho^2 - \lambda^2}{\rho} \right) d\rho = 0, \quad (7\text{-}24)$$

where $Q$ is the drilling fluid (mud) flow rate; $r$ is the radial coordinate; $\alpha$ is the ratio of the collar radius over the cutting radius ($R_i/R$) (Figure 7-6); $\Delta\Omega$ is the drill string angular velocity; $\eta$ is the viscosity of the drilling fluid; $\rho$ is the non-dimensional radial coordinate representing the ratio $r/R$; and $\lambda^2$, $RJ/2$ , and $C$ are parameters related to the fluid shear stresses. As long as annular flow remains in the laminar regime, the above three nonlinear integral equations can be solved numerically to determine the final eroded volume of the borehole (a function of the effective shear strength for erosion, $\tau_{fail}$) and the resulting total cavings volume.

### 7.7.2.2 TURBULENT FLOW

At a Reynolds number of about 3000, flow becomes fully turbulent; momentum effects dominate and fluid viscosity is no longer as important in characterizing pressure losses. A far more important parameter is the surface roughness past which the fluid must flow.

The increased complexity of turbulent flow makes empirical procedures necessary. For axial flow in an annulus, the pressure loss under turbulent conditions can be approximated by (Broc, 1982)

$$\Delta P = \frac{2 f L \bar{\rho} \bar{V}^2}{(0.8165) D}, \quad (7\text{-}25)$$

where $f$ is the coefficient of pressure head loss (Fanning friction factor), $D$ is the hydraulic diameter, $L$ is the borehole length, $\bar{V}$ is the average fluid velocity, and $\bar{\rho}$ is the drill fluid density.

If the shear stress due to the flowing fluid is assumed to be uniformly distributed on the inner and outer surfaces of the annulus, it can be easily shown using Equation 7-25 that the shear stress is related to the average fluid velocity through the relation

$$\tau = \frac{f\bar{\rho}\bar{V}^2}{2(0.8165)}, \tag{7-26}$$

The Fanning friction factor is empirically related to the Reynolds number and relative roughness by the equation (Whittaker, 1985)

$$\frac{1}{\sqrt{f}} = -4\log_{10}\left[\frac{\varepsilon}{3.72D} + \frac{1.255}{R_e\sqrt{f}}\right], \tag{7-27}$$

where $\varepsilon/D$ is the relative roughness and $R_e$ is the Reynolds number. For circular pipes, $D$ in this equation represents the inside diameter and $\varepsilon$ is the absolute roughness or the average depth of pipe wall irregularities. In the absence of a similar equation for flow in an annulus, it is assumed that this equation also applies here, where $D$ is the hydraulic diameter, and $\varepsilon$ is the absolute roughness of the waste-borehole interface.

The above three equations can be used to obtain the final eroded borehole radius under turbulent flow conditions by forcing the fluid shear stress acting on the borehole wall to equal the shear strength for erosion of the repository waste ($\tau_{fail}$).

### 7.7.3 Spallings

The spalling of borehole walls is a common occurrence in oil and gas drilling and can be caused by an encounter with a geopressurized formation; a similar event may occur if an exploratory drill bit penetrates a waste-filled, pressurized room at the WIPP. Corrosion and biodegradation of the waste will generate gas, raising the gas pore pressure in the waste to values approaching and perhaps exceeding the lithostatic level within the next 700 to 2,000 years. Because the permeability of the surrounding Salado Formation is expected to be 1 to 7 orders of magnitude less than that of the compacted waste, the Salado can be considered impermeable compared to the waste. The intrusion of a drill bit into the waste could therefore "suddenly" expose the waste with its high pore pressure (for example, 14.8 MPa) to the borehole hydrostatic pressure of 7.7 MPa (assuming a saturated salt solution is used while drilling), causing gas to escape to the borehole after flowing through the compacted waste. The escaping gas may compromise the stability of the borehole wall and contribute to the quantity of waste material that reaches the surface environment.

Spalling is a complex process that involves the flow of gas in a moving waste matrix, changing stress states, changing porosity and permeability of the waste, waste failure, and when the waste interacts with the drill bit, turbulent mixing of the three phases—solid waste, drilling fluid, and gas. The approach for modeling spalling caused by the intrusion of an exploratory drill bit is still being developed.

The current state of understanding for spall as related to WIPP is treated in Berglund (1992). In addition to a discussion of related literature, Berglund (1992) describes several types of calculations, each of which addresses a different aspect of gas flow and waste response from a penetrated, gas-pressurized, waste storage room. The waste response is found to be very dependent on the constitutive nature of the compacted composite waste, a feature

that is currently unknown. If the waste is assumed to behave as a granular, soil-like material with a nonlinear constitutive character and a small cohesive strength, the behavior of the waste subject to gas flow indicates a movement toward the borehole after penetration. In both the one- and two-dimensional computational models, where an instantaneous borehole pressure drop is assumed, the inward motion of the waste-borehole boundary would quickly (in milliseconds) be blocked by the presence of the drill string and would remain impressed against the drill string while a sufficient pore pressure gradient is maintained.

What happens to the waste as it is impressed against the drill string is not known because the interface between the waste and drill stem is very difficult to characterize without experimental verification. One possibility is the compressed waste will completely block the flow of drilling mud. Whether the drilling operation can proceed in such circumstances is unknown. Certainly the flow of gas out of the waste will be further restricted if not completely blocked. Such a restriction would prolong the compressive stresses acting between the drill string and the waste. Another possibility is that some drilling fluid may be able to channel its way through the waste-drill string boundary carrying eroded waste up into the upper borehole.

The driller may, however, be able to detect the resistance afforded by the waste pressing against the drill stem by the increase in torque, circulation pressure, and by a drop in mud flowrate (Austin, 1983). Under such conditions the driller may raise the cutting bit and allow the "spall" to continue naturally, eventually proceeding after the process diminishes (Short, 1982). Often under these conditions a repetitive process is undertaken of cleaning out, drilling ahead a few feet of new hole, picking up the drill bit to check for fill, then cleaning out again. This is repeated until spalling slows. The cleanout procedure can be used for 12 to 24 hours, or longer, if it shows sign of becoming effective (Short, 1982).

If drilling can proceed with the waste impressed against the drilling equipment, erosion will probably occur at the interface and could continue until a significant portion of the gas has leaked from the penetrated room or the target drill depth is reached. Based on leakage rates from the waste with uniform permeabilities, significant volumes of gas will be removed from the room only after several hours for the greatest waste permeability and hundreds of days for the least permeability. Moreover, the decrease in waste permeability caused by the compressive stress field at the drill string-waste interface is likely to decrease the gas leakage rates significantly.

In the analyses considered in Berglund (1992), actions to prevent a blowout taken by the driller after encountering a gas-pressurized formation are also discussed. When formation gas flow into a borehole is detected at the surface, such as by an increase in return mud volume, the driller usually will "close in" the well by engaging blowout preventers (BOPs) to prevent serious injury to personnel and damage to equipment. This action is usually taken within a minute or two after the "kick" is first observed, and the effect is that the gas flow from the formation to the borehole is effectively curtailed (Mills, 1984). The well is then "killed" by increasing the mud density in the borehole so that the formation (waste) pore pressure is in balance with the mud pressure. The drilling can then safely continue. With the pressure gradient in the borehole wall thus reduced to zero, spallation will cease and waste will be brought to the surface by erosion only. BOPs are engaged only if a blowout condition is detected. For high-permeability wastes ($k = 1 \times 10^{-13}$ $m^2$), the rate of flow of gas to the borehole will increase the mud volume in the annulus significantly, and it is very likely that the well will be "killed." However, for lower permeabilities, the gas flowrate is much reduced; the driller may not engage BOPs but continue drilling, thus allowing spall into the borehole to occur.

Estimating the amount of material that may eventually be passed into the borehole as the result of gas generation in the repository is difficult and speculative. However, based upon the analysis performed and the literature examined to date, it does not appear to be unreasonable that a volume of waste greater than the lower bound cuttings volume (bit area × waste depth) could eventually reach the ground surface. Currently, little data are available that predict the constitutive nature of the compacted, decomposed waste at the time of intrusion, nor have there been any experiments performed that could confirm the mechanisms for borehole spall as discussed. These data are currently being developed.

# 8. REFERENCES


Adams, J.E. 1944. "Upper Permian Ochoa Series of Delaware Basin, West Texas and Southeastern New Mexico," *Bulletin of the American Association of Petroleum Geologists.* Vol. 28, no. 11, 1596-1625.

Anderson, R.Y. 1981. "Deep-Seated Salt Dissolution in the Delaware Basin, Texas and New Mexico," *Environmental Geology and Hydrology in New Mexico.* Eds. S. G. Wells and W. Lambert. New Mexico Geological Society Special Publication No. 10. Roswell, NM: New Mexico Geological Society, 133-145.

Apostolakis, G., R. Bras, L. Price, J. Valdes, K. Wahi, and E. Webb. 1991. *Techniques for Determining Probabilities of Events and Processes Affecting the Performance of Geologic Repositories: Suggested Approaches.* NUREG/CR-3964, SAND86-0196. Albuquerque, NM: Sandia National Laboratories. Vol. 2.

Austin, E.H. 1983. *Drilling Engineering Handbook.* Boston, MA: International Human Resources Development Corporation.

Bachman, G.O. 1981. *Geology of Nash Draw, Eddy County, New Mexico.* U.S. Geological Survey Open-File Report 81-31. Denver, CO: U. S. Geological Survey.

Bachman, G.O. 1984. *Regional Geology of Ochoan Evaporites, Northern Part of Delaware Basin.* New Mexico Bureau of Mines and Mineral Resources Circular 184. Socorro, NM: New Mexico Bureau of Mines and Mineral Resources.

Bachman, G.O. 1987. *Karst in Evaporites in Southeastern New Mexico.* SAND86-7078. Albuquerque, NM: Sandia National Laboratories.

Beauheim, R.L. 1986. *Hydraulic-Test Interpretations for Well DOE-2 at the Waste Isolation Pilot Plant (WIPP) Site.* SAND86-1364. Albuquerque, NM: Sandia National Laboratories.

Beauheim, R.L. 1987a. *Interpretations of Single-Well Hydraulic Tests Conducted At and Near the Waste Isolation Pilot Plant (WIPP) Site, 1983-1987.* SAND87-0039. Albuquerque, NM: Sandia National Laboratories.

Beauheim, R.L. 1987b. *Analysis of Pumping Tests of the Culebra Dolomite Conducted At the H-3 Hydropad at the Waste Isolation Pilot Plant (WIPP) Site.* SAND86-2311. Albuquerque, NM: Sandia National Laboratories.

Beauheim, R.L. 1987c. *Interpretation of the WIPP-13 Multipad Pumping Test of the Culebra Dolomite at the Waste Isolation Pilot Plant (WIPP) Site.* SAND87-2456. Albuquerque, NM: Sandia National Laboratories.

Beauheim, R.L., and P.B. Davies. 1992. "Experimental Plan for Tracer Testing in the Culebra Dolomite at the WIPP Site." Revision A. Albuquerque, NM: Sandia National Laboratories.

Beauheim, R.L., and R.M. Holt. 1990. "Hydrogeology of the WIPP Site," *Geological and Hydrological Studies of Evaporites in the Northern Delaware Basin for the Waste Isolation Pilot Plant (WIPP), New Mexico.* Geological Society of America 1990 Annual Meeting Field Trip #14 Guidebook. Dallas, TX: Dallas Geological Society. 131-179.

Beauheim, R.L., G.J. Saulnier, Jr., and J. D. Avis. 1991. *Interpretation of Brine-Permeability Tests of the Salado Formation at the Waste Isolation Pilot Plant Site: First Interim Report.* SAND90-0083. Albuquerque, NM: Sandia National Laboratories.

Bechtel National, Inc. 1986. *Waste Isolation Pilot Plant Design Validation Final Report.* DOE/WIPP-86-010. Prepared for U.S. Department of Energy. San Fransisco, CA: Bechtel National, Inc.

Berglund, J.W. 1990. Appendix A, "Letter 1a: Bar Graphs Representing Range of Values for Drilling Operations Near WIPP Site," *Data Used in Preliminary Performance Assessment of the Waste Isolation Pilot Plant (1990).* R.P. Rechard, H. Iuzzolino, and J. S. Sandha (Report Authors). SAND89-2408. Albuquerque, NM: Sandia National Laboratories. A-157 through A-164.

Berglund, J.W. 1992. *Mechanisms Governing the Direct Removal of Wastes from the Waste Isolation Pilot Plant Repository Caused by Exploratory Drilling.* SAND92-7295. Albuquerque, NM: Sandia National Laboratories.

Bertram-Howery, S.G., and R.L. Hunter, eds. 1989. *Preliminary Plan for Disposal-System Characterization and Long-Term Performance Evaluation of the Waste Isolation Pilot Plant.* SAND89-0178. Albuquerque, NM: Sandia National Laboratories.

Bertram-Howery, S.G., and P.N. Swift. 1990. *Status Report: Potential for Long-Term Isolation by the Waste Isolation Pilot Plant Disposal System.* SAND90-0616. Albuquerque, NM: Sandia National Laboratories.

Bertram-Howery, S.G., M.G. Marietta, R.P. Rechard, P.N. Swift, D.R. Anderson, B.L. Baker, J.E. Bean, Jr., W. Beyeler, K.F. Brinster, R.V. Guzowski, J.C. Helton, R.D. McCurley, D.K. Rudeen, J.D. Schreiber, and P. Vaughn. 1990. *Preliminary Comparison with 40 CFR Part 191, Subpart B for the Waste Isolation Pilot Plant, December 1990.* SAND90-2347. Albuquerque, NM: Sandia National Laboratories.

Blom, G. 1989. *Probability and Statistics: Theory and Applications.* New York, NY: Springer-Verlag.

Bonano, E.J., S.C. Hora, R.L. Keeney, and D. von Winterfeldt. 1990. *Elicitation and Use of Expert Judgement in Performance Assessment for High-Level Radioactive Waste Repositories.* NUREG/CR-5411, SAND89-1821. Albuquerque, NM: Sandia National Laboratories.

Borns, D.J., and J.C. Stormont. 1988. *An Interim Report on Excavation Effect Studies at the Waste Isolation Pilot Plant: The Delineation of the Disturbed Rock Zone.* SAND87-1375. Albuquerque, NM: Sandia National Laboratories.

Borns, D.J., and J.C. Stormont. 1989. "The Delineation of the Disturbed Rock Zone Surrounding Excavations in Salt," *Rock Mechanics as a Guide for Efficient Ulilization of Natural Resources, Proceedings of the 30th U.S. Symposium, West Virginia University, Morgantown, WV. June 19-22, 1989.* Ed. A.W. Rhair. Brookfield, VT: A.A. Balkema. 353-360.

Borns, D.J., L.J. Barrows, D.W. Powers, and R.P. Snyder. 1983. *Deformation of Evaporites Near the Waste Isolation Pilot Plant (WIPP) Site.* SAND82-1069. Albuquerque, NM: Sandia National Laboratories.

Bredehoeft, J.D. 1988. "Will Salt Repositories Be Dry?" *EOS, Transactions, of the American Geophysical Union.* Vol. 69, no. 9.

Brinster, K.F. 1991. *Preliminary Geohydrologic Conceptual Model of the Los Medaños Region Near the Waste Isolation Pilot Plant for tne Purpose of Performance Assessment.* SAND89-7147. Albuquerque, NM: Sandia National Laboratories.

Broc, R., ed. 1982. *Drilling Mud and Cement Slurry Rheology Manual.* Houston, TX: Gulf Publishing Company.

Brodsky, N.S., and T.W. Pfeifle. 1992. *Consolidation of the Waste Isolation Pilot Plant Crushed Salt/Bentonite Mixtures as a Function of Confining Pressure and Moisture Content as Compared With Constitutive Model Predictions.* SAND91-7071. Albuquerque, NM: Sandia National Laboratories.

Brookins, D.G., S.J. Lambert, and D.B. Ward. 1990. *Authigenic Clay Minerals in the Rustler Formation, WIPP Site, New Mexico.* SAND89-1405. Albuquerque, NM: Sandia National Laboratories.

Brush, L.H. 1990. *Test Plan for Laboratory and Modeling Studies of Repository and Radionuclide Chemistry for the Waste Isolation Pilot Plant.* SAND90-0266. Albuquerque, NM: Sandia National Laboratories.

Brush, L.H., and D.R. Anderson. 1989a. Appendix E: "Estimates of Radionuclide Concentrations in Brines," *Performance Assessment Methodology Demonstration: Methodology Development for Purposes of Evaluating Compliance with EPA 40 CFR 191, Subpart B, for the Waste Isolation Pilot Plant.* M.G. Marietta, S.G. Bertram-Howery, D.R. Anderson, K.F. Brinster, R.V. Guzowski, H. Iuzzolino, and R.P. Rechard (Report Authors). SAND89-2027. Albuquerque, NM: Sandia National Laboratories. E-1 through E-14.

Brush, L.H., and D.R. Anderson. 1989b. Appendix A.2: "Effects of Microbial Activity on Repository Chemistry, Radionuclide Speciation, and Solubilities in WIPP Brines," *Systems Analysis, Long-Term Radionuclide Transport, and Dose Assessments, Waste Isolation Pilot Plant (WIPP), Southeastern New Mexico; March 1989.* Eds. A.R. Lappin, R.L. Hunter, D.P. Garber, and P.B. Davies. SAND89-0462. Albuquerque, NM: Sandia National Laboratories. A-31 through A-50.

Butcher, B.M., C.F. Novak, and M. Jercinovic. 1991. *The Advantages of a Salt/Bentonite Backfill for Waste Isolation Pilot Plant Disposal Rooms.* SAND90-3074. Albuquerque, NM: Sandia National Laboratories.

Cauffman, T.L., A.M. LaVenue, and J.P. McCord. 1990. *Ground-Water Flow Modeling of the Culebra Dolomite. Volume II: Data Base.* SAND89-7068/2. Albuquerque, NM: Sandia National Laboratories.

Chapman, J.B. 1986. *Stable Isotopes in the Southeastern New Mexico Groundwater: Implications for Dating Recharge in the WIPP Area.* EEG-35. Santa Fe, NM: Environmental Evaluation Group, Environmental Improvements Division, Health and Environment Department, State of New Mexico.

Chapman, J.B. 1988. *Chemical and Radiochemical Characteristics of Groundwater in the Culebra Dolomite, Southeastern New Mexico.* EEG-39. Santa Fe, NM: Environmental Evaluation Group, Environmental Improvement Division, Health and Environment Department, State of New Mexico.

Cheeseman, R.J. 1978. "Geology and Oil/Potash Resources of the Delaware Basin, Eddy and Lea Counties, New Mexico," *Geology and Mineral Deposits of Ochoan Rocks in Delaware Basin and Adjacent Areas.* Ed. G.S. Austin. New Mexico Bureau of Mines and Mineral Resources Circular 159. Socorro, NM: New Mexico Bureau of Mines and Mineral Resources. 7-14.

COHMAP (Cooperative Holocene Mapping Project) Members. 1988. "Climatic Changes of the Last 18,000 Years: Observations and Model Simulations," *Science.* Vol. 241, no. 4869, 1043-1052.

Cole, F.W. 1975. *Introduction to Meteorology.* 2nd. ed. New York, NY: John Wiley and Sons, Inc.

Cranwell, R.M., J.E. Campbell, J.C. Helton, R.L. Iman, D.E. Longsine, N.R. Ortiz, G.E. Runkle, and M.J. Shortencarier. 1987. *Risk Methodology for Geologic Disposal of Radioactive Waste: Final Report.* NUREG/CR-2452, SAND81-2573. Albuquerque, NM: Sandia National Laboratories.

Cranwell, R.M., R.V. Guzowski, J.E. Campbell, and N.R. Ortiz. 1990. *Risk Methodology for Geologic Disposal of Radioactive Waste: Scenario Selection Procedure.* NUREG/CR-1667, SAND80-1429. Albuquerque, NM: Sandia National Laboratories.

Darley, H.C.H. 1969. "A Laboratory Investigation of Borehole Stability," *JPT, Journal of Petroleum Technology.* Vol. 21, no. 7, 883-892.

Darley, H.C.H., and G.R. Gray. 1988. *Composition and Properties of Drilling and Completion Fluids.* Houston, TX: Gulf Publishing Company. 243.

Davies, P.B. 1984. "Deep-Seated Dissolution and Subsidence in Bedded Salt Deposits." Ph.D. dissertation. Stanford, CA: Department of Applied Earth Sciences, Stanford University.

Davies, P.B. 1989. *Variable-Density Ground-Water Flow and Paleohydrology in the Waste Isolation Pilot Plant (WIPP) Region. Southeastern New Mexico.* U.S. Geological Survey Open-File Report 88-490. Albuquerque, NM: U.S. Geological Survey.

de Marsily, G. 1986. *Quantitative Hydrogeology: Groundwater Hydrology for Engineers.* Orlando, FL: Academic Press, Inc.

Dosch, R.G. 1980. *Assessment of Potential Radionuclide Transport in Site-Specific Geologic Formations.* SAND79-2468. Albuquerque, NM: Sandia National Laboratories.

Dosch, R.G. 1981. *Solubility and Sorption Characteristics of Uranium (VI) Associated with Rock Samples and Brines/Groundwaters from WIPP and NTS.* SAND80-1595. Albuquerque, NM: Sandia National Laboratories.

Dosch, R.G., and A.W. Lynch. 1978. *Interaction of Radionuclides with Geomedia Associated with the Waste Isolation Pilot Plant (WIPP) Site in New Mexico.* SAND78-0297. Albuquerque, NM: Sandia National Laboratories.

Earth Technology Corporation. 1988. *Final Report for Time Domain Electromagnetic (TDEM) Surveys at the WIPP Site.* SAND87-7144. Albuquerque, NM: Sandia National Laboratories.

Freeze, R.A., and J.A. Cherry. 1979. *Groundwater.* Englewood Cliffs, NJ: Prentice-Hall, Inc.

Gallegos, D.P., P.I. Pohl, and C.D. Updegraff. 1992. *An Investigation of the Impact of Conceptual Model Uncertainty on the Estimated Performance of a Hypothetical High-Level Nuclear Waste Repository Site in Unsaturated, Fractured Tuff.* SAND90-2882. Albuquerque, NM: Sandia National Laboratories.

Gelhar, L.W., C. Welty, and K.R. Rehfeldt. 1992. "A Critical Review of Data on Field-Scale Dispersion in Aquifers," *Water Resources Research.* Vol. 28, no. 7, 1955-1974.

Geohydrology Associates, Inc. 1979. *Water-Resources Study of the Carlsbad Potash Area, New Mexico.* Consultant Report for the U.S. BLM. Contract No. YA-S12-CT8-195. (Copy on file in the Waste Management and Transportation Library, Sandia National Laboratories, Albuquerque, NM.)

Geological Society of America, Inc. 1984. *Decade of North American Geology Geologic Time Scale.* Geological Society of America Map and Chart Series MCH050. Boulder, CO: Geological Society of America, Inc.

Gilkey, A.P. 1986a. *SPLOT — A Distance-versus-Variable Plot Program for the Output of a Finite Element Analysis.* SAND86-0882. Albuquerque, NM: Sandia National Laboratories.

Gilkey, A.P. 1986b. *TPLOT — A Time History or X-Y Plot Program for the Output of a Finite Element Analysis.* SAND86-0883. Albuquerque, NM: Sandia National Laboratories.

Gilkey, A.P. 1988. *ALGEBRA - A Program That Algebraically Manipulates the Output of a Finite Element Analysis.* SAND88-1431. Albuquerque, NM: Sandia National Laboratories.

Gilkey, A.P., and D.P. Flanagan. 1987. *DETOUR — A Deformed Mesh/Contour Plot Program.* SAND86-0914. Albuquerque, NM: Sandia National Laboratories.

Guzowski, R.V. 1990. *Preliminary Identification of Scenarios That May Affect the Escape and Transport of Radionuclides From the Waste Isolation Pilot Plant, Southeastern New Mexico.* SAND89-7149. Albuquerque, NM: Sandia National Laboratories.

Guzowski, R.V. 1991. *Evaluation of Applicability of Probability Techniques to Determining the Probability of Occurrence of Potentially Disruptive Intrusive Events at the Waste Isolation Pilot Plant.* SAND90-7100. Albuquerque, NM: Sandia National Laboratories.

Hale, W.E., and A. Clebsch, Jr. 1958. *Preliminary Appraisal of Ground-Water Conditions in Southeastern Eddy County and Southwestern Lea County, New Mexico.* Trace Elements Memorandum Report 1045. United States Department of the Interior, Geological Survey. (Copy on file in the Waste Management and Transportation Library, Sandia National Laboratories, Albuquerque, NM.)

Hale, W.E., L.S Hughes, and E.R. Cox. 1954. *Possible Improvement of Quality of Water of the Pecos River by Diversion of Brine at Malaga Bend, Eddy County, New Mexico.* Carlsbad, NM: Pecos River Commission, New Mexico and Texas, in cooperation with United States Department of the Interior, Geological Survey, Water Resources Division.

Hansen, J., I. Fung, A. Lacis, D. Rind, S. Lebedeff, R. Ruedy, and G. Russell. 1988. "Global Climate Changes as Forecast by Goddard Institute for Space Studies Three-Dimensional Model," *Journal of Geophysical Research.* Vol. 93, no. D8, 9341-9364.

Harms, J.C., and C.R. Williamson. 1988. "Deep-Water Density Current Deposits of Delaware Mountain Group (Permian), Delaware Basin, Texas and New Mexico," *American Association of Petroleum Geologists Bulletin* . Vol. 72, no. 3, 299-317.

Haug, A., V.A. Kelley, A.M. LaVenue, and J.F. Pickens. 1987. *Modeling of Ground-Water Flow in the Culebra Dolomite at the Waste Isolation Pilot Plant (WIPP) Site: Interim Report.* SAND86-7167. Albuquerque, NM: Sandia National Laboratories.

Hays, J.D., J. Imbrie, and N.J. Shackleton. 1976. "Variations in the Earth's Orbit: Pacemaker of the Ice Ages," *Science.* Vol. 194, no. 4270, 1121-1132.

Helton, J.C. In press. "Drilling Intrusion Probabilities for Use in Performance Assessment for Radioactive Waste Disposal," *Reliability Engineering and System Safety.* (Copy on file as SAND93-7001J in Waste Management and Transportation Library, Sandia National Laboratories, Albuquerque, NM.)

Helton, J.C., J.W. Garner, R.D. McCurley, and D.K. Rudeen. 1991. *Sensitivity Analysis Techniques and Results for Performance Assessment at the Waste Isolation Pilot Plant.* SAND90-7103. Albuquerque, NM: Sandia National Laboratories.

Helton, J.C., J.W. Garner, R.P. Rechard, D.K. Rudeen, and P.N. Swift. 1992. *Preliminary Comparison with 40 CFR Part 191, Subpart B for the Waste Isolation Pilot Plant, December 1991—Volume 4: Uncertainty and Sensitivity Analysis Results.* SAND91-0893/4. Albuquerque, NM: Sandia National Laboratories.

Hills, J.M. 1984. "Sedimentation, Tectonism, and Hydrocarbon Generation in Delaware Basin, West Texas and Southeastern New Mexico," *American Association of Petroleum Geologists Bulletin.* Vol. 68, no. 3, 250-267.

Hiss, W.L. 1975. "Stratigraphy and Ground-Water Hydrology of the Capitan Aquifer, Southeastern New Mexico and West Texas." Ph.D. dissertation. Boulder, CO: University of Colorado.

Holt, R.M., and D.W. Powers. 1988. *Facies Variability and Post-Depositional Alteration Within the Rustler Formation in the Vicinity of the Waste Isolation Pilot Plant, Southeastern New Mexico.* DOE/WIPP-88-004. Carlsbad, NM. Westinghouse Electric Corporation.

Holt, R.M., and D.W. Powers. 1990. *Geologic Mapping of the Air Intake Shaft at the Waste Isolation Pilot Plant.* DOE-WIPP 90-051. Carlsbad, NM: Westinghouse Electric Corporation.

Hora, S.C., and R.L. Iman. 1989. "Expert Opinion in Risk Analysis: The NUREG-1150 Methodology." *Nuclear Science and Engineering.* Vol. 102, no. 4, 323-331.

Hora, S.C., D. von Winterfeldt, and K.M. Trauth. 1991. *Expert Judgment on Inadvertent Human Intrusion into the Waste Isolation Pilot Plant.* SAND90-3063. Albuquerque, NM: Sandia National Laboratories.

Houghton, J.T., G.J. Jenkins, and J.J. Ephraums. 1990. *Climate Change: The IPCC Scientific Assessment.* New York, NY: Cambridge University Press.

Hunter, R.L. 1985. *A Regional Water Balance for the Waste Isolation Pilot Plant (WIPP) Site and Surrounding Area.* SAND84-2233. Albuquerque, NM: Sandia National Laboratories.

Hunter, R.L., R.M. Cranwell, and M.S.Y. Chu. 1986. *Assessing Compliance with the EPA High-Level Waste Standard: An Overview.* SAND86-0121, NUREG/CR-4510. Albuquerque, NM: Sandia National Laboratories.

IAEA (International Atomic Energy Agency). 1989. *Evaluating the Reliability of Predictions Made Using Environmental Transfer Models.* Safety Series Report No. 100. Vienna: International Atomic Energy Agency.

Iman, R.L., and W.J. Conover. 1982. "A Distribution-Free Approach to Inducing Rank Correlation Among Input Variables," *Communications in Statistics: Simulation and Computation.* Vol. B11, no. 3, 311-334.

Iman, R.L. and W.J. Conover. 1983. *A Modern Approach to Statistics.* New York, NY: John Wiley & Sons, Inc.

Imbrie, J. 1985. "A Theoretical Framework for the Pleistocene Ice Ages," *Journal of the Geological Society.* Vol. 142, pt. 3, 417-432.

Imbrie, J., and J.Z. Imbrie. 1980. "Modeling the Climatic Response to Orbital Variations," *Science.* Vol. 207, no. 4334, 943-953.

Imbrie, J., J.D. Hays, D.G. Martinson, A. McIntryre, A.C. Mix, J.J. Morley, N.G. Pisias, W.L. Prell, and N.J. Shackleton. 1984. "The Orbital Theory of Pleistocene Climate: Support from a Revised Chronology of the Marine $\delta^{18}O$ Record," *Milankovitch and Climate, Proceedings of the NATO Advanced Research Workshop on Milankovitch, Palisades, NY, November 30-December 4, 1982.* Eds. A.L. Berger, J. Imbrie, J. Hays, G. Kukla, and B. Saltzman. Boston, MA: D. Reidel Publishing Co. Pt. 1, 269-305.

Jones, C.L., C.G. Bowles, and K.G. Bell. 1960. *Experimental Drill Hole Logging in Potahs Deposits of the Carlsbad District, New Mexico.* U.S. Geological Survey Open File Report 60-84. Denver, CO: U.S. Geological Survey.

Jones, T.L., V.A. Kelley, J.F. Pickens, D.T. Upton, R.L. Beauheim, and P.B. Davies. 1992. *Integration of Interpretation Results of Tracer Tests Performed in the Culebra Dolomite at the Waste Isolation Pilot Plant Site.* SAND92-1579. Albuquerque, NM: Sandia National Laboratories.

Journel, A.G., and Ch.J. Huijbregts. 1978. *Mining Geostatistics.* Orlando, FL: Academic Press, Inc.

Kaplan, S., and B.J. Garrick. 1981. "On the Quantitative Definition of Risk," *Risk Analysis.* Vol. 1, no. 1, 11-27.

Kelley, V.A., and J.F. Pickens. 1986. *Interpretation of the Convergent-Flow Tracer Tests Conducted in the Culebra Dolomite at the H-3 and H-4 Hydropads at the Waste Isolation Pilot Plant (WIPP) Site.* SAND86-7161. Albuquerque, NM: Sandia National Laboratories.

Kelley, V.A., and G.J. Saulnier, Jr. 1990. *Core Analyses for Selected Samples from the Culebra Dolomite at the Waste Isolation Pilot Plant.* SAND90-7011. Albuquerque, NM: Sandia National Laboratories.

Kunkler, J.L. 1980. *Evaluation of the Malaga Bend Salinity Alleviation Project, Eddy County, New Mexico.* U.S. Geological Survey Open-File Report 80-1111. Albuquerque, NM: U.S. Geological Survey/Water Resources Division and the Pecos River Commission.

Lambert, S.J. 1983. *Dissolution of Evaporites in and Around the Delaware Basin, Southeastern New Mexico and West Texas.* SAND82-0461. Albuquerque, NM: Sandia National Laboratories.

Lambert S.J. 1987. *Feasability Study: Applicability of Geochronologic Methods Involving Radiocarbon and Other Nuclides to the Groundwater Hydrology of the Rustler Formation, Southeastern New Mexico.* SAND86-1054. Albuquerque, NM: Sandia National Laboratories.

Lambert, S.J. 1991. Chapter 5: "Isotopic Constraints on the Rustler and Dewey Lake Groundwater Systems," *Hydrogeochemical Studies of the Rustler Formation and Related Rocks in the Waste Isolation Pilot Plant Area, Southeastern New Mexico.* Eds. M.D. Siegel, S.J. Lambert, and K.L. Robinson. SAND88-0196. Albuquerque, NM: Sandia National Laboratories. 5-1 through 5-79.

Lambert, S.J., and J.A. Carter. 1984. *Uranium-Isotope Disequilibrium in Brine Reservoirs of the Castile Formation, Northern Delaware Basin, Southeastern New Mexico, I: Principles and Methods.* SAND83-0144. Albuquerque, NM: Sandia National Laboratories.

Lambert, S.J., and J.A. Carter. 1987. *Uranium-Isotope Systematics in Groundwaters of the Rustler Formation, Northern Delaware Basin, Southeastern New Mexico. I. Principles and Preliminary Results.* SAND87-0388. Albuquerque, NM: Sandia National Laboratories.

Lambert, S.J., and D.M. Harvey. 1987. *Stable-Isotope Geochemistry of Groundwaters in the Delaware Basin of Southeastern New Mexico.* SAND87-0138. Albuquerque, NM: Sandia National Laboratories.

Lambert, S.J., and J.W. Mercer. 1978. *Hydrologic Investigations of the Los Medaños Area, Southeastern New Mexico, 1977.* SAND77-1401. Albuquerque, NM: Sandia National Laboratories.

Lappin, A.R. 1988. *Summary of Site-Characterization Studies Conducted from 1983 through 1987 at the Waste Isolation Pilot Plant (WIPP) Site, Southeastern New Mexico.* SAND88-0157. Albuquerque, NM: Sandia National Laboratories.

Lappin, A.R., R.L. Hunter, D.P. Garber, P.B. Davies, R.L. Beauheim, D.J. Borns, L.H. Brush, B.M. Butcher, T. Cauffman, M.S.Y. Chu, L.S. Gomez, R.V. Guzowski, H.J. Iuzzolino, V. Kelley, S.J. Lambert, M.G. Marietta, J.W. Mercer, E.J. Nowak, J. Pickens, R.P. Rechard, M. Reeves, K.L. Robinson, and M.D. Siegel. 1989. *Systems Analysis, Long-Term Radionuclide Transport, and Dose Assessments, Waste Isolation Pilot Plant (WIPP), Southeastern New Mexico; March 1989.* SAND89-0462. Albuquerque, NM: Sandia National Laboratories.

LaVenue, A.M., and B.S. RamaRao. 1992. A *Modeling Approach to Address Spatial Variability within the Culebra Dolomite Transmissivity Field.* SAND92-7306. Albuquerque, NM: Sandia National Laboratories.

LaVenue, A.M., A. Haug, and V.A. Kelley. 1988. *Numerical Simulation of Groundwater Flow in the Culebra Dolomite at the Waste Isolation Pilot Plant (WIPP) Site; Second Interim Report.* SAND88-7002. Albuquerque, NM: Sandia National Laboratories.

LaVenue, A.M., T.L. Cauffman, and J.F. Pickens. 1990. *Ground-Water Flow Modeling of the Culebra Dolomite: Volume I - Model Calibration.* SAND89-7068/1. Albuquerque, NM: Sandia National Laboratories.

Leigh, C.D., B.M. Thompson, J.E. Campbell, D.E. Longsine, R.A. Kennedy, and B.A. Napier. (In review). *User's Guide for GENII-S: A Code for Statistical and Deterministic Simulations of Radiation Doses to Humans from Radionuclides in the Environment.* SAND91-0561. Albuquerque, NM: Sandia National Laboratories. (Copy on file in the Waste Management and Transportation Library, Sandia National Laboratories, Albuquerque, NM.)

Lowenstein, T.K. 1988. "Origin of Depositional Cycles in a Permian "Saline Giant": The Salado (McNutt Zone) Evaporites of New Mexico and Texas," *Geological Society of America Bulletin.* Vol. 100, no. 4, 592-608.

Lynch, A.W., and R.G. Dosch. 1980. *Sorption Coefficients for Radionuclides on Samples from the Water-Bearing Magenta and Culebra Members of the Rustler Formation.* SAND80-1064. Albuquerque, NM: Sandia National Laboratories.

Mantoglou, A., and J.L. Wilson. 1982. "Turning Bands Method for Simulation of Random Fields Using Line Generation by a Spectral Method," *Water Resources Research.* Vol. 18, no. 5, 1379-1394.

Marietta, M.G., S.G. Bertram-Howery, D.R. Anderson, K.F. Brinster, R.V. Guzowski, H. Iuzzolino, and R.P. Rechard. 1989. *Performance Assessment Methodology Demonstration: Methodology Development for Evaluating Compliance With EPA 40 CFR Part 191, Subpart B, for the Waste Isolation Pilot Plant.* SAND89-2027. Albuquerque, NM: Sandia National Laboratories.

Matheron, G. 1971. *The Theory of Regionalized Variables and its Applications.* Fontainebleau, France: École National Supériéure des Mines.

Matheron, G. 1973. "The Intrinsic Random Functions and Their Applications," *Advances in Applied Probability.* Vol. 5, no. 3, 439-468.

McGrath, E.J., and D.C. Irving. 1975a. *Techniques for Efficient Monte Carlo Simulation. Volume II. Random Number Generation for Selected Probability Distributions.* ORNL-RSIC-38 (Vol. 2). Oak Ridge, TN: Oak Ridge National Laboratory.

McGrath, E.J., and D.C. Irving. 1975b. *Techniques for Efficient Monte Carlo Simulation. Volume III. Variance Reduction.* ORNL-RSIC-38 (Vol. 3). Oak Ridge, TN: Oak Ridge National Laboratory.

McGrath, E.J., S.L. Basin, R.W. Burton, D.C. Irving, and S.C. Jaquette. 1975. *Techniques for Efficient Monte Carlo Simulation. Volume I. Selecting Probability Distributions.* ORNL-RSIC-38. (Vol. 1). Oak Ridge, TN: Oak Ridge National Laboratory.

McKay, M.D., R.J. Beckman, and W.J. Conover. 1979. "A Comparison of Three Methods for Selecting Values of Input Variables in the Analysis of Output from a Computer Code," *Technometrics.* (Vol. 21). no. 2, 239-245.

Mejía, J.M., and I. Rodríguez-Iturbe. 1974. "On the Synthesis of Random Fields From the Spectrum: An Application to the Generation of Hydrologic Spatial Processes," *Water Resources Research.* Volume 10, no. 4, 705-711.

Mercer, J.W. 1983. *Geohydrology of the Proposed Waste Isolation Pilot Plant Site, Los Medaños Area, Southeastern New Mexico.* U.S. Geological Survey Water-Resources Investigations Report 83-4016. Albuquerque, NM: U.S. Geological Survey.

Mercer, J.W., and B.R. Orr. 1977. *Review and Analysis of Hydrogeologic Conditions Near the Site of a Potential Nuclear-Waste Repository, Eddy and Lea Counties, New Mexico.* U.S. Geological Survey Open-File Report 77-123. Albuquerque, NM: U.S. Geological Survey.

Mercer, J.W., and B.R. Orr. 1979. *Interim Data Report on Geohydrology of the Proposed Waste Isolation Pilot Plant Site, Southeast New Mexico.* U.S. Geological Survey Water-Resources Investigations 79-98. Albuquerque, NM: U.S. Geological Survey.

Mercer, J.W., R.L. Beauheim, R.P. Snyder, and G.M. Fairer. 1987. *Basic Data Report for Drilling and Hydrologic Testing of Drillhole DOE-2 at the Waste Isolation Pilot Plant (WIPP) Site.* SAND86-0611. Albuquerque, NM: Sandia National Laboratories.

Milankovitch, M. 1941. *Canon of Insolation and the Ice-age Problem.* Koniglich Serbische Akademie, Beograd. (English translation by the Israel Program for Scientific Translations; published by the U.S. Department of Commerce and the National Science Foundation, Washington, D.C.).

Mills, P.G. 1984. *Blowout Prevention Theory and Applications.* Boston, MA: International Human Resources Development Corporation. 27-28.

Mitchell, J.F.B. 1989. "The 'Greenhouse Effect' and Climate Change," *Reviews of Geophysics.* Vol. 27, no. 1, 115-139.

Munson, D.E., A.F. Fossum, and P.E. Senseny. 1989a. *Advances in Resolution of Discrepancies Between Predicted and Measured In Situ WIPP Room Closures.* SAND88-2948. Albuquerque, NM: Sandia National Laboratories.

Munson, D.E., A.F. Fossum, and P.E. Senseny. 1989b. *Approach to First Principles Model Prediction of Measured WIPP In Situ Room Closure in Salt.* SAND88-2535. Albuquerque, NM: Sandia National Laboratories.

NEA (Nuclear Energy Agency). 1992. *Safety Assessment of Radioactive Waste Repositories: Systematic Approaches to Scenario Development.* Paris: Nuclear Energy Agency, Organisation for Economic Co-Operation and Development.

Neuman, S.P. 1990. "Universal Scaling of Hydraulic Conductivities and Dispersivities in Geologic Media," *Water Resources Research.* Vol. 26, no. 8, 1749-1758.

Nowak, E.J. 1980. *Radionuclide Sorption and Migration Studies of Getters for Backfill Barriers.* SAND79-1110. Albuquerque, NM: Sandia National Laboratories.

Nowak, E.J., and J.C. Stormont. 1987. *Scoping Model Calculations of the Reconsolidation of Crushed Salt in WIPP Shafts.* SAND87-0879. Albuquerque, NM: Sandia National Laboratories.

Nowak, E.J., D.F. McTigue, and R. Beraun. 1988. *Brine Inflow to WIPP Disposal Rooms: Data, Modeling, and Assessment.* SAND88-0112. Albuquerque, NM: Sandia National Laboratories.

Nowak, E.J., J.R. Tillerson, and T.M. Torres. 1990. *Initial Reference Seal System Design: Waste Isolation Pilot Plant.* SAND90-0355. Albuquerque, NM: Sandia National Laboratories.

NuPac (Nuclear Packaging, Inc.). 1989. *Safety Analysis Report for the TRUPACT-II Shipping Package.* NuPac TRUPACT-II SAR Rev. 4. Washington, DC: Nuclear Packaging, Inc.

Oldroyd, J.G. 1958. "Non-Newtonian Effects in Steady Motion of Some Idealized Elastico-Viscous Liquids," *Proceedings of the Royal Society of London.* Series A, Vol. 245, no. 1241, 278-297.

Pace, B.O. 1990. Appendix A, "Letter 1b: Changes to Bar graphs," *Data Used in Preliminary Performance Assessment of the Waste Isolation Pilot Plant (1990).* R.P. Rechard, H. Iuzzolino, and J.S. Sandha (Report Authors). SAND89-2408. Albuquerque, NM: Sandia National Laboratories. A-165 through A-170.

Parry, G.W. 1988. "On the Meaning of Probability in Probabilistic Safety Assessment," *Reliability Engineering and System Safety.* Vol. 23, no. 4, 309-314.

Paté-Cornell, M.E. 1986. "Probability and Uncertainty in Nuclear Safety Decisions," *Nuclear Engineering and Design.* Vol. 93, no. 3, 319-327.

Peterson, E.W., P.L. Lagus, and K. Lie. 1987. *Fluid Flow Measurements of Test Series A and B for the Small Scale Seal Performance Tests.* SAND87-7041. Albuquerque, NM: Sandia National Laboratories.

Pfeifle, T.W., and N. S. Brodsky. 1991. *Swelling Pressure, Water Uptake, and Permeability of 70/30 Crushed Salt Bentonite.* SAND91-7070. Albuquerque, NM: Sandia National Laboratories.

Popielak, R.S., R.L. Beauheim, S.R. Black, W.E. Coons, C.T. Ellingson, and R.L. Olsen. 1983. *Brine Reservoirs in the Castile Fm., Waste Isolation Pilot Plant (WIPP) Project, Southeastern New Mexico.* TME-3153. Carlsbad, NM: U.S. Department of Energy.

Powers, D.W., and R.M. Holt. 1990. "Sedimentology of the Rustler Formation near the Waste Isolation Pilot Plant (WIPP) Site," *Geological and Hydrological Studies of Evaporites in the Northern Delaware Basin for the Waste Isolation Pilot Plant (WIPP), New Mexico, Geological Society of America 1990 Annual Meeting, Dallas, TX, October 29-November 1, 1990.* Geological Society of America 1990 Annual Meeting, Field Trip #14 Guidebook. Dallas, TX: Dallas Geological Society. 79-106.

Powers, D.W., S.J. Lambert, S-E. Shaffer, L.R. Hill, and W.D. Weart, eds. 1978a. *Geological Characterization Report, Waste Isolation Pilot Plant (WIPP) Site, Southeastern New Mexico.* SAND78-1596. Albuquerque, NM: Sandia National Laboratories. Vol. I.

Powers, D.W., S.J. Lambert, S-E. Shaffer, L.R. Hill, and W.D. Weart, eds. 1978b. *Geological Characterization Report, Waste Isolation Pilot Plant (WIPP) Site, Southeastern New Mexico.* SAND78-1596. Albuquerque, NM: Sandia National Laboratories. Vol. II.

Public Law 102-579. 1992. *Waste Isolation Pilot Plant Land Withdrawal Act.*

RamaRao, B.S., and M. Reeves. 1990. *Theory and Verification for the GRASP II Code for Adjoint-Sensitivity Analysis of Steady-State and Transient Ground-Water Flow.* SAND89-7143. Albuquerque, NM: Sandia National Laboratories.

Rechard, R.P. 1989. *Review and Discussion of Code Linkage and Data Flow in Nuclear Waste Compliance Assessments.* SAND87-2833. Albuquerque, NM: Sandia National Laboratories.

Rechard, R.P., ed. 1992. *User's Reference Manual for CAMCON: Compliance Assessment Methodology Controller Version 3.0.* SAND90-1983. Albuquerque, NM: Sandia National Laboratories.

Rechard, R.P., H.J. Iuzzolino, J.S. Rath, A.P. Gilkey, R.D. McCurley, and D.K. Rudeen. 1989. *User's Manual for CAMCON: Compliance Assessment Methodology Controller.* SAND88-1496. Albuquerque, NM: Sandia National Laboratories.

Rechard, R.P., H. Iuzzolino, and J.S. Sandha. 1990a. *Data Used in Preliminary Performance Assessment of the Waste Isolation Pilot Plant (1990).* SAND89-2408. Albuquerque, NM: Sandia National Laboratories.

Rechard, R.P., W. Beyeler, R.D., McCurley, D.K. Rudeen, J.E. Bean, and J.D. Schreiber. 1990b. *Parameter Sensitivity Studies of Selected Components of the Waste Isolation Pilot Plant Repository/Shaft System.* SAND89-2030. Albuquerque, NM: Sandia National Laboratories.

Robinson, T.W., and W.B. Lang. 1938. *Geology and Ground-Water Conditions of the Pecos River Valley in the Vicinity of Laguna Grande de la Sal, New Mexico, With Special Reference to the Salt Content of the River Water.* New Mexico State Engineer 12th-13th Biennial Reports 1934-1938. Santa Fe, NM: State Engineer. 77-100.

Saulnier, G.J., Jr. 1987. *Analysis of Pumping Tests of the Culebra Dolomite Conducted at the H-11 Hydropad at the Waste Isolation Pilot Plant (WIPP) Site.* SAND87-7124. Albuquerque, NM: Sandia National Laboratories.

Saulnier, G.J., Jr., and J.D. Avis. 1988. *Interpretation of Hydraulic Tests Conducted in the Waste-Handling Shaft at the Waste Isolation Pilot Plant (WIPP) Site.* SAND88-7001. Albuquerque, NM: Sandia National Laboratories.

Savins, J.G., and G.C. Wallick. 1966. "Viscosity Profiles, Discharge Rates, Pressures, and Torques for a Rheologically Complex Fluid in a Helical Flow," *A.I.Ch.E. Journal.* Vol. 12, no. 2, 357-363.

Scheidegger, A.E. 1960. *The Physics of Flow Through Porous Media.* Rev. ed. Toronto, Canada: University of Toronto Press.

Serne, R.J., D. Rai, M.J. Mason, and M.A. Molecke. 1977. *Batch Kd Measurements of Nuclides to Estimate Migration Potential at the Proposed Waste Isolation Pilot Plant in New Mexico.* PNL-2448. Richland, WA: Battelle Pacific Northwest Laboratories.

Sewards, T. 1991. *Characterization of Fracture Surfaces in Dolomite Rock, Culebra Dolomite Member, Rustler Formation.* SAND90-7019. Albuquerque, NM: Sandia National Laboratories.

Sewards, T., M.L. Williams, and K. Keil. 1991a. *Mineralogy of the Culebra Dolomite Member of the Rustler Formation.* SAND90-7008. Albuquerque, NM: Sandia National Laboratories.

Sewards, T., R. Glenn, and K. Keil. 1991b. *Mineralogy of the Rustler Formation in the WIPP-19 Core.* SAND87-7036. Albuquerque, NM: Sandia National Laboratories.

Sewards, T., A. Brearley, R. Glenn, I.D.R. MacKinnon, and M.D. Siegel. 1992. *Nature and Genesis of Clay Minerals of the Rustler Formation in the Vicinity of the Waste Isolation Pilot Plant in Southeastern New Mexico.* SAND90-2569. Albuquerque, NM: Sandia National Laboratories.

Shinozuka, M., and C-M. Jan. 1972. "Digital Simulation of Random Processes and Its Applications," *Journal of Sound and Vibration.* Vol. 25, no. 1, 111-128.

1 Short, J.A. 1982. *Drilling and Casing Operations.* Tulsa, OK: PennWell Books. 183-184.

2 Siegel, M.D. 1990. Appendix A, "Memo 3a: Representation of Radionuclide Retardation in the Culebra
3 Dolomite in Performance Assessment Calculations," *Data Used in Preliminary Performance Assessment*
4 *of the Waste Isolation Pilot Plant* (1990). R.P. Rechard, H. Iuzzolino, and J.S. Sandha (Report Authors).
5 SAND89-2408. Albuquerque, NM: Sandia National Laboratories. A-43 through A-62.

6 Siegel, M.D., J.O. Leckie, S.W. Park, S.L. Phillips, and T. Sewards. 1990. *Studies of Radionuclide Sorption*
7 *by Clays in the Culebra Dolomite at the Waste Isolation Pilot Plant Site, Southeastern New Mexico.*
8 SAND89-2387. Albuquerque, NM: Sandia National Laboratories.

9 Siegel, M.D., and S.J. Lambert. 1991. Chapter 1: "Summary of Hydrogeochemical Constraints on Groundwater
10 Flow and Evolution in the Rustler Formation," *Hydrogeochemical Studies of the Rustler Formation and*
11 *Related Rocks in the Waste Isolation Pilot Plant Area, Southeastern New Mexico.* Eds. M.D. Siegel, S.J.
12 Lambert, and K.L. Robinson. SAND88-0196. Albuquerque, NM: Sandia National Laboratories. 1-1
13 through 1-109.

14 Siegel, M.D., K.L. Robinson, and J. Myers. 1991. Chapter 2: "Solute Relationships in Groundwaters from the
15 Culebra Dolomite and Related Rocks in the Waste Isolation Pilot Plant Area, Southeastern New Mexico,"
16 *Hydrogeochemical Studies of the Rustler Formation and Related Rocks in the Waste Isolation Pilot Plant*
17 *Area, Southeastern New Mexico.* Eds. M. D. Siegel, S.J. Lambert, and K.L. Robinson. SAND88-0196.
18 Albuquerque, NM: Sandia National Laboratories.2-1 through 2-164.

19 Skokan, C., J. Starrett, and H.T. Anderson. 1988. *Final Report: Feasibility Study of Seismic Tomography to*
20 *Monitor Underground Pillar Integrity at the WIPP Site.* SAND88-7096. Albuquerque, NM: Sandia
21 National Laboratories.

22 Smith, L., and R.A. Freeze. 1979. "Stochastic Analysis of Steady State Groundwater Flow in a Bounded
23 Domain, 2. Two-Dimensional Simulations," *Water Resources Research.* Vol. 15, no. 6, 1543-1559.

24 Smith, L., and F.W. Schwartz. 1981. "Mass Transport, 2. Analysis of Uncertainty in Prediction," *Water*
25 *Resources Research.* Vol. 17, no. 2, 351-369.

26 Snyder, R.P. 1985. *Dissolution of Halite and Gypsum, and Hydration of Anydrite to Gypsum, Rustler*
27 *Formation, in the Vicinity of the Waste Isolation Pilot Plant, Southeastern New Mexico.* Open-File
28 Report 85-229. Denver, CO: U.S. Geological Survey.

29 Stone, C.M., R.D. Krieg, and Z.E. Beisinger. 1985. *SANCHO: A Finite Element Computer Program for the*
30 *Quasistatic, Large Deformation, Inelastic Response of Two-Dimensional Solids.* SAND84-2618.
31 Albuquerque, NM: Sandia National Laboratories.

32 Stormont, J.C. 1988. *Preliminary Seal Design Evaluation for the Waste Isolation Pilot Plant.* SAND87-3083.
33 Albuquerque, NM: Sandia National Laboratories.

Stormont, J.C., E.W. Peterson, and P.L. Lagus. 1987. *Summary of and Observations About WIPP Facility Horizon Flow Measurements Through 1986.* SAND87-0176. Albuquerque, NM: Sandia National Laboratories.

Swift, P.N. 1991. "Appendix A: Climate and recharge variability parameters for the 1991 WIPP PA calculations," *Preliminary Comparison with 40 CFR Part 191, Subpart B for the Waste Isolation Pilot Plant, December 1991 — Volume 3: Reference Data.* WIPP Performance Assessment Division (Report Author). SAND91-0893/3. Albuquerque, NM: Sandia National Laboratories. A-107 through A-122.

Swift, P.N. 1992. *Long-Term Climate Variability at the Waste Isolation Pilot Plant, Southeastern New Mexico, USA.* SAND91-7055. Albuquerque, NM: Sandia National Laboratories.

Taylor, L.M., D.P. Flanagan, and W.C. Mills-Curran. 1987. The GENESIS Finite Element Mesh File Format. SAND86-0910. Albuquerque, NM: Sandia National Laboratories.

Tien, P-L., F.B. Nimick, A.B. Muller, P.A. Davis, R.V. Guzowski, L.E. Duda, and R.L. Hunter. 1983. *Repository Site Data and Information in Bedded Salt: Palo Duro Basin, Texas.* SAND82-2223, NUREG/CR-3129. Albuquerque, NM: Sandia National Laboratories.

Tierney, M.S. 1990. *Constructing Probability Distributions of Uncertain Variables in Models of the Performance of the Waste Isolation Pilot Plant: The 1990 Performance Simulations.* SAND90-2510. Albuquerque, NM: Sandia National Laboratories.

Trauth, K.M., S.C. Hora, R.P. Rechard, and D.R. Anderson. 1992. *The Use of Expert Judgment to Quantify Uncertainty in Solubility and Sorption Parameters for Waste Isolation Pilot Plant Performance Assessment.* SAND92-0479. Albuquerque, NM: Sandia National Laboratories.

Tyler, L.D., R.V. Matalucci, M.A. Molecke, D.E. Munson, E.J. Nowak, and J.C. Stormont. 1988. *Summary Report for the WIPP Technology Development Program for Isolation of Radioactive Waste.* SAND88-0844. Albuquerque, NM: Sandia National Laboratories.

U.S. DOE (Department of Energy). 1980. *Final Environmental Impact Statement: Waste Isolation Pilot Plant.* DOE/EIS-0026. Washington, DC: U.S. Department of Energy. Vols. 1-2.

U.S. DOE (Department of Energy). 1990a. *WIPP Test Phase Plan: Performance Assessment.* DOE/WIPP 89-011, Rev. 0. Carlsbad, NM: U.S. Department of Energy, Waste Isolation Pilot Plant.

U.S. DOE (Department of Energy). 1990b. *Recommended Initial Waste Forms for the WIPP Experimental Test Program, May 1990, Engineered Alternatives Task Force.* DOE/WIPP 90-009. Carlsbad, NM: Westinghouse Electric Corporation.

U.S. DOE (Department of Energy). 1991a. *Waste Acceptance Criteria for the Waste Isolation Pilot Plant.* WIPP-DOE-069, Rev. 4.0. Carlsbad, NM: Westinghouse Electric Corporation.

U.S. DOE (Department of Energy). 1991b. *Integrated Data Base for 1991: U.S. Spent Fuel and Radioactive Waste Inventories, Projections, and Characteristics.* DOE/RW-0006, Rev. 7. Oak Ridge, TN: Oak Ridge National Laboratory.

U.S. DOE (Department of Energy). 1991c. *Draft Report: Evaluation of the Effectiveness and Feasibility of the Waste Isolation Pilot Plant Engineered Alternatives: Final Report of the Engineered Alternatives Task Force.* DOE/WIPP 91-007, Revision 0. Carlsbad, NM: Westinghouse Electric Corporation.

U.S. DOE (Department of Energy). 1992. *WIPP Test Phase Activities in Support of Critical Performance Assessment Information Needs (40 CFR 191, Subpart B).* Attachment I. Washington, DC: U.S. Department of Energy.

U.S. DOE (Department of Energy) and State of New Mexico. 1981, as modified. "Agreement for Consultation and Cooperation" on WIPP by the State of New Mexico and U.S. Department of Energy, modified 11/30/84, 8/4/87, and 4/18/88.

U.S. EPA (Environmental Protection Agency). 1985. "40 CFR Part 191: Environmental Standards for the Management and Disposal of Spent Nuclear Fuel, High-Level and Transuranic Radioactive Wastes Final Rule," *Federal Register.* Vol. 50, no. 182, 38066-38089.

U.S. EPA (Environmental Protection Agency). 1986. "40 CFR Part 268 Land Disposal Restrictions," as amended and published in the most recent *Code of Federal Regulations.* Washington, DC: Office of the Federal Register, National Archives and Records Administration.

University of New Mexico. 1989. *New Mexico Statistical Abstract 1989.* Albuquerque, NM: Bureau of Business and Economic Research, University of New Mexico.

Vesely, W.E., and D.M. Rasmuson. 1984. "Uncertainties in Nuclear Probabilistic Risk Analyses," *Risk Analysis.* Vol. 4, no. 4, 313-322.

Vine, J.D. 1963. *Surface Geology of the Nash Draw Quadrangle, Eddy County, New Mexico.* U.S. Geological Survey Bulletin 1141-B. Washington, DC: U.S. Government Printing Office.

Walker, R.E. 1976. "Hydraulic Limits are Set by Flow Restrictions," *Oil and Gas Journal.* Vol. 74, no. 40, 86-90.

Walker, R.E., and W.E. Holman. 1971. "Computer Program Predicting Drilling-Fluid Performance," *Oil and Gas Journal.* Vol. 69, no. 13, 80-90.

Ward, R.F., C.G. St. C. Kendall, and P.M. Harris. 1986. "Upper Permian (Guadalupian) Facies and Their Association with Hydrocarbons - Permian Basin, West Texas and New Mexico," *American Association of Petroleum Geologists Bulletin.* Vol. 70, no. 3, 239-262.

Wehr, R.M., J.A. Richards, Jr., and T.W. Adair III. 1984. *Physics of the Atom.* 4th ed. Reading, MA. Addison-Wesley Publishing Company.

Whittaker, A., ed. 1985. *Theory and Application of Drilling Fluid Hydraulics.* Boston, MA: International Human Resources Development Corporation.

Williamson, C.R. 1978. "Depositional Processes, Diagenesis and Reservoir Properties of Permian Deep-Sea Sandstone Bell Canyon Formation." Ph.D. dissertation. Austin, TX: University of Texas.

WIPP PA (Performance Assessment) Division. 1991a. *Preliminary Comparison with 40 CFR Part 191, Subpart B for the Waste Isolation Pilot Plant, December 1991 — Volume 1: Methodology and Results.* SAND91-0893/1. Albuquerque, NM: Sandia National Laboratories.

WIPP PA (Performance Assessment) Division. 1991b. *Preliminary Comparison with 40 CFR Part 191, Subpart B for the Waste Isolation Pilot Plant, December 1991— Volume 2: Probability and Consequence Modeling.* SAND91-0893/2. Albuquerque, NM: Sandia National Laboratories.

WIPP Performance Assessment Division (WIPP PA Division). 1991c. *Preliminary Comparison with 40 CFR Part 191, Subpart B for the Waste Isolation Pilot Plant, December 1991 — Volume 3: Reference Data.* SAND91-0893/3. Albuquerque, NM: Sandia National Laboratories.

Zimmerman, A., and J.L. Wilson. 1990. *Description of and User's Manual for TUBA: A Computer Code for Generating Two-Dimensional Random Fields via the Turning Bands Method.* Albuquerque, NM: Gram, Inc.

# APPENDIX A:
# BRAGFLO AND PANEL

# APPENDIX A: BRAGFLO AND PANEL

## A.1 Background

The WIPP PA Department has developed a computational model called BRAGFLO (BRine And Gas FLOw) to simulate two-phase flow through porous, heterogeneous reservoirs. BRAGFLO numerically solves the coupled nonlinear partial differential equations (PDEs) describing the mass conservation of the gas and brine components distributed between the gas and liquid phases. Finite difference methods are used to develop analogs of the mass conservation PDEs in two spatial dimensions. These analogs are integrated over time using a modified Newton-Raphson method and variable time spacing.

BRAGFLO output is used to provide input for an equilibrium-mixing cell mathematical model called PANEL to evaluate radionuclide concentrations resulting from the mixing of brine with waste. PANEL has no geometry; it can be thought of as a point. The brine flow up the borehole that is calculated by BRAGFLO is input to PANEL so that appropriate amounts of radionuclides determined by their respective solubilities can be added to the brine flow.

### A.1.1 BRAGFLO Features and Limitations

BRAGFLO is a modeling tool that can accommodate conceptual model changes and is therefore well suited to test various alternative conceptual models. This flexibility results, in part, from the highly structured and modular coding style used. BRAGFLO is also designed to be robust and numerically stable when simulating multiphase flow over a wide range of conditions and input property values.

Current limitations of BRAGFLO include:

- Only isothermal two-phase flow is modeled.
- Only two components or chemical species are modeled, and only one of the components can be distributed between both phases, such as a gas component existing in the gas phase and a water or oil phase as dissolved gas. In the case of the WIPP performance assessment, the waste-generated gas exists in both the gas phase and the brine phase, but the brine exists only in the brine phase (the brine has zero vapor pressure).
- The porous medium within each numerical grid block is treated as a single continuum; discrete fracturing or dual porosity is not considered.
- Grid block connectivity is not arbitrary and is fixed by spatial constraints. The solution domain cannot be modeled by mixed dimensionality.

- If two phases or components exist anywhere in the repository, both component mass balances must be solved everywhere in the repository even though isolated areas may be governed solely by single-phase flow.

- Non-Darcy flow, where flow is proportional to a potential gradient (for example, molecular diffusion) is not modeled.

- Fluids are assumed to exhibit Newtonian behavior (fluid viscosity does not vary with rate or time of shear).

## A.1.2 Performance Assessment Role of BRAGFLO and PANEL

The WIPP PA Department is using BRAGFLO to study the effects of gas on the flow of brine through the repository and up an intrusion borehole. Specifically, BRAGFLO models the effects of the interaction of the following phenomena:

- gas generation from corrosion and microbiological degradation of the waste,

- brine movement from the surrounding rock through the waste over time,

- possible saturation of the waste by mixing with brine from an underlying pressurized reservoir that reaches the waste through a borehole created by an exploratory drill bit, and

- creep closure of the surrounding host rock.

BRAGFLO uses wells to model gas generation from corrosion and microbiological degradation of the waste, the brine flow from a breached underlying pressurized brine pocket, and brine influx from the surrounding host rock. In BRAGFLO, wells may be accommodated by using simple well models or by directly including well geometry and properties in the numerical mesh. This process is described in detail in the 1991 performance assessment documentation (see Section 5.2.2.5 of WIPP PA Division, 1991).

PANEL uses the results of BRAGFLO to predict mixing of radionuclides with brine (see Section A.3).

Creep closure of the host rock surrounding the repository will result in pressurization or rock deformation, changing material porosities and permeabilities. Presently, BRAGFLO is capable of using as input varying room porosity, which changes with closure as predicted by SANCHO (Appendix B). Porosities and absolute permeabilities of all other materials in the modeled waste room are currently treated as imprecisely known constants.

# A.2 Flow (BRAGFLO)

## A.2.1 Fundamental Equations

The BRAGFLO flow model simultaneously solves five equations:

- a partial differential equation that describes the mass conservation of gas in the repository and surrounding formation,
- a partial differential equation that describes the mass conservation of the brine in the repository and surrounding formation,
- a saturation constraint equation,
- a mass fraction constraint equation on the components making up the brine phase, and
- a capillary pressure constraint equation.

The above equations, along with appropriate boundary and initial conditions and material property relationships, form the basis of the model's fundamental equations. These equations are described in detail in Volume 3 of this report (Section 1.4.1) and the 1991 performance assessment documentation (see Section 5.2 of WIPP PA Division, 1991).

## A.2.2 General Conceptualization

BRAGFLO can simulate the simultaneous flow of two immiscible phases through a porous anisotropic reservoir. The reservoir may consist of many materials with widely differing characteristics. Reservoir properties may also vary spatially within a particular material type.

A description of multiphase porous media flow is necessary to understand the assumptions involved in modeling multiphase flow through porous media. Details of the equations of motion for multiphase flow describing assumptions, derivations, and implementation are wide-spread throughout the petroleum literature (Bear et al., 1968; Bear, 1975, 1979; Dake, 1978; Crichlow, 1977; Collins, 1961; Aziz and Settari, 1979; Peaceman, 1977; Crookston et al., 1979; Coats, 1980; Vaughn, 1986; Rubin and Vinsome, 1979; Scheidegger, 1960). The nomenclature, assumptions, and conceptualization used here are typical of those found in much of the multiphase reservoir modeling literature referenced above.

BRAGFLO is based on a description of porous media presented by Bear (1975), Bear et al. (1968), and Bear and Bachmat (1967). The porous media is characterized as a portion of space occupied by heterogeneous matter made up of a solid phase and at least one fluid phase. The space that is occupied by the fluid phases is called the

pore or void space. Some of the pores are interconnected (effective porosity) and others are not. This void space forms a tortuous network of randomly sized and located channels. The porous medium forms a continuum with the solid matrix present in each representative volume.

The conceptualization of fluid flow through such a porous media is consistent with assumptions and descriptions presented in Bear (1975). The fluids are assumed to be Newtonian and may be compressible. The flow in the void space is laminar and confined to well-defined channels with fluid particles moving parallel to the channel walls. The forces acting on the fluid particles result only from pressure, gravity, capillary action, and shear. Flow in the network of channels contained in a given volume gives rise to average gradients that are independent of the geometry of individual channels.

BRAGFLO simulates multiphase flow through porous media. Two types of multiphase flow are possible, miscible and immiscible. BRAGFLO considers immiscible displacement only. In this case, both fluids flow simultaneously through the porous network. The two fluid phases are separated by an interface whose curvature and surface tension give rise to a capillary pressure difference across the interface (Brooks and Corey, 1964; Corey, 1986; Peaceman, 1977; Dake, 1978; Crichlow, 1977; Collins, 1961). The interface is assumed to be abrupt and any transitions from one phase to another occur over a distance of negligible length compared to the channel diameter (Bear, 1975).

The concept of saturation is introduced to describe the occupation of void space by more than one fluid. Saturation is defined as the volume fraction of void space occupied by a particular fluid. Interfacial tension exists where the two immiscible fluids contact each other. The shape of the resulting meniscus defines the wet ability of the system (Brooks and Corey, 1964; Bear, 1975). For example, the convex side of the meniscus faces toward the wetting phase, while the concave side faces toward the non-wetting phase. Interfacial tension and wettability may depend on the direction the interface is moving. This phenomenon is called hysteresis. Hysteresis is a secondary effect and is not currently modeled (Brooks and Corey, 1964).

Three saturation regions are differentiated in the two-phase system, brine and gas, for example. Assuming a brine-wet reservoir, at low brine saturations, brine forms in isolated rings or exists as a thin film. As brine saturation increases, a condition is reached where the brine forms a continuous phase that is capable of transmitting pressure. Above this critical saturation or "irreducible saturation," brine flow is possible. Potential flow of brine below the irreducible brine saturation will not occur. At high brine saturations, brine isolates the gas and the gas no longer forms a continuous phase. This occurs at the irreducible gas saturation.

Bear's continuum approach is assumed for multiphase flow (Bear, 1975). Each fluid is a continuum and the various continua occupy the void space simultaneously. The equations of motion for multiphase flow used here are based on heuristic extensions of Darcy's law (Hubbert, 1956; Bear, 1975, 1979; Dake, 1978; Crichlow, 1977; Collins, 1961; Dullien, 1979; Hiatt, 1968; de Marsily, 1986; De Wiest, 1965; Aziz and Settari, 1979).

The following is a statement of Darcy's law in differential form:

$$q_v = -\frac{k}{\mu}[\nabla P - \rho g] \qquad \text{(A-1)}$$

where $q_v$ is the volumetric flow rate per unit cross-sectional area, $k$ is the absolute or intrinsic permeability of the porous media, $\mu$ is the fluid viscosity, $\rho$ is the fluid density, $g$ is the gravitational constant, and $P$ is the fluid pressure.

Darcy's original observations were made on the one-dimensional vertical flow of water through a fully saturated porous medium (Hubbert, 1956). Darcy postulated the law, which states that the flow of water under these conditions is proportional to the change in potential. Many generalizations of Darcy's law can be found in the literature (Bear, 1975, 1979; Bear et al., 1968; Bear and Bachmat, 1967; Dake, 1978; Crichlow, 1977; Collins, 1961; Dullien, 1979; Hiatt, 1968; de Marsily, 1986; De Wiest, 1965; Aziz and Settari, 1979). These generalizations extend Darcy's observation to other fluids, to the simultaneous flow of immiscible fluids, to multiple dimensions, and to compressible fluids. These generalizations are used in obtaining the equations of motion governing the two-phase flow assumed in BRAGFLO.

The first extension is a generalization from an isotropic to an anisotropic medium. This extension is developed heuristically as well as theoretically in Bear (1975). Implicit in this generalization is the extension to two and three dimensions.

The second extension is that of accounting for fluid compressibility effects. Hubbert (1940) shows that extensions of Darcy's law to compressible fluids, such as gas, are valid provided the density of the fluid is a function of pressure only and the flow is irrotational.

The third extension of Darcy's law accounts for the presence and flow of multiple immiscible phases. Once steady-state flow is achieved, Darcy's law may be extended to describe the separate flow of each phase (Bear, 1975). This extension introduces the concept of effective permeabilities, relative permeabilities, and capillary pressure.

For each phase, the absolute permeability of Equation A-1 is replaced by the effective phase permeability, and the pressure of Equation A-1 is replaced by the phase pressure. These effective permeabilities are empirically determined by pressure drop and flow measurements. Numerous experiments verify the validity of this extension and suggest that the effective permeability depends on characteristics of the rock, the wettability characteristics, surface tension, the shape of the interface separating the phases, and phase saturation. The effective permeabilities do not appear to depend on fluid viscosities or their specific discharges (Bear, 1975; Scheidegger, 1960). Instead of using effective permeabilities, it is more convenient to refer to relative permeabilities, which are defined for each phase as the ratio of the effective phase permeability to the absolute or intrinsic permeability of the medium (measured when the medium is saturated with a single fluid).

## A.2.3. Geometry

BRAGFLO is developed in terms of a one-, two- or three-dimensional block-centered grid system. In general, the three-dimensional numerical methods are normally based on Cartesian $xyz$ coordinates. The finite difference formulations in BRAGFLO are sufficiently general to handle grid block "stretching" (variable grid spacing) in the directions of flow, as well as variable grid thickness or cross-sectional area in directions normal to flow. In

addition, the coordinate system may be rotated in three-dimensional space, with respect to the direction of gravity resulting in the generalized case of gravity components in each of the coordinate directions.

Because of these generalities, many geometries may be considered. Some of these include the following:

- Cartesian geometry (one-dimensional linear vertical, horizontal, or inclined flow; two-dimensional planar areal sweep, vertical or inclined flow; three-dimensional flow),
- Cylindrical geometry (two-dimensional axisymmetric cylindrical geometry with axis of symmetry oriented parallel, normal, or inclined to the direction of gravity),
- Spherical symmetry, and
- Non-Cartesian geometry (variable grid thickness and cross-sectional areas normal to flow).

To model in axisymmetric cylindrical geometry or spherical symmetry requires only an external transformation to obtain the equivalent Cartesian grid block sizes required for BRAGFLO. For example, consider the two-dimensional convergent flow toward a well in radial coordinates $r$ and $z$ (Figure A-1) (symmetry is assumed in the angular direction, $\theta$).

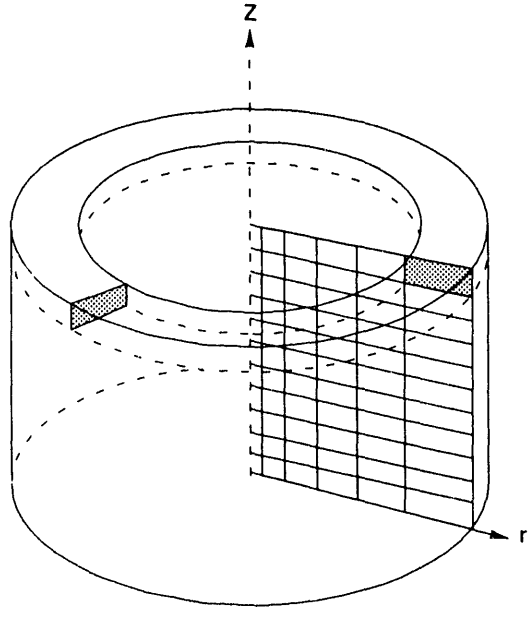


TRI-6342-1476-1

Figure A-1. Schematic representation of an axisymmetric cylindrical model.

If the coordinate transformations of $x(x,z) = r$, $y(x,z) = 2\pi r$ and $z(x,z) = z$, then an equivalent Cartesian system of the cylindrical geometry is defined. In the Cartesian system, flow is in the $x$ and $z$ directions. The length in the non-flow or symmetric direction, $y$, varies with $x$ and accounts for the increase in cross-sectional area (normal to radial flow) with radial distance from the well. The transformation are justified by the equivalence of the volume integration in the two coordinate systems. An arbitrary function of $r$ and $z$, $f(r,z)$ is integrated over the cylindrical element volume as

$$F = \int_{z_k}^{z_{k+1}} \int_{r_i}^{x_{i+1}} \int_{0}^{2\pi} f(r,z)\, r\, d\Theta\, dr\, dz \qquad \text{(A-2)}$$

When the above transformations are defined, Equation A-2 is identical to the integration in Cartesian coordinates carried out below:

$$G = \int_{z_k}^{z_{k+1}} \int_{x_i}^{x_{i+1}} \int_{0}^{2\pi r} g(x,z)\, dx\, dy\, dz \qquad \text{(A-3)}$$

Therefore, the conversion from radial geometry to the BRAGFLO Cartesian formulation requires only setting the mesh width ($y$) of each grid block equal to the circumference of a circle passing through the center of that grid block.

The way in which grid block sizes may vary is not arbitrary and depends on restrictions concerning grid block connectivity and interface cross-sectional areas. In BRAGFLO, two criteria determine valid grid block stretchings. First, grid-block stretchings are confined to certain directions dependent on the dimensionality of the flow. For example, in one-dimensional flow, the length of all grid blocks ($\Delta x$, $\Delta y$, and $\Delta z$) may vary in the direction of flow. In two-dimensional flow ($x$ and $y$ directions), the length $\Delta x$ can vary only in the $x$-direction while the length $\Delta y$ can vary only in the $y$-direction. For three-dimensional flow, the length of the grid blocks can only vary in the direction of flow coincident to their respective orientations. That is, $\Delta x$ varies only in $x$, $\Delta y$ varies only in $y$, and $\Delta z$ = varies only in $z$. The reasons for these restrictions arise when determining appropriate averages for flows across block interfaces, given values evaluated at the centers of adjacent blocks. Secondly, grid block sizes may vary only in a way that results in a one-to-one connectivity between grid blocks in each direction starting from the origin. Grid block stretchings that violate only the first criterion may or may not be physically valid and are acceptable by BRAGFLO, although a warning message alerts the user to possible problems. Stretchings that violate criterion two above will not run. The grid patterns of Figure A-2 (a, b, and c) depict grid stretchings in one, two, and three dimensions, respectively, which are consistent with both criteria above.

The reason that some violations of the first criterion above present problems is that they may require restrictive assumptions concerning the average cross-sectional area between adjacent grid blocks for calculating interblock transmissibilities, flow rates, and velocities. The reason violations of the second criterion are not acceptable is because they are inconsistent with the bookkeeping assumed in BRAGFLO for mapping the coordinates of the grid block centers from their spatial positions to their locations in the numerical space.

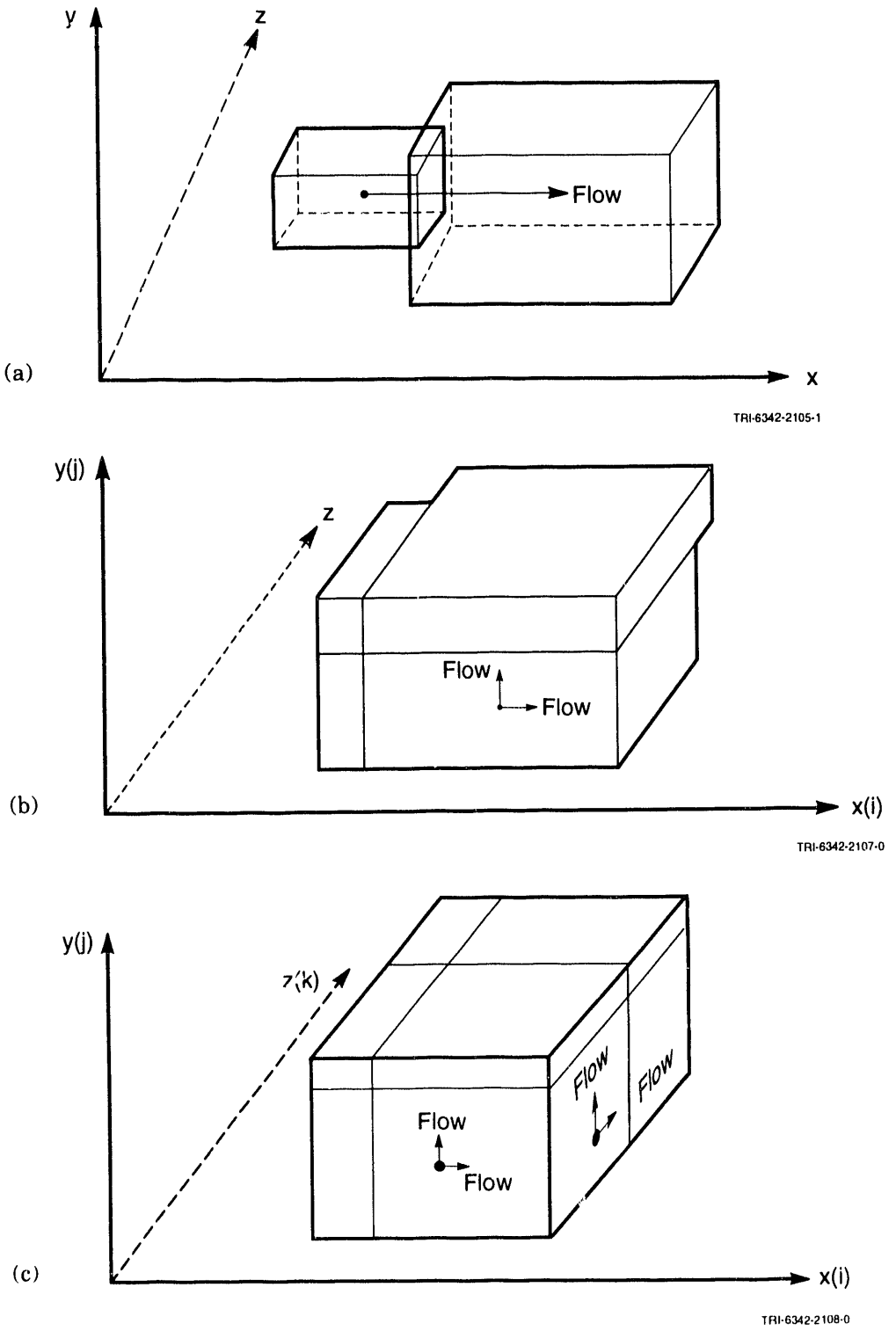


Figure A-2. Grid-block stretching for flow in (a) one, (b) two, or (c) three dimensions.

## A.2.4 Derivation of Flow Equations

The derivation of the flow equations begins by consideration of mass conservation in a differential volume element. The derivation will initially be presented for one-dimensional compressible flow and then generalized to other dimensionalities. The derivation is generalized to allow for the cross-sectional area normal to flow to vary in the direction of flow.

Consider the mass conservation of a single component in a two-phase system about the control volume depicted in Figure A-3.

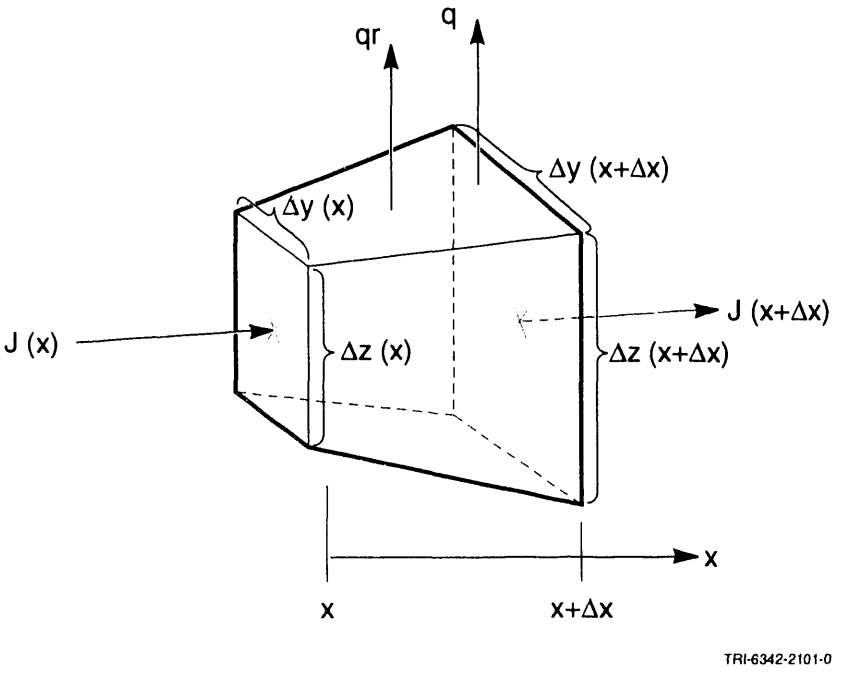


Figure A-3. Control volume for derivation of flow equations.

Flow is in the $x$ direction across a length $\Delta x$. The cross-sectional area normal to flow varies with $x$ as $A(x) = \Delta y(x) \bullet \Delta z(x)$. Therefore, the cross-section areas at the left boundary and right boundary are $\Delta y(x) \bullet \Delta z(x)$ and $\Delta y(x + \Delta x) \bullet \Delta z(x + \Delta x)$ respectively. The mass flux entering the element at the left face is $J(x)$, while the mass flux leaving at the right face is $J(x + \Delta x)$. Included in the mass balance are terms for mass rate of injection (per unit volume of reservoir) due to wells, $q$, and chemical reaction, $q_r$. We also acknowledge that the density and saturation of the component, as well as the porosity of the reservoir, may change with time.

The mass conservation equation simply states that

$$[\text{rate in}] - [\text{rate out}] + [\text{rate injected}] + [\text{rate reacted}] = [\text{rate accumulated}] \qquad \text{(A-4)}$$

The rate at which mass enters the element from the left boundary is

$$J(x) \bullet \Delta y(x) \bullet \Delta z(x)$$

The rate at which mass exits the element at the right boundary is

$$J(x+\Delta x) \bullet \Delta y(x+\Delta x) \bullet \Delta z(x+\Delta x)$$

The rate at which mass is injected or produced by or from a well into the element is

$$q \bullet \overline{\Delta y \bullet \Delta z} \bullet \Delta x = q \bullet \overline{A} \bullet \Delta x,$$

where $\overline{A}$ is an average value of the product of $\Delta y$ and $\Delta z$ across the block length $\Delta x$, the volume of the block being $\overline{\Delta y \bullet \Delta z} \bullet \Delta x$.

Similarly, the rate at which mass is reacted in the element is

$$q_r \bullet \overline{\Delta y \bullet \Delta z} \bullet \Delta x = q_r \bullet \overline{A} \bullet \Delta x$$

The rate at which mass is accumulated in the element volume is

$$\frac{\partial}{\partial t}\left(\bar{\phi}\bar{\rho}\bar{S}\right) \bullet \overline{A}\Delta x,$$

because $\bar{\phi} \bullet \bar{\rho} \bullet \bar{S} \bullet \overline{A}\ \Delta x$ is the mass contained in the element. The bars signify an average of the value in the element. We have assumed that the size of the element does not change with time.

The statement of component mass conservation (Equation A-4) is written as

$$\left[J_x \Delta y \Delta z\right]_x - \left[J_x \Delta y \Delta z\right]_{x+\Delta x} + \left[q\overline{\Delta y \Delta z}\Delta x\right] + \left[q_r \overline{\Delta y \Delta z}\Delta x\right] = \overline{\Delta y \Delta z}\Delta x \frac{\partial}{\partial t}\left(\bar{\phi}\bar{\rho}\bar{S}\right) \tag{A-5}$$

Dividing Equation A-5 by $\Delta x$ gives

$$\frac{-\left[J_x \Delta y \Delta z\right]_{x+\Delta x} + \left[J_x \Delta y \Delta z\right]_x}{\Delta x} + \left[q\overline{\Delta y \Delta z}\right] + \left[q_r \overline{\Delta y \Delta z}\right] = \overline{\Delta y \Delta z}\frac{\partial\left(\bar{\phi}\bar{\rho}\bar{S}\right)}{\partial t} \tag{A-6}$$

If we define a derivative to be

$$\frac{\partial f(x)}{\partial x} = \lim_{\Delta x \to 0} \frac{f(x+\Delta x) - f(x)}{\Delta x},$$

then in this limit, the differential form of the component mass conservation equation is

$$-\frac{\partial(J_x \Delta y \Delta z)}{\partial x} + q\Delta y\Delta z + q_r \Delta y \Delta z = \Delta y \Delta z \frac{\partial(\phi \rho S)}{\partial t} \tag{A-7}$$

where we have noted in the limit as $\Delta x \to 0$ that $\overline{\Delta y \Delta z} \to \Delta y(x)\Delta z(x)$, $\bar{\rho} \to \rho(x)$, $\bar{\phi} \to \phi(x)$, and $\bar{S} \to S(x)$.

Following a similar procedure in considering two-dimensional and three-dimensional flow results in the following differential forms of the component mass conservation equations:

Two-dimensional form:

$$-\frac{\partial(J_x \Delta z)}{\partial x} - \frac{\partial(J_y \Delta z)}{\partial y} + q\Delta z + q_r \Delta z = \Delta z \frac{\partial(\phi \rho S)}{\partial t} \tag{A-8}$$

Three-dimensional form:

$$-\frac{\partial(J_x)}{\partial x} - \frac{\partial(J_y)}{\partial y} - \frac{\partial(J_z)}{\partial z} + q + q_r = \frac{\partial(\phi \rho S)}{\partial t} \tag{A-9}$$

We have generalized to allow flux in the $y$ and $z$ directions, $J_y$ and $J_z$ respectively.

If Equations A-7, A-8, and A-9 are compared, the differential component mass conservation equations may be generalized for arbitrary dimensionality as follows:

$$-\nabla \bullet \alpha \vec{J} + \alpha(q + q_r) = \alpha \frac{\partial(\phi \rho S)}{\partial t} \tag{A-10}$$

where $\alpha$ is a geometric factor and depends on dimensionality as follows:

one dimension: $\alpha(x, y, z) = \Delta y(x)\Delta z(x)$,
two dimensions: $\alpha(x, y, z) = \Delta z(x, y)$,
three dimensions: $\alpha(x, y, z) = 1$,
and $\nabla \bullet \alpha \vec{J}$ is shorthand for $\frac{\partial(\alpha J_x)}{\partial x} + \frac{\partial(\alpha J_y)}{\partial y} + \frac{\partial(\alpha J_z)}{\partial z}$.

It is important to note that, in general, $\alpha$ varies spatially and, therefore, remains inside the above derivative terms. In two-dimensional flow, $J_z$ is zero, and in one-dimensional flow, both $J_y$ and $J_z$ are zero.

Equation (A-11) is written for one component. In multicomponent systems, the mass of each component must be conserved. This results in multiple conservation equations (one for each component) similar to Equation A-11.

The development leading up to Equation A-11 assumed that the component exists in one phase because its mass is assumed equal to the product $\phi\rho S$. We now relax this assumption and write the two mass conservation equations for a two-phase, two-component system in which each component may be distributed between each of the phases. Such conditions arise when gas dissolves in liquid or liquid vaporizes into gas.

For convenience and generality, the two phases will consist of a wetting and a non-wetting phase denoted by lowercase *w* and *n*, respectively. The two components will be distinguished according to wetting and non-wetting and denoted by uppercase W and *N*. We recognize that wettability is a characteristic of the phase and not a component property. The nomenclature "wetting component" is used to indicated that this component in general dominates the wetting phase and similarly for the non-wetting component.

Component concentrations are required when a phase may consist of more than one component. Define $C_{Ij}$ as the mass fraction of the Ith component in the jth phase. Using the above nomenclature, four concentration terms can be defined for the general two-component, two-phase system: $C_{Nw}$, $C_{Ww}$, $C_{Nn}$, and $C_{Wn}$. Because all the mass in a phase must come from the two components, then the component concentrations in each phase are related as

$$C_{Nw} + C_{Ww} = 1.0 \text{ and } C_{Nn} + C_{Wn} = 1.0 \tag{A-11}$$

With the above concepts and nomenclature defined, Equation A-10 is applied to both the wetting and non-wetting components as follows:

Non-wetting component mass balance:

$$-\nabla \bullet \alpha \vec{J}_N + \alpha(q_N + q_{rN}) = \alpha \frac{\partial}{\partial t}(\phi\rho_n S_n C_{Nn} + \phi\rho_w S_w C_{Nw}) \tag{A-12}$$

Wetting component mass balance:

$$-\nabla \bullet \alpha \vec{J}_W + \alpha(q_W + q_{rW}) = \alpha \frac{\partial}{\partial t}(\phi\rho_n S_n C_{Wn} + \phi\rho_w S_w C_{Ww}) \tag{A-13}$$

Comparison of Equations A-12 and A-13 with A-10 shows that aside from the addition of some subscripts, the major differences come from allowing for the possibility of component mass in the element volume to be distributed between the two phases. For example, in the wetting component mass balance (Equation A-13), the first term in the time derivative, $\phi\rho_n S_n C_{Wn}$ is the mass of the wetting component distributed to the non-wetting phase in the element volume. The second term in the time derivative, $\phi\rho_w S_w C_{Ww}$ is the mass of the wetting component distributed to the wetting phase in the element volume.

The component mass flux vectors $\vec{J}_N$ and $\vec{J}_W$ consist of contributions from both phases. The flux can be expanded and written to account for these contributions as follows:

$$\vec{J}_N = C_{Nn}\rho_n\vec{V}_n + C_{Nw}\rho_w\vec{V}_w \tag{A-14}$$

$$\vec{J}_W = C_{Wn}\rho_n\vec{V}_n + C_{Ww}\rho_w\vec{V}_w . \tag{A-15}$$

$\vec{V}_n$ and $\vec{V}_w$ are the superficial velocities for the non-wetting and wetting phases, respectively.

So far in this development, no assumptions have been made concerning the velocities or their relationships to pressure or potential. In BRAGFLO, Darcy's original law, extended to multiphase and multidimensional flow and accounting for gravity and capillary forces, relates superficial velocities to potential.

As mentioned in Section A.2.2, when two immiscible fluids occupy the pore space, they become separated by an interface. The curvature and surface tension of this interface produces a pressure difference called the capillary pressure. This capillary pressure has been experimentally observed to vary with saturation. In BRAGFLO, the capillary pressure is defined by Equation A-16 as the difference between non-wetting phase pressure and wetting phase pressure.

$$P_c(S_w) = P_n - P_w \tag{A-16}$$

Assuming each phase pressure is partially responsible for the flow of only that phase, Darcy's law in differential form becomes

$$\vec{V}_n = -\frac{K_n}{\mu_n}(\nabla P_n - \rho_n g \nabla D) \tag{A-17}$$

$$\vec{V}_w = -\frac{K_w}{\mu_w}(\nabla P_w - \rho_w g \nabla D), \tag{A-18}$$

where $g$ is the gravitational constant of acceleration and $D$ is the depth, which may vary spatially with all three coordinates.

In Equation A-17 and A-18, $K_n$ and $K_w$ are the effective permeabilities to flow for each phase. Unlike the absolute permeability of a porous medium in Darcy's original law that is independent of the flowing fluid (except for gas at low pressures), the effective permeability depends on the characteristics of the rock and fluid and has been experimentally observed to vary with the type and amount of fluid present (i.e., to vary with saturation). Instead of effective permeability, it is more common to encounter relative permeabilities in the reservoir literature. The relative permeabilities are defined as the ratio of the effective permeability of a phase to the absolute permeability (or single fluid permeability) of the porous medium.

$$k_{rn} = \frac{K_n}{K} \tag{A-19}$$

$$k_{rw} = \frac{K_w}{K} \tag{A-20}$$

The dependence of capillary pressure and relative permeability on fluid saturation is described in more detail in Volume 3, Section 2.3.1 of this report.

Substitution of Equations A-14, A-15, A-17, A-18, A-19, and A-20 into A-12 and A-13 results in the two-component mass conservation equations, A-21 and A-22.

$$-\nabla \bullet \left[ \frac{\alpha C_{Nn} \rho_n k_{rn} K}{\mu_n} (\nabla P_n - \rho_n g \nabla D) + \frac{\alpha C_{Nw} \rho_w k_{rw} K}{\mu_w} (\nabla P_w - \rho_w g \nabla D) \right] + \alpha (q_N + q_{rN})$$

$$= \alpha \frac{\partial}{\partial t} \left[ \phi \rho_n S_n C_{Nn} + \phi \rho_w S_w C_{Nw} \right] \tag{A-21}$$

$$-\nabla \bullet \left[ \frac{\alpha C_{Wn} \rho_n k_{rn} K}{\mu_n} (\nabla P_n - \rho_n g \nabla D) + \frac{\alpha C_{Ww} \rho_w k_{rw} K}{\mu_w} (\nabla P_w - \rho_w g \nabla D) \right] + \alpha (q_N + q_{rN})$$

$$= \alpha \frac{\partial}{\partial t} \left[ \phi \rho_n S_n C_{Wn} + \phi \rho_w S_w C_{Ww} \right] \tag{A-22}$$

Equations A-21 and A-22, along with A-11, A-16, and the phase saturation constraint, Equation A-23, form the system of equations solved simultaneously in BRAGFLO.

$$S_n + S_w = 1.0 \tag{A-23}$$

The constraint on saturation simply states that all of the pore space volume is occupied by the fluid phases.

The absolute permeability that appears in Equations A-21 and A-23 is directional and may be in general viewed as a second-order tensor. When the permeability of a porous medium depends on direction, the medium is characterized as being anisotropic. In BRAGFLO, the anisotropic porous medium is assumed to be orthotropic with the three orthogonal axes of the medium being aligned with the three coordinate axes. The off-diagonal elements of the permeability tensor are zero for an orthotropic porous medium. The diagonal permeabilities are $K_x$, $K_y$, and $K_z$. Some pre-processing of permeability data may be required if the data is taken in directions not aligned with the model's coordinate axes.

Assuming the concentrations and all of the physical properties of the fluids and the porous media are defined, the system of equations defines the spatial and temporal variation in the four dependent variables $S_n$, $S_w$, $P_n$, and $P_w$. The saturation constraint (Equation A-23) and the definition of capillary pressure (Equation A-16) are used to eliminate two of the dependent variables.

Theoretically, any two of the variables may be eliminated from the system, leaving two primary dependent variables. Some combinations may be numerically more advantageous than others. Selecting both phase pressures as primary dependent variables is not appropriate because saturation would then be obtained from the capillary pressure dependence on saturation, which may not be defined below residual saturations or capillary pressure may not uniquely specify a saturation.

In BRAGFLO, the primary dependent variables are selected as $S_n$ and $P_w$. $S_n$ is aligned with the non-wetting mass conservation partial differential equation (Equation A-21), while $P_w$ is aligned with Equation A-22. Equation A-23 determines $S_w$ from $S_n$, and Equation A-16 is used to obtain $P_n$ once $S_w$ and $P_w$ are known. No fundamental difference was observed when the primary dependent variables of $P_n$ and $S_w$ were used during simple test problems. Nevertheless, the current BRAGFLO formulation assumes $S_n$ and $P_w$ as primary dependent variables.

## A.2.5 Initial and Boundary Conditions

$S_n$, $S_w$, $P_n$, and $P_w$

Specification of boundary and initial conditions is required to complete the formulation. Upon examination of Equations A-21 and A-22, it is evident that they are second-order with respect to non-wetting phase pressure ($P_n$) and wetting phase pressure ($P_w$). Thus, two boundary conditions are required for each phase pressure in each dimension (two for $P_n$ and $P_w$ in $x$, two for $P_n$ and $P_w$ in $y$, and two for $P_n$ and $P_w$ in $z$). BRAGFLO handles boundary conditions in a way that typifies reservoir models; that is, the reservoir of interest in enclosed by a boundary across which there is no flow in the direction normal to it. Mathematically, these types of conditions are Neumann boundary conditions in which the normal derivative of pressure to the boundary is zero. In BRAGFLO, this is accomplished by assigning a zero value to the normal transmissibilities along each of the boundaries for both the gas and brine phases.

Through the use of wells, BRAGFLO has the capability to override the no-flow conditions. By locating pressure-constrained or flow-constrained fictitious wells along the boundaries, fixed pressures along the boundary or non-zero flow into or out of the reservoir across the boundary can be approximated.

No-flow boundary conditions may occur on two types of boundaries: one is the physical boundary of the reservoir being modeled; the other is along a line of symmetry. An implicit assumption in the use of no-flow boundaries is that the boundaries are located far enough away from the wells or other regions of interest that the boundaries exert negligible influence on the flow behavior in the reservoir over the duration of simulation time.

A number of variables and properties must be specified at time $t = 0$. These initial conditions consist of: (1) the two dependent variables aligned with Equation A-21 and Equation A-22 ($S_n$ and $P_w$), (2) the reservoir properties of porosity and the directional permeabilities, and (3) the concentrations of metal and cellulose. These variables must be specified throughout the simulation volume and along the boundaries. All other material properties (fluid and reservoir properties) must also be specified; however, properties such as relative

permeabilities, capillary pressures, densities, viscosities, dissolved gas, etc., are functions of the previously specified dependent variables and are calculated in BRAGFLO.

## A.2.6 Numerical Solution Techniques

The numerical techniques in the BRAGFLO flow model are based on a fully implicit finite difference representation of the nonlinear conservation equations. In implicit methods, the dependent variable at a particular location is evaluated as a function of the current values of its neighbors and the current value of any coefficients. In explicit methods, current values of the dependent variables are evaluated as a function of previously determined (or past-dated) values of dependent variables and coefficients. Implicit methods are inherently more numerically stable compared to their explicit or hybrid (IMPES) counterparts (Fanchi et al., 1982; Carnahan et al., 1969; Smith, 1965). The penalty for this increased stability is the increased computational effort associated with the simultaneous solution of the resulting finite difference analogs of the conservation equations at each grid block center. A complete discussion of numerical solution techniques is provided in the 1991 performance assessment documentation (see Section 5.2 of WIPP PA Division, 1991).

## A.2.7 Benchmark Results

BRAGFLO has been benchmarked against two other multiphase reservoir codes (BOAST II and TOUGH). The results of four one-dimensional, radial benchmarks (with/without dissolved gas and with/without gas generation) showed excellent agreement among the three codes. Benchmark results are provided in the 1991 performance assessment documentation (see Section 5.2.2.3 of WIPP PA Division, 1991).

## A.2.8 Postprocessing

BRAGFLO output has in the past consisted solely of various distributions—pressures, saturations, interblock, flows, etc. However, detailed analyses of the results, such as those discussed in the RCRA report (WIPP PA Department, 1992) and the 1991 sensitivity analysis report (Helton et al., 1992), require more detailed output. Examples include extents of gas flow in particular regions (such an the anhydrite layers) and especially numerous integrated quantities, such as integrated flows up intrusion boreholes or flows through drift or shaft seals.

Last year, these integrations and summary types of calculations were done externally to BRAGFLO using CAMCON postprocessing tools, in particular, ALGEBRA. However, the postprocessors can deal only with data in the BRAGFLO output files. Because the quantity of output from BRAGFLO can be vast, results are generally printed out only every 15 or 20 time steps. For most purposes, this provides an adequate amount of detail. However, some of the integrations are done on quantities that can vary extremely rapidly. For example, the rate of brine flow up an intrusion borehole can sometimes be very high immediately following the intrusion, but last for only a few time steps. Assuming that the high rate lasts for 15 or 20 steps, rather than just two steps, can seriously overestimate the quantity of brine that flowed up the borehole in that time period.

This shortcoming was corrected in 1992 by performing these integrations internally to BRAGFLO. All integrations and summary statistics used in detailed analysis of BRAGFLO output are now calculated at each step of a performance calculation. Thus, these results are as accurate as the fundamental solution quantities calculated in BRAGFLO (brine pressures and gas saturations). No additional errors are introduced by postprocessing partial results.

A drawback to performing these integrations internally to BRAGFLO is that portions of the code become mesh specific. In order to integrate flows up an intrusion borehole, for example, the location of the borehole must be "hardwired" into the code. In addition, quantities that are of interest in one mesh do not even exist in another mesh because the conceptual model differs. To program the integration and summary calculations to be completely general to enable it to perform on any mesh is not feasible under the PA time constraints. Thus, multiple versions of BRAGFLO currently are used, each one differing only in the number and type of output summary calculations that are done for the particular mesh and conceptual model being used. All other internal workings of the different versions are identical.

## A.3 Waste Mobilization (PANEL)

PANEL's waste mobilization model mathematically computes the radionuclide concentrations in the brine that result from the waste mixing with the brine. This model assumes that the concentrations of all species are uniform through the waste room, that the concentrations of all species are always in equilibrium, and that solubility limits for a given element are allocated among its isotopes on the basis of relative abundance. Radioactive decay based on the Bateman equations (Section 7.1 of this volume; WIPP PA Division 1991, Section 7.2.3) is also taken into consideration. A complete description of the waste mobilization model is provided in the PANEL discussions found in Volume 3 of this report (Section 1.4.4) and in the 1991 performance assessment documentation (see Section 5.3.2 of WIPP PA Division, 1991).

# Appendix A References


Aziz, K., and A. Settari. 1979. *Petroleum Reservoir Simulation.* London: Applied Science Publishers.

Bear, J. 1975. *Dynamics of Fluids in Porous Media.* New York, NY: Elsevier Publishing Company.

Bear, J. 1979. *Hydraulics of Groundwater.* New York, NY: McGraw-Hill, Inc.

Bear, J., and Y. Bachmat. 1967. "A Generalized Theory on Hydrodynamic Dispersion in Porous Media," *I.A.S.H. Symp. Artificial Recharge and Management of Aquifers.* IASH, P.N. 72. Haifa, Israel. 7-16.

Bear, J., D., I. H. Zaslovskii, and S. Irmay. 1968. *Physical Principles of Water Percolation and Seepage.* Paris: UNESCO.

Brooks, R.H., and A.T. Corey. 1964. *Hydraulic Properties of Porous Media.* Hydrology Paper No. 3. Fort Collins, CO: Civil Engineering Department, Colorado State University.

Carnahan, B., H.A. Luther, and J.O. Wilkes. 1969. *Applied Numerical Methods.* New York, NY: John Wiley & Sons, Inc.

Coats, K.H. 1980. "In-Situ Combustion Model," *Society of Petroleum Engineers Journal.* Vol. 26, no. 6, 533-554.

Collins, R.E. 1961. *Flow of Fluids Through Porous Materials.* New York, NY: Reinhold Publishing Corporation.

Corey, A.T. 1986. *Mechanics of Immiscible Fluids in Porous Media.* Littleton, CO: Water Resources Publications.

Crichlow, H.B. 1977. *Modern Reservoir Engineering - A Simulation Approach.* Englewood Cliffs, NJ: Prentice-Hall, Inc.

Crookston, R.B., W.E. Culham, and W.H. Chen. 1979. "Numerical Simulation Model for Thermal Recovery Processes," *Society of Petroleum Engineers Journal.* Vol. 19, no. 1, 37-58.

Dake, L.P. 1978. *Fundamentals of Reservoir Engineering.* New York, NY: Elsevier Scientific Publishing Company.

de Marsily, G. 1986. *Quantitative Hydrogeology: Groundwater Hydrology for Engineers.* Orlando, FL: Academic Press, Inc.

De Wiest, R.J.M. 1965. *Geohydrology.* New York, NY: John Wiley and Sons.

Dullien, F.A.L. 1979. *Porous Media Fluid Transport and Pore Structure.* New York, NY: Academic Press, Inc.

Fanchi, J.R., K.J. Harpole, and S.W. Bujnowsky. 1982. *BOAST: A Three-Dimensional Three-Phase Black Oil Applied Simulation Tool (Version 1).* DOE/BC/10033-3. Tulsa, OK: Keplinger and Associates, Inc.

Helton, J.C., J.W. Garner, R.P. Rechard, D.K. Rudeen, and P.N. Swift. 1992. *Preliminary Comparison with 40 CFR Part 191, Subpart B for the Waste Isolation Pilot Plant, December 1991—Volume 4: Uncertainty and Sensitivity Analysis Results.* SAND91-0893/4. Albuquerque, NM: Sandia National Laboratories.

Hiatt, W.N. 1968. "Mathematical Basis of Two-Phase, Incompressible, Vertical Flow Through Porous Media and Its Implications in the Study of Gravity-Drainage-Type Petroleum Reservoirs," *Society of Petroleum Engineers Journal.* Vol. 8, no. 3, *225-230.*

Hubbert, M.K. 1940. "The Theory of Ground-Water Motion," *The Journal of Geology.* Vol. 48, no. 8, pt. 1, 785-944.

Hubbert, M.K. 1956. "Darcy's Law and the Field Equations of the Flow of Underground Fluids," *Journal of Petroleum Technology.* Vol. 8, 222-239.

Peaceman, D.W. 1977. *Fundamentals of Numerical Reservoir Simulation.* New York: Elsevier Scientific Publishing Company.

Rubin, B., and P.K.W. Vinsome. 1979. "Simulation of the In-Situ Combusion Process in One Dimension Using a Highly Implici Finite Difference Scheme," *Preprint, 30th Annual Meeting of the Canadian Institute of Mining and Metallurgy, Banft, Canada, May 8-11, 1979.* Paper 79-30-14. Montreal, Quebec: Canadian Institute of Mining and Metallurgy, Petroleum Society.

Scheidegger, A. E. 1960. *The Physics of Flow Through Porous Media.* Rev. ed. Toronto, Canada: University of Toronto Press.

Smith, G.D. 1965. *Numerical Solution of Partial Differential Equations, with Exercises and Worked Solutions.* New York, NY: Oxford University Press.

Vaughn, P. 1986. *A Numerical Model for Thermal Recovery Processes in Tar Sand: Description and Application.* DOE/FE/60177-2219. (Available from National Technical Information Service, Springfield, VA.)

WIPP Performance Assessment (PA) Department. 1992. *Long-Term Gas and Brine Migration at the Waste Isolation Pilot Plant: Preliminary Sensitivity Analyses for Post-Closure 40 CFR 268 (RCRA), May 1992.* SAND92-1933. Albuquerque, NM: Sandia National Laboratories.

WIPP Performance Assessment (PA) Division. 1991. *Preliminary Comparison with 40 CFR Part 191, Subpart B for the Waste Isolation Pilot Plant, December 1991 - Volume 2: Probability and Consequence Modeling.* SAND91-0893/2. Albuquerque, NM: Sandia National Laboratories.

# APPENDIX B:
# SANCHO

# APPENDIX B: SANCHO

## B.1 Overview

SANCHO is a special purpose, finite-element computer program developed at Sandia National Laboratories to solve problems of the quasistatic, large-deformation, inelastic response of two-dimensional (i.e., planar or axisymmetric) solids (Stone et al., 1985). This program numerically solves the general, nonlinear partial differential equations that govern relaxation to equilibrium between stresses and applied loads in a solid body. Because the general equations are an underdetermined system, they must be supplemented with constitutive equations for up to three optional material models: a finite strain, elastic-plastic strain-hardening model; a volumetric plasticity model; and a metallic creep model. The material models actually used in the 1992 series of PA calculations are described in Section 1.4.7 of Volume 3.

SANCHO uses a finite-element method to obtain a numerical solution; the elements are bilinear, isoparametric quadrilaterals with constant bulk strain. The solution strategy for obtaining equilibrium includes the use of an iterative scheme designed around a self-adaptive, dynamic relaxation algorithm; the iterative scheme is an explicit, central-difference, pseudo-time integration with artificial damping. Because the scheme is explicit, no stiffness matrix is formed or factored — a feature that can reduce computer storage requirements.

## B.2 Summary of Theory and Fundamental Equations

The theory underlying SANCHO is that of the motion of point-like particles that are imbedded within a solid body $V$, which occupies a region of three-dimensional space and is subject to deformation under the influence of prescribed body and surface forces. These particles usually occupy the corners or centers of elements of a mesh that is placed over the volume $V$ at the time ($t = 0$) that deformation begins; the configuration at this time is called the *reference configuration* and the position of a particle is specified by its vector of material coordinates, $\mathbf{X}$. In the reference configuration, the solid body is assumed to be strain free, though not necessarily stress free. As time increases and the body deforms, the particles move with the material along trajectories denoted by

$$x = \xi(\mathbf{X}, t). \tag{B-1}$$

The vector function $\xi$ describes the motion of a particle that starts at $\mathbf{X}$ at $t = 0$; clearly

$$\xi(\mathbf{X}, 0) = \mathbf{X}.$$

It is the vector function $\xi$ that is the basic dependent variable in problems of this kind because knowledge of it permits graphic visualization of the change in shape of the deforming body. For purposes of computing the dynamics of deformation, however, it is more convenient to view the flow of the particles through three-dimensional space as though they were imbedded in a continuous fluid moving with a velocity field,

$$\mathbf{v} = \frac{\partial}{\partial t}\xi(\mathbf{X}, t) = \eta(\mathbf{x}, t), \tag{B-2}$$

defined for $t \geq 0$ and *any* point $\mathbf{x} \in R^3$ (note that $\mathbf{x}$ is now an arbitrary point in space); this is called the *Eulerian point of view.*

The Eulerian point of view permits the calculation of the true acceleration of an element of mass that is instantaneously located at $\mathbf{x}$: from (B-1) and (B-2) and the chain rule of calculus, it is seen that the true acceleration is just the material derivative of $V$,

$$\frac{d\mathbf{v}}{dt} = \frac{\partial \mathbf{v}}{\partial t} + v \bullet \nabla v \tag{B-3}$$

The fundamental equation governing the deformation of the solid body $V$ follows by application of Newton's Laws of Motion to an arbitrary element of mass in volume $V$ (see Malvern, 1969 Section 5.3):

$$\rho \frac{d\mathbf{v}}{dt} = \nabla \bullet \mathbf{T} + \rho \mathbf{b} \tag{B-4}$$

where

$\rho$ = mass density ($kg/m^3$)

$\mathbf{T}$ = the Canchy stress tensor $\left(kg/m \cdot s^2\right)$

$\mathbf{b}$ = sum of specific body forces (i.e., forces per unit mass: usually, gravity; $m/s^2$).

The mass density must also satisfy the continuity equation:

$$\frac{d\rho}{dt} = -\rho \nabla \bullet \mathbf{v} \tag{B-5}$$

SANCHO was actually designed to solve the equilibrium equations associated with (B-4) and (B-5), i.e., the dynamical equations that apply when $|\mathbf{v}|$ and the time rate-of-change of density are small or zero [but in numerical practice a "quasistatic" approximation is employed that requires the re-introduction of artificial time derivatives having much the same form as the left-hand sides of (B-4) and (B-5)]. The quasistatic approximation to the equations of motion takes the form (Stone et al., 1985)

$$\nabla \bullet \mathbf{T} + \rho \mathbf{b} = 0, \tag{B-6}$$

and allows for three kinds of boundary conditions:

1. Jump condition at a contact discontinuity defined by some *internal* surface $S_0$; this condition requires that

$$\left(\mathbf{T}^+ - \mathbf{T}^-\right) \bullet \mathbf{n}_0 = 0 \quad on\ S_0 \tag{B-7}$$

where $\mathbf{n}_0$ is the outward unit normal on $S_0$, and the (+) and (-) signs on the stress tensors signify respectively values taken on the outer and inner sides of $S_0$.

2. Traction boundary conditions on some *external* surface $S_1$, of the form

$$\mathbf{T} \bullet \mathbf{n}_1 = \mathbf{S}(t) \quad on\ S_1 \tag{B-8}$$

where $\mathbf{n}_1$ is the outward unit normal on $S_1$, and $S(t)$ is a prescribed vector function of time.

3. Displacement boundary conditions on some *external* surface $S_2$;

$$\xi(\mathbf{X}, t) = \mathbf{k}(t) \quad on\ S_2 \tag{B-9}$$

where $\mathbf{k}(t)$ is a prescribed vector function of time.

Taken alone, equations (B-6) and the boundary conditions (B-7) through (B-9) obviously do not determine stress distributions. In the two-dimensional geometries of the SANCHO code, the stress tensor has three independent components; in matrix notation,

$$\mathbf{T} = \begin{pmatrix} t_{11} & t_{12} \\ t_{21} & t_{22} \end{pmatrix}, \text{ with } t_{12} = t_{21},$$

and so one more relation is needed in order to make a determinate system of equations. The *constitutive equations* or the stress-strain relations defining the nature of the material under consideration are usually chosen in a way that supplies the required, addition relationships (note, however, that the form of the constitutive equations may vary in space because different kinds of materials may occupy different parts of the solid body $V$).

The constitutive equations in SANCHO are usually expressed as ordinary differential equations (ODEs) for the components of the stress tensor or the components of the deviatoric stress tensor,

$$\mathbf{T}' = \mathbf{T} - \sigma\mathbf{I} = \mathbf{T} + p\mathbf{I} \tag{B-10}$$

where $\sigma$ denotes the mean normal stress and p is the mean normal pressure. For examples of the ODEs governing material models used in the 1992 PA calculations, see Section 1.4.7 of Volume 3.

# Appendix B References

Malvern, L.E. 1969. *Introduction to the Mechanics of a Continuous Medium.* Englewood Cliffs, NJ: Prentice-Hall, Inc.

Stone, C.M., R.D. Kreig, and Z.E. Besinger. 1985. *SANCHO — A Finite Element Computer Program for the Quasistatic, Large Deformation, Inelastic Response of Two-Dimensional Solids.* SAND84-2618. Albuquerque, NM: Sandia National Laboratories.

# APPENDIX C:
# SECO FLOW AND TRANSPORT MODEL

# APPENDIX C: SECO FLOW AND TRANSPORT MODEL

## C.1 Flow

SECO_2DH calculates single-phase Darcy flow for groundwater flow problems in two dimensions. The formulation is based on a single partial differential equation for a hydraulic head using fully implicit time differencing. Both confined and unconfined aquifer conditions are simulated. The flow is solved in both a regional and a local grid, each of which is defined independently of the grid that defines the aquifer properties. A semi-coarsening multigrid solvers is used to increase solution efficiency for large array dimensions. High-order accuracy particle tracking is available for both grids. The codes are written in DEC VMS FORTRAN. The codes are designed specifically for execution on VAX computers operating under the VMS operating system. The guiding philosophy for the SECO codes is to make the problem definition convenient and to facilitate as much as possible the running of grid-convergence tests and local-area simulations within the larger regional-area simulation. The codes are particularly well suited for testing alternative conceptual models for flow and transport.

### C.1.1 Governing Equation

SECO_2DH simulates groundwater flow at regional and local scales within the Culebra Dolomite by solving the following partial differential equation in two dimensions $(x,y)$ in time $(t)$ for potentiometric head, $h$:

$$S_s \frac{\partial h}{\partial t} = \nabla \bullet (K \nabla h) - W \qquad \text{(C-1)}$$

where $K$ is the (tensor) hydraulic conductivity, $S_s$ is the specific storage of the porous material (the Culebra), $t$ is time, and $W$ is a volumetric flux (out of the Culebra) per unit volume of formation (used to simulate wells or recharge). The principal axes of $K$ must be aligned along the coordinate directions $x$ and $y$. $S_s$, $K$, and $W$ may be functions of $(x, y, t)$. For a derivation of this equation from Darcy's flow and the equation of mass conservation, see McDonald and Harbaugh (1988).

### C.1.2 Discretization and Solvers

Equation C-1 (or the steady-state version with $\partial h/\partial t = 0$) is discretized using standard second-order differences in space and first-order backward (fully implicit) differences in time (McDonald and Harbaugh, 1988; Roache, 1976). The fully implicit time differencing produces unconditional stability for this linear equation, but requires solution of an elliptic equation at each time step. In MODFLOW and other common groundwater hydrology codes, this linear, elliptic equation is solved by either the two-line successive over-relaxation (SOR) iterative method or by a direct solver. The direct solver is not considered to be practical for realistic grids (sufficiently fine resolution), being excessively sensitive to computer round-off error (especially on VAX-class computers) and very slow. In SECO_2DH, the solver options are point SOR, (single) line SOR (e.g., see Roache, 1976), and the

semi-coarsening multigrid solver MGSS2, which was developed at Ecodynamics (personal communication with P. Knapp, Ecodynamics Research Associates, Albuquerque, NM).

The semi-coarsening multigrid solver (MGSS2) is the default option. For very coarse resolution (e.g., a 6×6 grid that might be used for development of code enhancements), the point SOR solver is fastest. However, MGSS2 results in significantly increased efficiency for problems with fine resolution and strongly varying conductance (due to either hydraulic conductivity variations or highly stretched grids). Further, the MGSS2 solver does not require that the user estimate an optimum relaxation factor, as SOR solvers do.

### C.1.3 Block-Centered Discretization

SECO_2DH has been written with an option flag called MAC to select either the most common block-centered discretization (MAC=1), with the cell edge coincident with the aquifer edge, or node-centered discretization (MAC=0), with the cell center (or node) on the aquifer edge. Unless required by a specific study, the default cell configuration is MAC=1. This configuration clearly more accurately locates the aquifer edge for both Dirichlet (fixed-head) and Neumann (fixed-gradient) boundary conditions. For QA purposes, MAC=0 is unsupported in SECO_2DH.

### C.1.4 Problem Decoupling

To make the problem definition convenient and to facilitate the running of grid convergence tests and local-area simulations within the larger regional-area simulation, the problem definition is decoupled from the computational grid. The aquifer properties are defined on a discrete data base that can be independent of the computational grids. A sequence of grid solutions does not require the user to define aquifer properties point by point in each computational grid; likewise, the regional computational grid is decoupled from the local computational grid, both in space and time. A number of parameters, including the boundaries of the computational regions, the spatial increments (cell sizes), the simulation times, and the time steps, are all decoupled in both space and time. The only requirement is that the local grid-problem domain of definition must lie within the regional grid-problem domain of definition. Likewise, definition of boundary conditions (types and values) and wells (locations and pumping schedules) are decoupled from the computational grid and are defined in the continuum.

## C.2 Transport

SECO_TP uses a total variational diminishing (TVD) scheme to solve the two-dimensional radionuclide transport equation in a fractured porous medium (Salari et al., 1992). The TVD scheme employed by SECO_TP uses three-level time differencing and directional splitting to improve accuracy and execution time.

An overview theoretical development of SECO_TP that follows has been extracted from Salari et al. (1992). A more detailed explanation is available from Salari et al. (1992) and the work cited below.

## C.2.1 Governing Equation

The relevant partial differential equation contains advection, dispersion, absorption, source, and decay terms. The radionuclide transport problem consists of $N$ species equations, $k = 1,\ldots,N$:

$$\nabla \bullet \left[ D\nabla C_k - VC_k \right] = \phi R_k \frac{\partial C_k}{\partial t} + \phi R_k \lambda_k C_k - \phi R_{k-1} \lambda_{k-1} C_{k-1} - Q\hat{C}_k - \Gamma_k, \tag{C-2}$$

where the dependent variables are $C_k$, the concentration of the $k$th radionuclide. Physical parameters include $D(x,t)$, a $2\times 2$ hydrodynamic dispersion tensor (velocity-dependent); $V(\mathbf{x})$, the Darcy velocity; $\phi(\mathbf{x})$, the fracture porosity; $R_k$, the retardation coefficient; $\lambda_k$, the species decay constant; and $\hat{C}_k$, the concentration of the $k$th injected radionuclide. The well injection rate is $Q$. Detailed physical descriptions of these terms can be found in Huyakorn and Pinder (1983) and Bear and Bachmat (1990). A dual-continuum model requires the additional source term $\Gamma_k$ to represent the flux due to the exchange of contaminant between the fracture and matrix domain. Fracture flow (single-porosity) and fracture/matrix-flow (dual-porosity) versions of Equation C-2 are presented and discussed in detail in Volume 3 of this report (Section 1.4.6). The $N$ equations are linear and sequentially coupled.

A general Robin boundary condition is assumed:

$$\alpha C_k + \beta \frac{\partial C_k}{\partial n} = \gamma \tag{C-3}$$

on a planar rectangular domain $\Omega$. For various choices of $\alpha(\mathbf{x})$, $\beta(\mathbf{x})$, and $\gamma(\mathbf{x})$, one may obtain Dirichlet, Neumann, or Cauchy boundary conditions on different portions of the boundary. The flow field is obtained from SECO_2DH.

The two-dimensional governing equation is solved using an approximate factorization (Fletcher, 1988) with an implicit treatment of boundary conditions. The convective terms are modeled by TVD (Yee, 1987) and the remaining terms by central differencing. Solution of the governing equation is explained in detail in Salari et al. (1992).

## C.2.2 Code Verification

The SECO_TP code has been applied to test problems and is shown to be accurate for both high and low mesh Peclet numbers. SECO_TP has been verified for temporal and spatial accuracy using the following unsteady equation and its solution, with $V = ui$:

$$C_t + uC_x = \alpha_L u C_{xx} + \alpha_T u C_{yy} - g(x,y,t), \tag{C-4}$$

where

$$g(x,y,t) = (x-ut)^2 + y^2,$$

and $0 < x < 1$, $0 < y < 1$. The initial condition is given by

$$C(x,y,0) = \frac{1}{12u}\left[\frac{x^4}{\alpha_L} + \frac{y^4}{\alpha_T}\right] \tag{C-5}$$

The exact solution to Equation C-4 is

$$C(x,y,t) = \frac{1}{12u}\left[\frac{(x-ut)^4}{\alpha_L} + \frac{y^4}{\alpha_T}\right]. \tag{C-6}$$

Because the computational domain is finite, the Dirichlet boundary conditions are time dependent and may be obtained from the exact solution.

Table C-1 presents the computed solution to Equation C-4 at time = 25 for four different grid sizes and time steps. The magnitude of the coefficients are $u = 0.1$, $\alpha_L = 0.1$, and $\alpha_T = 0.1$. Examination of the ratio of root mean square (RMS) of errors shows that the overall solution is second-order accurate in time and space.

The SECO_TP code has also been benchmarked against exact transport solutions in Javandel et al. (1984), Tang et al. (1981), and Knupp and Salari (1992).

Table C-1. Convergence Results, Uniform Grid

| Size | $\Delta x$ | $\Delta y$ | RMS | RMS Ratio |
|---|---|---|---|---|
| 20×20 | 0.05 | 0.25 | 7.697E-3 | |
| 40×40 | 0.025 | 0.125 | 1.954E-3 | 3.94 |
| 80×80 | 0.0125 | 0.0625 | 4.921E-4 | 3.97 |
| 160×160 | 0.00625 | 0.03125 | 1.234E-4 | 3.99 |

# Appendix C References


Bear, J., and Y. Bachmat. 1990. *Introduction to Modeling of Transport Phenomena in Porous Media.* Dordrecht, Netherlands: Kluwer Academic Publishers.

Fletcher, C.A.J. 1988. *Computational Techniques for Fluid Dynamics.* New York, NY: Springer-Verlag. Vols. 1-2.

Huyakorn, P.S., and G.F. Pinder. 1983. *Computational Methods in Subsurface Flow.* New York, NY: Academic Press.

Javandel, I., C. Doughty, and C-F. Tsang. 1984. *Groundwater Transport: Handbook of Mathematical Models.* Water Resources Monograph No. 10. Washington, DC: American Geophysical Union.

Knupp, P.M., and K. Salari. 1992. *Contributions of an Analytical Solution to a 2D Radionuclide Transport Problem for Site Performance Assessment.* Albuquerque, NM: Ecodynamics Research Associates Technical Report. (Copy on file in Waste Management and Transportation Library, Sandia National Laboratories, Albuquerque, NM.)

McDonald, M.G., and A.W. Harbaugh. 1988. *A Modular Three-Dimensional Finite-Difference Ground-Water Flow Model.* Techniques of Water-Resources Investigations of the United States Geological Survey, Book 6, Modeling Techniques. Reston, VA: U.S. Geological Survey.

Roache, P.J. 1976. *Computational Fluid Dynamics.* Rev. printing. Albuquerque, NM: Hermosa Publishers.

Salari, K., P. Knupp, P. Roache, and S. Steinberg. 1992. "TVD Applied to Radionuclide Transport in Fractured Porous Media," *Proceedings of IX International Conference on Computational Methods in Water Resources, Denver, Colorado.* 141-148. (Copy on file in Waste Management and Transportation Library, Sandia National Laboratories, Albuquerque, NM.)

Tang, D.H., E.O. Frind, and E.A. Sudicky. 1981. "Contaminant Transport in Fractured Porous Media: Analytical Solution for a Single Fracture," *Water Resources Research.* Vol. 17, no. 3, 555-564.

Yee, H.C. 1987. "Construction of Explicit and Implicit Symmetric TVD Schemes and Their Applications," *Journal of Computational Physics.* Vol. 68, no. 1, 151-179.

# APPENDIX D:
# CULEBRA TRANSMISSIVITY FIELD SIMULATIONS

# APPENDIX D: CULEBRA TRANSMISSIVITY FIELD SIMULATIONS

The information presented in this appendix is extracted from LaVenue and RamaRao (1992).

## D.1 Background

Efforts to incorporate uncertainty in the Culebra transmissivity field into PA calculations have been somewhat evolutionary. In the 1990 PA calculations, the Culebra was divided into seven zones or regions. A mean transmissivity value and an associated standard deviation was assigned to each zone. By sampling from the distributions associated with each zone, multiple realizations of zonal transmissivity values were subsequently used as input to the flow and transport calculations. Although computationally elegant, the specification of zones significantly reduces the spatial variability within a given realization because each zone has a constant value. In addition, large differences in the values assigned to each zone in a given realization may occur generating severe step changes in the permeability field.

In an effort to improve the transmissivity field used in the 1991 PA calculations, conditional simulations (CS) of Culebra transmissivity fields were produced by conditioning upon the observed transmissivity values and the pilot points which were added in the LaVenue et al. (1990) model. The CS transmissivity fields were then used in a groundwater flow model (WIPP PA Division, 1991). The boundary conditions necessary to reduce the differences between the observed and calculated steady-state heads were then determined. Those realizations that did not meet a minimum error criteria were not considered adequate and were discarded. This work resulted in over 60 conditional simulations that had acceptable fits to the observed steady-state freshwater heads. These 60 fields were subsequently used in the calculations by sampling on a uniformly distributed variable assigned to each CS field (WIPP PA Division, 1991). The differences between each realization is depicted by a groundwater travel-time cumulative-distribution function, where travel times range from approximately 10,000 years to 30,000 years. These travel times are used as an internal diagnostic measure in the generation of CS transmissivity fields. Travel times used in the calculation of Environmental Protection Agency (EPA) normalized releases of radionuclides to the accessible environment are calculated using the CS transmissivity fields and the SECO flow and transport codes.

In March of 1991, a geostatistics/stochastic-hydrology expert panel (GXG) was convened to provide guidance for adequately incorporating the uncertainty of the Culebra transmissivity field into the PA calculations. After reviewing the previous work, the GXG had several concerns regarding the approach taken in LaVenue et al. (1990). One of the principal concerns raised by the GXG panel members related to the subjectivity inherent in the manual calibration approach. For example, the model was calibrated in a piecewise fashion by sequentially selecting regions to be calibrated, instead of calibrating the whole model area at the same time. The model was sequentially calibrated in the northwest (upgradient) region, southwest region, southern region, and central region or WIPP-site boundary area. As mentioned in the 1990 study, the regions upgradient and downgradient from the WIPP-site area were calibrated prior to making any changes within the WIPP-site boundary. This approach was employed in order to reproduce the regional hydraulic gradients across the northern and southern WIPP-site boundaries; it is analogous to producing a regional flow model to provide boundary conditions for a local scale

model. The GXG panel wondered whether there would be any major differences in the calibrated transmissivity field had the entire model area been calibrated at the same time.

Several recommendations were proposed by the GXG panel members and are described in detail in Gallegos (1992). One of their recommendations included repeating the modeling performed by LaVenue et al. (1990), which included steady-state and transient model calibration, numerous times. However, instead of simply kriging the transmissivities, conditional simulations would be generated and subsequently calibrated. The conditional simulations would allow for different transmissivity fields to be used as the initial fields for the model. These fields would initially be conditioned on the observed transmissivity data only. Subsequent model calibration would then condition each of the conditionally simulated fields to the observed steady-state and transient heads. Because the GXG panel also expressed concerns regarding the manual assignment of transmissivities to the pilot points, the approach used in LaVenue et al. (1990) was also enhanced to include optimization routines that were needed to assign transmissivity values to the pilot points once their location was selected.

The present study addresses the uncertainty in the travel time by embedding the problem in a probabilistic framework. The true transmissivity distribution at the WIPP site is conceptualized to be one realization of a stochastic process. Accordingly, a large number of realizations of this stochastic process, which are very plausible versions of the true transmissivity at the WIPP site, are generated. This ensemble of realizations is thus used with the groundwater flow model to generate an ensemble of the corresponding travel times. The distribution of the travel times provides an understanding of the uncertainty. While several statistical measures can be used to quantify the uncertainty, a complimentary cumulative distribution function (CCDF) is commonly used for a graphical display of the uncertainty in travel time.

This appendix describes the methodology of this new approach as it is used in the Culebra system. (A more complete explanation of this new approach and its application is provided in LaVenue and RamaRao [1992].) Seventy calibrated conditionally simulated (CCS) transmissivity fields were produced using this approach; these fields are discussed in Section 2.6.3 of Volume 3 of this report and are presented in Appendix C of Volume 3 of this report.

## D.2 Overview of Methodology

The solution methodology involves the generation of a large number of random transmissivity fields, each of which is in close agreement with all the measured data at the WIPP site. The collected data at the WIPP site is comprised of (1) transmissivity measurements, and (2) pressure measurements (both steady state and transient state). Conformity between a random transmissivity field and the measured data is achieved in stages, as described below. Figure D-1 presents an overview of the different steps in this study.

First, unconditional simulations of the WIPP transmissivity fields are generated. These are random fields, having the same statistical moments (the mean and the variance) and the same spatial correlation structure, as indicated by the transmissivity measurements. (These fields need not, however, match the measured transmissivities at the location of their measurements.)

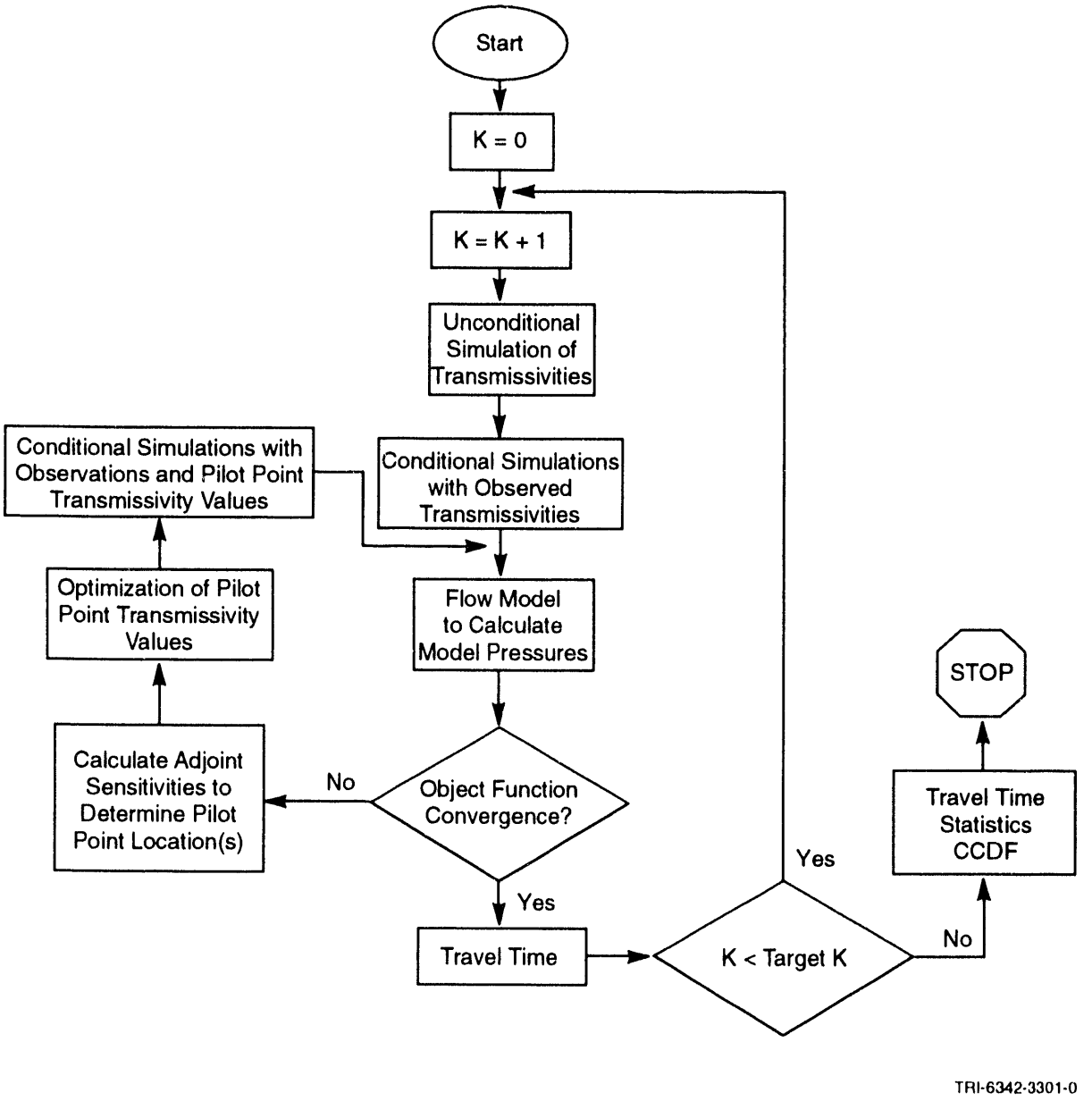


Figure D-1. Calibration of conditionally simulated transmissivity fields: flow chart.

These transmissivity fields are then conditioned, so that they honor exactly the measured transmissivities at the locations of their measurements. The resulting fields are called conditional simulations of the transmissivity fields.

The conditional simulations of transmissivity field are then further conditioned, such that the pressures computed by the groundwater flow model (both steady and transient state) agree closely with the measured pressures, in a least-square sense. This phase is known as calibration or the solution of inverse problem, and accounts for a large part of the time and effort in this study. When the calibration is completed, one obtains a random transmissivity field that is in conformity with all the data at the WIPP site, and may therefore be regarded as a plausible version of the true distribution of transmissivity at the WIPP site.

In this study model calibration is done by an indirect approach. An objective function is defined as the weighted sum of the squared deviations between the model computed pressures and the observed pressures, with the summation being extended in the spatial and temporal domain where pressure measurements are taken. The classical formulation of the calibration then requires the minimization of the objective function, subject to the constraints of the groundwater flow equations in the steady and transient state. This approach is implemented by iteratively adjusting the transmissivity distribution until the objective function is reduced to a prescribed minimum value.

A common approach to calibration consists in dividing the model domain into a few zones, in each of which the transmissivity is treated as constant. The transmissivities in the different zones constitute the parameters to be adjusted in the optimization process. Clearly, the delineation of zones is a subjective process and does affect the results of the calibration. Thus, it may become necessary to consider several alternative zonation patterns for calibration. Also, in this approach, uniform transmissivities are assigned to each zone. This representation may be considered as inadequate, particularly while addressing the issues of spatial variability (within a zone).

To avoid the above difficulties of the zonation approach, an approach using pilot points as parameters is adopted here. A pilot point is a synthetic transmissivity data point, that is added to an existing measured transmissivity data set during the course of calibration. A pilot-point is defined by its spatial location and by the transmissivity value assigned to it. After a pilot point is added to the transmissivity data set, the augmented data set is used to obtain kriged or conditionally simulated transmissivity fields, for a subsequent iteration in calibration. With the addition of a pilot point, the transmissivity distribution in the neighborhood of the pilot point gets modified with dominant modifications being closer to the pilot-point location. The modifications in the different grid blocks are determined by kriging weights and are not uniform (as in the zonation approach). Conceptually, a pilot point may be viewed as a simple model to effect realistic modifications of transmissivity in a large region of the model.

A coupled kriging-and-adjoint sensitivity analysis is used for the location of the pilot point; optimization algorithms are used for assigning the transmissivity of a pilot point. Thus, the pilot-point approach to calibration has been rendered objective, a feature considered very desirable for the WIPP site. Further, a multistage approach has been used in implementing this methodology. This aspect bears similarity to the dynamic programming method of optimization.

## D.3 Code Development: An Overview

A comprehensive code package has been assembled using many of the codes already developed and frequently used in groundwater flow simulations. They are listed below. For details of the theory and application of these codes, the following references cited may be consulted:

- TUBA, unconditional simulation of transmissivity field (Zimmerman and Wilson, 1990),
- AKRIP, generalized kriging (Kafritsas and Bras, 1981),
- SWIFT II, modeling pressures (steady and transient state) (Reeves et al., 1986a,b,c)
- GRASP II, adjoint sensitivity analysis (steady and transient state) (Wilson et al., 1986; RamaRao and Reeves, 1990), and
- STLINE, groundwater travel time and travel paths (Intera, Inc., 1989).

In addition to using the above codes, the following new codes have been developed in the present task. The details of the new codes are provided in LaVenue and RamaRao (1992).

- MAIN—drives the different modules
- CONSIM—generates conditional simulations of transmissivity from the unconditional simulations of transmissivity
- PILOTL—locates the pilot points based on sensitivity analysis
- PAREST—assigns the pilot point transmissivities by minimization of a least square objective function

## D.4 Simulated Transmissivities

In the earlier modeling efforts for WIPP (LaVenue et al., 1990), kriging has been employed to address the issue of spatial variability in transmissivity. In an effort where only one calibrated field is to be produced, kriging becomes an obvious choice. Kriging provides optimal estimate of the transmissivity at a point, thereby necessarily smoothing out the true variability between measurement points. On the contrary, simulated values reproduce the fluctuation patterns in transmissivity, which may lead to extreme values in travel times. Thus, simulated fields are useful to resolve the residual uncertainty not addressed by kriging.

## D.4.1 Unconditional Simulation

An unconditional simulation of transmissivity field is a random field having the same statistical moments (mean and variance) and the same spatial correlation structure as indicated by the measured transmissivities in the field. An unconditionally simulated transmissivity field is said to be isomorphic with the true field, and is independent of the true field. The following methods have been used earlier in groundwater hydrology for generating unconditional simulations:

- nearest neighbor method (Smith and Schwartz, 1981; Smith and Freeze, 1979),
- matrix decomposition,
- multidimensional spectral analysis (Shinozuka and Jan, 1972; Mejía and Rodríguez-Iturbe, 1974), and
- turning bands method (Matheron, 1971, 1973; Mantoglou and Wilson, 1982; Zimmerman and Wilson, 1990).

In this study, the turning bands method has been used. It is an extremely fast and efficient algorithm and the code TUBA to implement this, is available in public domain.

A two-dimensional (or a three-dimensional) stochastic process is generated in this method by the summation of a series of equivalent one-dimensional processes. Figure D-2 shows a definition sketch taken from Mantoglou and Wilson (1982). The region $P$ shows a grid of points at each of which the two-dimensional field is to be generated. In particular, consider a point $N$ in the grid where the two-dimensional field $[Z_s(N)]$ is to be simulated.

Consider a particular line $i$, the length along which, from the origin O, is measured by $\zeta_i$. This line is divided into a number of intervals (bands), of length $\Delta\zeta_i$, in each of which the one-dimensional process $Z_i$ is computed. Let $N_i$ be the projection of the point N onto the line i. Let $Z_i(\zeta_i)$ be the one-dimensional process in the band containing $N_i$. Then the two-dimensional process $[Z_s(N)]$ is obtained by summing the contributions from the different lines, by the relation

$$Z_s(N) = \frac{\sum_{i=1}^{L} Z_i(\zeta_{N_i})}{\sqrt{L}}, \qquad \text{(D-1)}$$

where $L$ is the number of lines selected. Usually $L$ is between 16 and 20.

LaVenue et al. (1990) analyzed the WIPP transmissivity data and identified the spatial structure of the two-dimensional transmissivity field. They modeled it as an isotropic process and as an intrinsic random function of order zero (IRF-0), with the generalized covariance function (GCF) given by

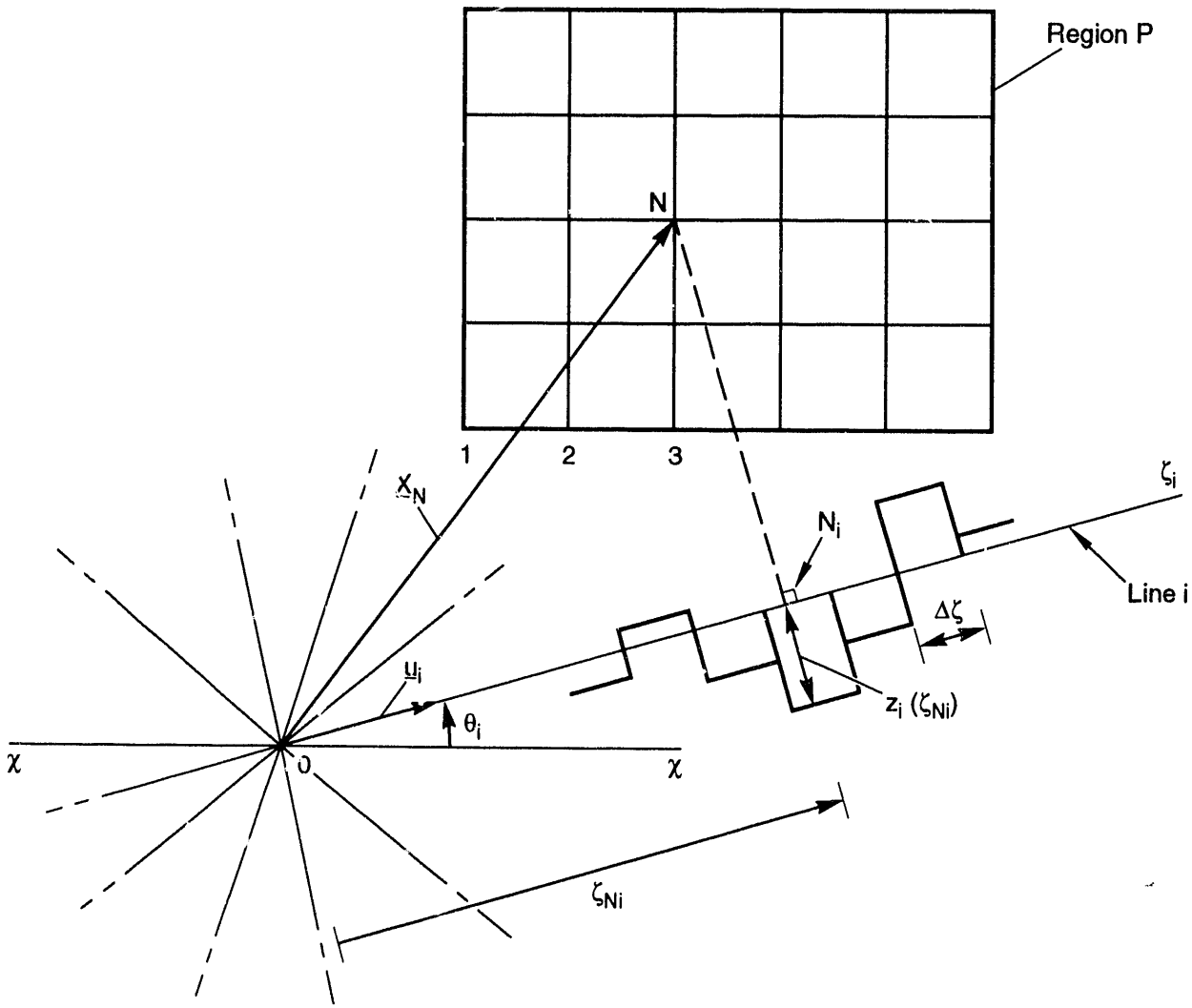


TRI-6342-3303-0

Figure D-2. Schematic representation of the field and turning bands lines (Mantoglou and Wilson, 1982).

$$k_2(r) = -a_0 r \quad \text{(GCF)}$$

$r$ = a radial distance (D-2)

$a_0$ = a constant

The subscript 2 denotes a two-dimensional process.

If $k_1(r)$ is the GCF for an equivalent one-dimensional process,

$$k_1(r) = -\left(\frac{\pi}{2}\right) a_0 r. \tag{D-3}$$

The Weiner-Levy process is known to be an IRF-0 process and is accordingly used to generate the line process. The relevant equations are given below.

$$Z_i(\zeta) = W(\zeta), \tag{D-4}$$

where $W(\zeta)$ is the Weiner-Levy Process.

$$W(0) = 0, \tag{D-5}$$

$$W(\zeta + \Delta\zeta) = W(\zeta) + gU(\zeta), \tag{D-6}$$

$$U(\zeta) = U\left[-\frac{1}{2}, \frac{1}{2}\right], \tag{D-7}$$

and

$$g = \sqrt{12\pi a_0 \Delta\zeta}, \tag{D-8}$$

where $U(\zeta)$ is a uniformly distributed random variable.

## D.4.2 Conditional Simulation

An unconditionally simulated transmissivity field, which is made to honor exactly the measured transmissivity at the locations of the measurements, is called a conditionally simulated transmissivity field. The procedure of conditioning is described below.

Let $Z(x)$ be the true value (not known) of the field at a point x. One may decompose $Z(x)$ as below:

$$Z(x) = Z_{ok}(x) + [Z(x) - Z_{ok}(x)], \tag{D-9}$$

where $Z_{ok}(x)$ is the kriged estimate of $Z$, at $x$, based on the observed values of $Z$ at the locations of the observations.

Here, $[Z(x) - Z_{ok}(x)]$ is a true kriging error and is unknown, since the true value of $Z(x)$ is unknown. It is possible to simulate this error.

Using the unconditionally simulated values ($Z_{uc}$) at the locations of the observations (not the actual observations), a kriged field ($Z_{uk}$) is generated. One may write, using a similar decomposition as above,

$$Z_{uc}(x) = Z_{uk}(x) + [Z_{uc}(x) - Z_{uk}(x)] \quad \text{(D-10)}$$

where $[Z_{uc}(x) - Z_{uk}(x)]$ is also a kriging error, and is known and may be called a simulated kriging error. This error is isomorphic with the true kriging error. More importantly, this error is independent of the kriged values:

$$E\left[Z_{ok}(x), \{Z_{uc}(y) - Z_{uk}(y)\}\right] = 0 \text{ for all } x,y \quad \text{(D-11)}$$

Substituting the known simulated kriging error for the true but unknown kriging error, in Equation D-9, one obtains:

$$Z(x) \approx Z_{ok}(x) + [Z_{uc}(x) - Z_{uk}(x)] \quad \text{(D-12)}$$

Equation D-12 clarifies the conditioning step as one of adding of simulated kriging error on a kriged field using the measured data. This step involves kriging twice, once with the measured transmissivities and another time with the unconditionally simulated transmissivities, both at the location of the observations. The superposition of the three different transmissivity fields is graphically illustrated in Figure D-3.

The (average) transmissivity of each grid block is obtained here, using Gaussian quadrature. A 2×2 Gauss point scheme is used for quadrature in each grid block.

The conditional simulations constitute the most important input to the groundwater flow model. It is useful to appreciate the following properties of a conditional simulation (CS):

1. **The CS field honors the measured values exactly at the measurement locations.** This follows from the fact the kriging is an exact interpolator, so that the simulated kriging error is zero at measurement locations and, further, the kriged value from observations ($Z_{ok}$) reduces to the measured value, for the same reason.

$$Z_{CS}(x) \approx Z_{OK}(x) + [Z_{UC}(x) - Z_{UK}(x)]$$

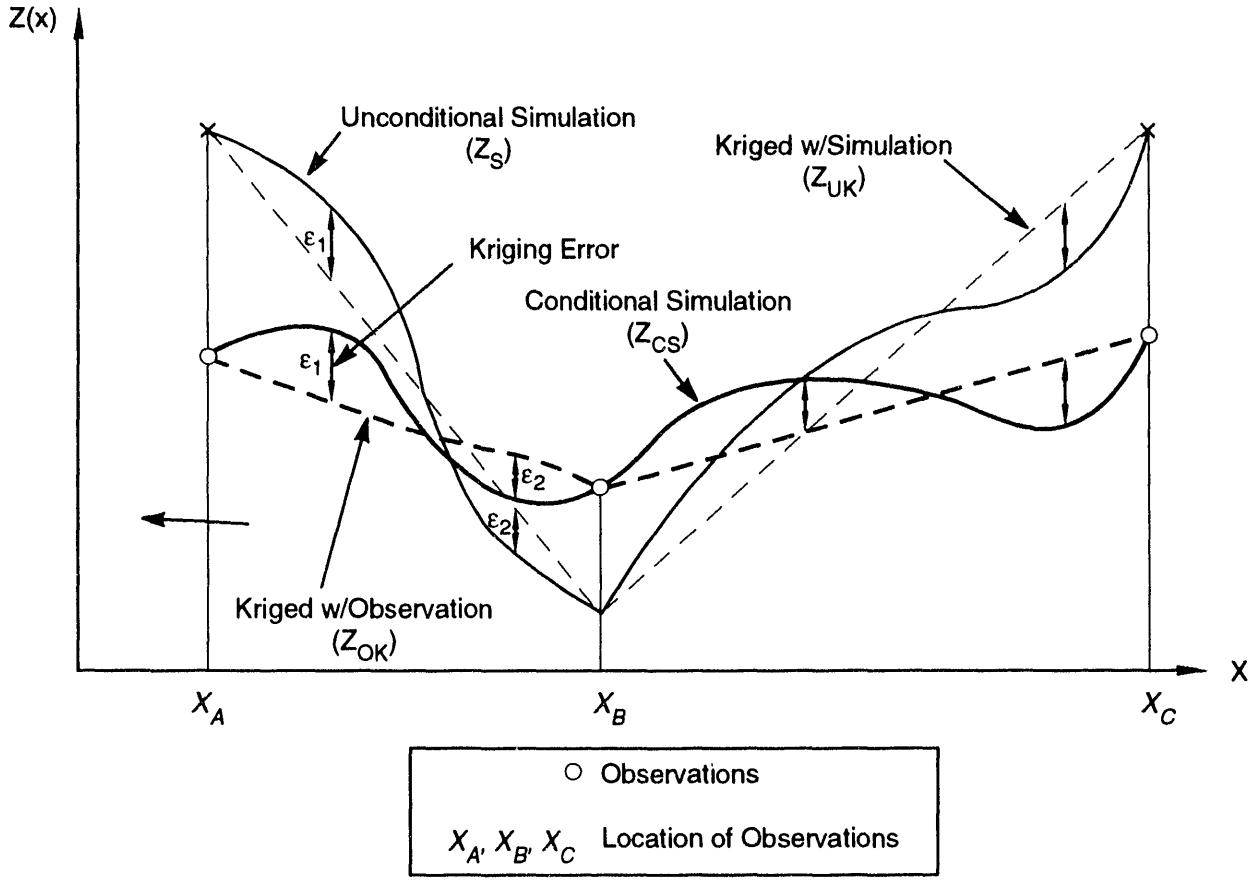


Figure D-3. Conditional and unconditional simulation: relationships.

2. **The CS field has the same spatial correlation structure as indicated by the measured data.** This follows from an orthogonality property of the kriging errors (Equation D-11), which states that the kriging errors (both true and simulated) are uncorrelated with any kriged values for stationary field and with generalized increments for the intrinsic fields (Delfiner, 1976; Delhomme, 1979). Accordingly, the addition of simulated kriging error field to a kriged field does not alter the spatial correlation structure of the kriged field. It may be recalled that the kriged field itself has the same correlation structure as implied by the data.

3. **The average of many CS fields at a location $x$, is merely the kriged estimate at $x$** $[Z_{ok}(x)]$.

4. **The variance of many CS fields at a location $x$ is given by the kriging variance.**

5. **The CS fields reproduce the true variability of the field, in contrast to a smoothed field given by kriging.**

6. **The conditioning step introduces a robustness with respect to the features of the reality that are not specifically known or imposed on the (unconditionally) simulated field.** This robustness increases with the amount of the conditioning data.

## D.4.3 Computational Options for Simulated Fields

The simulated kriging error is rendered zero at all observation points (see Figure D-4). When a pilot point is added to the observed transmissivity data set, two options exist:

- The pilot point may be given the full status of an observed data point. Then the simulated kriging error at the pilot point is also rendered zero. In this case, the simulated kriged error field varies from one iteration to the other, and needs to be computed at every iteration.

- The simulated kriging error is rendered zero only at the observed data point and not at the pilot points. Thus, the pilot points are used to obtain the kriged field using the 'augmented' data. But the simulated kriged error field remains the same as the initial field through all the iterations. It does not need to be recomputed during the various iterations.

While obtaining the kriged field using the simulated data at the measurement locations, two options exist:

- Assume that the simulated value ($Z_{uc}$) has the same errors as the actual measurements.

- Assume that the simulated value ($Z_{uc}$) has no errors.

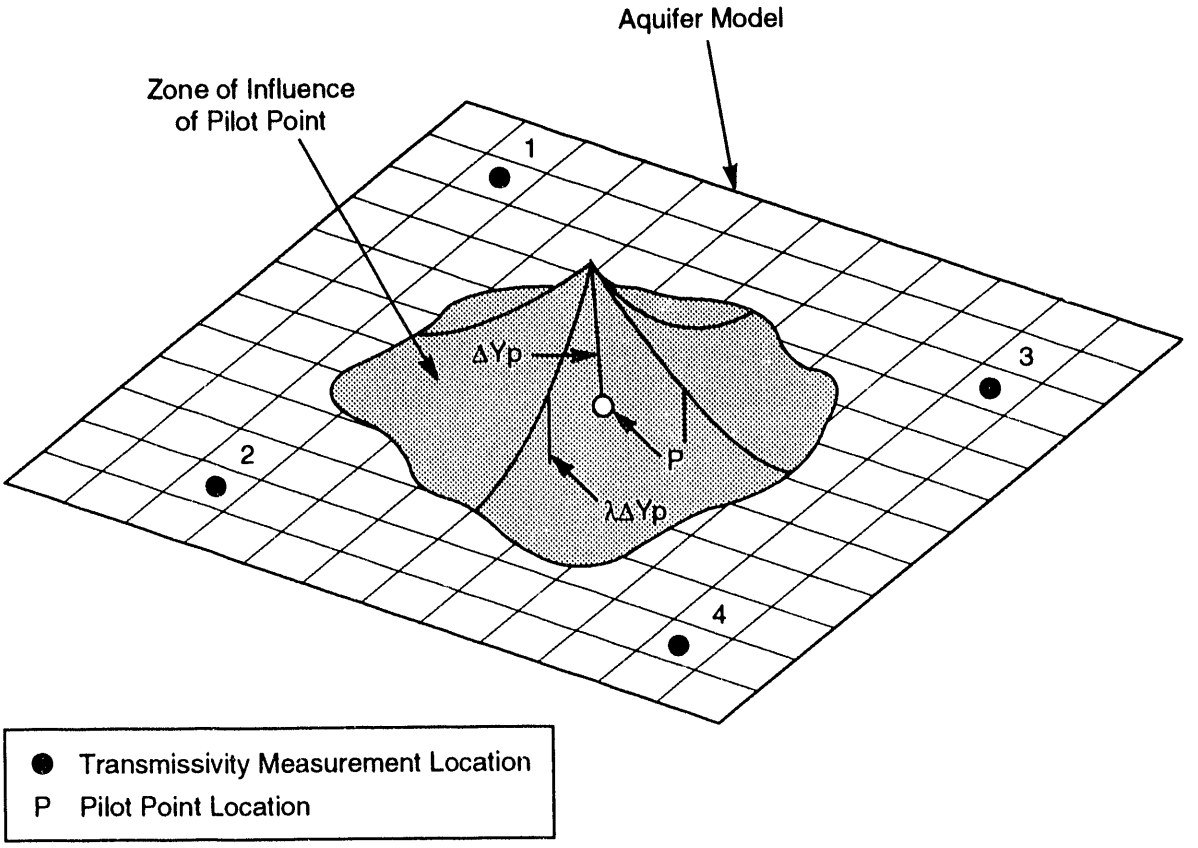


## Pilot Point - Schematic

| | | X | Y | T | y | $\sigma_y$ |
|---|---|---|---|---|---|---|
| Measured Transmissivity | 1 | 150 | 1050 | $10^{-3.1}$ | -3.1 | 0.5 |
| | 2 | | | | | |
| | ⋮ | | | | | |
| | 4 | | | | | |
| Pilot Points added in Calibration | $P_1$ | 650 | 620 | $10^{-4.81}$ | -4.81 | 0.84 |
| | $P_2$ | | | | | |
| | ⋮ | | | | | |
| | $P_n$ | | | | | |

TRI-6342-3305-0

Figure D-4. Pilot point: schematic.

## D.4.4 Validation of Simulations

For every CS field, the mean and variance of the transmissivity are computed and compared with that of the WIPP data. Also, using the code AKRIP, the generalized covariance function (GCF) of the field is obtained and is compared with that obtained from measured data at the WIPP. A close agreement between the two provides verification that the generated CS field is a plausible version of the reality at the WIPP site. The procedure is repeated for all the CS fields.

A collection of all the CS fields generated constitutes an ensemble. For any one location in the field, transmissivity values across all the fields in the ensemble are studied and their mean and variance computed. A spatial distribution of the ensemble mean and variance should closely agree with the spatial distribution of kriged values and kriging variance obtained from the kriging exercise itself.

# D.5 Automated Calibration

In an automatic algorithm, it becomes necessary to restrict the number of parameters (to be identified) to a small number; this step is called parameterization. The zonation approach and the pilot-point methodology can both be viewed as two alternative paths for parameterization. As shown above, the pilot-point approach eliminates an inherent subjectivity in the zonation approach and provides for the most objective inverse algorithm.

## D.5.1 Objective Function

The objective function that is to be minimized in the calibration is a weighted least-square-error criterion function. It comprises of two components, a model-fit criterion and a plausibility criterion. The model-fit criterion is a weighted sum of the squared deviations between the computed and measured pressures taken over all points in spatial and temporal domains, where pressure measurements have been made. The plausibility criterion demands that the calibrated transmissivities be not too far from their prior estimates. A relative weight $\eta$ between the plausibility criterion and the model-fit criterion has been used. In the present study, due to the nature of the pilot point methodology (de Marsily et al., 1984), the plausibility criterion is disregarded by setting $\eta = 0$; the code, however, has the capability to use it.

Equation D-13 defines the objective function in general terms:

$$J(\underline{u}) = \sum_{k=1}^{L} \underline{e}_p^T(k)\underline{\underline{R}}^{-1}(k)\underline{e}_p(k) \quad \text{(model fit)}$$

$$+\eta \bullet \underline{e}_u^T \bullet \underline{\underline{U}}^{-1} \bullet \underline{e}_u \quad \text{(plausibility)}, \tag{D-13}$$

where:

$J(\underline{u})$ = weighted least square (WLS) error criterion function

$\underline{e}_p = \left\{\underline{p}(k) - \underline{p}_{ob}(k)\right\}$

$\underline{e}_u = \left\{\underline{u} - \underline{u}_{est}\right\}$

$\underline{\underline{R}}$ = covariance matrix of errors in $\underline{p}_{ob}$

$\underline{\underline{U}}$ = covariance matrix of errors in $\underline{u}$

$\underline{u}$ = vector of parameters ($Y_p = \log_{10} T_p$)

$\eta$ = relative weight of the plausibility criterion to model fit criterion

$k$ = time step number

$\underline{p}(k)$ = pressures computed

$\underline{p}_{ob}(k)$ = pressures observed

$T$ = transpose

$T_p$ = pilot point transmissivity

$L$ = number of time steps.

After optimal estimates of $\underline{u}$ are obtained, the posterior covariance matrix of the parameters is given by

$$\underline{\underline{P}}_{uu} = \left\{\sum_{k=1}^{L} \underline{\underline{S}}^T(k)\underline{\underline{R}}^{-1}(k)\underline{\underline{S}}(k) + \underline{\underline{U}}^{-1}\right\}^{-1} \tag{D-14}$$

$$\underline{\underline{S}}^T(k) = \text{Jacobian Matrix} = \left[\frac{dp(k)}{d\underline{u}'}\right],$$

where $\underline{\underline{P}}_{uu}$ is the posterior covariance matrix of the parameters.

## D.5.2 Parameters of Calibration

The pilot-point transmissivities are the parameters that are adjusted for calibration. However, in the mathematical implementation, the logarithms (to base 10) of the transmissivities (and not the transmissivity) are treated as parameters. The calibration parameters are given by

$$Y_p = \log_{10} T_p$$

where $T_p$ is the transmissivity at a pilot point (suffix $p$ denotes pilot point). Figure D-4 illustrates the concepts of pilot points presented above.

## D.5.3 Pilot-Point Location

Pilot points are placed at locations where their potential for reducing the objective function is the highest. This potential is quantified by the sensitivity coefficients ($dJ/dY$) of the objective function J, with respect to Y, the logarithm (to base 10) of pilot-point transmissivity. A large number of candidate pilot points are considered, usually the centroids of all the grid blocks in the flow-model grid. The selected candidate pilot points are ranked in the descending order of the magnitude of their absolute sensitivity coefficients, i.e., $|dJ/dY|$. The required number of pilot points is chosen from the top of the ranked list of points.

Coupled adjoint sensitivity analysis and kriging is used to compute the required derivatives, and the procedure is documented in RamaRao and Reeves (1990). It is described briefly here.

Let $P$ be a pilot point added to a set of $N$ observation points. Let $T_p$ be the transmissivity assigned to pilot point $P$. Kriging is done using $Y_p$, where

$$Y_p = \log_{10} T_p \tag{D-15}$$

The kriged estimate ($Y^*$) at the centroid of a gridblock m, is given by

$$Y_m^* = \sum_{k=1}^{N} Y_k \bullet \gamma_{m,k} + Y_p \bullet \gamma_{m,p}\,, \tag{D-16}$$

where $k$ is the subscript for observation point, $p$ is the subscript for pilot point, and $\gamma_{m,k}$ and $\gamma_{m,p}$ are the kriging weights for the interpolation point $m$ and data point $k$ and interpolation point $m$ and data point $p$, respectively.

When a pilot point transmissivity is perturbed, the kriged transmissivities and, hence, the permeabilities in all gridblocks are altered, causing the objective function $J$ to change. Accordingly, using the chain rule,

$$\frac{dJ}{dY_p} = \sum_{m=1}^{M} \frac{dJ}{dY_m^*} \frac{dY_m^*}{dY_p} \tag{D-17}$$

where $M$ is the total number of grid blocks in the flow model.

$$\frac{dY_m^*}{dY_p} = \gamma_{m,p} \quad \text{(from Equation D-16)}$$

$$\frac{dJ}{dY_p} = \sum_{m=1}^{M} \frac{dJ}{dY_m^*} \bullet \gamma_{m,p} \tag{D-18}$$

$$Y_m^* = \log_{10}\left(T_m^*\right)$$

$$T_m^* = K_m \frac{\rho_m}{\mu_m} g b_m$$

$$\frac{dJ}{dY_m^*} = \ln(10) K_m \frac{dJ}{dK_m} \tag{D-19}$$

where $T^*$ is the estimated transmissivity, $K^*$ is the estimated permeability, $\rho$ is fluid density, $\mu$ is fluid viscosity, $g$ is acceleration due to gravity, $b$ is gridblock thickness, and $m$ is the subscript denoting gridblock.

Combining Equations D-18 and D-19

$$\frac{dJ}{dY_p} = \ln(10) \sum_{m=1}^{M} \gamma_{m,p} K_m \frac{dJ}{dK_m} \tag{D-20}$$

The sensitivity coefficient, $dJ/dK_m$ of the objective function with respect to the permeability in a gridblock $m$ is obtained by adjoint sensitivity analysis.

Adjoint sensitivity analysis provides an extremely fast algorithm, particularly when, for a given objective function $J$, the sensitivity coefficients are to be computed for a large number of parameters (permeabilities in thousands of grid blocks, as is the case here).

Let the groundwater flow model be represented by the following matrix equation:

$$\underline{\underline{A}}\,\underline{p}^n = \underline{\underline{B}}\,\underline{p}^{n-1} + \underline{f}^n \tag{D-21}$$

where for a fully implicit scheme of time integration adopted here,

$\underline{p}$ = vector of gridblock pressures
$\underline{\underline{A}}$ = $\underline{\underline{C}} + \underline{\underline{B}}$
$\underline{\underline{B}}$ = $\underline{\underline{S}}/\Delta t$
$\underline{\underline{C}}$ = conductance matrix
$\underline{\underline{S}}$ = storativity matrix
$\underline{f}^n$ = vector of source terms
$\Delta t$ = $t^n - t^{n-1}$
$t$ = time
$n$ = time level (1,2,3 .... L)

$L$ = maximum time level of the simulation.

First, an adjoint state vector $\{\lambda\}$ is obtained by the solution of the following equation:

$$\underline{\underline{A}}\underline{\lambda}^{n-1} = \underline{\underline{B}}\underline{\lambda}^{n} + \left[\frac{\partial J}{\partial \underline{p}^{n}}\right]^{T} \tag{D-22}$$

where $T$ denotes the transpose of the matrix.

Equation D-22 is solved backwards in time, from $n = L$ to $n = 1$ with

$$\underline{\lambda}^{L} = 0 \tag{D-23}$$

If $\alpha_i$ is a generic sensitivity parameter in the gridblock $i$, the sensitivity coefficient $dJ/d\alpha_i$ is evaluated by the expression:

$$\frac{dJ}{d\alpha_i} = \frac{\partial J}{\partial \alpha_i} + \sum_{n=1}^{L} \underline{\lambda}^{nT} \bullet \left[\frac{\partial \underline{\underline{A}}}{\partial \alpha_i}\underline{p}^{n} - \frac{\partial \underline{\underline{B}}}{\partial \alpha_i}\underline{p}^{n-1} - \frac{\partial \underline{f}^{n}}{\partial \alpha_i}\right] \tag{D-24}$$

Here, the Equation D-24 is evaluated with $\alpha_i = K_i$, the permeability in the $i^{th}$ gridblock.

## D.5.4 Pilot Points: Transmissivities

The transmissivities at pilot points are assigned by an unconstrained optimization algorithm and a subsequent imposition of constraints.

The optimization algorithm chosen here belongs to a class of iterative search algorithms. It involves a repeated application of the following equation until convergence is achieved:

$$\underline{Y}_{i+1} = \underline{Y}_i + \beta_i \bullet \underline{d}_i, \tag{D-25}$$

where i is the iteration index, $\underline{d}_i$ is the direction vector, $\beta_i$ is the step length (a scalar), and $\underline{Y}_i$ is the vector of parameters to be optimized (i.e., logarithms of pilot-point transmissivities to base 10).

The steps in the implementation of this algorithm are as follows:

1. For the selected number of pilot points, choose the initial estimates of the parameters ($Y_p = \log_{10} T_p$). These are taken to be the kriged or the conditionally simulated values in the gridblocks, where pilot points are located depending upon the option chosen.

2. Compute the direction vector, $\underline{d}_i$, as per one of the three algorithms discussed below (Fletcher-Reeves, Broyden's, or Davidon-Fletcher-Powell). The direction vector constitutes a direction in the hyperspace of the parameters, and advancing along this direction, yields new values of the parameters. The step-length $\beta$ determines the actual advance along this direction.

3. Determine the optimal step-length $\beta$, which minimizes the objective function. (How the step length is determined is explained in detail in LaVenue and RamaRao [1992].)

4. Update the parameters:

$$\underline{Y}_{i+1} = \underline{Y}_i + \beta_i \underline{d}_i$$

5. Impose the constraints, as explained in Section D.5.5.

6. Check for convergence.

7. If convergence is achieved, the optimization algorithm is completed, the pilot points are added to the data, and execution of the main algorithm continues.

8. If convergence is not achieved, let $i = i + 1$, and go to Step 9.

9. Using the augmented data set, generate a new conditional simulation of transmissivity field, derive the corresponding pressure field, and recompute the gradient vector using the already selected pilot-point locations. (The pilot-point selection process will be skipped.)

10. Go to Step 2.

The code includes three options for the computation of the direction vector $\underline{d}_i$. They are the algorithms due to (1) Fletcher-Reeves, (2) Broyden, and (3) Davidon-Fletcher-Powell (Luenberger, 1973; Gill et al., 1981; Carrera and Neuman, 1986). (These options are explained in detail in LaVenue and RamaRao [1992].)

## D.5.5 Pilot Point Transmissivities: Constraints

It is possible that the optimization algorithms may dictate large changes in the parameters and bring about an impressive reduction in the objective function. Such recommended large changes may be viewed as undesirable for several reasons. At any point in the field, one can obtain a kriged estimate of transmissivity and its variance (kriging variance). One may construct a confidence interval (assuming a normal distribution of kriging errors) for the transmissivity. It is reasonable to expect the calibrated value to be within the confidence band. A constraint may be imposed to achieve this.

Further, situations may exist where the confidence band may be large. A large change in the parameter value, even if contained within the confidence band, can cause a large change in the spatial-correlation structure of

the transmissivity field. One of the objectives in calibration can then be to limit the maximum charge to a specified value, so that the geostatistical structure is not altered significantly.

Consider the $k$th parameter, whose value is $Y_k$ ($k$th element in the vector of parameters, $\underline{Y}$). Then,

$$\begin{aligned} \Delta Y_{k,i} &= \left(Y_{k,i+1} - Y_{k,i}\right) \\ &= \beta_i \bullet d_{k,i} \end{aligned} \quad , \tag{D-26}$$

where $i$ is an iteration index.

Constraint 1: The parameter value should lie within the confidence band.

$$Y_{k,o} - m\sigma_{yo} \le Y_{k,i} \le Y_{k,o} + m\sigma_{yo}, \tag{D-27}$$

where the subscript $o$ indicates initially kriged value, based on the measured data only. Thus $Y_{k,o}$ gives the initially kriged value at the location of the $k^{th}$ pilot point, and $\sigma^2_{yo}$ gives the initially computed kriging variance at the same location, $m$ is the multiplier of the standard deviation, which gives the semi width of the confidence band. If normal distribution is assumed for kriging errors, and if 95% confidence levels are desired; $m = 2$.

Constraint 2: The change in any parameters must be limited to $\Delta Y_{max}$.

$$\Delta Y_{k,i} \le \Delta Y_{max} \tag{D-28}$$

After the optimization, these constraints are implemented for each parameter. In reality, only one constraint is active for a pilot-point. Also, in implementation, the optimal step length computed is reduced if the constraint became active, still preserving the direction.

## D.5.6 Convergence Criteria

It may be noted that there are two levels of iteration, designated as inner and outer iterations. An inner iteration relates to the iterations needed to optimize the transmissivities of the pilot points. Thus, when an inner iteration is repeated, the pilot-point locations are fixed as at the beginning of the sequence of inner iterations. When the convergence of an inner iteration is achieved, the pilot points are added to the transmissivity data set. This then sets the stage for an outer iteration. During the course of outer iteration, optimal location of the next set of pilot points is done using coupled kriging and adjoint sensitivity analysis. Subsequently, their transmissivities are optimized by a sequence of inner iterations. Figure D-5 clarifies these points.

It may be noted that both inner and outer iterations go through all phases of the algorithm, except that inner iterations skip the phase of selecting pilot points from a grid of candidate pilot points.

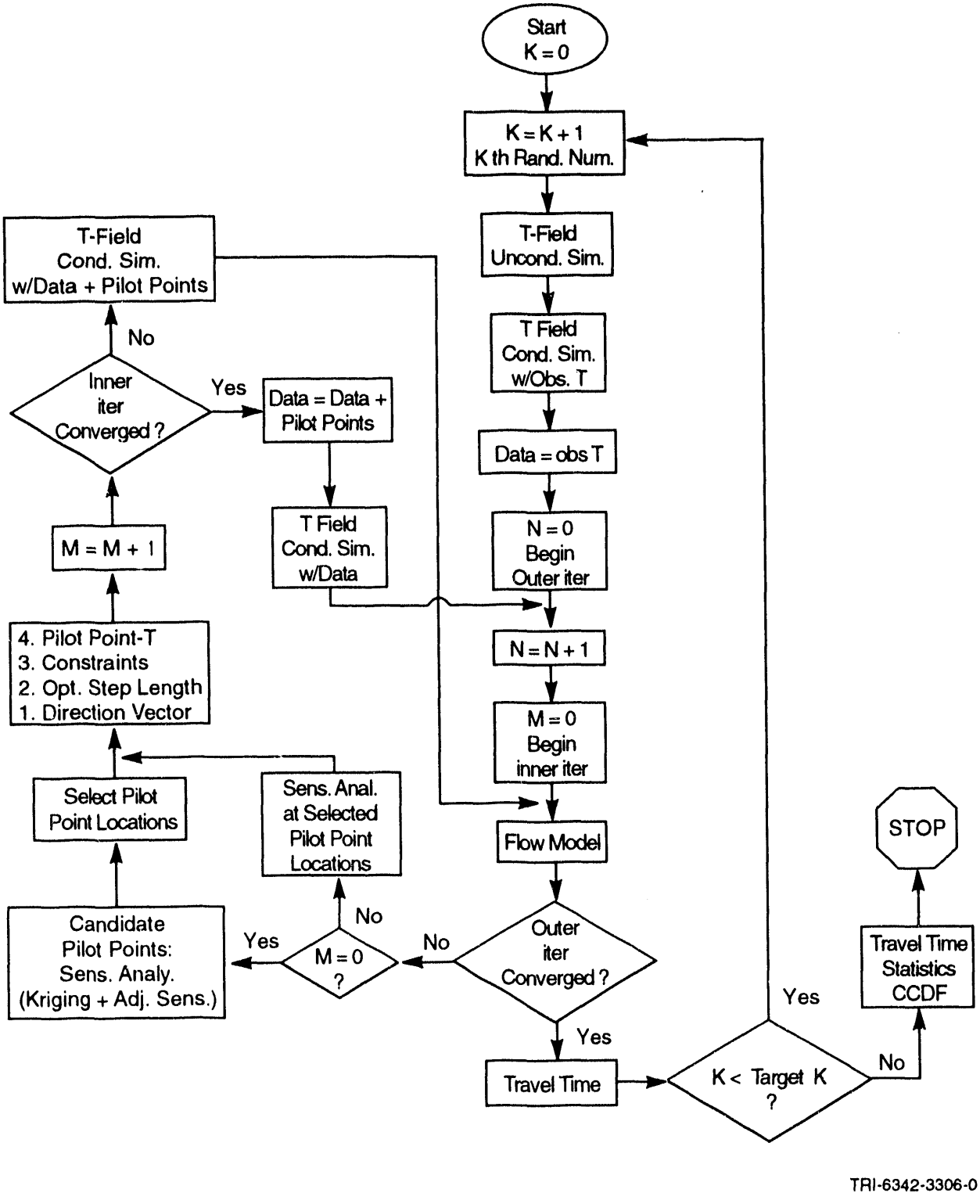


Figure D-5. Inner and outer iterations of calibration.

### D.5.6.1 CONVERGENCE CRITERIA: INNER ITERATIONS.

1. The performance measure $J$ drops below a prescribed minimum value (JMIN):

$$J \leq \text{JMIN} \tag{D-29}$$

2. The number of iterations (NITER) equals a prescribed maximum number of iterations, for the inner iterations (ITERMX1):

$$\text{NITER} \geq \text{ITERMX1} \tag{D-30}$$

3. The ratio of the norm of the gradient, to the initial-gradient norm reduces below a prescribed value (GRNR):

$$\frac{\|\underline{g}\|}{\|\underline{g}_0\|} \leq \underset{\text{(gradient norm ratio)}}{\text{GRNR}} \tag{D-31}$$

4. The gradient norm $\|\underline{g}\|$ is less than a prescribed minimum (GRMIN):

$$\|\underline{g}\| \leq \text{GRMIN} \tag{D-32}$$

5. The relative change in objective function is defined, as $\Delta J/J$, where $\Delta J$ is the change in the objective function during one iteration. Iterations are terminated if this relative change falls below a prescribed value (RELCJ):

$$\frac{\Delta J}{J} \leq \text{RELCJ} \tag{D-33}$$

### D.5.6.2 CONVERGENCE CRITERIA: OUTER ITERATIONS.

Outer iterations are terminated essentially on criteria (1) and (2) of inner iterations. They are not repeated.

# Appendix D References


Carrera, J., and S.P. Neuman. 1986. "Estimation of Aquifer Parameters Under Transient and Steady State Conditions 2, Uniqueness, Stability, and Solution Algorithms," *Water Resources Research.* Vol. 22, no. 2, 211-227.

Delfiner, P. 1976. "Linear Estimation of Non Stationary Spatial Phenomena," *Advanced Geostatistics in the Mining Industry, Proceedings of the NATO Advanced Study Institute, University of Rome, October 13-25, 1975.* Eds. M. Guarescio, M. David, and C. Huijbregts. Hingham, MA: D. Reidel, 49-68.

Delhomme, J.P. 1979. "Spatial Variability and Uncertainty in Groundwater Flow Parameters: A Geostatistical Approach," *Water Resources Research.* Vol. 15, no. 2, 269-280.

de Marsily, G, G. Lavedan, M. Boucher, and G. Fasanino. 1984. "Interpretation of Interference Tests in a Well Feild Using Geostatistical Techniques to Fit the Permeability Distribution in a Reservoir Model," *Geostatistics for Natural Resources Characterization, South Lake Tahoe, CA, Sept. 6-17, 1983.* Eds. G. Verly, M. David, A.G. Journel, and A. Marechai. Hingham, MA: D. Reidel, Pt. 2, 831-849.

Gallegos, D.P., P.I. Pohl , and C.D. Updegraff. 1992. *An Investigation of the Impact of Conceptual Model Uncertainty on the Estimated Performance of a Hypothetical High-Level Nuclear Waste Repository Site in Unsaturated, Fractured Tuff.* SAND90-2882. Albuquerque, NM: Sandia National Laboratories.

Gill, P.E., W. Murray, and M.H. Wright. 1981. *Practical Optimization.* New York, NY: Academic Press, Inc.

Intera, Inc. 1989. *Users Manual for STLINE.* 097B-12C-001B.

Kafiitsas, J., and R.L. Bras. 1981. *The Practice of Kriging.* Technical Report 263. Cambridge, MA: Ralph M. Parsons Laboratory, Massachusetts Institute of Technology.

LaVenue, A.M., T.L. Cauffman, and J.F. Pickens. 1990. *Ground-Water Flow Modeling of the Culebra Dolomite. Volume I: Model Calibration.* SAND89-7068/1. Albuquerque, NM: Sandia National Laboratories.

LaVenue, A.M., and B.S. RamaRao. 1992. *A Modeling Attempt to Address Spatial Variability within the Culebra Dolomite Transmissivity Field.* SAND92-7306. Albuquerque, NM: Sandia National Laboratories.

Luenberger, D.G. 1973. *Introduction to Linear and Nonlinear Programming.* Reading, MA: Addison-Wesley Publishing Co.

Mantoglou, A., and J.L. Wilson. 1982. "Turning Bands Method for Simulation of Random Fields Using Line Generation by a Spectral Method," *Water Resources Research.* Vol. 18, no. 5, 1379-1394.

Matheron, G. 1971. *The Theory of Regionalized Variables and its Applications.* Paris, France: École National Supérieure des Mines.

Matheron, G. 1973. "The Intrinsic Random Functions and Their Applications," *Advances in Applied Probability.* Vol. 5, no. 3, 439-468.

Mejía, J. M., and I. Rodríguez-Iturbe. 1974. "On the Synthesis of Random Fields Sampling From the Spectrum: An Application to the Generation of Hydrologic Spatial Processes," *Water Resources Research.* Vol. 10, no. 4, 705-711.

RamaRao, B.S., and M. Reeves. 1990. *Theory and Verification for the GRASP II Code for Adjoint-Sensitivity Analysis of Steady-State and Transient Ground-Water Flow.* SAND89-7143. Albuquerque, NM: Sandia National Laboratories.

Reeves, M., D.S. Ward, N.D. Johns, and R.M. Cranwell. 1986a. *Theory and Implementation for SWIFT II, the Sandia Waste-Isolation Flow and Transport Model for Fractured Media, Release 4.84.* NUREG/CR-3328. SAND83-1159. Albuquerque, NM: Sandia National Laboratories.

Reeves, M., D.S. Ward, N.D. Johns, and R.M. Cranwell. 1986b. *Data Input Guide for SWIFT II, The Sandia Waste-Isolation Flow and Transport Model for Fractured Media, Release 4.84.* NUREG/CR-3162. SAND83-0242. Albuquerque, NM: Sandia National Laboratories.

Reeves, M., D.S. Ward, P.A. Davis, and E.J. Bonano. 1986c. *Swift II Self-Teaching Curriculum: Illustrative Problems for the Sandia Waste Isolation Flow and Transport Model for Fractured Media.* NUREG/CR-3925. SAND84-1586. Albuquerque, NM: Sandia National Laboratories.

Shinozuka, M., and C-M. Jan. 1972. "Digital Simulation of Random Processes and Its Applications," *Journal of Sound and Vibration.* Vol. 25, no. 1, 111-128.

S ıith, L., and R.A. Freeze. 1979. "Stochastic Analysis of Steady State Groundwater Flow in a Bounded Domain. 2. Two-dimensional Simulations," *Water Resources Research.* Vol. 15, no. 6, 1543-1559.

Smith, L., and F.W. Schwartz. 1981. "Mass Transport. 2. Analysis of Uncertainty in Prediction," *Water Resources Research.* Vol. 17, no. 2, 351-369.

Wilson, J.L., B.S. RamaRao, and J.A. McNeish. 1986. *GRASP: A Computer Code to Perform Post-SWENT Adjoint Sensitivity Analysis of Stead-State Ground-Water Flow.* BMI/ONWI-625. Columbus, OH: Office of Nuclear Waste Isolation, Battelle Memorial Institute.

WIPP Performance Assessment (PA) Division. 1991. *Preliminary Comparison with 40 CFR Part 191, Subpart B for the Waste Isolation Pilot Plant, December 1991 — Volume 2: Probability and Consequence Modeling.* SAND91-0893/2. Albuquerque, NM: Sandia National Laboratories.

Zimmerman, D.A., and J.L. Wilson. 1990. *Description of and User's Manual for TUBA: A Computer Code for Generating Two-Dimensional Random Fields via the Turning Bands Method.* Albuquerque, NM: Gram, Inc.

# DISTRIBUTION

(Send Distribution list changes to M.M. Gruebel, Dept. 6342, Sandia National Laboratories, PO Box 5800, Albuquerque, NM 87185-5800)

## Federal Agencies

US Department of Energy (2)
Office of Environmental Restoration and Waste Management
Attn: L.P. Duffy, EM-1
C. Frank, EM-50
Washington, DC 20585

US Department of Energy (3)
Office of Environmental Restoration and Waste Management
Attn: M. Frei, EM-34 (Trevion II)
Director, Waste Management Projects
Washington, DC 20585-0002

US Department of Energy
Office of Environmental Restoration and Waste Management
Attn: J. Lytle, EM-30 (Trevion II)
Washington, DC 20585-0002

US Department of Energy
Office of Environmental Restoration and Waste Management
Attn: S. Schneider, EM-342 (Trevion II)
Washington, DC 20585-0002

US Department of Energy (3)
WIPP Task Force
Attn: G.H. Daly
S. Fucigna
B. Bower
12800 Middlebrook Rd.
Suite 400
Germantown, MD 20874

US Department of Energy (4)
Office of Environment, Safety and Health
Attn: R.P. Berube, EH-20
C. Borgstrum, EH-25
R. Pelletier, EH-231
K. Taimi, EH-232
Washington, DC 20585

US Department of Energy (5)
WIPP Project Integration Office
Attn: W.J. Arthur III
R. Becker
P. Dickman
L.W. Gage
P.J. Higgins
D.A. Olona
PO Box 5400
Albuquerque, NM 87115-5400

US Department of Energy (10)
WIPP Project Site Office (Carlsbad)
Attn: A. Hunt (4)
V. Daub (4)
J. Lippis
K. Hunter
PO Box 3090
Carlsbad, NM 88221-3090

US Department of Energy, (5)
Office of Civilian Radioactive Waste Management
Attn: Deputy Director, RW-2
Associate Director, RW-10
Office of Program Administration and Resources Management
Associate Director, RW-20
Office of Facilities Siting and Development
Associate Director, RW-30
Office of Systems Integration and Regulations
Associate Director, RW-40
Office of External Relations and Policy
Office of Geologic Repositories
Forrestal Building
Washington, DC 20585

US Department of Energy
Attn: National Atomic Museum Library
Albuquerque Operations Office
PO Box 5400
Albuquerque, NM 87185

US Department of Energy
Research & Waste Management Division
Attn: Director
PO Box E
Oak Ridge, TN 37831

US Department of Energy (2)
Idaho Operations Office
Fuel Processing and Waste
Management Division
785 DOE Place
Idaho Falls, ID 83402

US Department of Energy
Savannah River Operations Office
Defense Waste Processing
Facility Project Office
Attn: W.D. Pearson
PO Box A
Aiken, SC 29802

US Department of Energy (2)
Richland Operations Office
Nuclear Fuel Cycle & Production
Division
Attn: R.E. Gerton
825 Jadwin Ave.
PO Box 500
Richland, WA 99352

US Department of Energy (3)
Nevada Operations Office
Attn: J.R. Boland
D. Livingston
P.K. Fitzsimmons
2753 S. Highland Drive
Las Vegas, NV 89183-8518

US Department of Energy (2)
Technical Information Center
PO Box 62
Oak Ridge, TN 37831

US Department of Energy (2)
Chicago Operations Office
Attn: J.C. Haugen
9800 South Cass Avenue
Argonne, IL 60439

US Department of Energy
Los Alamos Area Office
528 35th Street
Los Alamos, NM 87544

US Department of Energy (3)
Rocky Flats Area Office
Attn: W.C. Rask
G. Huffman
T. Lukow
PO Box 928
Golden, CO 80402-0928

US Department of Energy
Dayton Area Office
Attn: R. Grandfield
PO Box 66
Miamisburg, OH 45343-0066

US Department of Energy
Attn: E. Young
Room E-178
GAO/RCED/GTN
Washington, DC 20545

US Bureau of Land Management
101 E. Mermod
Carlsbad, NM 88220

US Bureau of Land Management
New Mexico State Office
PO Box 1449
Santa Fe, NM 87507

US Environmental Protection
Agency (2)
Office of Radiation Protection Programs
(ANR-460)
Washington, DC 20460

US Nuclear Regulatory Commission
Division of Waste Management
Attn: H. Marson
Mail Stop 4-H-3
Washington, DC 20555

US Nuclear Regulatory Commission (4)
Advisory Committee on Nuclear Waste
Attn: D. Moeller
M.J. Steindler
P.W. Pomeroy
W.J. Hinze
7920 Norfolk Avenue
Bethesda, MD 20814

Defense Nuclear Facilities Safety Board
Attn: D. Winters
625 Indiana Avenue, NW
Suite 700
Washington, DC 20004

Nuclear Waste Technical Review
Board (2)
Attn: Library
Suite 910
1100 Wilson Blvd.
Arlington, VA 22209-2297

Energy and Science Division
Office of Management and Budget
Attn: K. Yuracko
725 17th Street NW
Washington, DC 20503

US Geological Survey (2)
Water Resources Division
Attn: C. Peters
Suite 200
4501 Indian School NE
Albuquerque, NM 87110

### New Mexico Congressional Delegation

Jeff Bingaman
U.S. Senate
110 Hart SOB
Washington, DC 20510-3102

Pete V. Domenici
U.S. Senate
427 Dirksen Bldg.
Washington, DC 20510-3101

Bill Richardson
House of Representatives
2349 Rayburn HOB
Washington, DC 20515

Steven H. Schiff
House of Representatives
1009 Longworth HOB
Washington, DC 20515

Joe Skeen
House of Representatives
2367 Rayburn HOB
Washington, DC 20515

### State Agencies

New Mexico Bureau of Mines
and Mineral Resources
Socorro, NM 87801

New Mexico Energy, Minerals and Natural
Resources Department
Attn: Librarian
2040 South Pacheco
Santa Fe, NM 87505

New Mexico Energy, Minerals and Natural
Resources Department
New Mexico Radioactive Task Force (2)
(Governor's WIPP Task Force)
Attn: A. Lockwood, Chairman
C. Wentz, Coordinator/Policy Analyst
2040 South Pacheco
Santa Fe, NM 87505

Bob Forrest
Mayor, City of Carlsbad
PO Box 1569
Carlsbad, NM 88221

Executive Director
Carlsbad Department of Development
Attn: C. Bernard
PO Box 1090
Carlsbad, NM 88221

New Mexico Environment Department
Secretary of the Environment (3)
Attn: J. Espinosa
PO Box 968
1190 St. Francis Drive
Santa Fe, NM 87503-0968

New Mexico Environment Department
Attn: P. McCasland
WIPP Project Site Office
PO Box 3090
Carlsbad, NM 88221-3090

New Mexico State Engineer's Office
Attn: M. Chudnoff
PO Box 25102
Santa Fe, NM 87504-5102

Environmental Evaluation Group (5)
Attn: R. Neill
Suite F-2
7007 Wyoming Blvd. NE
Albuquerque, NM 87109

### Advisory Committee on Nuclear Facility Safety

John F. Ahearne
Executive Director, Sigma Xi
99 Alexander Drive
Research Triangle Park, NC 27709

James E. Martin
109 Observatory Road
Ann Arbor, MI 48109

**WIPP Panel of National Research Council's Board on Radioactive Waste Management**

Charles Fairhurst, Chairman
Department of Civil and
Mineral Engineering
University of Minnesota
500 Pillsbury Dr., SE
Minneapolis, MN 55455-0220

John O. Blomeke
3833 Sandy Shore Drive
Lenoir City, TN 37771-9803

John D. Bredehoeft
Western Region Hydrologist
Water Resources Division
US Geological Survey (M/S 439)
345 Middlefield Road
Menlo Park, CA 94025

Fred M. Ernsberger
1325 NW 10th Avenue
Gainsville, FL 32601

Rodney C. Ewing
Department of Geology
University of New Mexico
200 Yale, NE
Albuquerque, NM 87131

B. John Garrick
PLG, Inc.
Suite 400
4590 MacArthur Blvd.
Newport Beach, CA 92660-2027

Leonard F. Konikow
US Geological Survey
431 National Center
Reston, VA 22092

Jeremiah O'Driscoll
505 Valley Hill Drive
Atlanta, GA 30350

Christopher Whipple
Clement International Corp.
160 Spear St.
Suite 1380
San Francisco, CA 94105-1535

National Research Council (3)
Board on Radioactive
Waste Management
RM HA456
Attn: P.B. Myers,
Staff Director (2)
G.J. Grube
2101 Constitution Avenue
Washington, DC 20418

**Performance Assessment Peer Review Panel**

G. Ross Heath
College of Ocean and
Fishery Sciences HN-15
583 Henderson Hall
University of Washington
Seattle, WA 98195

Thomas H. Pigford
Department of Nuclear Engineering
4159 Etcheverry Hall
University of California
Berkeley, CA 94720

Thomas A. Cotton
JK Research Associates, Inc.
4429 Butterworth Place, NW
Washington, DC 20016

Robert J. Budnitz
President, Future Resources
Associates, Inc.
2000 Center Street
Suite 418
Berkeley, CA 94704

C. John Mann
Department of Geology
245 Natural History Bldg.
1301 West Green Street
University of Illinois
Urbana, IL 61801

Frank W. Schwartz
Department of Geology and Mineralogy
The Ohio State University
Scott Hall
1090 Carmack Rd.
Columbus, OH 43210

**National Laboratories**

Argonne National Laboratory (2)
Attn: A. Smith
D. Tomasko
9700 South Cass, Bldg. 201
Argonne, IL 60439

Battelle Pacific Northwest Laboratory (3)
Attn: R.E. Westerman
S. Bates
H.C. Burkholder
Battelle Boulevard
Richland, WA 99352

Idaho National Engineering Laboratory (2)
Attn: H. Loo
R. Klinger
Mail Stop 5108
Idaho Falls, ID 83403-4000

Los Alamos National Laboratory
Attn: B. Erdal, CNC-11
PO Box 1663
Los Alamos, NM 87545

Los Alamos National Laboratory
Attn: A. Meijer
PO Box 1663, Mail Stop J514
Los Alamos, NM 87545

Los Alamos National Laboratory (3)
HSE-8
Attn: M. Enoris
L. Soholt
J. Wenzel
PO Box 1663
Los Alamos, NM 87545

Los Alamos National Laboratory
EM-7
Attn: S. Kosiewicz
PO Box 1663, Mail Stop J595
Los Alamos, NM 87545

Oak Ridge National Laboratory
Transuranic Waste Manager
Attn: D.W. Turner
PO Box 2008, Bldg. 3047
Oak Ridge, TN 37831-6060

Pacific Northwest Laboratory
Attn: B. Kennedy
PO Box 999
Richland, WA 99352

Savannah River Laboratory (3)
Attn: N. Bibler
M.J. Plodinec
G.G. Wicks
Aiken, SC 29801

Savannah River Plant (2)
Attn: R.G. Baxter
Bldg. 704-S
K.W. Wierzbicki
Bldg. 703-H
Aiken, SC 29808-0001

**Corporations/Members of the Public**

Benchmark Environmental Corp.
Attn: C. Frederickson
4501 Indian School NE
Suite 105
Albuquerque, NM 87110

City of Albuquerque
Public Works Department
Utility Planning Division
Attn: W.K. Summers
PO Box 1293
Albuquerque, NM 87103

Deuel and Associates, Inc.
Attn: R.W. Prindle
7208 Jefferson NE
Albuquerque, NM 87109

Disposal Safety, Inc.
Attn: B. Ross
1660 L Street NW
Suite 314
Washington, DC 20036

Ecodynamics (2)
Attn: P. Roache
R. Blaine
PO Box 9229
Albuquerque, NM 87119-9229

EG & G Idaho (3)
1955 Fremont Street
Attn: C. Atwood
C. Hertzler
T.I. Clements
Idaho Falls, ID 83415

Geomatrix
Attn: K. Coppersmith
100 Pine Street, Suite 1000
San Francisco, CA 94111

Golder Associates, Inc. (3)
Attn: M. Cunnane
R. Kossik
I. Miller
4104 148th Avenue NE
Redmond, WA 98052

INTERA, Inc. (2)
Attn: J.F. Pickens
A.M. LaVenve
6850 Austin Center Blvd.
Suite 300
Austin, TX 78731

INTERA, Inc.
Attn: W. Stensrud
PO Box 2123
Carlsbad, NM 88221

INTERA, Inc.
Attn: W. Nelson
101 Convention Center Drive
Suite 540
Las Vegas, NV 89109

IT Corporation (2)
Attn: R.F. McKinney
J. Myers
Regional Office, Suite 700
5301 Central Avenue NE
Albuquerque, NM 87108

John Hart and Associates, P.A.
Attn: J.S. Hart
2815 Candelaria Road NW
Albuquerque, NM 87107

John Hart and Associates, P.A.
Attn: K. Lickliter
1009 North Washington
Tacoma, WA 98406

MACTEC (2)
Attn: J.A. Thies
D.K. Duncan
8418 Zuni Road SE, Suite 200
Albuquerque, NM 87108

Newman and Holtzinger
Attn: C. Mallon
1615 L Street NW, Suite 1000
Washington, DC 20036

RE/SPEC, Inc. (2)
Attn: W. Coons
4775 Indian School NE, Suite 300
Albuquerque, NM 87110

RE/SPEC, Inc.
Attn: J.L. Ratigan
PO Box 725
Rapid City, SD 57709

Reynolds Elect/Engr. Co., Inc.
Attn: E.W. Kendall
Building 790, Warehouse Row
PO Box 98521
Las Vegas, NV 89193-8521

Roy F. Weston, Inc.
CRWM Tech. Supp. Team
Attn: C.J. Noronha
955 L'Enfant Plaza SW
North Building, Eighth Floor
Washington, DC 20024

Science Applications International Corporation (SAIC)
Attn: H.R. Pratt
10260 Campus Point Drive
San Diego, CA 92121

Science Applications International Corporation (2)
Attn: D.C.Royer
C.G. Pflum
101 Convention Center Dr.
Las Vegas, NV 89109

Science Applications International Corporation (2)
Attn: M. Davis
J. Tollison
2109 Air Park Road SE
Albuquerque, NM 87106

Science Applications International Corporation (2)
Attn: J. Young
D. Lester
18706 North Creek Parkway, Suite 110
Bothell, WA 98011

Southwest Research Institute
Center for Nuclear Waste Regulatory Analysis (2)
Attn: P.K. Nair
6220 Culebra Road
San Antonio, TX 78228-0510

Systems, Science, and Software (2)
Attn: E. Peterson
P. Lagus
Box 1620
La Jolla, CA 92038

TASC
Attn: S.G. Oston
55 Walkers Brook Drive
Reading, MA 01867

Tech Reps, Inc. (6)
Attn: J. Chapman
C. Crawford
D. Marchand
J. Stikar
P. Oliver
D. Scott
5000 Marble NE, Suite 222
Albuquerque, NM 87110

Tolan, Beeson & Associates
Attn: T.L. Tolan
2320 W. 15th Avenue
Kennewick, WA 99337

TRW Environmental Safety Systems
Attn: I. Sacks
2650 Park Tower Drive, Suite 800
Vienna, VA 22180

Westinghouse Electric Corporation (5)
Attn: Library
L. Trego
C. Cox
L. Fitch
R.F. Kehrman
PO Box 2078
Carlsbad, NM 88221

Westinghouse Hanford Company
Attn: D. E. Wood
MSIN HO-32
PO Box 1970
Richland, WA 99352

Western Water Consultants
Attn: D. Fritz
1949 Sugarland Drive #134
Sheridan, WY 82801-5720

Western Water Consultants
Attn: P.A. Rechard
PO Box 4128
Laramie, WY 82071

P. Drez
8816 Cherry Hills Road, NE
Albuquerque, NM 87111

D.W. Powers
Star Route Box 87
Anthony, TX 79821

Shirley Thieda
PO Box 2109, RR1
Bernalillo, NM 87004

Jack Urich
c/o CARD
144 Harvard SE
Albuquerque, NM 87106

**Universities**

University of California
Mechanical, Aerospace, and
Nuclear Engineering Department (2)
Attn: W. Kastenberg
D. Browne
5532 Boelter Hall
Los Angeles, CA 90024

University of California
Mine Engineering Dept.
Attn: Neville Cook
Rock Mechanics Engineering
Berkeley, CA 94720

University of Hawaii at Hilo
Attn: S. Hora
Business Administration
Hilo, HI 96720-4091

University of New Mexico
Geology Department
Attn: Library
Albuquerque, NM 87131

University of New Mexico
Research Administration
Attn: H. Schreyer
102 Scholes Hall
Albuquerque, NM 87131

University of Wyoming
Department of Civil Engineering
Attn: V.R. Hasfurther
Laramie, WY 82071

University of Wyoming
Department of Geology
Attn: J.I. Drever
Laramie, WY 82071

University of Wyoming
Department of Mathematics
Attn: R.E. Ewing
Laramie, WY 82071

**Libraries**

Thomas Brannigan Library
Attn: D. Dresp
106 W. Hadley St.
Las Cruces, NM 88001

Hobbs Public Library
Attn: M. Lewis
509 N. Ship Street
Hobbs, NM 88248

New Mexico State Library
Attn: N. McCallan
325 Don Gaspar
Santa Fe, NM 87503

New Mexico Tech
Martin Speere Memorial Library
Campus Street
Socorro, NM 87810

New Mexico Junior College
Pannell Library
Attn: R. Hill
Lovington Highway
Hobbs, NM 88240

Carlsbad Municipal Library
WIPP Public Reading Room
Attn: L. Hubbard
101 S. Halagueno St.
Carlsbad, NM 88220

University of New Mexico
General Library
Government Publications Department
Albuquerque, NM 87131

**NEA/Performance Assessment Advisory Group (PAAG)**

P. Duerden
ANSTO
Lucas Heights Research Laboratories
Private Mail Bag No. 1
Menai, NSW 2234, AUSTRALIA

Gordon S. Linsley
Division of Nuclear Fuel Cycle and Waste Management
International Atomic Energy Agency
PO Box 100
A-1400 Vienna, AUSTRIA

Nicolo Cadelli
Commission of the European Communities
200, Rue de la Loi
B-1049 Brussels, BELGIUM

R. Heremans
Organisme Nationale des Déchets Radioactifs et des Matiéres Fissiles
ONDRAF
Place Madou 1, Boitec 24/25
B-1030 Brussels, BELGIUM

J. Marivoet
Centre d'Etudes de l'Energie Nucléaire
CEN/SCK
Boeretang 200
B-2400 Mol, BELGIUM

P. Conlon
Waste Management Division
Atomic Energy Control Board (AECB)
PO Box 1046
Ottawa, Canada KIP 559, CANADA

A.G. Wikjord
Manager, Environmental and Safety Assessment Branch
Atomic Energy of Canada Limited
Whiteshell Nuclear Research Establishment
Pinewa, Manitoba ROE 1LO, CANADA

Jukka-Pekka Salo
Teollisuuden Voima Oy (TVO)
Fredrikinkatu 51-53 B
SF-00100 Helsinki, FINLAND

Timo Vieno
Technical Research Centre of Finland (VTT)
Nuclear Energy Laboratory
PO Box 208
SF-02151 Espoo, FINLAND

Timo Äikäs
Teollisuuden Voima Oy (TVO)
Fredrikinkatu 51-53 B
SF-00100 Helsinki, FINLAND

M. Claude Ringeard
Division de la Sécurité et de la Protection de l'Environment (DSPE)
Commissariat á l'Energie Atomique
Agence Nationale pour la Gestion des Déchets Radioactifs (ANDRA)
Route du Panorama Robert Schuman
B. P. No. 38
F-92266 Fontenay-aux-Roses Cedex
FRANCE

Gérald Ouzounian
Agence Nationale pour la Gestion des Déchets Radioactifs (ANDRA)
Route du Panorama Robert Schuman
B. P. No. 38
F-92266 Fontenay-aux-Roses Cedex
FRANCE

Claudio Pescatore
Division of Radiation Protection and Waste Management
OECD Nuclear Energy Agency
38, Boulevard Suchet
F-75016 Paris, FRANCE

M. Dominique Greneche
Commissariat á l'Energie Atomique
IPSN/DAS/SASICC/SAED
B. P. No. 6
F-92265 Fontenay-aux-Roses Cedex,
FRANCE

Robert Fabriol
Bureau de Recherches Géologiques et Miniéres (BRGM)
B. P. 6009
45060 Orléans Cedex 2, FRANCE

P. Bogorinski
Gesellschaft für Reaktorsicherheit (GRS) mbH
Schwertnergasse 1
D-5000 Köln 1, GERMANY

R. Storck
GSF - Institut für Tieflagerung
Theodor-Heuss-Strabe 4
D-3300 Braunschweig, GERMANY

Ferrucio Gera
ISMES S.p.A
Via del Crociferi 44
I-00187 Rome, ITALY

Hiroyuki Umeki
Isolation System Research Program
Radioactive Waste Management Project
Power Reactor and Nuclear Fuel Development Corporation (PNC)
1-9-13, Akasaka
Minato-ku
Tokyo 107, JAPAN

P. Carboneras Martinez
ENRESA
Calle Emilio Vargas 7
R-28043 Madrid, SPAIN

Tönis Papp
Swedish Nuclear Fuel and Waste Management Co.
Box 5864
S 102 48 Stockholm, SWEDEN

Conny Hägg
Swedish Radiation Protection Institute (SSI)
Box 60204
S-104 01 Stockholm, SWEDEN

J. Hadermann
Paul Scherrer Institute
Waste Management Programme
CH-5232 Villigen PSI, SWITZERLAND

J. Vigfusson
USK- Swiss Nuclear Safety Inspectorate
Federal Office of Energy
CH-5303 Würenlingen, SWITZERLAND

D.E. Billington
Departmental Manager - Assessment Studies
Radwaste Disposal R&D Division
AEA Decommissioning & Radwaste
Harwell Laboratory, B60
Didcot Oxfordshire OX11 ORA
UNITED KINGDOM

P. Grimwood
Waste Management Unit
BNFL
Sellafield
Seascale, Cumbria CA20 1PG
UNITED KINGDOM

Alan J. Hooper
UK Nirex Ltd
Curie Avenue
Harwell, Didcot
Oxfordshire, OX11 ORH
UNITED KINGDOM

Jerry M. Boak
Yucca Mountain Project Office
US Department of Energy
PO Box 98608
Las Vegas, NV 89193

Seth M. Coplan (Chairman)
US Nuclear Regulatory Commission
Division of High-Level Waste Management
Mail Stop 4-H-3
Washington, DC 20555

A.E. Van Luik
INTERA/M&O
The Valley Bank Center
101 Convention Center Dr.
Las Vegas, NV 89109

**NEA/PSAG User's Group**

Shaheed Hossain
Division of Nuclear Fuel Cycle and Waste Management
International Atomic Energy Agency
Wagramerstrasse 5
PO Box 100
A-1400 Vienna, AUSTRIA

Alexander Nies (PSAC Chairman)
Gesellschaft für Strahlen- und
Institut für Tieflagerung
Abteilung für Endlagersicherheit
Theodor-Heuss-Strasse 4
D-3300 Braunschweig, GERMANY

Eduard Hofer
Gesellschaft für Reaktorsicherheit (GRS) MBH
Forschungsgelände
D-8046 Garching, GERMANY

Andrea Saltelli
Commission of the European Communities
Joint Resarch Centre of Ispra
I-21020 Ispra (Varese), ITALY

Alejandro Alonso
Cátedra de Tecnología Nuclear
E.T.S. de Ingenieros Industriales
José Gutiérrez Abascal, 2
E-28006 Madrid, SPAIN

Pedro Prado
CIEMAT
Instituto de Tecnología Nuclear
Avenida Complutense, 22
E-28040 Madrid, SPAIN

Miguel Angel Cuñado
ENRESA
Emilio Vargas, 7
E-28043 Madrid, SPAIN

Francisco Javier Elorza
ENRESA
Emilio Vargas, 7
E-28043 Madrid, SPAIN

Nils A. Kjellbert
Swedish Nuclear Fuel and Waste Management Company (SKB)
Box 5864
S-102 48 Stockholm, SWEDEN

Björn Cronhjort
Swedish National Board for Spent Nuclear Fuel (SKN)
Sehlsedtsgatan 9
S-115 28 Stockholm, SWEDEN

Richard A. Klos
Paul-Scherrer Institute (PSI)
CH-5232 Villingen PSI
SWITZERLAND

NAGRA (2)
Attn: C. McCombie
F. Van Dorp
Parkstrasse 23
CH-5401 Baden, SWITZERLAND

N. A. Chapman
Intera Information Technologies
Park View House, 14B Burton Street
Melton Mowbray
Leicestershire, LE13 1AE
UNITED KINGDOM

Daniel A. Galson
Galson Sciences Ltd.
35, Market Place
Oakham
Leicestershire LE15 6DT
UNITED KINGDOM

David P. Hodgkinson
Intera Information Technologies
Chiltern House
45 Station Road
Henley-on-Thames
Oxfordshire RG9 1AT, UNITED KINGDOM

Brian G.J. Thompson
Department of the Environment: Her Majesty's Inspectorate of Pollution
Room A5.33, Romney House
43 Marsham Street
London SW1P 2PY, UNITED KINGDOM

Intera Information Technologies
Attn: M.J.Apted
3609 South Wadsworth Blvd.
Denver, CO 80235

US Nuclear Regulatory Commission (2)
Attn: R. Codell
N. Eisenberg
Mail Stop 4-H-3
Washington, DC 20555

Battelle Pacific Northwest Laboratories
Attn: P.W. Eslinger
PO Box 999, MS K2-32
Richland, WA 99352

Center for Nuclear Waste Regulatory Analysis (CNWRA)
Southwest Research Institute
Attn: B. Sagar
PO Drawer 28510
6220 Culebra Road
San Antonio, TX 78284

**Geostatistics Expert Working Group (GXG)**

Rafael L. Bras
R.L. Bras Consulting Engineers
44 Percy Road
Lexington, MA 02173

Jesus Carrera
Universidad Politécnica de Cataluña
E.T.S.I. Caminos
Jordi, Girona 31
E-08034 Barcelona, SPAIN

Gedeon Dagan
Department of Fluid Mechanics and Heat Transfer
Tel Aviv University
PO Box 39040
Ramat Aviv, Tel Aviv 69978, ISRAEL

Ghislain de Marsily (GXG Chairman)
University Pierre et Marie Curie
Laboratorie de Geologie Applique
4, Place Jussieu - T.26 - 5e etage
75252 Paris Cedex 05, FRANCE

Alain Galli
Centre de Geostatistique
Ecole des Mines de Paris
35 Rue St. Honore
77035 Fontainebleau, FRANCE

Steve Gorelick
Department of Applied Earth Sciences
Stanford University
Stanford, CA 94305-2225

Peter Grindrod
INTERA Information Technologies Ltd.
Chiltern House, 45 Station Road
Henley-on-Thames
Oxfordshire, RG9 1AT
UNITED KINGDOM

Alan Gutjahr
Department of Mathematics
New Mexico Institute of Mining and Technology
Socorro, NM 87801

C. Peter Jackson
Harwell Laboratory
Theoretical Studies Department
Radwaste Disposal Division
Bldg. 424.4
Oxfordshire Didcot Oxon OX11 ORA
UNITED KINDGOM

Peter Kitanidis
60 Peter Coutts Circle
Stanford, CA 94305

Rae Mackay
Department of Civil Engineering
University of Newcastle Upon Tyne
Newcastle Upon Tyne NE1 7RU
UNITED KINGDOM

Dennis McLaughlin
Parsons Laboratory
Room 48-209
Department of Civil Engineering
Massachusetts Institute of Technology
Cambridge, MA 02139

Shlomo P. Neuman
College of Engineering and Mines
Department of Hydrology and Water Resources
University of Arizona
Tucson, AZ 85721

Christian Ravenne
Geology and Geochemistry Division
Institut Francais du Pétrole
1 & 4, av. de Bois-Préau BP311
92506 Rueil Malmaison Cedex
FRANCE

Yoram Rubin
Department of Civil Engineering
University of California
Berkeley, CA 94720

**Foreign Addresses**

Studiecentrum Voor Kernenergie
Centre D'Energie Nucleaire
Attn: A. Bonne
SCK/CEN
Boeretang 200
B-2400 Mol, BELGIUM

Atomic Energy of Canada, Ltd. (3)
Whiteshell Research Estab.
Attn: M.E. Stevens
B.W. Goodwin
D. Wushke
Pinewa, Manitoba
ROE 1L0, CANADA

Esko Peltonen
Industrial Power Company Ltd.
TVO
Fredrikinkatu 51-53
SF-00100 Helsinki 10, FINLAND

Jean-Pierre Olivier
OECD Nuclear Energy Agency (2)
38, Boulevard Suchet
F-75016 Paris, FRANCE

D. Alexandre, Deputy Director
ANDRA
31 Rue de la Federation
75015 Paris, FRANCE

Claude Sombret
Centre D'Etudes Nucleaires
De La Vallee Rhone
CEN/VALRHO
S.D.H.A. BP 171
30205 Bagnols-Sur-Ceze, FRANCE

Bundesministerium fur Forschung und
Technologie
Postfach 200 706
5300 Bonn 2, GERMANY

Bundesanstalt fur Geowissenschaften
und Rohstoffe
Attn: M. Langer
Postfach 510 153
3000 Hanover 51, GERMANY

Gesellschaft fur Reaktorsicherheit (GRS) (2)
Attn: B. Baltes
W. Muller
Schwertnergasse 1
D-5000 Cologne, GERMANY

Institut fur Tieflagerung (2)
Attn: K. Kuhn
Theodor-Heuss-Strasse 4
D-3300 Braunschweig, GERMANY

Physikalisch-Technische
Bundesanstalt
Attn: P. Brenneke
Postfach 33 45
D-3300 Braunschweig, GERMANY

Shingo Tashiro
Japan Atomic Energy Research Institute
Tokai-Mura, Ibaraki-Ken
319-11, JAPAN

Netherlands Energy Research
Foundation (ECN)
Attn: L.H. Vons
3 Westerduinweg
PO Box 1
1755 ZG Petten, THE NETHERLANDS

Johan Andersson
Swedish Nuclear Power Inspectorate
Statens Kärnkraftinspektion (SKI)
Box 27106
S-102 52 Stockholm, SWEDEN

Fred Karlsson
Svensk Karnbransleforsorjning
AB SKB
Box 5864
S-102 48 Stockholm, SWEDEN

Nationale Genossenschaft fur die Lagerung
Radioaktiver Abfalle (NAGRA) (2)
Attn: S. Vomvoris
P. Zuidema
Hardstrasse 73
CH-5430 Wettingen, SWITZERLAND

AEA Technology
Attn: J.H. Rees
D5W/29 Culham Laboratory
Abington
Oxfordshire OX14 3DB, UNITED KINGDOM

AEA Technology
Attn: W.R. Rodwell
O44/A31 Winfrith Technical Centre
Dorchester
Dorset DT2 8DH, UNITED KINGDOM

AEA Technology
Attn: J.E. Tinson
B4244 Harwell Laboratory
Didcot, Oxfordshire OX11 ORA
UNITED KINGDOM

D.R. Knowles
British Nuclear Fuels, plc
Risley, Warrington
Cheshire WA3 6AS, 1002607
UNITED KINGDOM

**Internal**

| | |
|---|---|
| 1 | A. Narath |
| 20 | O.E. Jones |
| 1502 | J.C. Cummings |
| 1511 | D.K. Gartling |
| 6000 | D.L. Hartley |
| 6115 | P.B. Davies |
| 6119 | E.D. Gorham |
| 6119 | Staff (14) |
| 6121 | J.R. Tillerson |
| 6121 | Staff (7) |
| 6233 | J.C. Eichelberger |
| 6300 | D.E. Ellis |
| 6302 | L.E. Shephard |
| 6303 | S.Y. Pickering |
| 6303 | W.D. Weart |
| 6305 | S.A. Goldstein |
| 6306 | A.L. Stevens |
| 6312 | F.W. Bingham |
| 6313 | L.S. Costin |
| 6331 | P.A. Davis |
| 6341 | Sandia WIPP Central Files (300) |
| 6342 | D.R. Anderson |
| 6342 | Staff (30) |
| 6343 | S.A. Orrell, Acting |
| 6343 | Staff (3) |
| 6345 | R.C. Lincoln |
| 6345 | Staff (9) |
| 6347 | D.R. Schafer |
| 6348 | J.T. Holmes |
| 6351 | R.E. Thompson |
| 6352 | D.P. Garber |
| 6352 | S.E. Sharpton |
| 6400 | N.R. Ortiz |
| 6613 | R.M. Cranwell |
| 6613 | R.L. Iman |
| 6613 | C. Leigh |
| 6622 | M.S.Y. Chu |
| 6641 | R.E. Luna, Acting |
| 7141 | Technical Library (5) |
| 7151 | Technical Publications |
| 7613-2 | Document Processing for DOE/OSTI (10) |
| 8523-2 | Central Technical Files |
| 9300 | J.E. Powell |
| 9310 | J.D. Plimpton |
| 9330 | J.D. Kennedy |



☆ U.S. GOVERNMENT PRINTING OFFICE 1992—774-122/80126

# END

DATE
FILMED
9/8/93